2-2011

Engineering Nanoparticles Surface for Biosensing: "Chemical Noses" to Detect and Identify Proteins, Bacteria and Cancerous Cells

Oscar Ramon Miranda-Sanchez
University of Massachusetts Amherst

ENGINEERING NANOPARTICLES SURFACE FOR BIOSENSING: "CHEMICAL NOSES" TO DETECT AND IDENTIFY PROTEINS, BACTERIA AND CANCEROUS CELLS

A Dissertation Presented

by

OSCAR RAMON MIRANDA-SANCHEZ

Submitted to the Graduate School of the
University of Massachusetts Amherst in partial fulfillment
of the requirements for the degree of

DOCTOR OF PHILOSOPHY

February 2011

Chemistry

ENGINEERING NANOPARTICLES SURFACE FOR BIOSENSING: "CHEMICAL NOSES" TO DETECT AND IDENTIFY PROTEINS, BACTERIA AND CANCEROUS CELLS

A Dissertation Presented

by

OSCAR RAMON MIRANDA-SANCHEZ

Approved as to style and content by:

_____
Vincent M. Rotello, Chair

_____
Todd S. Emrick, Member

_____
Michael J. Knapp, Member

_____
Edward G. Voigtman, Jr., Member

_____
Craig T. Martin, Head,
Department of Chemistry

DEDICATION

To my parents, Oscar and Raquel
my brothers, Juan, Walter, Freddy, Lester and Ridder
my sisters, Maria and Magdalena
all my friends
all Rotello group members
my adviser, Prof. Vincent M. Rotello
and The Department of Chemistry

ACKNOWLEDGMENTS

First and foresmost I would like to thank Prof. Vincent M. Rotello, Charles A. Goessmann Professor of Chemistry, for his support, intellectual discussion, personal encouragement, advice, pacience during my time in his lab (LRGT 1315) and the most important friendship. I also thanks to him for installing the confidence in me to pursue my academics goals. I have been lucky over the past five years to have published several papers, attending national meetings, and even win an award, The William E. McEwen Outstanding Graduate Student Award. Without him, this project would not have been possible. So for all the above described I want to say "Prof. Rotello thanks so much for everything! " and I wish you all the best ! .

I am also extremely thankful to my research committee members, Prof. Michael Knapp, Prof. Edward Voigtman, and Prof. Todd Emrick, for their detailed and constructive comments, thoughts, suggestions and constant academic support throughout this work, making possible to finish this dissertation.

I wish to express my warm and sincere gratitude to Prof. Uwe H. F. Bunz, his research group, especially to Dr. Ronnie L. Phillips, Dr. Ik-Bum Kim, and Psaras in Georgia Institute of Technology for such a successful and productive collaboration regarding to the fluorescent conjugated polymes (PPEs) used in this project. I would also like to thanks to Prof. D. Joseph Jerry from the department of veterinary and animal science at UMass-Amherst, for such a great collaboration regarding to the mammalian cells including the cancerous cells. I want to thanks to Prof. Richard W. Vachet for a successful collaboration using his expertise in analytical chemistry and co-advice two members of our group (Jiang and Bo).

I thank my past and present group members in Rotello's group for their friendship and wonderful collaboration throughout my PhD years. I specifically like to thank Dr. Chang-Cheng You for all of his helpful advice, training, collaboration, friendship and his great support at my early stage of Ph.D program and Dr. Avinash Bajaj also for helpful advice, training, collaboration, and friendship at my last stage of my PhD carrier. My warm thanks to Belma, Tommy, Pops, Yuval, Rochelle, Mrinmoy, Partha, Bappa, Basar, Deb, Appiwat, Sarit, Myoung, Jiang, Xi Y., Handan, Subinoy, Chandra, Bo, Xiao-Chao, Xiaoning, Brian C., Youngdo, David S., Krish, Yi-Cheun, Archana, David, Joe Y., and Daniel for their teamwork. I want also to thank Carol Greene, for her inconditional help to the Rotello group and also for her friendship. You know, working in the rotello group is stressful enough, but having good people around you to vent frustrations to about the latest rejection of failed experiment has made coming into everyday much more enjoyable.

I would like to thank to the the UMass-Amherst Department of Chemistry faculty and staff for all their technical and financial support in the Chemistry Graduate Program over the past five years. I would specially like to thanks to Kathy Tobiassen and J. M. Stowe (jms) for their direction in my first and last years of my PhD. I do not know how anyone gets any thing done without their help. I would also like to thank to the Office of Graduate School, College of Natural Sciences at University of Massachusetts for all its technical support during my graduate studies.

I am truly grateful to have met all my friends, especially to Ricardo Jose Alvarado-Noguera, Father Ricardo Apicci, Stephen MacWilliams, Louise/Aideen/Mercy O'Malley, Roger and Dorothy Bins, Arthur and Mary O'Neill, Temer S. Ahmadi, Marta Jimenez and family, Arthur and Mary O'Neill, Chang Cheng, Avinash, Deb, Vannesa, Andrea,

Ron, Phey, Partha, Gan, Rochelle, Brian J., Brian C., Mrinmoy, Brad, Gokhan, Bappa, Sarit, David S., Krish, Abby, Siriporn (A), Carol G., Kay, Jiang, Bo, Rui, Subinoy, Xi Y., Yi-Cheun, Xiaoning, Malar, Chandra, Nitai, Daniel, Elih, Witold, Kristen H., Shanon, Kevin, Dipankar, Xiaochao, Chaekyu, Amherstpals, Facebook friends……I would like to write the names of each one of you guys but the list is too big, my more sincere apology to this issue. However, I want to say to all of you thanks for your support, advice and friendship. You were always with me in fun as well as difficult times.

Finally I want to thank to my parents in Nicaragua: Oscar and Raquel, my sisters: Maria and Magdalena and my brothers: Juan, Walter, Freddy, Lester and Ridder and all new members of my family for all their unrelenting love, patience, inspiration, motivation, strength, and constant support they always gave me in my difficult moments. I am truly grateful for all their gifts and teaching in my life. I have been blessed with such a wonderful family and they have definitely played an integral role in my success. Thanks to GOD for all his blessing.

ABSTRACT

ENGINEERING NANOPARTICLES SURFACE FOR BIOSENSING:
"CHEMICAL NOSES' TO DETECT AND IDENTIFY PROTEINS,
BACTERIA AND CANCEROUS CELLS

FEBRUARY 2011

OSCAR R. MIRANDA, B.E., NATIONAL UNIVERSITY OF ENGINEERING

MBA (POST-GRADUATE), CENTRAL AMERICAN UNIVERSITY

M.Sc., VILLANOVA UNIVERSITY, PENNSYLVANIA

Ph.D., UNIVERSITY OF MASSACHUSETTS-AMHERST

Directed by: Professor Vincent M. Rotello

Rapid and sensitive detection of biomolecules is an important issue in nanomedicine. Many disorders are manifested by changes in protein levels of serum and other biofluids. Rapid and effective differentiation between normal and cancerous cells is an important challenge for the diagnosis and treatment of tumor. Likewise, rapid and effective identification of pathogens is a key target in both biomedical and environmental monitoring. Most biological recognition processes occur via specific interactions. Gold nanoparticles (**AuNP**s) feature sizes commensurate with biomacromolecules, coupled with useful physical and optical properties. A key issue in the use of nanomaterials is controlling the interfacial interactions of these complex systems. Modulation of these physicochemical properties can be readily achieved by engineering nanoparticles surface. Inspired by the idea of mimicking nature, a convenient, precise and rapid method for sensing proteins, cancerous cells and bacteria has been developed by overtaking the superb performance of biological olfactory systems in odor detection, identification, tracking, and location. On the fundamental side, an array-based/'chemical nose' sensor composed of cationic functionalized **AuNP**s as receptors and anionic fluorescent conjugated polymers or green fluorescent proteins or enzyme/substrates as transducers that can properly detect and identify proteins, bacteria, and cancerous cells has been successfully fabricated.

TABLE OF CONTENTS

Page

LIST OF TABLES

Table Page

LIST OF FIGURES

Figure Page

LIST OF SCHEMES

Scheme Page

CHAPTER 1

INTRODUCTION

The detection and quantification of cells, proteins, and other biosystems in complex matrices is important for disease detection. There are wide varieties of methods available to approach this goal, including antibodies used in ELISA-type tests, proteomics and related approaches coupled with mass spectrometry, as well as widely employed techniques such as gel electrophoresis to detect serum imbalances in patients with liver failure or other gross metabolic problems.[1] For the detection of microorganisms, plating and culturing as well as PCR are standard; viral infections are generally detected by ELISA type tests, or in the case of early detection of HIV also by PCR.[2] Other methods for the detection of microorganisms, including electrochemical assays, have been suggested.[3] However, the field is open when it comes to simple and rapid assays that indicate the presence of an analyte by color or fluorescence change; in such a case one "strip" might even contain a small library of indicators, the combined responses of which would indicate the presence or absence of specific analytes. The combination of selective instead of specific sensors or indicators into a sensor array generates a chemical nose or tongue, in which the combined response of the library of these sensors identifies analytes or disease states.

This dissertation will focus on array-based sensing using gold nanoparticles (**AuNP**s) and fluorescent conjugated polymer or green fluorescent proteins or enzyme/substrate complexes as 'chemical noses' to detect and identify protein, bacteria and cancerous cell. The read-out of these systems is based on optical methods i.e fluorescence or UV-vis spectroscopy.

1.1 Nanoparticles Surfaces: An Excellent Scaffold for Biological Applications

Nanobiotechnology has emerged as a new exciting field in recent years with much promise.[4] The use of nanomaterials in nanomedicine merges the interfaces among the fields of material science, chemistry and biology. Gold nanoparticles (**AuNP**s) used as receptors, offer a useful platform for biomolecular surface recognition, providing unique properties with potentially wide-ranging therapeutic applications.[5] The utility of **AuNPs** arises from a variety of desirable structural attributes, including the similar size of nanoparticles and biomolecules such as proteins and polynucleic acids (Figure 1.1).[6] The size of the asotropic **NP**s core can be tuned from 1.5 to more than 10 nm which can provides a suitable platform for the interaction of **AuNP**s with protein and other biomolecule surfaces

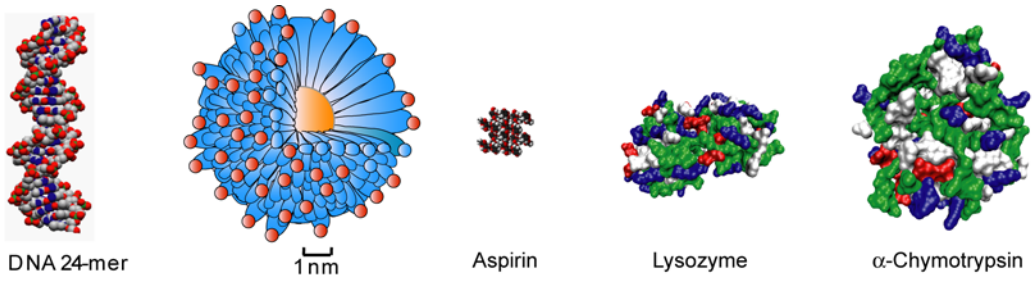

Figure 1.1 Schematic representation of a 2 nm core gold nanoparticle with 11-mercaptoundecanoic acids monolayer and relative sizes of aspirin crystal (small molecule), lysozyme and α-chymotrypsin (proteins), and a 24-mer DNA duplex (Reproduced from Ref. 6).

Nanoparticles can be fabricated with a wide range of surface functionality providing a versatile system for creation of surface-specific receptors and can be fashioned with a wide range of metal and semiconductor core materials that impart useful properties such as fluorescence and magnetic behavior.[7] The applicable properties of some well known core materials and corresponding possible ligands used for surface functionalization with

their possible applications are summarized in Table 1.1. From Table 1.1, 3 metallic and 2 non-metallic nanoparticles (i.e. Au, Ag etc.) are become more popular for molecular recognition, delivery and sensing where as semiconductor and magnetic nanoparticles are drawing interest as imaging agents.[8]

Table 1.1: Characteristics, ligands and representative applications for various metal and semiconductor materials (Reproduced from Ref. 8).

Core material	Characteristics	Ligand	Applications
Au	Optical absorption, fluorescence and fluorescence quenching, stability	Thiol, disulfide, phosphine, amine	Biomolecular recognition, delivery, *sensing*
Ag	Surface-enhanced fluorescence	Thiol	*Sensing*
Pt	Catalytic property	Thiol, phosphine, amine, isocyanide	Bio-catalyst, *sensing*
CdSe	Luminescence, photo-stability	Thiol, phosphine, pyridine	Imaging, *sensing*
Fe_2O_3	Magnetic property	Diol, dopamine derivative, amine	MR imaging and biomolecule purification, *sensing*
SiO_2	Biocompatibility	Alkoxysilane	Biocompatible by surface coating,

Finally, the self-template nature of this system to guest molecules is allowing an increase in the affinity and selectivity upon incubation with the guest molecules. Applying these characteristic to the selective recognition of biomacromolecules, however, requires suitable surface functionality which can be solved by using reported synthetic methods. [9] There are several examples on nanoparticle-biomolecule interactions have been reported based on various biological and diagnostic applications.[8] Nanoparticles can be made-up with a diverse array of metal, alloy, oxide and semiconductor materials, using standard reported procedure available in literatures which already mention before (Table 1.1). As

an example Brust and coworkers have developed a widely used particle preparation procedure for metallic nanoparticles by the reduction of metal salt in the presence surfactant and coating ligands (Figure 1.2).[10] This synthetic approach, known as Brust-Schiffrin method, involves the transfer of hydrogen tetrachloroaurate from aqueous phase to toluene phase by using surfactant TOAB and the subsequent reduction by sodium borohydride in the presence of alkanethiols to generate nanoparticles that are soluble in organic solvents. This reaction leads to the relatively monodisperse **AuNP**s protected by thiol ligands with diameters ranging from 1.5 to 5 nm. The alkanethiols generally possess a footprint of ca. 0.2 nm^2, while sterically bulky thiol ligands require much larger footprints for encapsulation on gold surfaces. The nanoparticle size might be readily controlled by varying the reaction conditions including gold-to-thiol ratio, reduction rate and reaction temperature, etc.[11] Thiol-protected **AuNP**s possess superior stability due to the synergic effect of strong thiol-gold interactions and van der Waals attractions of neighboring ligands. The nanoparticles of this kind can then be thoroughly dried and redispersed in solution without any aggregation. Single-phasic reduction of gold salts by sodium borohydride in the presence of thiols has also been developed,[12] through which water-soluble **AuNP**s could be prepared in a single step. In the biphasic reduction protocol, the absence of thiol ligands can lead to slightly larger nanoparticles stabilized by quaternary ammonium, which show considerable stability in solution and serve as excellent precursors for other functionalized nanoparticles.[13]

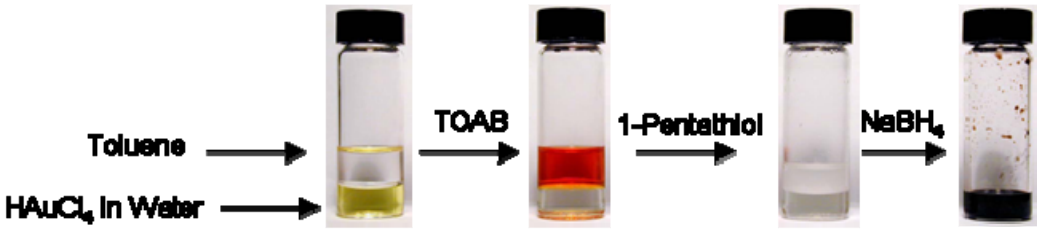

Figure 1.2. Synthesis of metal core gold nanoparticles through Brust-Schiffrin reduction. This synthesis involves transfer of hydrogen tetrachloroaurate from aqueous phase to toluene phase by using surfactant TOAB and the subsequent reduction by sodium borohydride in the presence of alkanethiols to generate nanoparticles that are soluble in organic solvents. The diameters of this asotropic gold nanoparticles ranging from 1.5 to 5 nm.

Using this method various metallic nanoparticles (such as Ag, Pt, Pd, Cu etc.) have been prepared. In this protocol the size of the particle can be controlled by varying the metal-ligand ratio and reaction conditions. For efficient biological applications, the most important requirements of the nanoparticle are surface functionality and water-solubility.

To introduce the surface functionality, the most acceptable method is the Murray's place-exchange process (Figure 1.3a),[14] where the initial ligands on the nanoparticle surface are replaced by external ligands of similar functionality as an instance, thiol or disulfide ligands for gold and silver particle. The other well known method is direct synthesis of metallic nanoparticles in presence of corresponding ligand to generate monolayer-protected clusters (**MPC**s) and mixed monolayer-protected clusters (**MMPC**s). According to the necessity further functionality can be introduced through conventional organic protocols.[15] Recently, another kind of watersoluble functionalized nanoparticles were reported by the incorporation of hydrophobic nanoparticles into the hydrophobic interiors of surfactant micelles.[16,17] To improve the biocompatibility oligo(ethylene glycol) (OEG) and poly(ethylene glycol) (PEG) are commonly incorporated into the monolayers.[12] The OEG or PEG are hydrophilic in nature to improve the water solubility with the added benefit these ligand resist the nonspecific interactions with biomolecules.

Therefore the slandered nanoparticle for controlled biomolecular interactions consists of hydrophobic interior, an OEG or PEG layer, and recognition elements on the surface (Figure 1.3b).

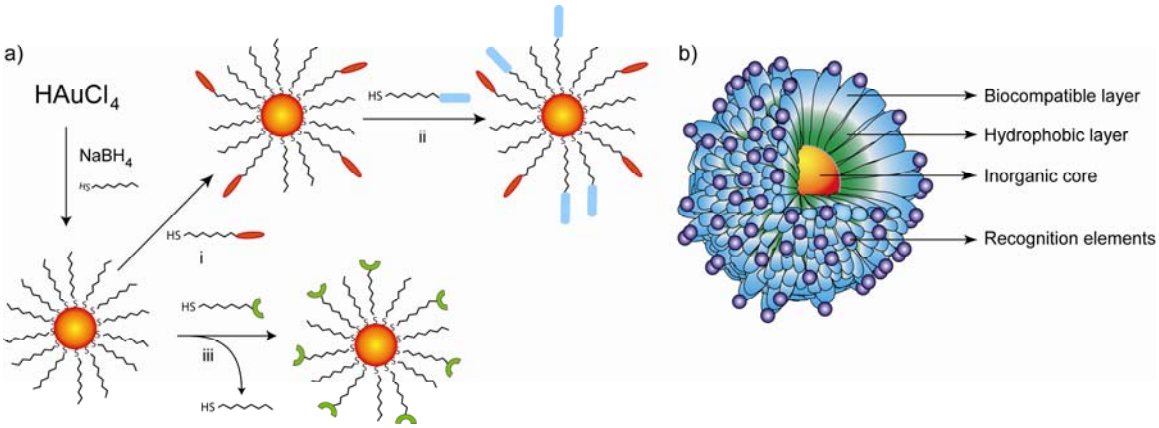

Figure 1.3 a) Construction of nanoparticles through Brust reduction and subsequent modification such as Murray place-exchange reaction (i), (ii) and encapsulation of hydrophobic MPCs into surfactant micelles (iii). b) Multifunctional particle monolayers featuring a hydrophobic core for stability, OEG or PEG layer for biocompatibility, and recognition elements on the surface for interaction with biomolecules (Reproduced from Ref. 14).

1.2 Physical Properties of Gold Nanoparticles

AuNPs possess unique optical, magnetic and electronic properties that are vitally related to their size and shape. Solutions of spherical **AuNP**s exhibit colors ranging from dark brown to burgundy red to red violet with the core size increase (from 1 to 100 nm). UV/vis investigation reveals that **AuNP**s generally show an intensive absorption peak from 500 to 550 nm.[18] This absorption band is usually referred to as "surface plasmon band", which arises from the collective oscillation of the conduction electrons due to the resonant excitation by the incident photons (Figure 1.4). This surface plasmon band is absent in both small nanoparticles (d < 2 nm) and bulk materials. Mie theoretically interpreted the surface plasmon resonance (SPR) phenomena in 1908[19] and his theory has been extensively correlated with the experimental results.[20,21] The SPR is sensitive not

only to nanoparticle size, but also to the surrounding environment such as ligand, solvent and temperature. Particularly, the SPR frequency is dependent on the proximity to other nanoparticles. Thus, under nanoparticle aggregation the surface plasmon band shows significant red-shifting (to ca. 650 nm) and broadening and the solution displays red-to-blue color change due to the interparticle plasmon coupling.[22] This phenomenon constitutes the cornerstone for their application in colorimetric sensing, which will be discussed in detail in the following sections.

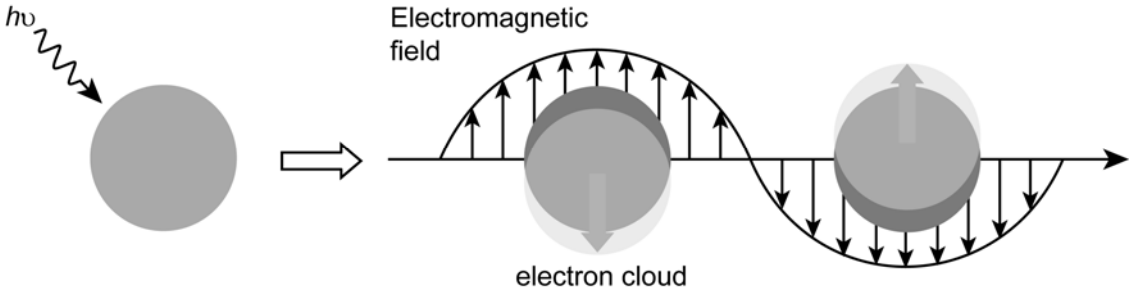

Figure 1.4 Schematic representation of the oscillation of conduction electrons across the nanoparticle in the electromagnetic field of the incident light (Reproduced from Ref(s). 22 and 23).

For the application of **AuNP**s in solution, it is not a trivial task to determine their concentrations. As the molar extinction coefficient of colloid gold (520 nm) is around 4000 M^{-1} cm^{-1} per gold atom,[23] the nanoparticle concentration can then be roughly estimated based on the number of gold atoms. The extinction coefficients of **AuNP**s with different sizes and capping ligands have also been measured experimentally.[24] A linear relationship is observed between logarithms of molar extinction coefficient (ε) and core diameter (d), essentially irrespective of the ligands and solvents:

$$\ln \varepsilon = k \ln d + c \qquad (1.1)$$

where k = 3.32 and c = 10.8 (λ = 506 nm). Therefore, the nanoparticle concentrations can be readily deduced from Beer-Lambert Law once the nanoparticle size is known (from TEM). According to equation (1.1), it is estimated that the **AuNP** of 20 nm diameter has a molar extinction coefficient of 1×10^9 M^{-1} cm^{-1}. This value is at least three orders higher than that of common organic dyes (10^4-10^6 M^{-1} cm^{-1}), indicating that AuNPs may serve as excellent light collectors.[25]

AuNPs show photoluminescence under certain conditions[26],[27] and they can also enhance fluorescence at appropriate fluorophore-to-metal distances on solid substrates.[28] Nevertheless, much attention has been focused on the superb quenching ability of **AuNP**s to the proximal fluorescent molecules. Fluorescence resonance energy transfer (FRET) is an important deactivation pathway for the excited fluorophores on the nanoparticle surfaces in case of a good overlap between the donor's emission spectrum and the gold surface plasmon band.[29] The energy transfer efficiency is correlated not only with the spectral overlap, donor-acceptor distance and mutual orientation as those existing in the conventional FRET systems, but also with the size and shape of the **AuNP**s used.[30] Both radiative and nonradiative decay rates of fluorescent molecules are distinctly affected, so that highly efficient fluorescence quenching is observed even in the presence of small nanoparticles of 1 nm diameter. Photoinduced electron transfer (PET) makes great contribution to the deactivation of the fluorophores in the vicinity of **AuNP**s, where the nanoparticles act as electron acceptors.[31] The electron transfer process can be modulated by charging/discharging the gold core, providing an interesting opportunity for sensor fabrication.[32]

In contrast to bulk metals, a band gap exists between the valence and the conduction bands of metal nanoparticles. Small metal nanoparticles would therefore display size-dependent quantization effects, leading to the discrete electron-transition energy levels. For example, 15 redox states have been observed for hexanethiol-capped **AuNP**s (Au_{147}, r = 0.81 nm) at room temperature due to the quantized double layer charging.[33] This result explicitly indicates that molecular-protected **AuNP**s are multivalent redox species which display molecule-like redox properties.[34] The quantized capacitance charging behavior of **AuNP**s is distinctly affected by electrolyte ions, external ligands, and magnetic field applied. Such unique electrochemical properties expand their practical interests of applications in electronic devices and electrochemical labels.[35] Furthermore, the conductivity of **AuNP** assemblies relies on the interparticle space as well as the chemical environment, providing another important handle over tailoring electronic and electrochemical sensors.

1.3 Nanoparticle-Biomolecule Surface Interactions

Creation of nanoparticle-based artificial receptors for biomacromolecular surface recognition provides a potential tool for controlling cellular and extracellular processes in numerous biological applications such as enzymatic inhibition, transcription regulation, delivery and sensing.

The conjugation of nanoparticles with biomolecules, such as proteins and DNA, can be done using two different approaches: direct covalent linkage and non-covalent interactions.[36,37,38,39,40] The most direct approach involves covalent attachment.[41] This conjugation can be achieved through either chemisorption of the biomolecule to the

particle surface or through the use of heterobifunctional linkers. Chemisorption of proteins onto the surface of nanoparticles (usually containing a core of Au, ZnS, CdS and CdSe/ZnS) can be done through cysteine residues that are present on the protein surface (e.g. oligopeptide, serum albumin),[42] or chemically using 2-iminothiolane (Traut's reagent).[43,44] Bifunctional linkers provide a more versatile means of bioconjugation. Biomolecules are often covalently linked to ligands on the **NP** surface via traditional coupling strategies such as carbodiimide-mediated amidation and esterfication.[45] For biological applications, OEG or PEG is used in the linker to enhance the stability of the attached biomolecules and minimize non-specific adsorption of other materials.

Non-covalent assembly provides a highly modular approach to the biofunctionalization of nanoparticles. The use of cationic ligands on the nanoparticle surface provides a complementary surface for binding the negatively charged backbone of DNA, for example the use of **NP1** to bind to a 37-mer DNA duplex (Figure 1.5a).[46] Another approach to DNA conjugation exploits the high affinity and specificity of base-paring between DNA strands (Figure 1.5b).[47] It has been reported that cationic tetra-alkyl ammonium functionalized **AuNP**s recognize the surface of an anionic protein through complementary electrostatic interaction and inhibit its activity. The activity was recovered due to release of free protein by treating the protein–particle complex with GSH, showing **AuNP**s as potential protein transporters (Figure 1.5c).[48] In another approach has been demonstrated that cationic gold mixed monolayer protected clusters (**MMPC**s) with ~2 nm core diameter were used to induce folding of negatively charged peptide (tetraaspartate peptide, **TAP**) into an α-helix conformation (Figure 1.5d).[49]

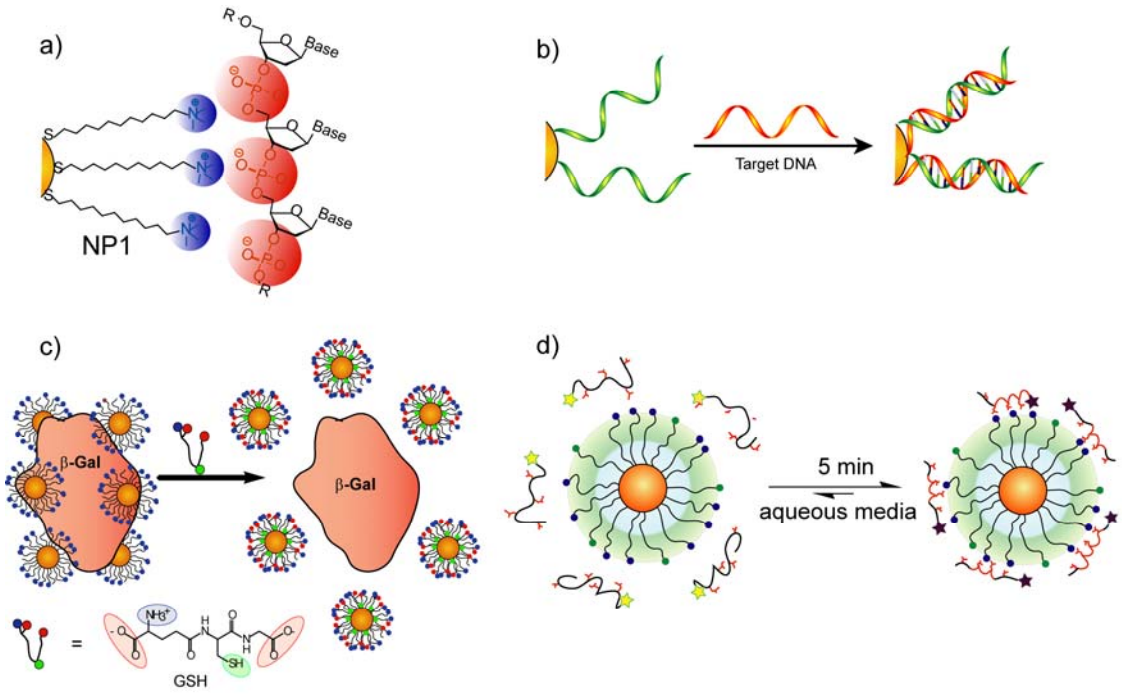

Figure 1.5 The DNA-nanoparticle interactions. (a) Structure of **NP1** scaffold and the DNA backbone. The interaction is directed by electrostatic interaction. b) Binding of DNA thtough complementay oligonucleotide hybridization. c) **AuNPs** interact with the surface of an anionic protein through complementary electrostatic interaction and inhibit its activity. d) Schematic depiction of the peptide binding in helical conformation on MMPCs surface (Reproduced from Ref(s). 47-50).

1.4. Poly(*para*phenyleneethynylene)s (PPEs): A Multivalent Water Soluble Conjugate Polymer as a Tranducer

Water soluble poly(*para*phenyleneethynlene)s conjugated polymers (**PPE**s) have received much attention and have shown great promise as highly sensitive fluorescent sensory materials for chemical analytes and biomolecules. The multivalent capabilities and sensitivity of conjugated polymers to minor conformational or environmental changes make them ideal candidates for biosensing applications. The electrochemical and optoelectronic properties of π-conjugated polymers can be modified by environmental stimuli to detect chemical or bioactive species. Water-soluble **PPE**s are accessible by introducing ionic side groups to solubilize the otherwise hydrophobic polymer

backbones. These polymers can have high fluorescence quantum yields in aqueous solution, unique solution behavior, ability to interact electrostatically with other charged species, and display an extraordinarily high sensitivity to fluorescence quenchers (picomolar level) because of the "molecular wire effect".[50] Ionic groups such as carboxylic, sulfonic, ammonium or phosphonate have been grafted on the side chains of these conjugated polymers as well as neutral groups such as sugars[51] and highly branched hydroxyls.[52] A number of useful sensor applications for ions, peptides and proteins, bacteria and nucleic acids have been reported using such polymers.[53]

Compared to quenching of the corresponding monomers, only one recognition element binding to a quencher is enough to shut down the fluorescence of a whole polymer chain, creating strong signal amplification. This "amplified quenching" or "superquenching" process of the **PPE** fluorescence is caused by either electron or energy transfer and is useful to transmit information and monitor binding events either directly or by displacement assays through removal of the pre-bound quencher and turning on the fluorescence of a conjugated polymer. Many groups have utilized the intrinsic fluorescence signal amplification properties of **PPE**s, and developed sensitive assays for biologically relevant targets including proteins, DNA, glycopeptides and carbohydrates. Fluorescent "superquenching" of **PPE**s by oppositely charged analytes was discovered in 1998 by Whitten *et al.*[54] and opened a new door to specific sensing applications by **PPE**s.[55] They are used in direct or competitive assay technology for high-throughput screening of protease enzyme activity,[56] nucleic acid hybridization[57] and kinase[58] and phosphatase activities by metal ion mediation.[59] Ionic **PPE**s were employed to detect conformational changes of biomolecules (Figure 1.6)[60] or negatively charged nucleic

acids,[61] differentiate ssDNA from dsDNA,[62] and recognize the DNA's tertiary structure. In the case of the detection of conformational change of biomolecule, a negatively charged conjugated polyelectrolyte (poly(thiophene acetic acid), PTAA-Li) when interaction with native bovine insuline (nBI) or bovine insuline in amyloid fibrillar (fBI) form a complex, displaying different characteristic optical changes that can be detected visually or by absorption and emission, the absorption maximum is red shifted to 463 nm. This result strongly suggests that binding of PTAA to amyloid fibrils of BI will force the polyelectrolyte backbone to adopt a more rod-shaped conformation. The planarization of the polymer backbone might be a result of the change in the secondary structure of the BI, as the polyelectrolyte will most likely interact differently with the α-helical nBI molecule and the fBI molecule that contains more β-sheet structure. Hence, the alteration of the optical properties from the conjugated polyelectrolyte should be due to a change in the secondary structure of the protein molecule. Interestingly, the shift in absorption for the two different solutions is clearly visible for the human eye. The PTAA/nBI solution is yellow, and the PTAA/fBI solution is orange (Figure 1.6).

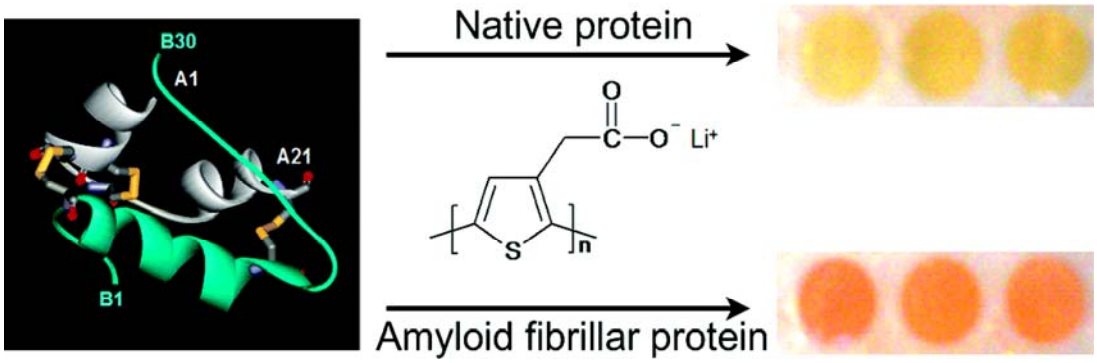

Figure 1.6 Structure of the insulin monomer (right), chemical structure of the repeating unit of poly(thiophene acetic acid) (PTAA-Li) (middle) and the microtiter plate wells (right) containing PTAA/nBI (top) and PTAA/fBI (bottom) (Reproduced from Ref. 61).

PPEs form stable complexes with some proteins. However, even with simple electrostatic interactions, Heeger et al.[63] and Bunz et al.[51c] showed that proteins can be distinguished by their overall charges and electron transfer reactivities. Recently, Swager *et. al*.[51b] showed that *E. coli* can be detected in moderately concentrated cell suspensions by using a water-soluble, carbohydrate functionalized PPEs. Fluorescent cell clusters formed in 10-15 min. through multivalent interactions with mannose receptors located on the bacterial pili of *E. coli* with the mannosylated polymer.[64]

PPEs are typically synthesized according to Heck-Cassar-Sonogashira-Hagihara (HCSH) reaction conditions which employs a palladium catalyzed process to yield moderate to high molecular weight **PPE**s (Scheme 1.1).[65] This method is advantageous due to its tolerance of monomer functionality, variability of reaction conditions, and simplicity of reaction workup.

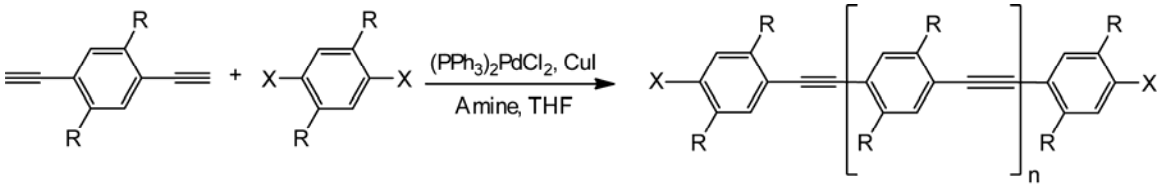

Scheme 1.1 General synthetic scheme for **PPE**s under HCSH reaction conditions (Reproduced from Ref. 67).

Due to the ease of synthesis, **PPE**s can be synthesized in large quantities with high purities. Typically, the **PPE**s are a yellow-orange solid and exhibit a blue-green fluorescence ($\lambda_{emission}$ = 455-465 nm). With the incorporation of heterocyclic monomers such as benzothiadiazole, **PPE**s with a yellow-orange emission ($\lambda_{emission}$ = 500-550 nm) can be easily achieved.

1.5. Nanoparticles in Biosensing

Sensors are a class of devices that produce measurable responses to changes in physical conditions or chemical concentration.[66] Biosensors, first reported in 1962,[67] are generally defined as sensors that consists of two components: 1) biological recognition element for target binding, often called bioreceptors, 2) transduction element for signaling the binding event that produces a signal proportional to the analyte concentration. The large surface to-volume ratio with the electronic and optical properties makes the nanoparticles as a potential system in sensor application. Nanoparticles are applied in the detection of various biomolecules such as, oligonucleotides, proteins, microorganisms and mammalian cells. Based on the regulating properties such as absorbance, quenching, conductivity etc. the nanoparticle based biological sensing can be sub-categorized in several group, such as, 1) colorimetric sensing,[68] 2) fluorescence sensing[69] 3) electrochemical sensing [70] 4) surface enhanced raman scattering (SERS),[71] etc. Some of the very interesting studies of each group have been highlighted here. In the first group, a colorimetric method of sensing proteins using aptamer and gold nanoparticles functionalized with citrate was used.[68] In this study, the specific recognition of a particular protein is realized through the aptamer structure change which occurs during the binding process. This structural change is then detected by the color change of gold nanoparticles (Figure 1.7). The analyte thrombin and its 29-mer binding aptamer (TBA) were taken as model. Significant color change is visible at as low as 83 nM using this calorimetric aptasensor, with UV-visible spectroscopic measurement used to obtain this detection limit.

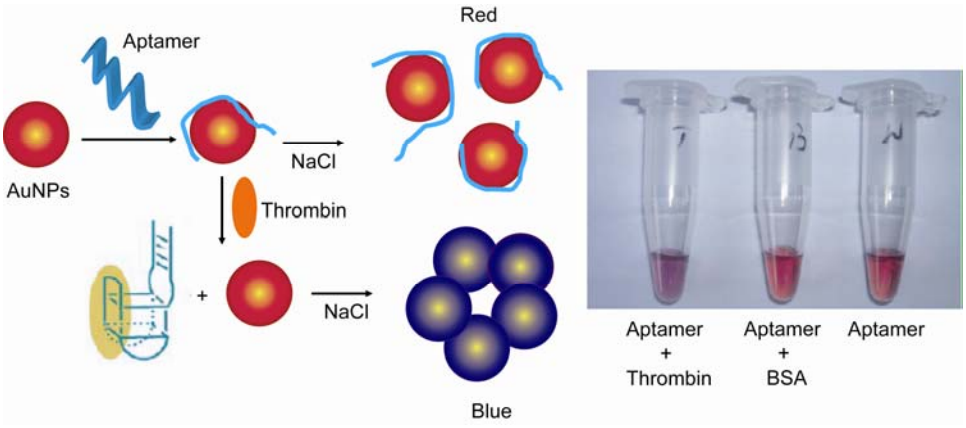

Figure 1.7 AuNPs colometric strategy for thrombin detection**.** By exploiting interactions between **AuNP**s and the DNA sequences, color changes could sensitively differentiate the conformational change of TBA before and after adding thrombin. Photographs of 200 mL 13 nm **AuNP**s stabilized by the aptamer (30 mL 4.59 mM) after the addition of salt (100 mL 0.5 M NaCl) in the presence and absence of target protein (from left to right: 83 nM thrombin, 83 nM BSA and water as control) (Reproduced from Ref. 70).

In the second group, for the develop of a fluorescent biosensor the high quenching ability of gold nanoparticles was used for molecular beacons construction for sensing the DNA strands using the intensity of fluorescence responses.[69] According to the reported design, initially the dye molecule remains close to the nanoparticle surface due to hairpin structure of the attached DNA, resulting in an effective fluorescence quenching through FRET (Figure 1.8). As shown in the hybridization of target DNA opens up the hairpin structure and increase the distance between nanoparticle and dye, results in a significant increase in fluorescence. As the fluorescent intensity was only depends on the concentration of the target DNA, this system was used for DNA sensing. A range of ssDNA and DNA cleavages ware detected using this molecular beacon approach.

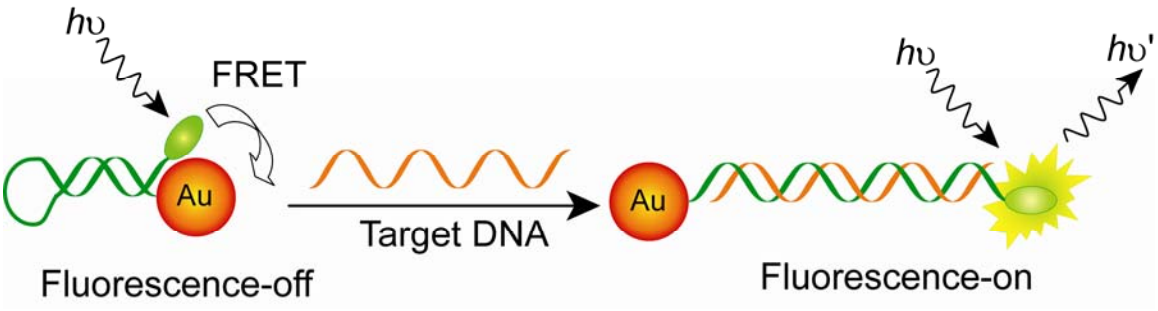

Figure 1.8 Schematic representation of molecular beacon for the detection of target DNA (Reproduced from Ref. 71).

In the third group, a bioelectrocatalytic system was constructed by connecting the redox enzyme glucose oxidase (apo-GOx) onto a gold nanoparticle that was functionalized with N^6-(2-aminoethyl) flavin adenine (FAD) (Figure 1.9).[70] This enzyme-nanoparticle hybrid system was linked to the electrode through dithiols, or alternatively the FAD-functionalized nanoparticle was assembled onto the electrode followed by the addition of apo-GOx. This system exhibited a highly efficient electrical communication with the enhanced turnover rates as compared to native Gox, and provided an effective sensor for glucose in the physiological concentration regime. An analogous electron transfer from protein to nanoparticles was used for monitoring hydrogen evolution from zinc-substituted cytochrome c immobilized TiO_2 nanoparticles as reported by Yeni Astuti *et al.*[72]

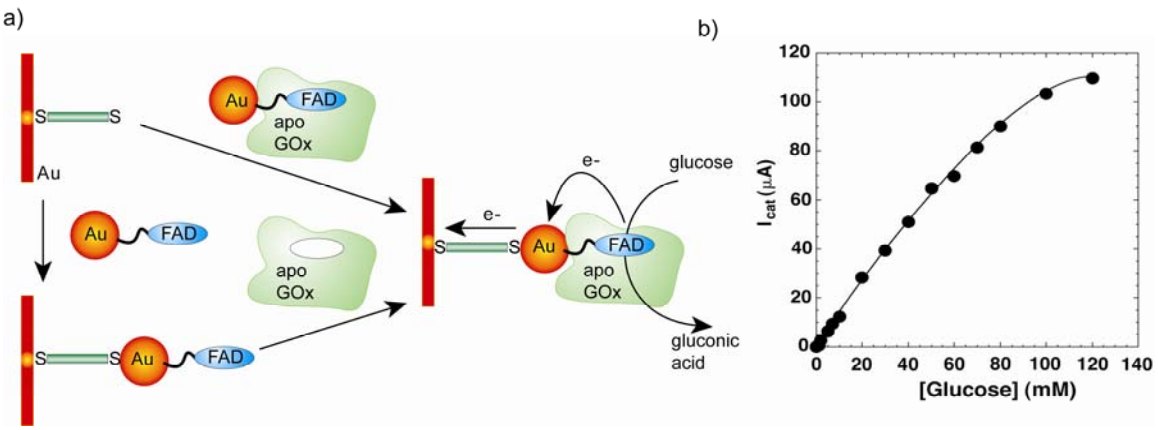

Figure 1.9 a) Fabrication of GOx electrode by the reconstitution of apo-enzyme on a FAD-functionalized gold nanoparticle. b) Plot of the current developed by the reconstituted GOx electrode in the presence of different concentrations of glucose (Reproduced from Ref. 72).

The last group of sensing system, SERS, an ultra-sensitive 'bio-barcode' biosensor for proteins and nucleic acids has been developed by Mirkin's group, where the oligonucleotide is amplified and then detected either by surface hybridization or by PCR amplification, providing a means for detection of both proteins and DNA (Figure 1.10). In case of DNA detection, a magnetic microparticle carrying partially complementary to target DNA was hybridized with bio-barcoded gold nanoparticles in presence of target DNA (Figure 10.a). After the magnetic separation of the sandwich assemblies and thermal dehybridization, the barcode was released for analysis. The detection limit of this method was found at 500 zeptomolar, comparable to many PCR-based approaches. For protein detection the magnetic microparticles carry antibodies that specifically bind the target protein (Figure 10.b). The magnetic microparticle-bound protein subsequently interacts with gold nanoparticles by antigen-antibody interaction. The detection limit for the chip-based sandwich hybridization process was observed at 30 attomolar, which was reduced using PCR amplification to 3 attomolar.[73] This approach is also used for

multiplexed detection of protein and DNAs by using mixture of different biobarcoded gold nanoparticle probes. [74]

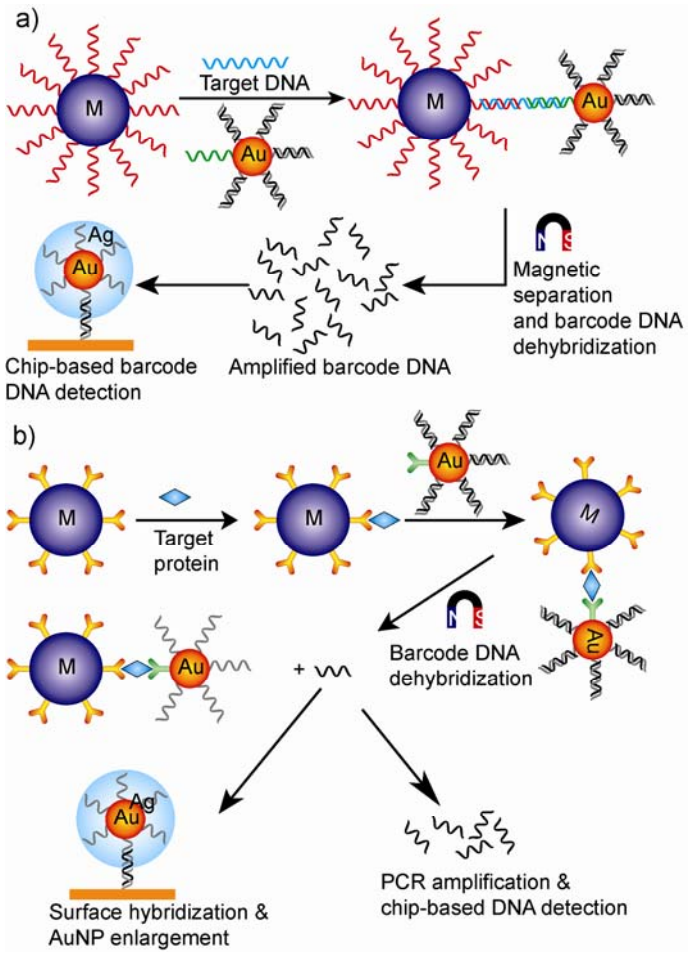

Figure 1.10 Schematic illustration of 'bio-barcode' assays for a) DNA and b) proteins (Reproduced from Ref. 73).

1.6 Chemical Tongue/Nose Sensors

Most biomolecular recognition processes in biology occur via specific interactions. Sensory processes such as taste and smell, however, use "differential" binding where the receptors bind to their analytes by different binding characteristics that are selective rather then specific.[75] These arrays, a.k.a. "electronic tongues"[76] provide highly versatile sensors (Figure 1.11). They have been used to sense calcium and metal ions, pH levels,

sugars as well as cholesterol levels in blood, cocaine in urine, and toxins in water.[77] A variety of other analytes such as including metal ions,[78] volatile agents,[79] aromatic amines,[80] amino acids,[81,82] and carbohydrates.[83,84] have also been successfully identified using this approach.

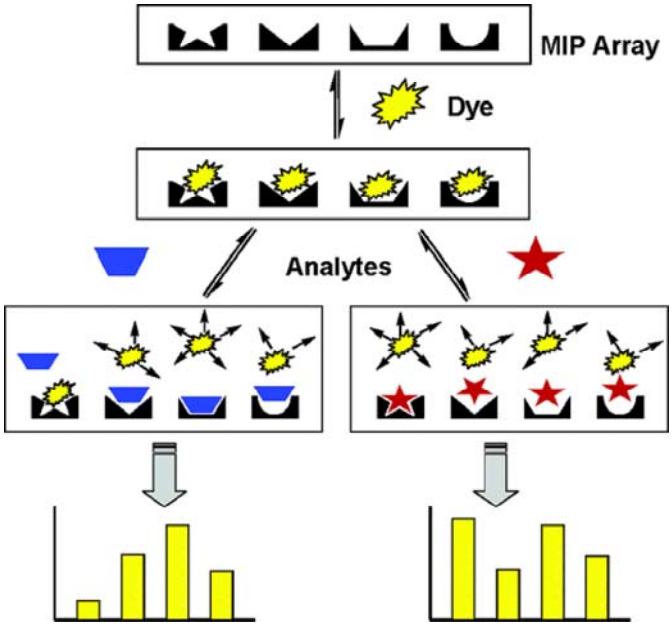

Figure 1.11. A Representative scheme of an molecularly imprinted polymers (MIP) sensor array that uses a dye-displacement strategy to give an easily visualized and unique colorimetric response pattern for each analyte (Reproduced from Ref. 82).

1.7 Protein Sensing using Chemical Noses

The emergence of abnormal proteins and/or irregular protein concentrations are indicative of cancers and diseases.[85,86] Therefore, sensitive, convenient, and precise protein sensing methods are required to obtain early diagnosis of diseases and successful treatment of patients. Currently, the most extensively used detection method for proteins is enzyme-linked immunosorbent array (ELISA).[87] In this system, the capture antibodies immobilized onto surfaces bind the antigen through a "lock-key" approach and another enzyme-coupled antibody is combined to react with chromogenic or fluorogenic substrates to generate detectable signals. Despite of the high sensitivity, the application of

this method is restricted due to its high production cost, instability, and challenges for quantification. On the other hand, synthetic agents with high affinity and specificity for proteins are scarcely available although they possess better chemical and thermal stability.

Recently, the "chemical nose/tongue" approach has been applied to protein sensing. Hamilton's group has used eight tetra-*meso*-carboxylphenyl-porphyrins carrying peripheral amino acid functionalities to identify four metal and nonmetal-containing proteins, with a detection limit between 7.5 ~ 15 μM (Figure 1.12a).[88,89] Anslyn et al. have employed 29 boronic acid-containing oligopeptide functionalized resin beads to differentiate 5 proteins and glycoproteins through an indicator-uptake colorimetric analysis, with a limit of detection of 355 μM (Figure 1.12b).[90]

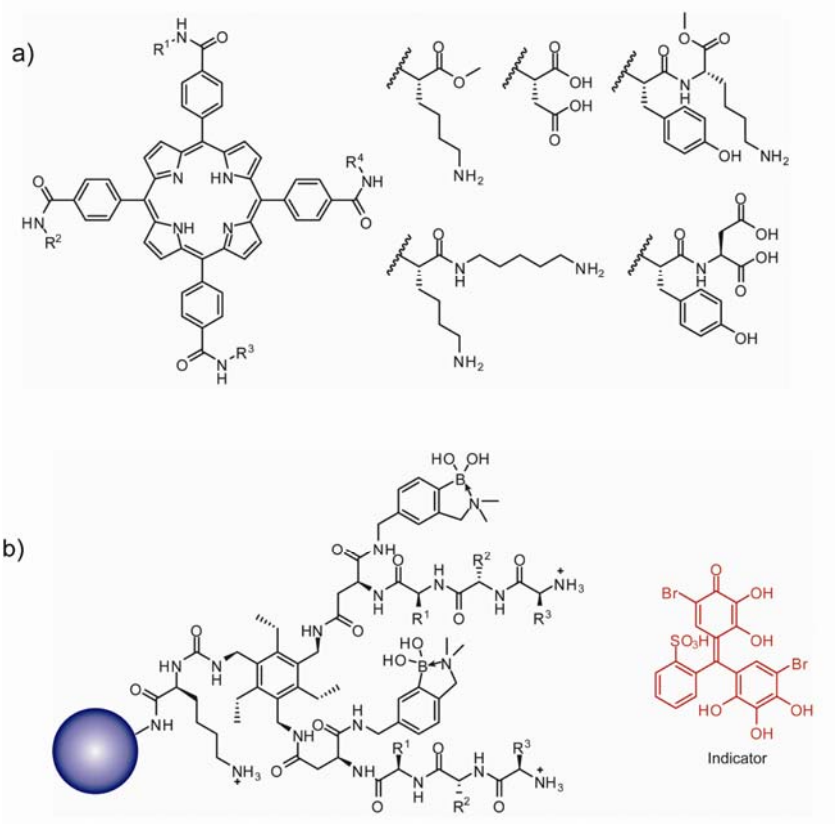

Figure 1.12 a) A library of tetra-meso-carboxylphenylporphyrin (TCPPs) conjugated with amino acids or amino acid derivatives used for protein sensing by Hamilton's group. b) Structure of receptors which incorporates one of 19 natural amino acids at each of three sites that are biased towards particular analyte classes. Bromopyrogallol red is used for the indicator-uptake colorimetric analysis (Reproduced from Ref(s). 90-92).

It has more recently been shown that non-selective electrostatic interaction in combination with covalently or non-covalently bound fluorophores are sufficient to differentiate between a number of biological relevant metalloproteins. Thayumanavan et al. exploited eight different fluorescence dye molecules non-covalently bound to the micellar interiors of an amphiphilic homopolymer to generate a pattern and differentiate four different metalloproteins, with limits of detection between 1-200 μM (Figure 1.12).[91]

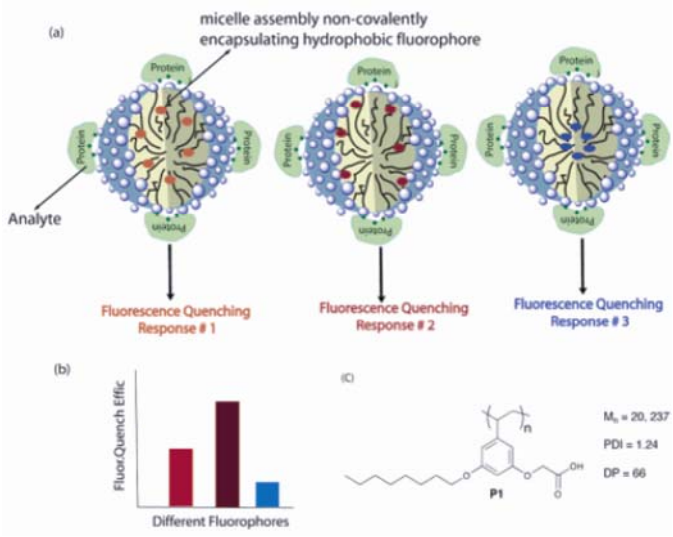

Figure 1.13 a) Schematic of the differential transducer approach using amphiphilic homopolymer micelles. b) Fluorescence quenching response for a hypothetical analyte. c) Structure of polymer P1 (Reproduced from Ref. 93).

1.8 Chemometric Analysis: A Powerful Tool to Discriminate Biomolecules in Chemical Noses Approach

As a consequence of having an array of differentially selective, rather than specific, responses to protein, bacteria, cancerous cells or other analytes, the raw PPE fluorescence responses of the sensor arrays are a matrix of noiselike signals from which we must accurately and quickly extract patterns with which to classify bacteria, cancerous cells or changed protein levels in serum samples. As there is no universally accepted optimal chemometric technique for chemical sensor array processing and pattern recognition, it is invariably necessary to be flexible and pragmatic in the application and evaluation of any such technique thought, *a priori*, to be a suitable starting point. Neural nets have previously been shown to be effective in the processing of fluorescence sensor array data.[92] Subsequently, Shaffer *et al*. performed quantitative comparisons of seven well-regarded chemometric techniques for chemical sensor array pattern recognition.[93] They used speed, training difficulty, memory requirements, robustness to outliers, and ability

to produce an uncertainty measure as qualitative performance measures, classification accuracy as the quantitative measure and concluded that the two neural network techniques they tested, *i.e*., learning vector quantization (LVQ) and probabilistic neural network (PNN), were clearly superior in performance. These measures, and their results, are directly relevant to our proposed work. Subsequent work by Shaffer and Rose-Pehrssen resulted in an improved probabilistic neural network (IPNN)[94] that reduced computational requirements, speeded training and decreased the false alarm rate. Further improvement can be obtained using the IPNN chemometric methodology of Shaffer and Rose-Pehrssen with a complementary filters provided by applying additional analysis techniques.[95]

As described before, there is no universally accepted optimal chemometric technique for chemical sensor array processing and pattern recognition. However, in this dissertation the discrimination of biomolecules was carried out using classical linear discriminant analysis (LDA) using SYSTAT software (version 11).[96] This statistical analysis method is used to recognize the linear combination of features that differentiate two or more classes of objects or events. Stepwise analysis with different sensor set(s) gives certain separatability between all the analytes through jackknifed classification and it is possible to be maximizing it using several analysis combinations to determine which sensor set can best differentiate between the biomolecules. The *Jackknifed classification matrix* is an attempt to approximate cross-validation. The *Jackknifed classification matrix* use functions computed from all of the data except the case being classified.

1.9 Concluding Remarks

To achieve highly efficient sensors, it is crucial to engineering the nanoparticle surface functionality for selective target analytes. **AuNP**s present a versatile scaffold for the creation of biological sensors. On the one hand, the particles provide an adaptable platform for the incorporation of various functionalities ranging from small organic ligands to giant biomacromolecules, allowing the binding of target molecules with appropriate affinity and selectivity. On the other hand, the physical attributes of **AuNP**s such as their environment-sensitive optoelectronic properties can be harnessed to realize the transduction of the binding events. Based on the results presented in this dissertation, it is apparent that nanoparticle-based sensors provide a powerful platform for analysis of proteins and cell surfaces. Through variation of sensor design it would appear that almost any system could be differentiated through appropriate sensor design. As we learn the strategies required for this differentiation, however, we will have to address the complexity of the target systems. Biofluids, such as undiluted human serum, contains a large amount of various proteins, salts, and cells that not only can inhibit or alter the sensing elements' ability to detect target analytes, but also complicate pattern generation. Clearly, creation of clinically useful sensor will require co-evolution of chemical and data analysis strategies.

1.10 References

1. McPherson, R. A.; Pincus, M. R. Henry's Clinical Diagnosis and Management by Laboratory Methods, *21st Edition, Elsevier*, Philadelphia, **2007**.

2. Laure, F.; Rouzioux, C.; Veber, F.; Jacomet, C.; Courgnaud, V.; Blanche, S.; Burgard,M.; Griscelli, C.; Brechot, C. *Lancet* **1988**, 332, 538.

3. Deisingh, A. K.; Thompson, M. *Analyst* **2002**, 127, 567.

4. Peer, D.; Karp, J.; Hong, S.; Farokhzad, O.; Margalit, R.; Langer, R. *Nature Nanotech.* **2007**, *2*, 751.

5. Gao, X.; Cui, Y.; Levenson, R. M.; Chung, L. W. K.; Nie, S. *Nat. Biotechnol.* **2004**, *22*, 969.

6. Verma, A.; Rotello, V. M. *Chem. Commun.* **2005**, 303.

7. Ferrari, M. *Nat. Rev. Cancer* **2005**, *5*, 161.

8. De, M.; Ghosh, P. S.; Rotello, V. M. *Adv. Mater.* **2008**, *20*, 4225.

9. Euliss, L. E.; DuPont, J. A.; Gratton, S.; DeSimone, J. *Chem. Soc. Rev.* **2006,** *35*, 1095.

10. Brust, M.; Walker, M.; Bethell, D.; Schiffrin, D. J.; Whyman, R. *J. Chem. Soc. Chem. Commun.*, **1994**, 801.

11. Hostetler, M. J.; Wingate, J. E.; Zhong, C. -J.; Harris, E.; Vachet, R. W.; Clark, M. R.; Londono, J. D.; Green, S. J.; Stokes, J. J.; Wignall, G. D.; Glish, G. L.; Porter, M. D.; Evans, N. D.; Murray, R. W. *Langmuir* **1998**, 14, 17.

12. Kanaras, A. G.; Kamounah, F. S.; Schaumburg, K.; Kiely, C. J.; Brust, M. *Chem. Commun.* **2002**, 2294.

13. Fink, J.; Kiely, C. J.; Bethell D.; Schiffrin, D. J. *Chem. Mater.* **1998**, 10, 922.

14. Templeton, A. C.; Wuelfing, M. P.; Murray, R. W. *Acc. Chem. Res.* **2000**, *33*, 27.

15. Rothrock, A. R.; Donkers, R. L.; Schoenfisch, M. H. *J. Am. Chem. Soc.* **2005**, *127*, 9362.

16. Fan, H. Y.; Chen, Z.; Brinker, C. J.; Clawson, J.; Alam, T., *J. Am. Chem. Soc.* **2005**, *127*, 13746.

17. Fan, H. Y.; Leve, E. W.; Scullin, C.; Gabaldon, J.; Tallant, D.; Bunge, S.; Boyle, T.; Wilson, M. C.; Brinker, C. J., *Nano Lett.* **2005**, *5*, 645.

18. Jain, P. K.; Lee, K. S.; El-Sayed I. H.; El-Sayed, M. A. *J. Phys. Chem. B* **2006**, 110, 7238.

19. Mie, G. *Ann. Phys.*, **1908**, 25, 377.

20. Kelly, K. L.; Coronado, E.; Zhao, E. L.; Schatz, G. C. *J. Phys. Chem. B* **2003**, 107, 668.

21. El-Sayed, E.; El-Sayed, M A. *Chem. Soc. Rev.*, **2006**, 35, 209.

22. Su, K.-H.; Wei, Q.-H.; Zhang, X.; Mock, J. J.; Smith, D. R.; Schultz, S. *Nano Lett.* **2003**, 3, 1087.

23. Link, S.; Wang, Z. L.; El-Sayed, M. A. *J. Phys. Chem. B* **1999**, 103, 3529.

24. Liu, X.; Atwater, M.; Wang, J.; Huo, Q. *Colloid Surf. B: Biointerfaces* **2006**, 58, 3.

25. Jain, P. K.; El-Sayed, I. H.; El-Sayed, M. A. *Today* **2007**, 2, 18.

26. Zheng, J.; Zhang C.; Dickson, R. M. *Phys. Rev. Lett.*, **2004**, 93, 077402.

27. van Dijk, M. A.; Lippitz M.; Orrit, M. *Acc. Chem. Res.* **2005**, 38, 594.

28. Lakowicz, J. R. *Anal. Biochem.* **2005**, 337, 171.

29. Sapsford, K. E.; Berti, L.; Medintz, I. L. *Angew. Chem. Int. Ed.* **2006**, 45, 4562.

30. Dulkeith, E.; Morteani, A. C.; Niedereichholz, T.; Klar, T. A.; Feldmann, J.; Levi, S. A.; van Veggel, F. C. J. M.; Reinhoudt, D. N.; Möller, M.; Gittins, D. I. *Phys. Rev. Lett.* **2002**, 89, 203002.

31. Thomas, K. G.; Kamat, P. V. *Acc. Chem. Res.* **2003**, 36, 888.

32. Kamat, P. V.; Barazzouk, S.; Hotchandani, S. *Angew. Chem. Int. Ed.* **2002**, 41, 2764.

33. Quinn, B. M.; Liljeroth, P.; Ruiz, V.; Laaksonen, T.; Kontturi, K. *J. Am. Chem. Soc.* 2003, **125**, 6644.

34. Antonello, S.; Holm, A. H.; Instuli, E.; Maran, F. *J. Am. Chem. Soc.* **2007**, 129, 9836.

35. Schmid, G.; Simon, U. *Chem. Commun.* **2005**, 697.

36. Niemeyer, C. M. *Angew. Chem., Int. Ed.* **2001**, *40*, 4128.

37. Sastry, M.; Rao, M.; Ganesh, K. N. *Acc. Chem. Res.* **2002**, *35*, 847.

38. Katz, E.; Willner, I. *Angew. Chem., Int. Ed.* **2004**, *43*, 6042.

39. Pellegrino, T.; Kudera, S.; Liedl, T.; Javier, A. M.; Manna, L.; Parak, W. J. *Small* **2005**, *1*, 48.

40. You, C. C.; De, M.; Rotello, V. M. *Curr. Opin. Chem. Biol.* **2005**, *9*, 639.

41. Caruso, F. *Adv. Matter.* **2001,** *13,* 11.

42. Naka, K.; Itoh, H.; Tampo, Y.; Chujo, Y. *Langmuir* **2003,** *19*, 5546.

43. Ghosh, S. S.; Kao, P. M.; McCue, A.W.; Chappelle, H. L. *Bioconjugate Chem*. **1990**, *1*, 71.

44. Droz, E.; Taborelli, M.; Descouts, P.; Wells, T. N. C.; Werlen, R. C. *J. Vac. Sci. Technol. B* **1996**, *14*, 1422.

45. Wang, J. *Anal. Chim. Acta* **2003**, *500*, 247.

46. McIntosh, C. M.; Esposito, E. A.; Boal, A. K.; Simard, J. M.; Martin, C. T.; Rotello, V. M. *J. Am. Chem. Soc.* **2001**, *123*, 7626.

47. Mirkin, C. A.; Letsinger, R. L.; Mucic, R. C.; Storhoff, J. J. *Nature* **1996**, *382*, 607.

48. Verma, A.; Simard, J.M.; Worrall, J.W.E.; Rotello, V.M. *J. Am. Chem. Soc.* **2004**, 126, 13987.

49. Ghosh, P. S.; Verma, A.; Rotello, V. M. *Chem. Commun.* **2007**, 2796.

50. a) Zhou, Q.; Swager, T. M. *J. Am. Chem. Soc*. **1995**, *117*, 12593-12602. b) Swager, T. M. *Acc. Chem. Res.* **1998**, *31*, 201.

51. a) Erdogan, B.; Wilson, J. N.; Bunz, U. H. F. *Macromolecules* **2002**; *35,* 7863. b) Disney, M. D.; Zheng, J.; Swager, T. M., Seeberger, P. H. *J. Am. Chem. Soc*. **2004**, *126*, 13343. c) Kim, I. B.; Dunkhorst, A.; Bunz, U. H. F. *Langmuir* **2005**, *21*, 7985.

52. Wilson, J. N.; Wang, Y.; Lavigne, J. J.; Bunz, U. H. F. *Chem. Comm*. **2003**, 1626.

53. Thomas, S. W.; Joly, G. D.; Swager, T. M. *Chem. Rev.* **2007,** *107*, 1339.

54. a) Chen, L.; McBranch D. W.; Wang, H. L.; Helgeson, R.; Wudl, F.; Whitten, D. G. *Proc. Natl. Acad. Sci, U. S. A.* **1999**, *96*, 12287. b) Achutyan, K. E.; Bergstedt, T. S.; Jones, R. M.; Chen, L.; Kumaraswamy, S.; Kushon, S. A.; Lu, L.; Ley, K. D.; McBranch, D.; Mukundan, H.; Rininsland, F.; Shi, X.; Xia, W.; Whitten, D. G. *J. Mater. Chem.* **2005**, *15*, 2648.

55. a) Liu, B.; Bazan, G. C. *Proc. Natl. Acad. Sci, U. S. A.* **2005**, *102*, 589. b) Song, X.; Wang, H. L.; Shi, J.; Park, J. W.; Swanson, B. I. *Chem. Mater*. **2002**, *14*, 2342. c) Liu, B.; Bazan, G. C. *Chem. Mater.* **2004**, *16*, 4467. d) Wang, D.; Gong, X.; Heeger, P. S.; Rininsland, F.; Bazan, G. C.; Heeger, A. J. *Proc. Natl. Acad. Sci, U. S. A.* **2002**, *99*, 49.

56. a) Pinto, M. T.; Schanze, K. S. *Proc. Natl. Acad. Sci, U. S. A.* **2004**, *101*, 7505. b) Kumaraswamy, S.; Bergstedt, T.; Shi, X.; Rininsland, F.; Kushon, S. A.; Xia, W.; Ley, K. D.; Achyuthan, K.; McBranch, D.; Whitten, D. *Proc. Natl. Acad. Sci, U. S. A.* **2004**, *101*, 7511. c) Wosnick, J. H.; Mello, C. M.; Swager, T. M. *J. Am. Chem. Soc*. **2005**, *127*, 3400.

57. a) Kushon, S. A.; Ley, K. D.; Bradford, K.; Jones, R. M.; McBranch, D.; Whitten, D. *Langmuir* **2002**, *18*, 7246. b) Gaylord, B. S.; Heeger, A. J.; Bazan, G. C. *J. Am. Chem. Soc*. **2003**, *125*, 896.

58. Rininsland, F.; Stankewicz, C.; Weatherford, W.; McBranch, D. *BMC Biotech*. **2005**, *5*, 1.

59. Rininsland, F.; Xia, W.; Whittenburg, S.; Shi, X.; Stankewicz, C.; Achyuthan, K.; McBranch, D.; Whitten, D. *Proc. Natl. Acad. Sci, U. S. A.* **2004**, *101*, 15295.

60. a) Nilsson, K. P.; Inganas, O. *Macromolecules*, **2004**, *37*, 9109-9113. b) Nilsson, K. P.; Herland, A.; Hammarstrom, P.; Inganas, O. *Biochemistry* **2005**, *44*, 3718.

61. Gaylord, B. S.; Heeger, A. J.; Bazan, G. C. *Proc. Natl. Acad. Sci, U. S. A.* **2002**, *99*, 10954.

62. a) Wang, S.; Liu, B.; Gaylord, B. S.; Bazan, G. C. *Adv. Func. Mat*. **2003**, *13*, 463. b) Bera-Aberam, M.; Ho, H. A.; Leclerc, M. *Tetrahedron* **2004**, *60*, 11169. c) Dore, K.; Dubus, S.; Ho, H. A.; Levesque, I.; Brunette, M.; Corbeil, G.; Boissinot, M. ; Boivin, G. ; Bergeron, M. G. ; Boudreau, D.; Leclerc, M. *J. Am. Chem. Soc*. **2004**, *126*, 4240.

63. Fan, C.; Plaxco, K. W.; Heeger, A. J. *J. Am. Chem. Soc*. **2002**, *124*, 5642.

64. a) Mammen, M.; Choi, S. K.; Whitesides, G. M. *Angew. Chem. Int. Ed*. **1998**, *37*, 2755. b) Kiessling, L. L.; Pohl N. L. *Chemistry & Biology* **1996**, *3*, 71. c) Kiessling, L. L.; Gestwicki, J. E.; Strong, L. E. *Current Opinion Chem. Biol.* **2000**, *4*, 696.

65. a) Dieck, H. A.; Heck, R. F. *J. Organomet. Chem.* **1975**, 93, 259. b) Cassar, I. *J. Organomet. Chem.* **1975**, 93, 253. c) Sonogashira, K.; Tohda, Y.; Hagihara, N. *Tetrahedron Lett.* **1975**, 16, 4467.

66. Norton, N. N. 'Biomedical sensors: Fundamentals and Applications, ed. N. M. Norton, Noyes Publications, Inc., **1982**, pp.1-44.

67. Clark, L. C. Jr.; Lyons, C. *Ann. NY Acad. Sci*. **1962**, 102, 29.

68. Wei, H.; Li, B.; Li, J.; Wang, E.; Dong, S. *Chem. Comm.* **2007**, 3735.

69. Dubertret, B.; Calame, M.; Libchaber, A. J. *Nat. Biotechnol.* **2001**, *19*, 365.

70. Xiao, Y.; Patolsky, F.; Katz, E.; Hainfeld, J.F.; Willner, I. *Science* **2003**, *299*, 1877.

71. Nam, J .M.; Stoeva, S. I.; Mirkin, C. A. *J. Am. Chem. Soc.* **2004**, *126*, 5932.

72. Astuti, Y.; Palomares, E.; Haque, S. A.; Durrant, J. R. *J. Am. Chem. Soc.* **2005**, *127*, 15120.

73. Nam, J. M.; Thaxton, C. S.; Mirkin, C. A. *Science* **2003**, *301*, 1884.

74. Stoeva, S. I.; Lee, J. S.; Thaxton, S. S.; Mirkin, C. A. *Angew. Chem. Int. Ed.* **2006**, *45*, 3303.

75. Lavigne, J. J.; Anslyn, E. V. *Angew. Chem. Int. Ed*. **2001**, *40*, 3118.

76. Goodey, A.; Lavigne, J. J.; Savoy, S. M.; Rodriguez, M. D.; Curey, T.; Tsao, A.; Simmons, G.; Wright, J.; Yoo, S. J.; Sohn, Y.; Ansyln, E. V.; Shear, J. B.; Neikirk, D. P.; McDevitt, J. T. *J. Am. Chem. Soc*. **2001**, *123*, 2559.

77. a) Wiskur, S. L.; Floriano, P. N., Anslyn, E. V.; McDevitt, J. T. *Angew. Chem. Int. Ed*. **2003**, *42*, 2070. b) Lavigne, J. J.; Savoy, S. M.; Clevenger, M. B.; Ritchie, J. E.; McDoniel, B.; Yoo, S. J.; Anslyn, E. V.; McDevitt, J. T.; Shear, J. B.; Neikirk, D. P. *J. Am. Chem. Soc*. **1998**, *120*, 6429. c) Curey, T. E.; Goodey, A.; Tsao, A.; Lavigne, J. J.; Sohn, Y.; McDevitt, J. T.; Anslyn, E. V.; Neikirk, D.; Shear, J. B. *Anal. Biochem*. **2001**, *293*, 178. d) McCleskey, S. C.; Griffin, M. J.; Schneider, S. E.; McDevitt, J. T.; Anslyn, E. V. *J. Am. Chem. Soc*. **2003**, *125*, 1114.

78. Lee, J. W.; Lee, J. S.; Kang, M.; Su, A. I.; Chang, Y. T. *Chem. Eur. J.* **2006**, *12*, 5691.

79. Rakow, N. A.; Suslick, K. S. *Nature* **2000**, *406*, 710.

80. Greene, N. T.; Shimizu, K. D. *J. Am. Chem. Soc.* **2005**, *127*, 5695.

81. Folmer-Andersen, J. F.; Kitamura M.; Anslyn E. V. *J. Am. Chem. Soc.* **2006**, *128*, 5652.

82. Buryak, A.; Severin, K. *J. Am. Chem. Soc.* **2005**, *127*, 3700.

83. Wright, A. T.; Anslyn, E. V. *Chem. Soc. Rev.* **2006**, 35, 14.

84. Lee, J. W.; Lee, J.-S.; Chang, Y.-T. *Angew. Chem. Int. Ed.* **2006**, *45*, 6485.

85. Daniels, M. J.; Wang, Y.; Lee, M.-Y.; Venkitaraman, A. R. *Science* **2004**, *306*, 876.

86. Ross, J. S.;Fletcher, J. A. *Stem Cells* **1998**, *16*, 413.

87. Haab, B. B. *Curr. Opin. Biotech.* **2006**, *17*, 415.

88. Baldini, L.; Wilson, A. J.; Hong, J.; Hamilton, A. D. *J. Am. Chem. Soc.* **2004**, *126*, 5656.

89. Zhou, H.; Baldini, L.; Hong, J.; Wilson, A. J.; Hamilton, A. D. *J. Am. Chem. Soc.* **2006**, *128*, 2421.

90. Wright, A. T.; Griffin, M. J.; Zhong, Z.; McCleskey, S. C.; Anslyn, E. V.; McDevitt, J. T. *Angew. Chem. Int. Ed.* **2005**, *44*, 6375.

91. a) Sandanaraj, B. S., Demont, R., Aathimanikandan, S. V., Savariar, E. N., Thayumanavan, S. *J. Am. Chem. Soc.* **2006**, *128*, 10686. b) Sandanaraj, B. S., Demont, R., Thayumanavan, S. *J. Am. Chem. Soc.* **2007**, *129*, 3506.

92. Sutter, J. M.; Jurs, P. C. *Anal. Chem*. **1997**, *69*, 856.

93. Shaffer, R. E.; Rose-Pehrssen, S. L.; McGill, R. A. *Anal. Chim. Acta* **1999**, *384*, 305.

94. Shaffer, R. E.; Rose-Pehrssen, S. L *Anal. Chem.* **1999**, *71*, 4263.

95. Brown, R. G., "Introduction to Random Signal Analysis and Kalman Filtering", John Wiley & Sons, Inc., New York, **1983**, pp. 165-169.

96. *SYSTAT11.0*, SystatSoftware, Richmond, CA 94804, USA, **2004**.

CHAPTER 2

INTERACTION OF NANOPARTICLES WITH CONJUGATED POLYMER: BUILDING "CHEMICAL NOSES"

2.1 Introduction

The combination of gold nanoparticles (**AuNP**s) with conjugated polymers (CPs) is a powerful one that has lead to novel biomolecular and bio-inspired materials with hierarchical structures.[1] This alliance is attractive not only from a structural standpoint, as the properties of both components are easily modified, but from an electronic one as well: **AuNPs** and CPs interact by energy transfer and both have transitions in the visible or in the UV-vis range. These interactions are examplified by reported combinations of poly(*p*-phenylenevinylene)s (PPV), polyfluorenes (PF) and poly(p-phenyleneethynylene)s (**PPE**) with **AuNP**s.[2,3] A seminal study on the interaction of CPs and **AuNP**s was published by Heeger and Bazan.[2] They observed that electrostatic interactions between a negatively charged **AuNP** and positively charged conjugated polymers of the PPV and the PF types lead to efficient binding between the **AuNP** and the CP as indicated by the **AuNP**s' ability to quench the fluorescence of the CP.

In this dissertation, we have employed hydrophobically functionalized **AuNP**s in combination with CPs **Sw-CO_2/PPECO_2** as powerful constructs to discern biomolecules and cell surfaces (Chapters 3, 6 and 8) through fluorescence recovery via displacement assays. In the course of these investigations we noted significant variance in the binding of the positively charged **AuNP**s to negatively charged CPs depending on the structural features of the **AuNP**.

It is not clear how the hydrophobicity of a monolayer protected **AuNP** influences the magnitude of the interaction between **AuNP** and CP (in this case the highly fluorescent **Sw-CO$_2$** with a quantum yield (Φ_F greater than 0.3). As such, we were interested in preparing a series of nanoparticles (**NP$_1$-NP$_{11}$**) that differed only in the size and structure of their exterior ammonium group (Figure 2.1). Though there has been a thorough study on the quenching of **AuNP**s by CPs by Bazan and Heeger, these authors used citrate-coated **AuNP**s that interacted with positively charged CPs; modulation of the binding between **AuNP** and CP by changing the exposed end of the protective monolayer has not been reported. A technical issue we have found necessary to address is how to perform the data analysis pertaining to the quenching experiments between **AuNP**s and CPs. Results of quenching experiments involving CPs are analyzed using a simple Stern-Volmer formalism,[4] by which, if static quenching can be assumed,[5] the binding constant between an **AuNP** and a fluorophore is extracted from the following equation (Eq. 2.1):

$$\frac{I_0}{I_{[Q]}} = 1 + K_{SV}[Q] \qquad \text{(Eq. 2.1)}$$

$I_0/I_{[Q]}$ is the quotient of the fluorescence intensity in the absence (I_0) and the presence of a specific concentration [Q] of the quencher Q ($I_{[Q]}$). K_{sv} represents the binding constant between **AuNP** and CP. From this simple equation Heeger and Bazan calculated binding constants between **AuNP** and conjugated polymer that were in excess of $K_{SV} = 10^{10}\ M^{-1}$. While this data workup is simple, it is not without problems (vide infra). The highly efficient quenching process brought on by complexation of the **AuNP** and the CP is of unusually large magnitude and may be a consequence of both the molecular wire effect and the efficient Förster type energy transfer from the excited state of the conjugated polymer to the plasmon band of the **AuNP**. Polyvalency[6,7] is probably also involved, as it

can be reasonably assumed that multiple electrostatic interactions occur between polymer chain and a single **AuNP**. Despite the strength of the interaction between CP and **AuNP**, their affinity for one another can be modulated by varying the structure of the positively charged monolayer ensheathing the **AuNP**.

AuNPs are easily synthesized[8,9,10] and monolayer functionalized with different and suitably substituted thiols or disulfides that chemisorb and oxidatively add to the gold surface after **AuNP** formation. As the number of potential disulfide and thiol ligands is essentially unlimited, different ligand coating can give **AuNP** unique physical and chemical properties; **AuNP**-conjugated polymer constructs form when the two components are mixed. Upon addition of a sufficient amount of nanoparticle to the system, the fluorescence of the conjugated polymer is fully quenched.[11] These **AuNP-PPE** complexes can be disrupted by the introduction of a suitable, charged analyte, which leads to free **PPE** chains in solution and a subsequent fluorescence turn-on.

We have exploited this principle for the successful sensing of proteins (Chapter 3),[11] bacteria (Chapter 6)[12] and cancerous cells (Chapter 8).[13] As we have created libraries of nanoparticles, we can influence both the binding of the employed PPE as well as its decomplexation from the **AuNP** by an analyte.

As an example for **AuNP-PPE** conjugate sensing system, we employing three and six simple **AuNP-PPE** constructs showed impressive selectivity (Chapters 3, 6, and 8); however, it is also helped to illustrate the effect of increasing salt concentration on the binding between **AuNP** and conjugated polymers, as well as to demonstrate the influence of the hydrophobic character of the monolayer protected **AuNP**s on the binding constant K_B between **AuNP** and CP. Herein we investigate the influence of increasing

hydrophobic character on the **AuNP**/CP binding and examine its dependence upon ionic strength.

2.2 Results and Discussion

The Ligands $\mathbf{L_1}$-$\mathbf{L_{11}}$ were synthesized according to Scheme 2.1 through quaternization of the tertiary amines **1-11** by the mesylate $\mathbf{L_0}$. Deprotection with trifluoroacetic acid in the presence of triisopropylsilane as a reducing agent gave $\mathbf{L_1}$-$\mathbf{L_{11}}$ as yellowish oils.

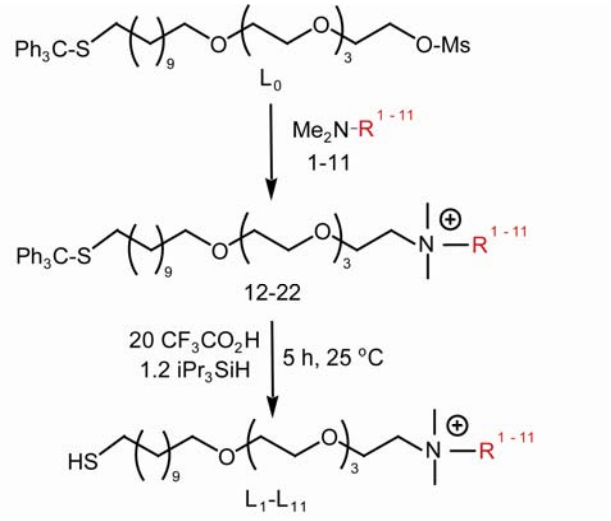

L	R	L	R
1	—Ethyl	**7**	—Cyclododecyl
2	—Butyl	**8**	—4-phenylcyclohexyl
3	—Hexyl	**9**	—Phenyl
4	—Decyl	**10**	—Benzyl
5	—Cyclohexyl	**11**	—3-oxa-4,4-diphenylbutyl
6	—4-t-Butylcyclohexyl		

Scheme 2.1. Synthesis of the thiols $\mathbf{L_1}$-$\mathbf{L_{11}}$. Yields of $\mathbf{L_1}$-$\mathbf{L_{11}}$ are above 95% in all cases starting from $\mathbf{L_0}$.

The $\mathbf{NP_1}$-$\mathbf{NP_{11}}$ were synthesized by dissolving pentanethiol-protected **AuNP**s generated from a literature procedure[3] in dried dichloromethane (DCM) and subsequently adding thiols $\mathbf{L_1}$-$\mathbf{L_{11}}$ respectively. Removal of solvent, dialysis in water and

lyophilization afforded **NP$_1$-NP$_{11}$** as brownish-red powders, which freely re-dispersed in water (Figure 2.1).

The PPE **Sw-CO$_2$** was prepared according to a literature procedure[14] and used as a 5 micromolar solution in buffer. The polymer had a degree of polymerization (P_n) of 12 and a molecular weight (M_n) of 14 KDa with a polydispersity index (PDI) of 1.8.

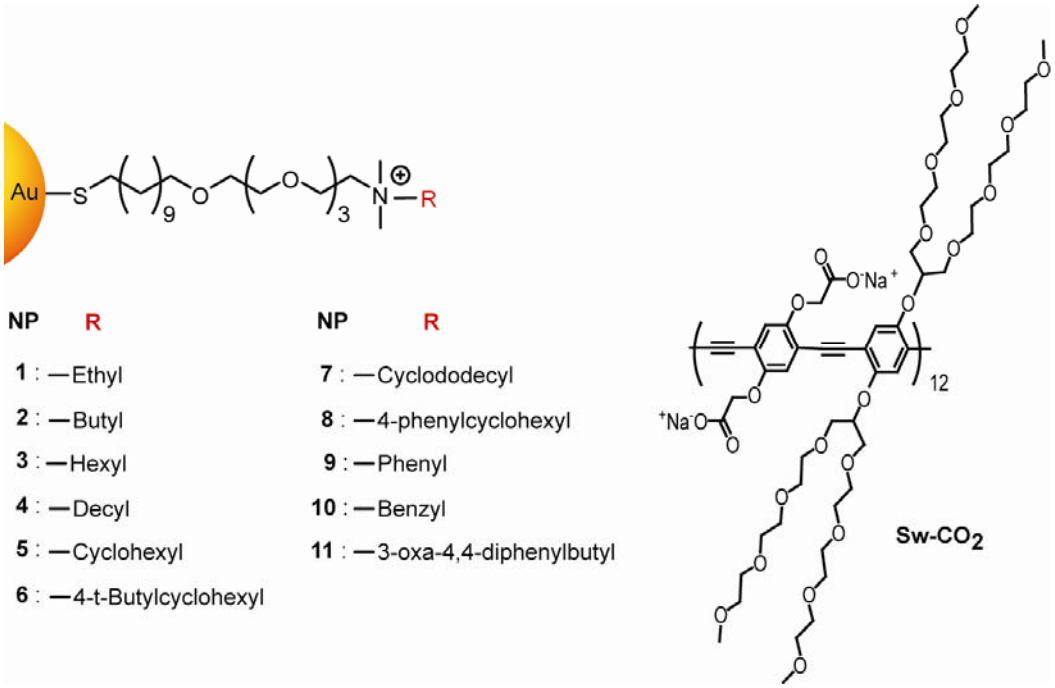

Figure 2.1 Monolayer protected gold nanoparticles (**AuNP**s) and structure of **PPE Sw-CO$_2$** investigated in this study.

The quenching of **Sw-CO$_2$** by the **AuNP** is a static process in terms of the Stern-Volmer formalism, as the emission lifetimes of the PPEs are generally between 150 and 450 ps.[15] Hence, any dynamic quenching effects, while present, have only a minute influence. We have recently developed the following binding model, which we exploit to investigate the quenching processes of the PPE by the **AuNP**s (Eq. 2.2).[16]

$$I_{[Q]} = I_0 + \frac{\alpha}{2}\left[\left([F]_0 + n[Q]_{tot} + \frac{1}{K_{SV}}\right) - \left\{\left([F]_0 + n[Q]_{tot} + \frac{1}{K_{SV}}\right)^2 - 4n[F]_0[Q]_{tot}\right\}^{1/2}\right]$$

(Eq. 2.2)

I_0 is the fluorescence intensity of the PPE at a concentration $[F]_0$ in the absence of quencher [Q] (in this case nanoparticles), $I_{[Q]}$ is the fluorescence intensity of the PPE in the presence of a concentration [Q] of gold nanoparticle, $[Q]_{tot}$ is the total concentration of the added quencher, and n denotes the valency of the **AuNP**, i.e. how many sites the **AuNP** has to quench multiple PPE chains. The term α is used to correlate the fluorescence intensities and concentrations of the two species. This factor is constant if the instrumental variables (e.g. slit width, excitation wavelength, sensitivity, etc.) and the nanoparticle and polymer identities are fixed.

In obtaining the Stern-Volmer binding constant, the current form of the equation (Eq. 2.2) allows us to approximate K_{sv} by performing a curve fitting analysis using ten different concentrations of nanoparticle quencher.

The formula in Eq. 2.2 is considerably more complex than Eq. 2.1, as the Stern-Volmer formalism makes assumptions that do not hold well in the high binding regimen we are investigating. In these cases, the SV-plots curve upward and are not linear as would be expected. One of the reasons for the non-linear behavior is the expression of the term [Q] in Eq. 3.1, as it refers to the concentration of free quencher and *not* to the easily measured total concentration of quencher $[Q]_{tot}$. If $[F]_0/K_{sv} < 1$ the assumption that $[Q]_{free} \approx [Q]_{tot}$ is justified and the Stern-Volmer approximation provides a simple and convenient but powerful tool for extracting binding constants in an analytical way. If $[F]_0/K_{sv} > 1$, the assumption that $[Q]_{free} \approx [Q]_{tot}$ breaks down and the observed Stern-Volmer plots are

invariably upwardly sloped. An analytical expression for the concentration of free quencher is unfortunately not available and most literature studies make use of $[Q]_{total}$ instead of $[Q]_{free}$. Consequently, one finds an innate upward curvature to the Stern-Volmer plot if $[F]_0/K_{sv} > 1$. While this upward curvature is often attributed to superquenching or other effects such as Dexter energy transfer, we suspect that it is due, at least in part, to the incorrect use of $[Q]_{total}$ instead of $[Q]_{free}$.[17] There is a second minor issue with the Stern-Volmer formalism in that it assumes the formation of a 1:1 complex that is fully quenched and does not display any residual fluorescence. Use of Eq. 2.2 resolves all of these issues.

In our first experiments we explored the influence of different buffers on the binding strengths between **AuNP** and **Sw-CO$_2$**. As shown in Figure 2.2 the binding curves are nearly superimposable in PB, PIPES, HEPES and TRIS-HCl buffers at a 5 mmol concentration. In the case of phosphate buffered saline (PBS) the binding constant is lower and there is a significant final residual fluorescence at high **AuNP** concentration. As **Sw-CO$_2$** has a P_n of 12 and a PDI of 1.8, there is expected to be a fraction of short oligomers in such polymer solutions. Since shorter polymer chains do not support polyvalent interactions to the **AuNP** as well, their binding will be considerably less efficient, and addition of salt will screen the electrostatic attractions between polymer and **AuNP** more so for short polymer chains than for longer ones.

In another series of experiments we investigated the influence of **PPE** concentration on K_{sv}. Figure 2.3 shows the dependence of the binding constant upon the concentration of the PPE. Binding constants obtained from a 10 nM solution of **PPE** are identical to those obtained from a 1 μM solution of **PPE** as predicted by Eq. 2.2, because they are not affected by the Stern-Volmer equation.

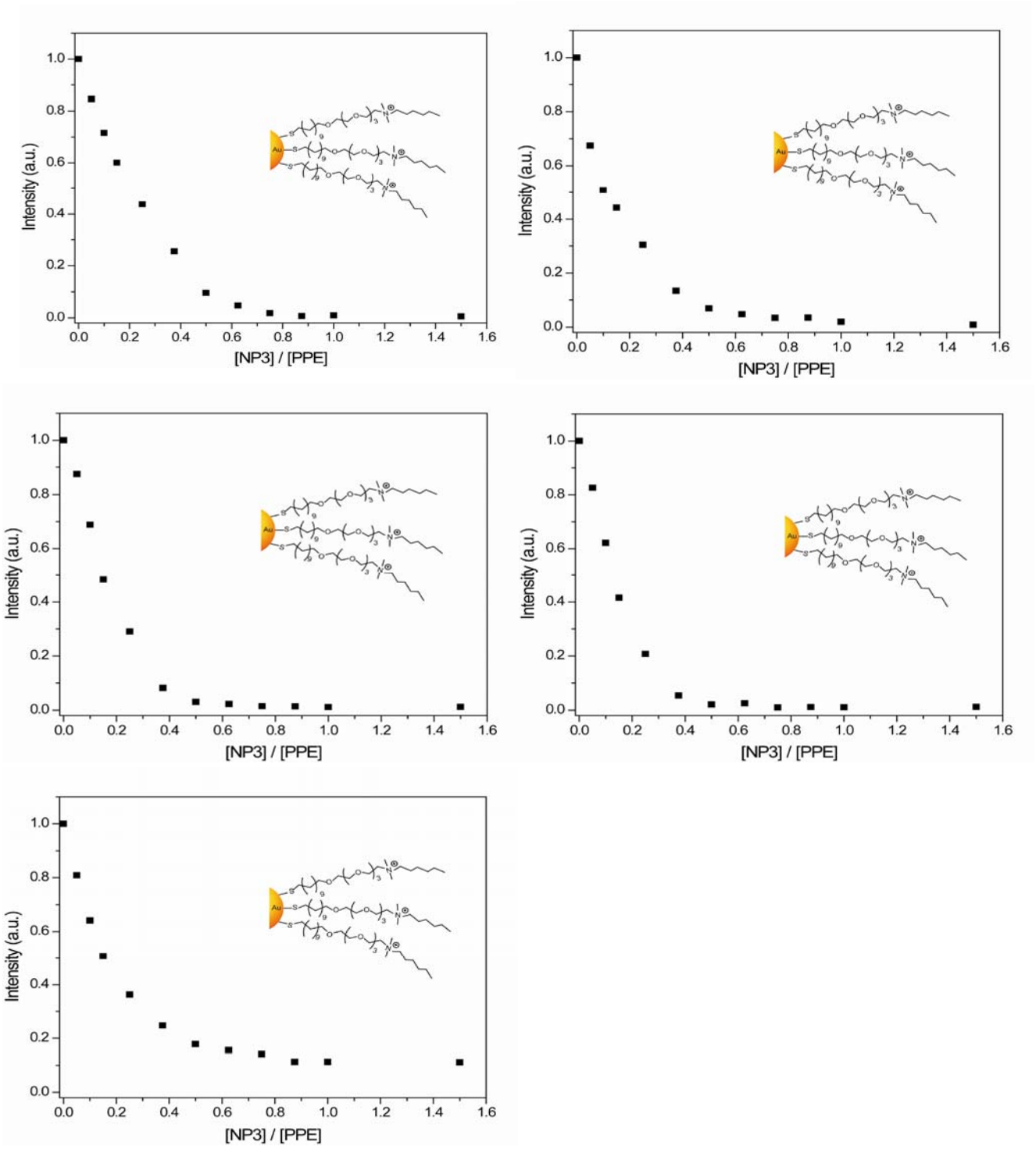

Figure 2.2 Fluorescence titration curves for the complexation of $\mathbf{NP_3}$ with $\mathbf{Sw\text{-}CO_2}$ in PB (top left), PIPES (top right), HEPES (middle left), Tris-HCl (middle right), and PBS (bottom left)

After performing these preliminary studies, we investigated the eleven nanoparticles **NP_1-NP_{11}** (Figure 2.1) for their ability to quench the fluorescence of **Sw-CO_2** in the presence of 0, 100, 250, 500 and 1000 mM of NaCl to determine and evaluate the relationship between electrostatic and hydrophobic effects (Figure 2.2). Figure 2.1 shows that **NP_1-NP_4** display increasingly long hydrocarbon tails while **NP_5-NP_7** feature cyclic hydrophobic substituents on the ammonium functionality. The **NP_8-NP_{11}** contain aromatic residues and are therefore grouped together.

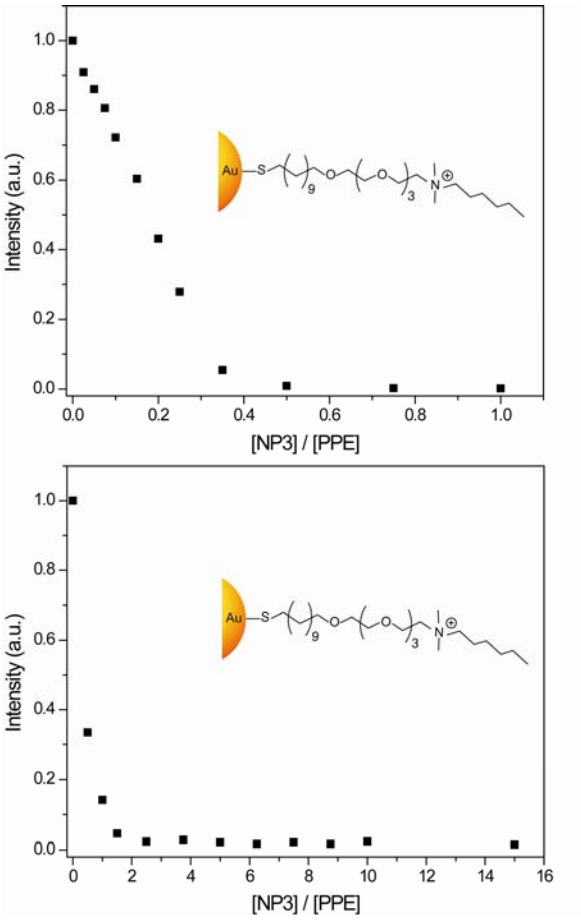

Figure 2.3 Quenching of PPE by **NP_3** for a PPE concentration of 1 µm (top; 8.5 x 10^7 M^{-1}) and 10 nm (bottom; 8.6 x 10^7 M^{-1}). Experimental values for Ksv's are nearly concentration independent.

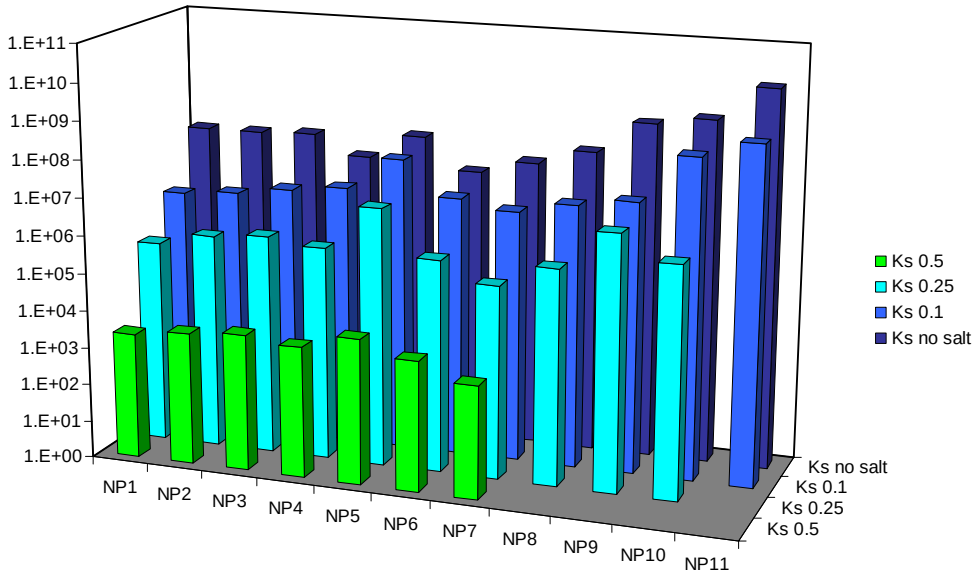

Figure 2.4 Logarithmic plot of binding constants between **NP_1-NP_{11}** and **Sw-CO_2** in the presence of different concentrations of sodium chloride.

Table 2.1 and Figure 2.4 display the results of the binding studies of **NP_1-NP_{11}** to **Sw-CO_2** in the presence of increasingly concentrated sodium chloride solutions. The binding between the negatively charged PPE and the positively charged **AuNP**s is dependent upon the structure of the **AuNP** and the salt concentration.

Table 2.1. Binding ratio "n" and binding constant K_a values for the complexation **NP_1-NP_{11}** with **Sw-CO_2** in PB with 0, 100, 250, 500, and 1000 mM NaCl. At higher NaCl concentrations, values could not be accurately determined for all nanoparticle-conjugated polymer constructs.

	n				$K_a * 10^{-6} (M^{-1})$			
NaCl (mM)	0	100	250	500	0	100	250	500
NP1	2.9	2.4	2.1	1.9	75	2.5	0.25	0.0022
NP2	7.3	6.8	6.4	5.9	76	3.4	0.54	0.0033
NP3	4.6	4.3	3.8	3.5	89	5.6	0.72	0.0043
NP4	3.7	3.4	3.2	2. 8	27	8.4	0.50	0.0031
NP5	5.7	5.5	5.0	4.5	130	62	7.5	0.0073
NP6	10.4	9.7	9.3	8.8	19	7.9	4.7	0.0029
NP7	12.9	12.1	11.4	10	42	4.8	0.14	0.0010
NP8	6.0	5.4	5.1	NA	110	9.7	0.55	NA
NP9	6.1	5.9	5.2	NA	780	16	6.1	NA
NP10	6.0	5.6	5.1	NA	1300	310	1.4	NA
NP11	5.7	5.5	NA	NA	10000	857	NA	NA

Increasing ionic strength screens the electrostatic interactions between **AuNP** and PPE. In a 1 molar NaCl solution binding between PPE and **AuNP** is weak, as the electrostatic interaction between **AuNP** and PPE is greatly attenuated. Static quenching is interrupted by the addition of salt, but dynamic quenching should be independent of the presence of binding sites or salt concentration. At high salt concentrations we observe values of K_{sv} of around 1 x 10^3 M^{-1} for **NP_1-NP_7** while the binding constants for **NP_8-NP_{11}** are negligible. From these experiments we can conclude that the contribution of dynamic quenching to the overall quenching process is minor and that it does not influence the outcome of the binding experiments done at low salt concentrations. According to Eq. 2.2 the analysis of the binding curves gives the number of binding sites n that are available on a single nanoparticle. The aromatic nanoparticles **NP_8-NP_{11}** give

values for n of around 6, i.e. 6 repeat units with 12 carboxylate functionalities are bound to one nanoparticle.

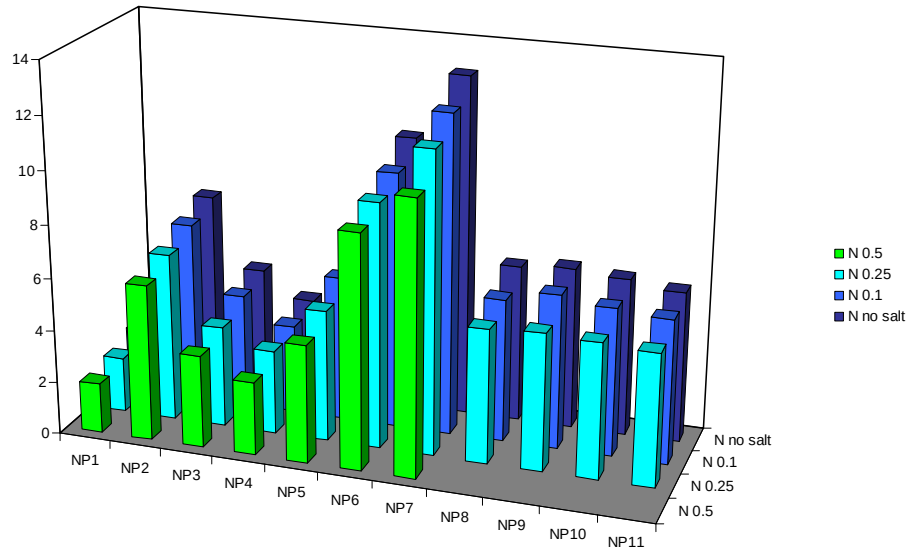

Figure 2.5 Number of binding sites n as obtained from Eq. 2.2. This value n refers to the binding sites of the **AuNP-PPE** construct.

As we have a degree of polymerization of 12 for the PPE, this means that either several PPE molecules could interact using only one or two of their carboxylate groups, or that only one PPE chain is bound per **AuNP** but with up to six contacts. From this model it is not possible to discern between these two scenarios. Overall, the n-values vary from 2-12, with the least hydrophobic **AuNPs** having the least number of binding sites. Figure 2.5 depicts the obtained results.

In the absence of salt, the **AuNP**s with aromatic ammonium species bind by far the strongest to the conjugated polymer. We rationalize this as a prevalence of π-π-interactions, i.e. the phenyl groups of the nanoparticle ligands bind strongly to the aromatic backbone of the PPE.

Although the partition coefficient *P* of a molecule alone does not provide an understanding of hydrophobic interactions of **AuNP**s to **Sw-CO$_2$**, it does offer a means of characterizing the effect of hydrophobicity when it is combined with another parameter. Therefore, we explored the relation between logK_a and log*P* to elucidate the interaction between the hydrophobicity of the **AuNPs** and **Sw-CO$_2$**. As shown in Figure 2.6, **NP$_{10}$** and **NP$_{11}$** that display aromatic units on their surface are the most efficient at quenching the fluorescence of the **Sw-CO$_2$**. As mentioned before, we presume that this is due to π-π-interactions between the aromatic groups on the surface of the **AuNP** and the hydrophobic backbone of the PPE. In the case of the cyclic units, **NP$_5$** (R = cyclohexyl), **NP$_6$** (R= tert-butyl) and **NP$_7$** (R= cyclododecyl) the binding interaction in terms of logK_a is lower by orders of magnitude, and this is assumed to be the result of two factors: a) they do not have aromatic units to interact with PPE and b) they feature bulky cyclic functionalities that reduce the electrostatic interaction with **Sw-CO$_2$**. However, a phenyl addition to the cyclohexane unit (**NP$_8$**) increases the binding interaction. In the case of **NP$_1$** (R= ethyl), **NP$_2$** (R= butyl) and **NP$_3$** (R= hexyl) the elongation of the aliphatic R group on the quaternary amine increases sligthly the strength of the binding. This is not the case for **NP$_4$** (R = decyl) where a weak binding interaction with **Sw-CO$_2$** is observed.

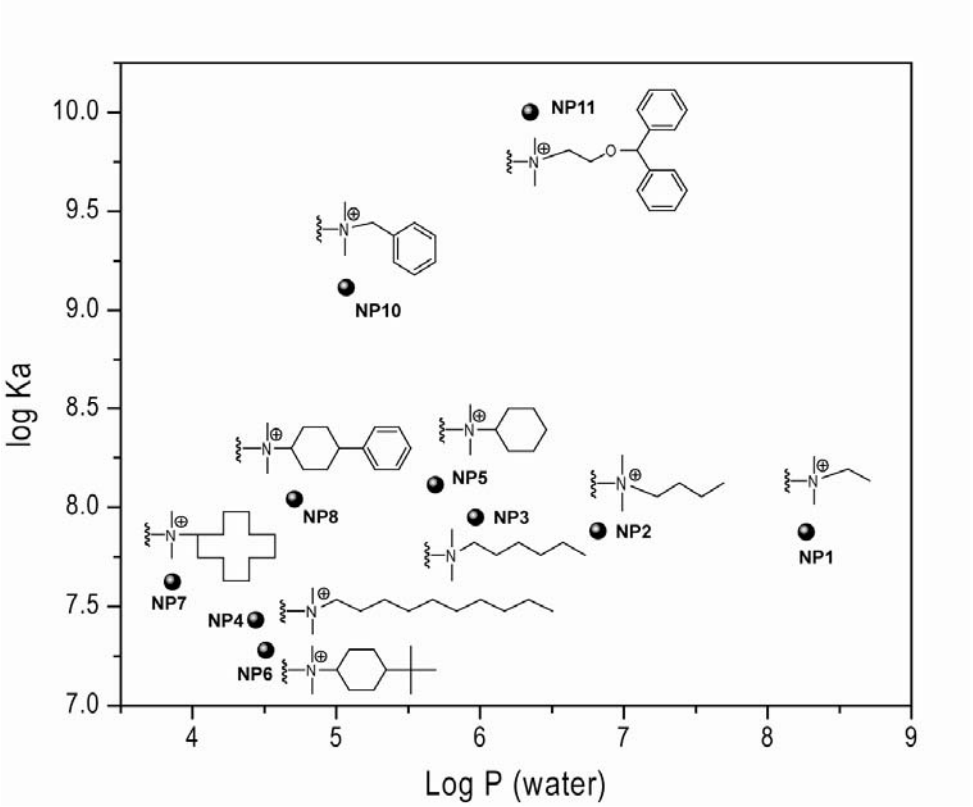

Figure 2.6. Logarithmic relation of binding constants (K_a, **AuNP-SwCO$_2$**) and partition coefficient of **NP$_1$-NP$_{11}$** (**NP$_9$** is not plotted due to the force field interaction).

Surprisingly, the strongest binding **AuNPs** (**NP$_{10}$** and **NP$_{11}$**) also display the highest sensitivity towards the addition of sodium chloride, while **NP$_5$** is the least sensitive to an increase in ionic strength. Conclusions that might be drawn to aid in the development of further **AuNP**-CP constructs are: 1) Electrostatic interactions between PPE and **AuNP** can be modulated and even turned off by an increase in ionic strength. 2) Aromatic side chains are more sensitive towards interruption of binding than aliphatic and specifically cycloaliphatic ammonium groups are. 3) Aromatic ammonium side chains display the highest association constants and promote the interaction between PPE and **AuNP**, presumably through aromatic stacking with the PPE backbone.

2.3 Conclusion

In conclusion, we have investigated the quenching of **Sw-CO_2** by 11 monoloayer protected, ammonium-functionalized nanoparticles (**NP_1-NP_{11}**) with varying hydrophobicity. **AuNP**s that feature aromatic units on their surfaces are most effective in quenching the fluorescence of the PPE perhaps due to efficient edge to face interactions between the aromatic groups on the surface of the **AuNP** and the hydrophobic backbone of the PPE in the fashion explained by Hunter and Sanders.[18] In all cases, however, increasing the ionic strength of the medium dramatically decreases the strength of the interaction between the two oppositely charged species i.e. **AuNP** and CP.

In the aliphatic systems, an *increase* in hydrophobicity is counterbalanced by a *decrease* in the electrostatic interactions, thus it does not lead to an increase in binding between **AuNP** and CP. In the aromatic **AuNP**s, however, the binding constant between **AuNP** and **Sw-CO_2** correlates well with the hydrophobicity of the aromatic tail on the ammonium group, suggesting that at low salt concentrations the contribution of the hydrophobic arenes is significant. Overall, we demonstrated that simple manipulation of the surface functionality of **AuNP**s by varying their hydrophobicity allows for a large range of binding constants to be attained by molecular tailoring, particularly if ammonium salts with aromatic substituents are employed to stabilize the **AuNP**s.

2.4 Experimental Section

2.4.1 Instrumentation and Materials. Swallowtail-substituted carboxylate PPE (**Sw-CO_2**) was synthesized according to published procedure.[14] Fluorescence intensity changes at 465 nm were recorded in 96-well plates (300 μL Whatman® Glass Bottom

microplate) on a Molecular Devices SpectraMax M5 micro plate reader with an excitation wavelength of 405 nm. Phosphate buffer (PB), phosphate buffered saline (PBS), piperazine-1,4-bis(2-ethanesulfonic acid) (PIPES), N-2-hydroxyethylpiperazine-N'-2-ethanesulfonic acid (HEPES), and tris(hydroxymethyl)aminomethane hydrochloride (Tris-HCl) were purchased from Sigma-Aldrich. The buffers were diluted to a concentration of 5 mM and a pH of 7.2 with DI H_2O. To calculate log P, computational program Maestro 8.0 was used.

2.4.2 General Procedure for the Synthesis of Cationic Ligands[11]

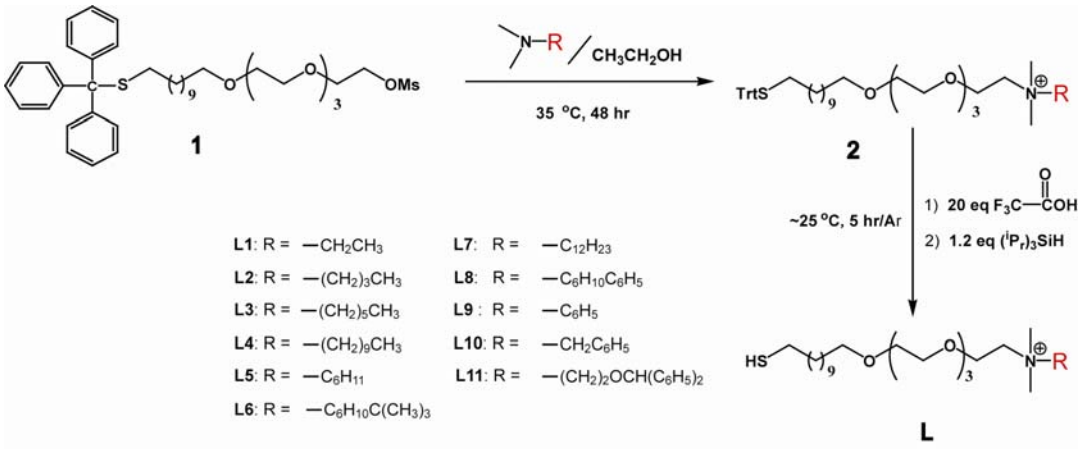

Scheme 2.2. Synthesis of ligands[11]

General procedure: Compound **2** bearing ammonium end groups were synthesized through the reaction of 1,1,1-triphenyl-14,17,20,23-tetraoxa-2-thiapentacosan-25-yl methanesulphonate (**1**) with corresponding substituted N,N-dimethylamines during 48 h at ~35 ^{o}C. The trityl protected thiol ligand **(2)** was dissolved in dry dichloromethane (Methylene Chloride, DCM) and an excess of trifluoroacetic acid (TFA, ~ 20

equivalents) was added. The color of the solution was turned to yellow immediately. Subsequently, triisopropylsilane (TIPS, ~ 1.2 equivalents) was added to the reaction mixture. The reaction mixture was stirred for ~5 h under Ar condition at room temperature. The solvent and most TFA and TIPS were distilled off under reduced pressure. The pale yellow residue was further dried in high vacuum. The product (**L**) formation was quantitative and their structure was confirmed by NMR. The yields were >95%.

Compound L_1: ^{1}H NMR (400MHz, $CDCl_3$, TMS): δ 3.94 (br, 2H, -CH_2N-), 3.69-3.56 (m, 14H, -CH_2O- + -OC$\underline{H}_2$-(CH_2N)-), 3.44 (t, 2H, -CH_2O-), 3.40-3.32 (m, 2H,-NCH_2-), 3.23 (s, 6H, -$(CH_3)_2$N-), 2.78 (s, 3H, -$CH_3SO^-_3$-), 2.51 (q, 2H, -CH_2S-), 1.69-1.149 (m, 4H, (SCH_2)C$\underline{H}_2$ + -C$\underline{H}_2$(CH_2O)-) , 1.44-1.24 (m, 18H, -SH + -CH_2- + -(NCH_2)C$\underline{H}_3$).

Compound L_2: ^{1}H NMR (400MHz, $CDCl_3$, TMS): δ 3.96 (br, 2H, -CH_2N-), 3.68-3.57 (m, 14H, -CH_2O- + -OC$\underline{H}_2$-(CH_2N)-), 3.49 (t, 2H, -CH_2O-), 3.39-3.33 (m, 2H,-NCH_2-), 3.17 (s, 6H, -$(CH_3)_2$N-), 2.91 (s, 3H, -$CH_3SO^-_3$-), 2.52 (q, 2H, -CH_2S-), 1.78-1.52 (m, 6H, -(NCH_2)C$\underline{H}_2$-) + (SCH_2)C$\underline{H}_2$ + -C$\underline{H}_2$(CH_2O)-) , 1.44-1.24 (m, 17H, -SH + -(NCH_2CH_2-)C$\underline{H}_2$-) + -CH_2-), 0.98 (t, 3H, - CH_3-).

Compound L_3: ^{1}H NMR (400MHz, $CDCl_3$, TMS): δ 3.95 (br, 2H, -CH_2N-), 3.68-3.56 (m, 14H, -CH_2O- + -OC$\underline{H}_2$-(CH_2N)-), 3.46 (t, 2H, -CH_2O-), 3.40-3.33 (m, 2H,-NCH_2-), 3.19 (s, 6H, -$(CH_3)_2$N-), 2.87 (s, 3H, -$CH_3SO^-_3$-), 2.52 (q, 2H, -CH_2S-), 1.76-1.53 (m, 6H, -(NCH_2)C$\underline{H}_2$-) + (SCH_2)C$\underline{H}_2$ + -C$\underline{H}_2$(CH_2O)-) , 1.41-1.22 (m, 21H, -SH + -(NCH_2CH_2-)C$\underline{H}_2$-) + -CH_2-), 0.89 (t, 3H, - CH_3-).

Compound L_4: ^{1}H NMR (400MHz, $CDCl_3$, TMS): δ 3.94 (br, 2H, -CH_2N-), 3.67-3.54 (m, 14H, -CH_2O- + -OC$\underline{H}_2$-(CH_2N)-), 3.48 (t, 2H, -CH_2O-), 3.41-3.32 (m, 2H,-NCH_2-), 3.17 (s, 6H, -$(CH_3)_2$N-), 2.90 (s, 3H, -$CH_3SO^-_3$-), 2.51 (q, 2H, -CH_2S-), 1.78-1.52 (m, 6H, -(NCH_2)C$\underline{H}_2$-) + (SCH_2)C$\underline{H}_2$ + -C$\underline{H}_2$(CH_2O)-) , 1.45-1.15 (m, 29H, -SH + -(NCH_2CH_2-)C$\underline{H}_2$-) + -CH_2-), 0.87 (t, 3H, - CH_3-).

Compound L_5: ^{1}H NMR (400MHz, $CDCl_3$, TMS): δ3.95 (br, 2H, -CH_2N-), 3.81-3.72 (m, 1H, H_{Cyclo}), 3.69-3.53 (m, 14H, -CH_2O- + -OC$\underline{H}_2$-(CH_2N)-), 3.49 (t, 2H, -CH_2O-), 3.11 (s, 6H, -$(CH_3)_2$N-), 2.91 (s, 3H, -$CH_3SO^-_3$-), 2.52 (q, 2H, -CH_2S-), 2.23 (d, 2H, H_{Cyclo}), 1.99 (d, 2H, H_{Cyclo}), 1.78-1.52 (m, 4H, -(SCH_2)C$\underline{H}_2$ + -C$\underline{H}_2$(CH_2O)-), 1.51-1.12 (m, 21H, SH + -CH2- + H_{Cyclo}).

Compound L_6: ^{1}H NMR (400MHz, $CDCl_3$, TMS): δ 3.96 (br, 2H, -CH_2N-), 3.79-3.75 (m, 1H, H_{Cyclo}), 3.66-3.57 (m, 14H, -CH_2O- + -OC$\underline{H}_2$-(CH_2N)-), 3.46 (t, 2H, -CH_2O-), 3.12 (s, 6H, -$(CH_3)_2$N-), 2.89 (s, 3H, -$CH_3SO^-_3$-), 2.52 (q, 2H, -CH_2S-), 2.28 (d, 2H, H_{Cyclo}), 2.01 (d, 2H, H_{Cyclo}), 1.64-1.54 (m, 4H, -(SCH_2)C$\underline{H}_2$ + -C$\underline{H}_2$(CH_2O)-), 1.47 (q,

2H, H_{Cyclo}), 1.33 (t, ^3J = 8.0 Hz, 1H, -SH), 1.30-1.22 (m, 14H, -CH2-), 1.16 (q, 2H, H_{Cyclo}) 1.04 (td, 1H -CHC-), 0.86 (s, 9H, -C(CH_3)$_3$-).

Compound L_7: ^{1}H NMR (400MHz, $CDCl_3$, TMS): δ 3.98 (br, 2H, -CH_2N-), 3.78-3.75 (m, 1H, H_{Cyclo}), 3.64-3.55 (m, 14H, -CH_2O- + -OC$\underline{H}_2$-(CH_2N)-), 3.46-3.42 (dt, 2H, -CH_2O-), 3.16 (s, 6H, -(CH_3)$_2$N-), 2.86 (s, 3H, -$CH_3SO^-_3$-), 2.52 (q, 2H, -CH_2S-), 1.93-1.40 (m, 26H, SCH_2)C$\underline{H}_2$ + -C$\underline{H}_2$(CH_2O)- + H_{Cyclo}), 1.33 (t, ^3J = 7.82 Hz, 1H, -SH), 1.29-1.24 (m, 14H, -CH2-).

Compound L_8: ^{1}H NMR (400MHz, $CDCl_3$, TMS): δ 7.4-7.2 (m, 4H, H_{Ar}), 7.17 (d, 1H, H_{Ar}), 3.95 (d and br, 2H, -CH_2N-), 3.79-3.52 (m, 14H, -CH_2O- + -OC$\underline{H}_2$-(CH_2N)-), 3.45 (q, 2H, -CH_2O-),3.29-3.22 (m and br, 1H, H_{Cyclo}), 3.01-2.92 (m and br, 1H, H_{Cyclo}) 2.87 (s, 3H, -$CH_3SO^-_3$-), 2.81 (d and br, 6H, -(CH_3)$_2$N-), 2.52 (q, 2H, -CH_2S-), 2.39-2.26 (m, 2H, H_{Cyclo}), 2.19-2.06 (m, 2H, H_{Cyclo}), 1.96-1.84 (m, 4H, H_{Cyclo}), 1.72-1.53 (m, 4H, -(SCH_2)C$\underline{H}_2$ + -C$\underline{H}_2$(CH_2O)-), 1.42-1.1.19 (m, 15H, -SH + -CH_2-).

Compound L_9: ^{1}H NMR (400MHz, $CDCl_3$, TMS): δ 7.82 (d, 2H, H_{Ar}), 7.66-7.51 (m, 3H, H_{Ar}), 4.24 (br, 2H, -CH_2N-), 3.78 (s, 6H, -(CH_3)$_2$N-), 3.68-3.52 (m, 14H, -CH_2O- + -OC$\underline{H}_2$-(CH_2N)-), 3.47-3.36 (m, 2H, -CH_2O-), 2.87 (s, 3H, -$CH_3SO^-_3$-), 2.52 (q, 2H, -CH_2S-), 1.70-1.46 (m, 4H, -(SCH_2)C$\underline{H}_2$ + -C$\underline{H}_2$(CH_2O)-), 1.42-1.1.16 (m, 15H, -SH + -CH_2-).

Compound L_{10}: ^{1}H NMR (400MHz, $CDCl_3$, TMS): δ 8.37 (d, 1H, H_{Ar}), 7.98 (d, 1H, H_{Ar}), 7.69-7.61 (m, 3H, H_{Ar}), 7.59-7.48 (m, 1H, H_{Ar}), 4.38 (br, 2H,-NCH_2-Ar)), 3.76 (br, 2H, -CH_2N-) 3.72-3.62 (m, 14H, -CH_2O- + -OC$\underline{H}_2$-(CH_2N)-), 3.61-3.55 (m, 2H, -CH_2O-), 3.23 (s, 6H, -(CH_3)$_2$N-), 3.07 (s, 3H, -$CH_3SO^-_3$-), 2.52 (q, 2H, -CH_2S-), 1.67-1.51 (m, 4H, -(SCH_2)C$\underline{H}_2$ + -C$\underline{H}_2$(CH_2O)-), 1.35-1.21 (m, 15H, -SH + -CH_2-).

Compound L_{11}: ^{1}H NMR (400MHz, $CDCl_3$, TMS): δ 7.42 (d, 2H, H_{Ar}), 7.37-2.27 (m, 8H, H_{Ar}), 7.25-7.18 (t, 2H, H_{Ar}), 5.13 (s, 1H, H_{Ar}), 4.12 (br, 2H, -CH_2N-)), 3.96 (br, 2H, -N$\underline{CH}_2$(CH_2OCAr), 3.64-3.51 (m, 14H, -CH_2O- + -OC$\underline{H}_2$-(CH_2N)-), 3.45 (t, 2H, -CH_2O-), 3.29-3.34 (m, 2H, -CH_2OCAr-), 3.28 (s, 6H, -(CH_3)$_2$N-), 2.86 (s, 3H, -$CH_3SO^-_3$-), 2.52 (q, 2H, -CH_2S-), 1.60-1.48 (m, 4H, -(SCH_2)C$\underline{H}_2$ + -C$\underline{H}_2$(CH_2O)-), 1.34-1.16 (m, 15H, -SH + -CH_2-).

2.4.3 General Procedure for the Synthesis of Cationic Nanoparticles

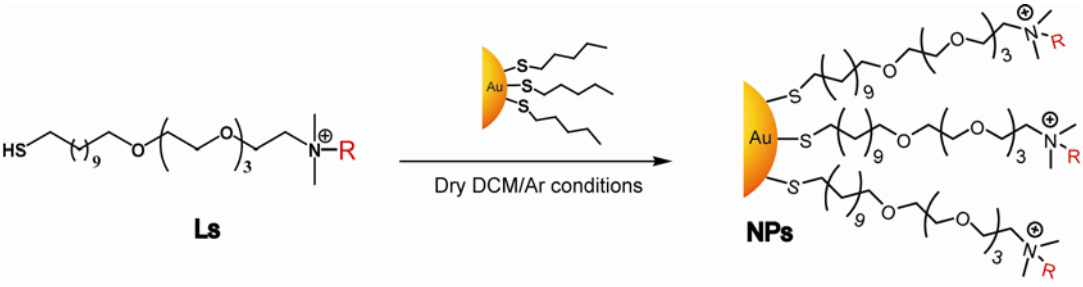

Scheme 2.3 Synthesis of cationic gold nanoparticles **(NP_1-NP_{11})**

General Procedure: 1-Pentanethiol coated gold nanoparticles (*d* = ~2 nm) were prepared according to the previously reported protocol.[9] Place-exchange reaction[19] of compound **Ls** dissolved in DCM with pentanethiol-coated gold nanoparticles (d~2 nm) was carried out for 3 days at environmental temperature. Then, DCM was evaporated under reduced pressure. The residue was dissolved in a small amount of distilled water and dialyzed (membrane MWCO = 1,000) to remove excess ligands, acetic acid and the other salts present with the nanoparticles. After dialysis, the particles were lyophilized to afford a brownish solid. The particles (**NPs**) are redispersed in water and/or ionized water (18 MΩ-cm). ^{1}H NMR spectra in D_2O showed substantial broadening of the proton signals and no free ligands were observed.

2.5 References

1. Sih, B. C.; Wolf, M. O. *Chem. Commun.* **2005**, 3375.

2. Fan, C. H.; Wang, S.; Hong, J. W.; Bazan, G. C.; Plaxco, K. W.; Heeger, A. J. *Proc. Nat. Acad. Sci.* **2003**, 100, 6297.

3. Brust, M.; Bethell, D.; Schiffrin, D. J.; Kiely, K. J. *Adv. Mater.* **1995**, 7, 795; Advincula, R. C. *Dalton Trans.* **2006**, 2778.

4. Stern, O.; Volmer, M. *Phys. Zeitschrift* **1919**, 20**,** 183.

5. Swager, T. M.; Zhou, Q. *J. Am. Chem. Soc.* **1995**, 117, 12593.

6. Mammen, M.; Choi, S. K.; Whitesides, G. M. *Angew. Chem.* **1998**, 37, 2755.

7. Lee, J. S.; Seferos, D. S.; Giljohann, D. A.; Mirkin, C. A. *J. Am. Chem. Soc.* **2008**, 130, 5430.

8. Simard, J.; Briggs, C.; Boal, A. K.; Rotello, V. M. *Chem. Commun.* **2000**, 1943.

9. Brust, M.; Walker, M.; Bethell, D.; Schiffrin, D. J.; Whyman, R. *Chem. Commun.* ***1*994**, 801.

10. Daniel, M. C.; Astruc, D. *Chem. Rev.* **2004**, 104, 293.

11. You, C. C.; Miranda, O. R.; Gider, B.; Ghosh, P. S.; Kim, I. B.; Erdogan, B.; Krovi, S. A.; Bunz, U. H. F.; Rotello, V. M. *Nature Nanotechnol.* **2007**, 2, 318.

12. Phillips, R. L.; Miranda, O. R.; You, C. C.; Rotello, V. M., Bunz, U. H. F. *Angew. Chem. Int. Ed.* **2008**, 47, 2590.

13. Bajaj, A.; Miranda, O. R.; Kim, I.-B.; Phillips, R. L.; Jerry, D. J.; Bunz, U. H. F.; Rotello, V. M. *Proc. Nat. Acad. Sci. USA* **2009**, 106, 10912.

14. Kim, I. B.; Phillips, R.; Bunz, U. H. F. *Macromolecules* **2007**, 40, 5290.

15. Bunz, U. H. F. *Chem. Rev*. **2000**, 100, 1605.

16. You, C. C.; De, M.; Han, G.; Rotello, V. M. *J. Am. Chem. Soc*. **2005**, 127, 12873.

17. a) Wang, J.; Wang, D. L.; Miller, E. K.; Moses, D.; Bazan, G.C.; Heeger, A. J. *Macromolecules* **2000**, 33, 5153. b) Fan, L.J.; Zhang, Y.; Jones, W.E. *Macromolecules* **2005**, 38, 2844.

18. Hunter, C. J.; Sanders, J. K. M. *J. Am. Chem. Soc.* **1990**, 112, 5525.

19. Hostetler, M. J.; Templeton, A. C.; Murray, R. W. *Langmuir* **1999**, 15, 3782.

CHAPTER 3

NANOPARTICLES-FLUORESCENT POLYMER "CHEMICAL NOSE" SENSOR: DETECTION AND IDENTIFICATION OF PROTEINS

3.1 Introduction

The presence of biomarker proteins and/or irregular protein concentrations is a consequence of cancer and other disease states.[1,2] Sensitive, convenient, and precise protein sensing methods provide crucial tools for the early diagnosis of diseases and successful treatment of patients. However, protein detection is a challenging prospect due to the structural diversity and complexity of the target analytes. Currently, the most extensively used detection method for proteins is enzyme-linked immunosorbent assay (ELISA).[3] In this system, the capture antibodies immobilized onto surfaces bind the antigen through a "lock-key" approach and another enzyme-coupled antibody is combined to react with chromogenic or fluorogenic substrates to generate detectable signals. Despite its high sensitivity, the application of this method is restricted due to its high production cost, instability, and challenges for quantification. While synthetic systems would alleviate some of these concerns, obtaining high affinity and specificity is quite challenging.

The "chemical nose/tongue" approach provides an alternative to the sensing protocol on the basis of exclusive analyte-receptor binding pairs.[4] In this strategy, a sensor array featuring *selective* receptors, as opposed to 'lock-key' specific recognition, is used for analyte detection. Strategically, the array presents chemical diversity to respond differentially to a variety of analytes. During the past few years, this approach has been harnessed to detect a wide range of analytes including metal ions,[5] volatile agents,[6]

aromatic amines,[7] amino acids,[8,9] and carbohydrates.[10,11] There have been preliminary studies into the application of this strategy to protein sensing, including Hamilton's porphyrin-based sensors used to identify four metal and nonmetal-containing proteins,[12,13] and Anslyn's use of 29 boronic acid-containing oligopeptide functionalized resin beads to differentiate 5 proteins and glycoproteins through an indicator-uptake colorimetric analysis.[14]

The first key challenge for effective protein sensors is the creation of materials featuring appropriate surface areas for binding protein exteriors, coupled with the control of structure and functionality required for selectivity. Nanoparticles provide versatile scaffolds for targeting biomacromolecules that feature sizes commensurate with proteins,[15,16,17] a challenging prospect with "small molecule"-based systems. Moreover, the self-assembled monolayer on these systems allows facile tuning of a range of surface properties in a highly divergent fashion, enabling diverse receptors to be rapidly and efficiently produced. For example, charged ligand-protected clusters can effectively recognize the protein surface through complementary electrostatic and hydrophobic interactions.[18,19,20]

The second challenge in protein sensing is the transduction of the binding event. Our strategy for the creation of protein sensors is to use the particle surface for protein recognition, with displacement of a fluorophore generating the output. As depicted in Figure 3.1a, the nanoparticles associate with charge complementary fluorescent dyes to give quenched complexes. The subsequent binding of protein analytes displaces the dyes, regenerating the fluorescence. By modulating the nanoparticle-protein and/or nanoparticle-dye association, distinct signal response patterns can then be employed to

differentiate the proteins (Figure 3.1b). The fluorescent indicator displacement assay does not require special instruments and its sensitivity (due in large part to the high surface area provided by nanoparticles) and rapidity facilitates protein detection.

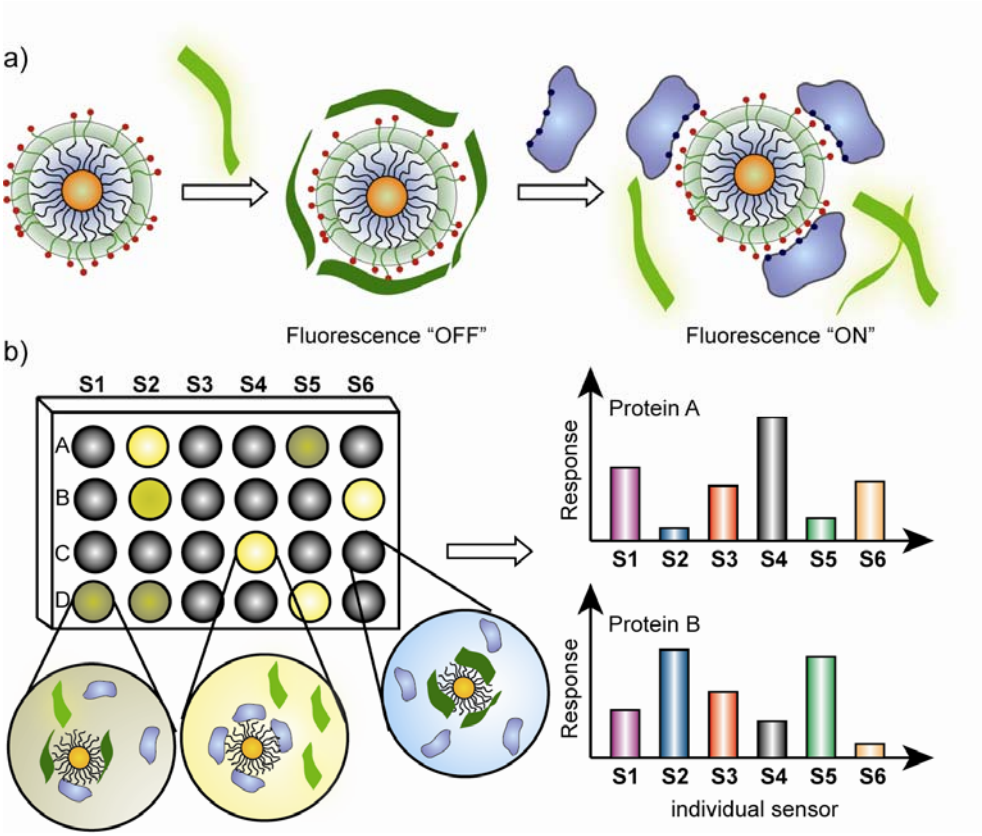

Figure 3.1 Fluorophore displacement-based protein sensor array. a) Displacement of quenched fluorescent polymer by protein analyte with concomitant restoration of fluorescence. b) Pattern generation through differential release of fluorescent polymers from gold nanoparticles.

In the current study, we employed six readily fabricated structurally related cationic gold nanoparticles (**NP1-NP6**) to create protein sensors (Figure 3.2a). These particles serve as both selective recognition elements as well as quenchers for the polymer. For our studies, we chose gold relative to other potential core materials (e.g. silver) due to its extraordinary stability, in particular resistance to exchange by amines (e.g. lysine residues) [21] and strong quenching ability.[22] The nanoparticle end groups carry additional

hydrophobic, aromatic or hydrogen-bonding functionality engineered to tune nanoparticle-polymer and nanoparticle-protein interactions. For the fluorescent transduction element we used a highly fluorescent poly(*p*-phenyleneethynylene) (PPE)[23,24] derivative, **PPE-CO$_2$**,[25] as a fluorescence indicator. Seven proteins with diverse structural features (Mw, pI) were used as the target analytes (Figure 3.2b). Using these components, we have created a competent sensor array, rendering distinct fluorescence response fingerprints for individual proteins. Linear discriminant analysis (LDA) was performed to identify the protein patterns with a high degree of accuracy.

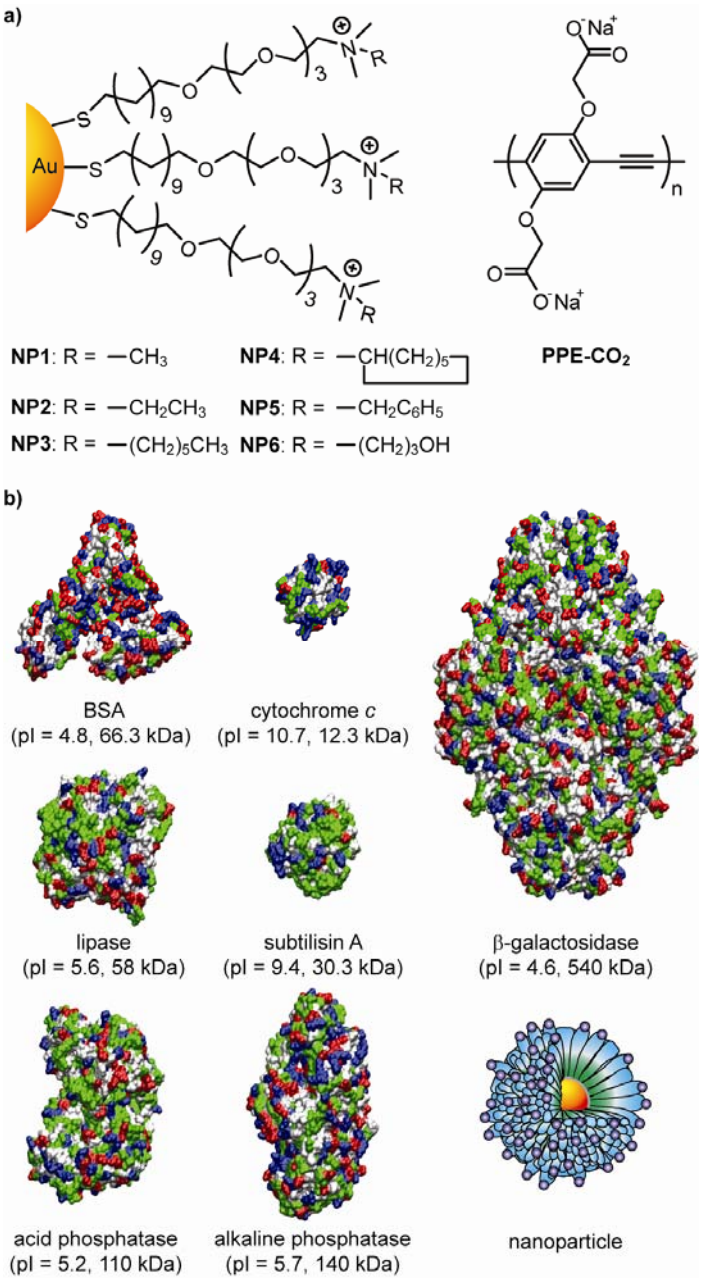

Figure 3.2 Structural features of protein receptors, signal transducer, and target analytes. a) Chemical structure of cationic gold nanoparticles (**NP1**-**NP6**) and anionic fluorescent polymer **PPE-CO$_2$** (n ~ 12). b) Surface structural feature and relative size of seven proteins and the nanoparticles used in the sensing study. Color scheme for the proteins: non-polar residues (gray), basic residues (blue), acidic residues (red) and polar residues (green).

3.2 Results and Discussion

Fluorescence titration was first conducted to assess the complexation between anionic **PPE-CO$_2$** and cationic gold nanoparticles **NP1**-**NP6**. The intrinsic fluorescence of **PPE-CO$_2$** was significantly quenched and slightly blue shifted upon addition of all nanoparticles (Figure 3.3 for **NP3**, for the others refer Figure 3.S1). The absorption effect of gold cores was obtained through control experiments using neutral particles[26] and the normalized fluorescence intensities of **PPE-CO$_2$** at 465 nm were subsequently plotted versus the ratio of nanoparticle to polymer. The complex stability constants (K_S) and association stoichiometries (n) were obtained through nonlinear least-squares curve-fitting analysis (Table 3.1). [24] Complex stabilities vary within *ca.* one order of magnitude ($\Delta\Delta G \sim 6$ kJ mol^{-1}), while the binding stoichiometry ranges from 0.8 for **NP6** to 2.9 for **NP2**. The observation indicates that the subtle structural changes of nanoparticle end groups significantly affect their affinity for the polymer. Significantly, all particle-polymer conjugates were optically transparent over the concentration range studied.

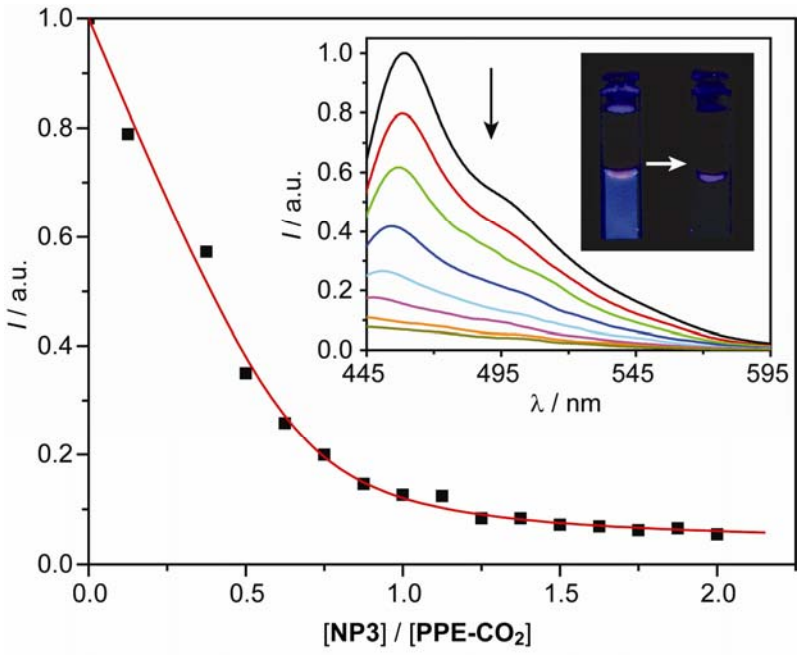

Figure 3.3 Fluorescence intensity changes of **PPE-CO_2** (100 nM) at 465 nm upon addition of cationic **NP3**. To eliminate the absorption effect of gold core, the fluorescence intensity was calibrated with that in the presence of respective concentrations of tetra(ethylene glycol)-functionalized gold nanoparticle which does not associate with **PPE-CO_2**. Inset shows the fluorescence spectra and the images of **PPE-CO_2** solution before and after addition of **NP3**.

Table 3.1 Binding constants (log K_S) and binding stoichiometries (n) between polymer **PPE-CO_2** and various cationic nanoparticles (**NP1**-**NP6**) as determined from fluorescence titration.

Nanoparticle	K_S / 10^8 M^{-1}	$-\Delta G$ / kJ mol^{-1}	n
NP1	3.0	48.4	2.0
NP2	2.1	47.5	2.9
NP3	1.7	47.0	1.5
NP4	21.0	53.2	1.8
NP5	3.6	48.8	2.4
NP6	25.0	53.6	0.8

Once the different binding characteristics of **PPE-CO_2** with **NP1**-**NP6** were established, the particle-polymer conjugates were used to sense proteins. The proteins

were chosen to display a variety of sizes and charges: the isoelectric points (pI) of the seven proteins vary from 4.6 to 10.7 and molecular weights range from 12.3 to 540 kDa. Within this set there are several pairs of proteins that have comparable molecular weights and/or pI values, providing a challenging testbed for protein discrimination. In the initial sensing study, 200 μL of fluorescent polymer **PPE-CO_2** (100 nM) and stoichiometric nanoparticles **NP1**-**NP6** (the stoichiometric values were taken from Table 3.1) were respectively loaded onto 96-well plates for recording the initial fluorescence intensities at 465 nm. Under these conditions, it is estimated that > 80% of polymer is bound to the nanoparticles based on the binding constants listed in Table 3.1, allowing fluorescent enhancement via subsequent displacement. As illustrated in Figure 3.4a, addition of aliquots of protein (5 μM) resulted in a variety of fluorescence responses. By contrast, the addition of proteins (5 μM) into **PPE-CO_2** (100 nM) induces only marginal fluorescence changes (Figure 3.S2 in experimental data), confirming the disruption of nanoparticle-**PPE-CO_2** interactions by proteins. BSA, β-galactosidase, acid phosphatase and alkaline phosphatase induce different levels of fluorescence increase, while cytochrome *c*, the only metal-containing protein, further attenuates the fluorescence of the systems presumably *via* an energy or electron transfer process.[27] Lipase and subtilisin A lead to smaller but still significant fluorescence changes for most nanoparticle-PPE systems. Notably, each protein possesses a unique response pattern. Such an outcome is reasonable since their interaction with the protein-detecting array is dependent on their surface characteristics such as the distribution of hydrophobic, neutral, and charged amino acid residues. For each protein, we have tested its fluorescence responses against the six nanoparticle-PPE assemblies for six times, generating a $6 \times 6 \times 7$ matrix.

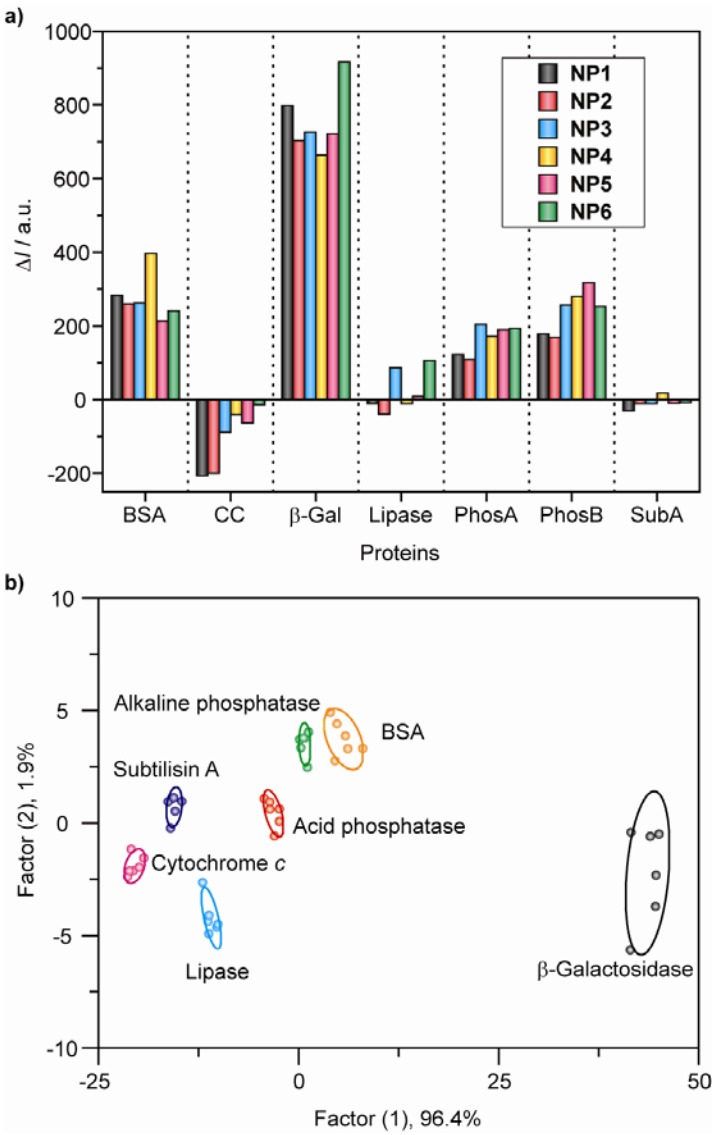

Figure 3.4 Array-based sensing of 5 μM protein analytes. a) Fluorescence response (ΔI) patterns of the **NP**-PPE sensor array (**NP1**–**NP6**) against various proteins (CC: cytochrome *c*, β-Gal: β-galactosidase, PhosA: acid phosphatase, PhosB: alkaline phosphatase, SubA: subtilisin A). Each value is an average of six parallel measurements. b) Canonical score plot for the first two factors of simplified fluorescence response patterns obtained with **NP**-PPE assembly arrays against 5 μM proteins. The canonical scores were calculated by LDA for the identification of seven proteins. The 95% confidence ellipses for the individual proteins are also shown.

The raw data obtained were subjected to linear discriminant analysis (LDA) to differentiate the fluorescence response patterns of the nanoparticle-PPE systems against the different protein targets.[28] LDA can maximize the ratio of between-class variance to the within-class variance in any particular data set thereby enabling maximal separability.

This analysis reduced the size of the training matrix (6 nanoparticles × 7 proteins × 6 replicates) and transformed them into canonical factors that are linear combinations of the response patterns (5 factors × 7 proteins × 6 replicates). The five canonical factors contain 96.4%, 1.9%, 0.8%, 0.6%, and 0.3% of the variation, respectively. The first two factors were visualized in a two-dimensional plot as presented in Figure 3.4b. In this plot, each point represents the response pattern for a single protein to the nanoparticle-PPE sensor array.

The canonical fluorescence response patterns of 5 μM proteins against the nanoparticle-PPE sensor array are clustered to seven distinct groups according to the protein analyte, with no overlap between the 95% confidence ellipses (Figure 3.4a, see also Table 3.S1 in experimental data). This result demonstrates that LDA allows the discrimination of very subtle differences in protein structure. Moreover, LDA provides in-depth quantitative analysis of the fluorescence responses of protein analytes. The assignment of the individual case was based on its Mahalanobis distances to the centroid of each group in a multidimensional space. The 42 training cases (7 proteins × 6 replicates) can be totally correctly assigned to their respective groups using LDA, giving a 100% accuracy. Furthermore, another 56 protein samples were prepared randomly and used as unknowns in a "blind" experiment, i.e. the individual performing the analysis did not know the identity of the solutions. During LDA analysis, the new cases were classified to the groups generated through the training matrix according to their Mahalanobis distances. Out of 56 cases, 54 were correctly classified, affording an identification accuracy of 96.4%. This result confirms not only the reproducibility of our

fluorescence patterns, but also the feasibility of practical application of such nanoparticle-conjugated polymer sensor array in detection and identification of proteins.

Real-world applications, however, require identification of proteins at varying concentrations. Varying protein concentrations would be expected to lead to the drastic alteration of fluorescence response patterns for the proteins, making identification of proteins with both unknown identity and concentration challenging. To enable the detection of unknown proteins, we have designed a protocol combining LDA and UV measurements. In this approach, a set of fluorescence response patterns were generated at analyte protein concentrations that generated a standard UV absorption value at 280 nm (A_{280} = 0.005), the lowest concentration that the proteins could be substantially differentiated using the given sensor array followed by LDA. Therefore, this concentration could also be treated as the detection limit of this assay, with molar concentrations ranging from 4 nM for β-galactosidase to 215 nM for cytochrome *c* (see Figure 3.5 for other proteins). In our unknown identification protocol, the A_{280} value of the protein was determined, and an aliquot subsequently diluted to A_{280} = 0.005 for recording the fluorescence response pattern against the NP-PPE sensing array. Once the identity of the protein was established by LDA, its initial concentration could be determined from the initial A_{280} value and corresponding molar extinction coefficient (ε_{280}) according to Beer-Lambert Law.

The fluorescence response patterns where the protein concentration is A_{280} = 0.005 are distinctly different from those generated from 5 μM of proteins, but retain a high degree of reproducibility (Figure 3.5a, see also Table 3.S2 in experimental data). As before, LDA accurately differentiate the protein patterns. As shown in Figure 3.5b, the

canonical fluorescence response patterns display excellent separation, except for a minor overlap between lipase and subtilisin A. According to the Jackknifed classification matrix, only one subtilisin A sample is misclassified, affording a classification accuracy of 97.6% (41 out of 42). As a control, analogous analyses were performed using polymer ([**PPE-CO$_2$**] = 100 nM) in the absence of nanoparticles. These studies show that the polymer itself can only substantially differentiate cytochrome *c*,[27] the metalloprotein, from the other proteins (see ESI). For the other six proteins, merely 50% classification accuracy is obtained on the basis of 6 replicates of measurement, only modestly higher than the statistical possibility (i.e. 17%). A further in-depth examination on the classification accuracy of the polymer in the absence and presence of individual nanoparticles revealed that the latter generally afforded better differentiation abilities than the former (see Tables 3S3 and 3S4 in Experimental data), demonstrating the role of the nanoparticle in providing selectivity, and hence the differentiation between proteins required for effective sensing.

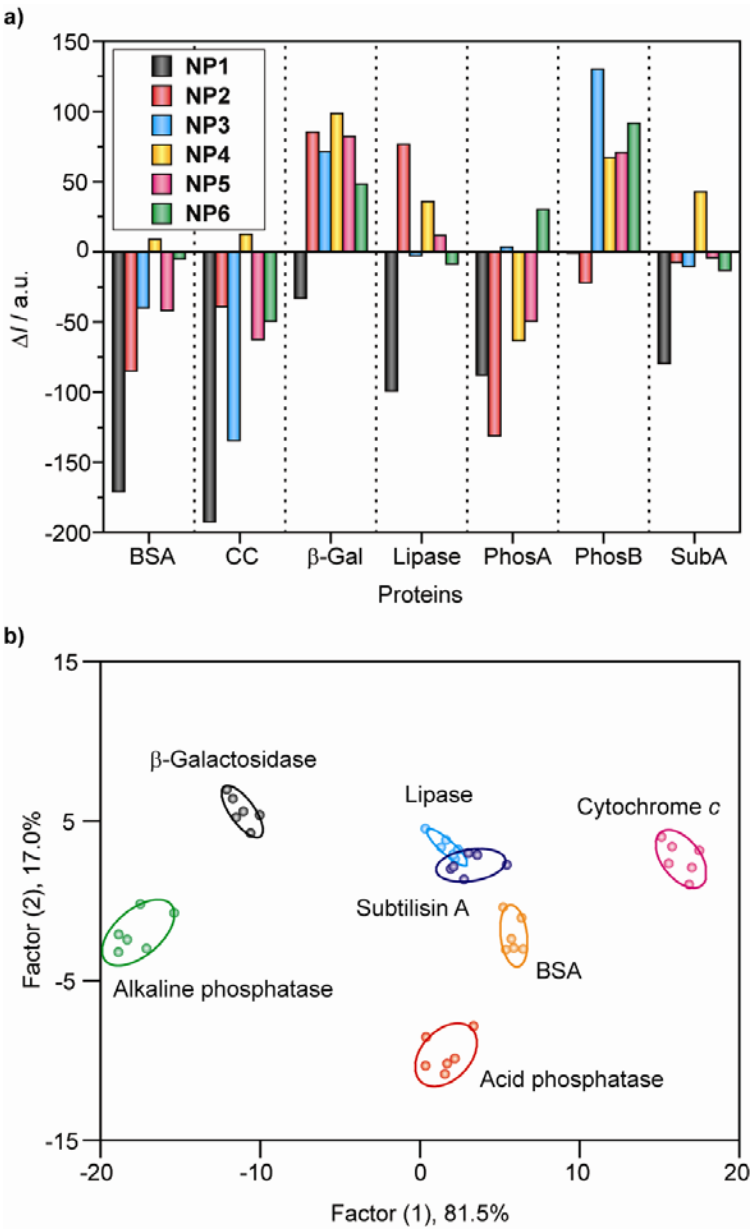

Figure 3.5 Array-based sensing of protein analytes with identical absorbance at 280 nm. a) Fluorescence response (ΔI) patterns of the **NP**-PPE sensor array. b) Canonical score plot for the first two factors of simplified fluorescence response patterns obtained with **NP**-PPE assembly arrays against proteins with identical absorption values of A = 0.005 at 280 nm. The canonical scores were calculated by LDA for the identification of seven proteins, with 95% confidence ellipses for the individual proteins shown. [BSA] = 110 nM; [cytochrome c] = 215 nM; [β-galactosidase] = 4 nM; [lipase] = 90 nM; [acid phosphatase] = 20 nM; [alkaline phosphotase] = 80 nM; [Subtilisin A] = 190 nM.

A series of unknown protein solutions were subsequently used for quantitative detection. To facilitate solution preparation and UV-vis measurement, the unknown

proteins were prepared at varying concentrations (120 nM - 50 μM). In principle, lower concentrations can also be employed since the detection limit of this method is nanomolar (*vide supra*). The unknown protein solutions were submitted to the testing procedures including determination of A_{280}, dilution of solution to A_{280} = 0.005, fluorescence response recording against the sensor array, and LDA. Of the 52 unknown protein samples; only 3 samples were incorrectly identified, affording an identification accuracy of 94.2% (see Table 3.S5 for original data). In addition, the protein concentration was assessed generally within ±5% once it was identified (Table 3.S5). This result unambiguously manifests that our sensor array holds substantial promise for both the identification and quantification of protein analytes.

3.3 Conclusion

In conclusion, we have demonstrated that the assemblies of gold nanoparticles with fluorescent PPE polymer provide efficient sensors of proteins, achieving both detection and identification of analytes. This strategy exploits the size and tunability of the nanoparticle surface to provide selective interactions with proteins, and the efficient quenching of fluorophores by the metallic core to impart efficient transduction of the binding event. Through application of linear discriminant analysis, we are able to use these fluorescence changes to identify and quantify proteins in a rapid, efficient, and general fashion. The robust characteristics of the nanoparticle and polymer components coupled with diversity of surface functionality that can be readily obtained using nanoparticles makes this array approach a promising technique to biomedical diagnostics.

3.4 Experimental Section

3.4.1 Metods, Instrumentation and Materials

Carboxylate-substituted PPE (**PPE-CO_2**) was synthesized according to the reported procedure.[25] The weight and number average molecular weights of the polymer are 6600 and 3500, respectively. The polydispersity index (PDI) and degree of polymerization of the conjugated polymer are 1.88 and 12, respectively. Thiol ligands bearing ammonium end groups were synthesized through the reaction of 1,1,1-triphenyl-14,17,20,23-tetraoxa-2- thiapentacosan-25-yl methanesulfonate with corresponding substituted *N*,*N*-dimethylamines followed by deprotection in the presence of trifluoroacetic acid (TFA) and triisopropylsilane (TIPS). Subsequent place-exchange reaction with petanethiol-coated gold nanoparticles ($d \sim 2$ nm)[29] afforded cationic gold nanoparticles **NP1**-**NP6** in high yields. ^{1}H NMR investigation revealed that the place-exchange reaction proceeds almost quantitatively and the coverage of cationic ligands on the nanoparticles is near unit. Bovine serum albumin (BSA), cytochrome *c* (from horse heart), β-galactosidase (from *E. coli*), lipase (from *Candida rugosa*), acid phosphatase (from potato), alkaline phosphatase (from bovine intestinal mucosa), and subtilisin A (from *Bacillus licheniformis*) were purchased from Sigma-Aldrich and used as received. Phosphate buffered saline (PBS, pH 7.4, 1×) was purchased from Invitrogen and used as the solvent throughout the fluorescence assays.

In the fluorescence titration study, fluorescence spectra were measured in a conventional quartz cuvette (10 × 10 × 40 mm) on a Shimadzu RF-5301 PC spectrofluorophotometer at room temperature (ca. 25 °C). During the titration, 2 mL of **PPE-CO_2** (100 nM) was placed in the cuvette and the initial emission spectrum was

recorded with excitation at 430 nm. Aliquots of a solution of **PPE-CO_2** (100 nM) and nanoparticles were subsequently added to the solution in the cuvette. After each addition, a fluorescence spectrum was recorded. The normalized fluorescence intensities calibrated by respective controls (tetra(ethylene glycol)-functionalized neutral nanoparticle with the same core) at 465 nm were plotted against the molar ratio of nanoparticle to **PPE-CO_2**. Nonlinear least-squares curve-fitting analysis was conducted to estimate the complex stability as well as the association stoichiometry using a calculation model in which the nanoparticle is assumed to possess *n* equivalent and independent binding sites.[19]

In the protein sensing study, fluorescent polymer **PPE-CO_2** and stoichiometric nanoparticles **NP1**-**NP6** (determined by fluorescence titration, ref. Table 1) was placed into six separate glass vials and diluted with PBS buffer to afford mixture solutions where the final concentration of **PPE-CO_2** was 100 nM. Then each solution (200 μL) was respectively loaded into a well on a 96-well plate (300 μL Whatman® Glass Bottom microplate) and the fluorescence intensity value at 465 nm was recorded on a Molecular Devices SpectraMax M5 micro plate reader with excitation at 430 nm. Subsequently, 10 μL of protein stock solution (105 μM) was added to each well (final concentration 5 μM) and the fluorescence intensity values at 465 nm were recorded again. The difference between two reads before and after addition of proteins is treated as the fluorescence response. Such process was repeated for seven protein targets to generate six replicates of each. Thus, the seven proteins were tested against the six nanoparticle array (**NP1**-**NP6**) six times to give a 6 × 6 × 7 training data matrix. The raw data matrix was processed using a classical linear discriminant analysis (LDA) in SYSTAT (version

11.0). Similar procedures were also performed to identify 56 randomly selected protein samples.

In the studies featuring unknown analyte protein concentrations, the sensor array was tested against 7 proteins (A_{280} = 0.005) for 6 times to generate the training data matrix. Fifty-two unknown protein solutions were subjected successively to UV absorption measurement at 280 nm, dilution to A_{280} = 0.005, fluorescence response pattern recording against the sensor array, and LDA. After the protein identity was recognized by LDA, the initial protein concentration (c) was deduced from the A_{280} value and corresponding molar extinction coefficient (ε_{280}) on the basis of Beer-Lambert Law ($c = A_{280}/(\varepsilon_{280} \cdot l)$). In the experimental setup, the protein samples were randomly selected from the 7 protein species and the solution preparation, data collection and LDA analysis were performed by different persons.

3.4.2 Experimental data

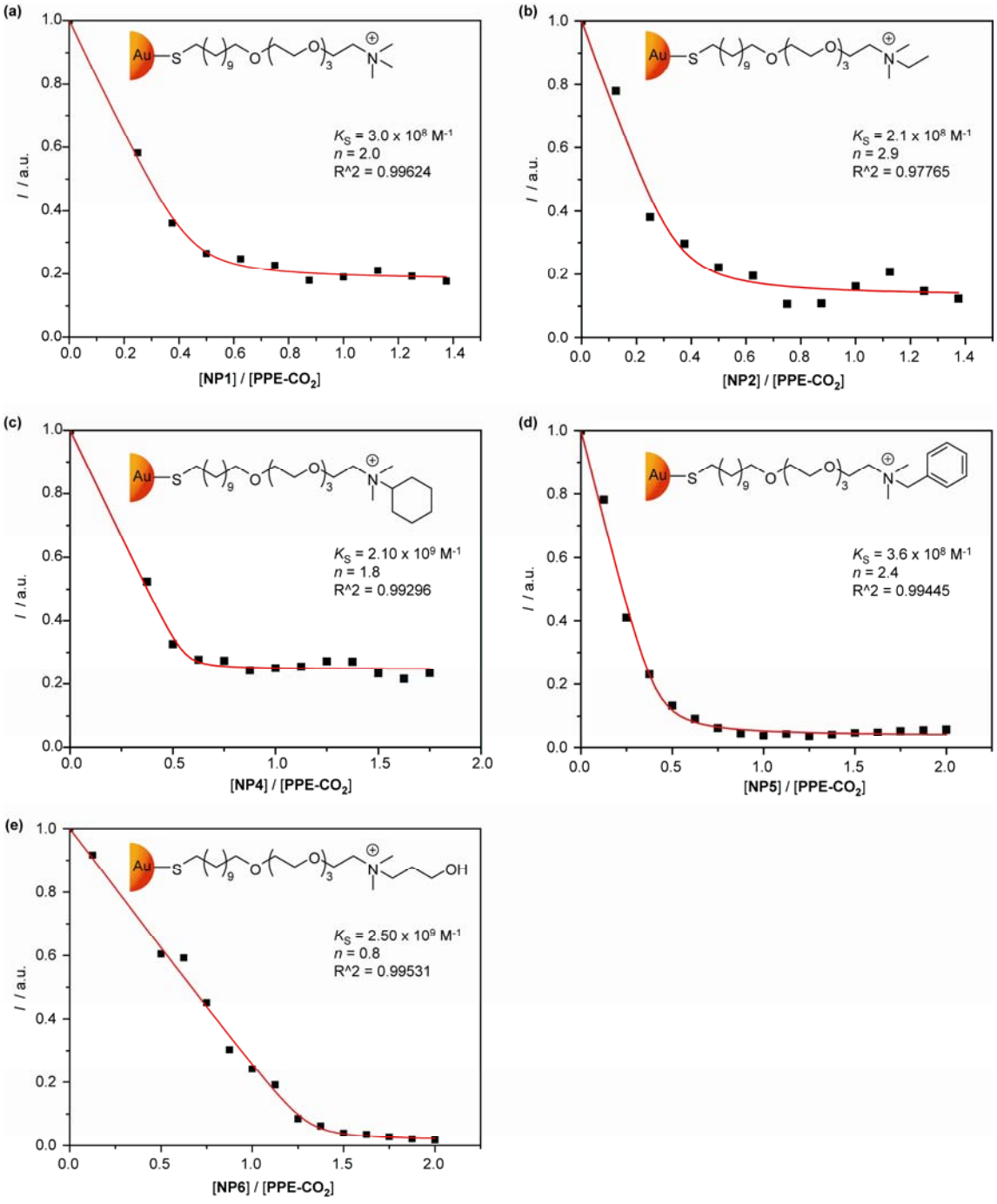

Figure 3.S1 Fluorescence titration curves for the complexation of **PPE-CO$_2$** (100 nM) with various cationic gold nanoparticles. The intensity changes at 465 nm were followed by the addition of various concentrations of **NP**s with an excitation wavelength of 430 nm. The red solid lines represent the best curve-fitting using a calculation model of single set of identical binding sites.

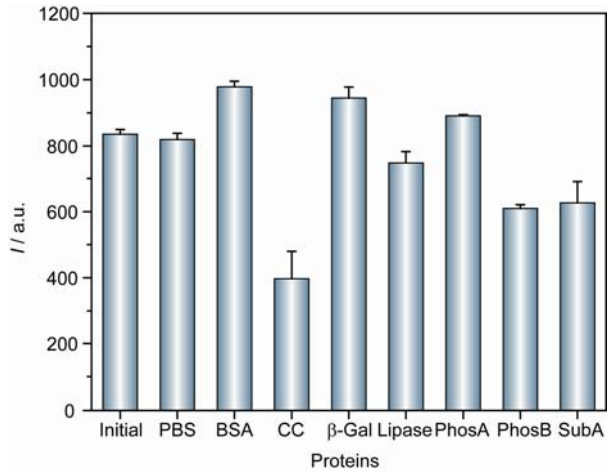

Figure 3.S2 Fluorescence intensities of **PPE-CO_2** (100 nM, 200 μL) in the 96-well microplate upon addition of PBS (10 μL) or various protein solutions (10 μL, 105 μM). The intensities were recorded at 465 nm with an excitation wavelength of 430 nm.

Table 3.S1 Training matrix of fluorescence response patterns of NP-PPE sensor array (**NP1** – **NP6**) against various proteins (5 μM). Table continues on the next page.

Protein	**NP1**	**NP2**	**NP3**	**NP4**	**NP5**	**NP6**
BSA	257.301	225.6705	264.481	414.337	232.6915	271.8175
BSA	340.96	306.497	286.159	389.051	255.113	289.169
BSA	286.309	269.784	298.041	375.189	277.446	266.679
BSA	274.95	230.364	270.385	385.978	270.743	255.996
BSA	248.114	227.807	219.887	406.811	118.506	205.777
BSA	289.53	301.474	233.368	411.579	126.498	156.355
Cytochrome *c*	-173.239	-243.7695	-98.33	-42.106	-67.827	-6.100
Cytochrome *c*	-212.689	-253.748	-96.444	-50.032	-70.193	-11.864
Cytochrome *c*	-211.989	-176.255	-96.533	-28.81	-75.472	-10.474
Cytochrome *c*	-226.049	-249.75	-101.088	-39.883	-56.252	-2.608
Cytochrome *c*	-218.562	-159.429	-89.063	-45.986	-53.261	-27.726
Cytochrome *c*	-194.438	-113.668	-48.999	-37.641	-56.521	-22.668
β-Galactosidase	685.72	717.134	675.0985	540.824	669.4222	922.738
β-Galactosidase	799.231	718.938	755.872	658.867	775.697	953.258
β-Galactosidase	749.614	732.453	695.919	734.933	710.618	902.833
β-Galactosidase	889.984	646.159	717.96	637.393	712.389	954.118
β-Galactosidase	864.656	656.946	733.992	661.197	731.902	871.314
β-Galactosidase	805.633	747.617	779.35	744.682	729.5	895.446
Lipase	-43.738	-39.656	91.944	-22.739	-1.6697	106.3148
Lipase	-2.394	-59.968	96.99	1.132	15.709	126.414
Lipase	89.814	-129.488	89.227	-14.037	-2.891	105.287
Lipase	3.47	-9.823	111.726	-9.262	5.724	108.542
Lipase	-56.325	-3.53	69.104	-1.982	34.993	88.651
Lipase	-57.092	7.63	63.602	-17.495	0.618	100.479
Acid phosphatase	94.092	91.365	201.777	175.071	200.925	180.196
Acid phosphatase	122.214	102.202	199.684	181.79	193.317	214.438
Acid phosphatase	107.14	109.187	248.382	160.445	177.163	188.247
Acid phosphatase	127.16	111.545	196.917	174.477	186.309	181.137
Acid phosphatase	151.778	136.102	183.673	174.045	186.81	202.74
Acid phosphatase	131.67	99.933	195.84	163.312	194.355	192.107
Alkaline phosphatase	213.327	147.464	292.456	255.852	318.939	263.11

Alkaline phosphatase	190.598	135.389	230.212	279.278	311.824	252.339
Alkaline phosphatase	160.721	205.114	245.772	285.58	311.061	248.009
Alkaline phosphatase	142.322	160.667	251.252	272.127	326.608	258.939
Alkaline phosphatase	175.056	170.559	268.359	287.199	317.05	243.648
Alkaline phosphatase	184.905	193.269	249.972	297.744	315.026	250.946
Subtilisin A	-30.425	6.563	-22.139	11.007	-3.126	-9.373
Subtilisin A	-36.602	-28.967	4.15	13.281	0.197	-16.321
Subtilisin A	-38.18	-2.424	-10.839	12.274	-6.559	-0.836
Subtilisin A	-18.079	-1.368	-22.089	21.301	-12.414	-11.739
Subtilisin A	-48.413	-38.422	13.29	6.327	-28.12	-13.824
Subtilisin A	-9.517	0.942	-25.906	39.032	-12.308	5.541

Table 3.S2 Training matrix of fluorescence response patterns of NP-PPE sensor array (**NP1**–**NP6**) against various proteins with identical absorption values of $A = 0.005$ at 280 nm. Table continues on the next page.

Protein	**NP1**	**NP2**	**NP3**	**NP4**	**NP5**	**NP6**
BSA	-207.251	-80.4074	-41.0494	3.556583	-41.3954	-3.76742
BSA	-152.201	-77.1674	-55.7804	-1.94342	-49.7074	4.588583
BSA	-251.316	-0.11142	-31.9444	25.40958	-39.3404	-11.0144
BSA	-98.0724	-65.7634	-43.7164	22.97658	-43.5624	-7.16342
BSA	-211.026	-66.2634	-39.8604	-7.87942	-43.6464	-3.81042
BSA	-105.233	-220.02	-26.8694	10.40658	-33.0744	-9.22942
Cytochrome *c*	-172.652	-50.1355	-146.265	10.8245	-47.6265	-40.3145
Cytochrome *c*	-190.972	-82.9625	-137.953	3.2665	-73.4645	-47.1625
Cytochrome *c*	-232.23	4.8425	-140.34	2.4305	-73.3435	-49.6205
Cytochrome *c*	-230.869	-122.978	-145.803	34.3415	-67.2365	-57.2915
Cytochrome *c*	-164.136	10.4385	-122.127	0.3655	-60.3585	-48.4655
Cytochrome *c*	-163.889	6.6535	-116.073	23.3225	-52.0905	-54.5375
β-Galactosidase	19.0285	107.7135	60.0105	113.7165	83.2875	61.1885
β-Galactosidase	9.1095	96.5955	77.4785	125.5305	53.7755	39.4995
β-Galactosidase	-19.4815	101.9385	69.9525	73.7525	94.1465	47.2445
β-Galactosidase	1.2955	41.5925	74.2685	123.5115	94.1875	49.3605
β-Galactosidase	-196.846	119.6175	62.6425	61.8325	80.0215	48.0035
β-Galactosidase	-11.7785	44.9365	83.1515	92.8155	88.1445	43.2705
Lipase	-79.0774	86.93458	-6.73842	27.82958	2.912583	-6.25842
Lipase	-42.0344	73.02458	-0.80742	24.90658	10.39558	-10.2144
Lipase	-134.166	26.16258	-0.72042	51.70958	12.93158	-13.5724
Lipase	-23.2854	96.48058	-3.04842	32.51358	4.503583	-10.3044
Lipase	-120.295	90.46358	-0.58542	57.46258	18.25058	-2.08742
Lipase	-196.312	86.72058	-4.36842	20.83658	20.81058	-8.69742
Acid phosphatase	-128.351	-188.015	2.1795	-79.1105	-46.9325	31.7065
Acid phosphatase	-77.2075	-44.4985	4.4975	-75.2075	-60.4315	28.5805
Acid phosphatase	-86.9055	-146.495	4.1835	-56.7145	-59.1445	31.3135
Acid phosphatase	-99.9655	-119.904	-8.0655	-62.6845	-42.9485	15.1155
Acid phosphatase	-111.126	-122.595	4.9705	-70.9985	-25.8015	33.4465
Acid phosphatase	-22.4615	-165.882	12.7355	-35.2555	-62.1085	40.8975
Alkaline phosphatase	28.025	45.951	142.938	71.48	77.665	77.528
Alkaline phosphatase	-14.702	-43.38	118.72	56.961	64.276	97.109
Alkaline phosphatase	-31.212	-32.501	105.815	81.159	62.164	82.984
Alkaline phosphatase	18.479	-30.982	119.467	63.77	73.137	106.726
Alkaline phosphatase	-13.647	-44.002	151.862	61.725	69.491	90.719
Alkaline phosphatase	7.936	-26.84	142.162	68.08	76.484	94.309
Subtilisin A	-131.396	25.0715	1.9835	47.1915	-6.7715	-10.0785
Subtilisin A	-2.9055	-10.7465	11.8125	47.2905	-15.1505	-17.8985

Subtilisin A	-78.4445	-41.6635	-32.2655	29.5855	12.6455	-7.0365
Subtilisin A	-80.4355	-30.6755	-24.3905	33.4205	-10.8945	-24.7975
Subtilisin A	-9.2595	7.0255	-13.5505	43.6225	-0.6355	1.8175
Subtilisin A	-175.215	4.4625	-6.6085	55.0065	-5.0035	-19.8595

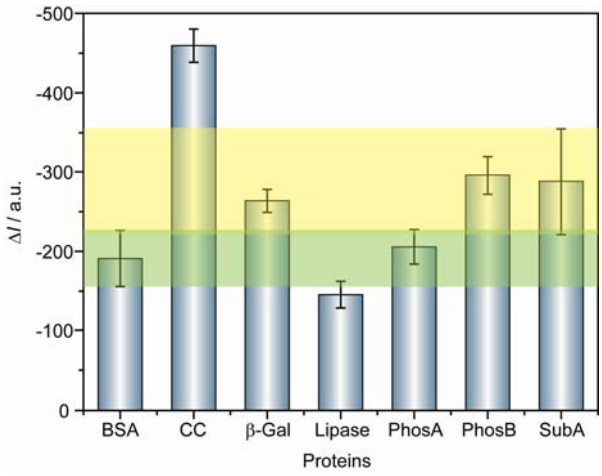

Figure 3.S3 Fluorescence responses (ΔI) of fluorescent polymer **PPE-CO$_2$** (100 nM) against various proteins with identical absorbance of A = 0.005 at 280 nm (BSA, 110 nM; CC: cytochrome *c*, 215 nM; β-Gal: β-galactosidase, 4 nM; Lipase, 90 nM; PhosA: acid phosphatase, 20 nM; PhosB: alkaline phosphatase, 80 nM; SubA: subtilisin A, 190 nM). Each fluorescence response value is an average of six parallel measurements. There are significant response overlaps between the proteins except for CC, as denoted by the shaded regions. LDA analysis on the raw data affords only a 57% classification accuracy.

Table 3.S3 LDA classification accuracy of protein analytes (5 μM) by using the fluorescent polymer and the complexes of the fluorescent polymer with individual nanoparticles as sensors. The values are taken from the Jackknifed classification matrix based on LDA analysis of the raw data (6 replicates) listed in Figure 3.S2 and Table 3.S1. The average classification accuracy of 6 polymer-nanoparticle complexes is 81.5%.

Proteins	Polymer	Polymer/**NP1**	Polymer/**NP2**	Polymer/**NP3**	Polymer/**NP4**	Polymer/**NP5**	Polymer/**NP6**
BSA	83	100	100	50	100	33	0
CC	100	100	83	83	100	100	50
β-Gal	83	100	100	100	83	100	100
Lipase	100	33	33	100	100	67	100
PhosA	100	83	83	83	100	83	100
PhosB	33	83	83	50	100	100	83
SubA	0	67	67	100	100	83	50
Total	71	81	79	81	98	81	69

Table 3.S4 LDA classification accuracy of protein analytes (A_{280} = 0.005) by using the fluorescent polymer and the complexes of the fluorescent polymer with individual nanoparticles as sensors. The values are taken from the Jackknifed classification matrix based on LDA analysis of the raw data (6 replicates) listed in Figure 3.S3 and Table 3.S2. The average classification accuracy of 6 polymer-nanoparticle complexes is 61.5%.

Proteins	Polymer	Polymer/**NP1**	Polymer/**NP2**	Polymer/**NP3**	Polymer/**NP4**	Polymer/**NP5**	Polymer/**NP6**
BSA	17	17	67	100	67	83	50
CC	100	50	17	100	17	67	100
β-Gal	83	17	67	100	67	83	83
Lipase	83	17	17	83	33	83	50
PhosA	50	17	83	83	100	17	83
PhosB	50	83	17	100	100	67	100
SubA	17	33	67	17	50	83	50
Total	57	33	48	83	62	69	74

Table 3.S5 Detection and identification of unknown proteins using LDA combined with UV measurements.[a] Table continues on the next page.

#	Fluorescence response pattern						Identification			Verification	
	NP1	**NP2**	**NP3**	**NP4**	**NP5**	**NP6**	Protein	A_{280}	Conc.	Protein/Conc.	Deviation
1	-55.3435	51.7795	-16.3605	26.5705	-4.4815	-2.796	SubA	1.2182	46.8 μM	SubA/48.6 μM	-3.7%
2	-159.922	-200.188	-33.567	-1.8505	-27.8385	15.6485	BSA	0.96539	20.6 μM	BSA/20.7 μM	-0.5%
3	60.447	24.348	-22.804	-51.3415	-27.869	46.857	PhosA	0.28217	1.09 μM	PhosA/1.15 μM	-5.2%
4	18.986	4.8175	30.6935	82.7865	86.03	55.373	β-Gal	0.16012	141.9 nM	β-Gal/132.5 nM	+7.1%
5	-153.174	76.981	-107.443	39.1415	-43.0145	-20.585	CC	0.27177	11.7 μM	CC/11.6 μM	+0.9%
6	140.3665	77.798	125.5305	57.021	29.3225	97.9345	PhosB	1.10921	17.7 μM	PhosB/18.2 μM	-2.7%
7	30.9535	-73.4045	-24.526	-58.722	-32.537	41.9955	PhosA	0.57403	2.23 μM	PhosA/2.29 μM	-2.6%
8	-32.722	-83.1245	1.01	26.369	-16.3085	-6.646	SubA	0.91653	35.2 μM	SubA/36.4 μM	-3.3%
9	-170.571	-176.652	-2.443	-10.5135	-20.1085	4.8575	BSA	0.25960	5.54 μM	BSA/5.17 μM	+7.2%
10	110.9075	75.605	120.6435	58.417	38.8035	96.4325	PhosB	0.84386	13.4 μM	PhosB/13.7 μM	-2.2%
11	-52.4345	-90.4335	-31.8315	39.614	-40.355	7.283	BSA	0.21278	4.54 μM	BSA/4.27 μM	+6.3%
12	132.2205	14.8855	48.0685	88.9575	60.5765	46.69	β-Gal	0.30713	272.1 nM	β-Gal/265.1 nM	+2.6%
13	-53.007	-26.357	2.4935	-0.6355	-18.5085	-2.031	SubA	0.64011	24.6 μM	SubA/24.3 μM	+1.2%
14	-89.257	-30.347	-95.7465	29.4355	-42.224	-25.484	CC	0.51375	22.1 μM	CC/23.7 μM	-6.8%
15	74.92	34.4575	122.4875	58.0585	30.54	90.445	PhosB	0.58285	9.32 μM	PhosB/9.11 μM	+2.3%
16	69.74	-59.9385	-22.9405	-54.0895	-38.892	46.379	PhosA	0.87457	3.39 μM	PhosA/3.44 μM	-1.5%
17	-46.589	-41.161	-45.58	28.9365	-18.155	-5.202	SubA	1.03644	39.8 μM	BSA/22.2 μM	Fail
18	-1.3855	123.234	40.306	104.191	53.1025	60.338	β-Gal	0.45375	402.0 nM	β-Gal/397.6 nM	+1.1%
19	8.744	-47.9015	-10.503	23.4455	-2.786	-0.551	SubA	0.29871	11.5 μM	SubA/12.1 μM	-5.0%
20	-127.88	10.989	-111.602	25.039	-42.7185	-31.055	CC	1.10620	47.4 μM	CC/47.4 μM	0%
21	80.646	77.4045	122.2085	49.6575	28.364	108.999	PhosB	0.30431	4.85 μM	PhosB/4.55 μM	+6.6%
22	-34.1755	-62.086	-39.003	-49.7855	-42.4565	47.0585	PhosA	1.12450	4.36 μM	PhosA/4.58 μM	-4.8%
23	-171.657	26.51	-108.075	33.099	-54.846	-23.0465	CC	0.22161	9.55 μM	CC/10.7 μM	-10.7%
24	66.1835	65.6285	43.726	85.35	63.9405	58.366	β-Gal	0.60837	539.0 nM	β-Gal/530.2 nM	+1.7%
25	-62.507	-77.425	-13.4925	-67.5525	-53.5785	45.438	PhosA	1.13410	4.40 μM	PhosA/4.37 μM	+0.7%
26	125.019	99.546	94.4245	92.824	95.8115	67.8245	β-Gal	0.13440	119.1 nM	β-Gal/114.6 nM	+3.9%
27	67.929	6.440	-24.355	21.209	5.599	9.609	SubA	0.28359	10.9 μM	Lipase/5.05 μM	Fail
28	-44.821	-8.148	-12.4455	42.5155	-8.811	19.273	SubA	0.31565	12.1 μM	SubA/11.5 μM	+5.2%
29	-1.7445	-53.0475	134.7005	77.0995	26.2465	93.0025	PhosB	1.16620	18.6 μM	PhosB/18.4 μM	+1.1%
30	-12.801	-213.077	-26.6465	14.8225	-20.1955	3.6715	BSA	0.31933	6.81 μM	BSA/6.40 μM	+6.4%
31	113.935	22.192	108.781	67.868	52.256	88.252	PhosB	0.89032	14.2 μM	PhosB/13.8 μM	+2.9%
32	-49.831	-201.661	-13.814	-70.416	-21.3195	42.461	PhosA	0.88471	3.43 μM	PhosA/3.27 μM	+4.9%

33	120.276	127.391	100.1595	73.635	79.0325	59.9445	β-Gal	0.27235	241.3 nM	β-Gal/229.1 nM	+5.3%
34	-37.397	-27.0225	16.458	27.685	5.337	-5.986	SubA	0.58273	22.4 μM	SubA/22.9 μM	-2.2%
35	4.1795	11.8585	139.236	85.6165	17.748	94.747	PhosB	0.87407	13.9 μM	PhosB/13.8 μM	+0.7%
36	-3.5925	-92.691	-34.049	12.4535	-36.709	19.2155	BSA	0.61183	13.1 μM	BSA/12.8 μM	+2.3%
37	35.837	9.911	-9.081	15.321	6.598	5.385	Lipase	0.58135	10.7 μM	Lipase/10.1 μM	+7.9%
38	30.6755	16.9725	98.9435	63.948	113.2	59.3525	β-Gal	0.38936	345.0 nM	β-Gal/344.8 nM	+0.1%
39	-58.207	-152.25	-15.833	18.004	-25.175	1.521	BSA	0.89327	19.1 μM	BSA/19.2 μM	-0.5%
40	-43.3685	-71.0225	-20.966	-70.314	-44.754	40.6875	PhosA	0.59783	2.32 μM	PhosA/2.18 μM	+6.4%
41	-11.573	-6.737	8.481	18.5585	20.9805	-8.1385	Lipase	0.91641	16.9 μM	SubA/34.5 μM	Fail
42	3.5915	-32.2335	152.74	48.9305	33.6155	98.29	PhosB	0.58425	9.31 μM	PhosB/9.22 μM	+1.0%
43	2.341	69.094	83.720	67.793	64.218	38.548	β-Gal	0.27904	247.2 μM	β-Gal/249.7 nM	-1.0%
44	-41.8565	-138.779	-20.7295	-75.9705	-26.236	54.806	PhosA	0.24280	941 nM	PhosA/1.09 μM	-13.7%
45	9.074	-60.2835	166.391	54.379	35.2185	113.06	PhosB	0.30505	4.86 μM	PhosB/4.61 μM	+5.4%
46	32.227	99.8215	96.609	77.601	94.505	68.7545	β-Gal	0.50911	451.1 nM	β-Gal/458.3 nM	-1.6%
47	27.6605	-39.711	1.79	18.2735	5.9905	-5.728	SubA	1.16410	44.7 μM	SubA/46.0 μM	-2.8%
48	-74.983	-150.324	-70.2795	24.0015	-55.487	-25.0155	BSA	1.30270	27.8 μM	BSA/25.7 μM	+8.6%
49	-29.81	71.8155	3.726	25.9465	2.937	-6.1615	Lipase	1.13742	20.9 μM	Lipase/20.2 μM	+3.5%
50	-61.873	99.490	80.315	81.070	77.443	36.694	β-Gal	0.45795	405.8 nM	β-Gal/374.6 nM	+8.3%
51	2.728	10.573	-9.496	23.268	12.090	15.387	Lipase	0.84971	15.6 μM	Lipase/15.2 μM	+2.6%
52	94.083	-32.448	117.772	74.158	73.077	104.623	PhosB	0.59023	9.40 μM	PhosB/9.23 μM	+1.8%

[a] BSA: bovine serum albumin, ε (280 nm) = 46860 M^{-1} cm^{-1}; CC: cytochrome *c*, ε (280 nm) = 23200 M^{-1} cm^{-1}; β-Gal: β-galactosidase, ε (280 nm) = 1128600 M^{-1} cm^{-1}; Lipase: ε (280 nm) = 54350 M^{-1} cm^{-1}; PhosA: acid phosphatase, ε (280 nm) = 257980 M^{-1} cm^{-1}; PhosB: alkaline phosphatase, ε (280 nm) = 62780 M^{-1} cm^{-1}; SubA: subtilisin A, ε (280 nm) = 26030 M^{-1} cm^{-1}.

3.5 References

1. Daniels, M. J.; Wang, Y.; Lee, M.-Y; Venkitaraman, A. R. *Science* **2004**, 306, 876.
2. Ross, J. S.; Fletcher, J. A. *Stem Cells* **1998**, 16, 413.
3. Haab, B. B. *Curr. Opin. Biotech.* **2006**, 17, 415.
4. Albert, K. J.; Lewis, N. S.; Schauer, C. L.; Sotzing, G. A.; Stitzel, S. E.; Vaid, T. P; Walt, D. R. *Chem. Rev.* **2000**, 100, 2595.
5. Lee, J. W.; Lee, J. S.; Kang, M.; Su, A. I.; Chang, Y. T. *Chem. Eur. J.* **2006**, 12, 5691.
6. Rakow, N. A; Suslick, K. S. *Nature* **2000**, 406, 710.
7. Greene, N. T.; Shimizu, K. D. *J. Am. Chem. Soc.* **2005**, 127, 5695.
8. Folmer-Andersen, J. F.; Kitamura M.; Anslyn E. V. *J. Am. Chem. Soc.* **2006**, 128, 5652.
9. Buryak, A.; Severin, K. A. *J. Am. Chem. Soc.* **2005**, 127, 3700.
10. Wright, A. T.; Anslyn, E. V. *Chem. Soc. Rev.* **2006**, 35, 14.
11. Lee, J. W.; Lee, J.-S.; Chang, Y.-T. *Angew. Chem. Int. Ed.* **2006**, 45, 6485.

12. Baldini, L.; Wilson, A. J.; Hong, J.; Hamilton, A. D. *J. Am. Chem. Soc.* **2004**, 126, 5656.

13. Zhou, H.; Baldini, L.; Hong, J.; Wilson, A. J.; Hamilton, A. D. *J. Am. Chem. Soc.* **2006**, 128, 2421.

14. Wright, A. T.; Griffin, M. J.; Zhong, Z.; McCleskey, S. C.; Anslyn, E. V.; McDevitt, J. T. *Angew. Chem. Int. Ed.* **2005**, 44, 6375.

15. You, C.-C.; Verma, A.; Rotello, V. M. *Soft Matter* **2006**, 2, 190.

16. Rosi, N. L.; Mirkin C. A. *Chem. Rev.* **2005**, 105, 1547.

17. Katz, E.; Willner I. *Angew. Chem. Int. Ed.* **2004**, 43, 6042.

18. Fischer, N. O.; McIntosh, C. M.; Simard, J. M.; Rotello V. M. *Proc. Natl. Acad. Sci. USA* **2002**, 99, 5018.

19. You, C.-C.; De, M., Han; G. Rotello V. M. *J. Am. Chem. Soc.* **2005**, 127, 12873.

20. Bayraktar, H.; Ghosh, P. S.; Rotello, V. M.; Knapp, M. J. *Chem. Commun.* **2006**, 1390.

21. Nath, S.; Ghosh, S. K.; Kundu, S.; Praharaj, S.; Panigrahi, S.; Pal, T. *J. Nanoparticle Res.* **2006**, 8, 111.

22. Fan, C.; Wang, S.; Hong, J. W.; Bazan, G. C.; Plaxco, K. W.; Heeger, A. J. *Proc. Natl. Acad. Sci. USA* **2003**, 100, 6297.

23. Bunz, U. H. F. *Adv. Polym. Sci.* **2005**, 177, 1.

24. Zheng, J.; Swager, T. M. *Adv. Polym. Sci.* **2005**, 177, 151.

25. Kim, I.-B.; Dunkhorst, A.; Gilbert, J.; Bunz, U. H. F. *Macromolecules* **2005**, 38, 4560.

26. Aguila, A.; Murray, R. W. *Langmuir* **2000**, 16, 5949.

27. Sandanaraj, B. S.; Demont, R.; Aathimanikandan, S. V.; Savariar, E. N.; Thayumanavan, S. *J. Am. Chem. Soc.* **2006**, 128, 10686.

28. Jurs, P. C.; Bakken, G. A.; McClelland, H. E. *Chem. Rev.* **2000**, 100, 2649.

29. Brust, M.; Walker, M.; Bethell, D.; Schiffrin, D. J.; Whyman, R. *J. Chem. Soc. Chem. Commun.* **1994**, 801.

CHAPTER 4

SNIFFING SERUM PROTEIN IN HUMAN SERUM: A NANOPARTICLE-GFP CONJUGATE BASED ARRAY SENSING

4.1 Introduction

Personalized medicine[1] requires *personalized* diagnostics to achieve *personalized* treatment of specific diseases. While treatment with personalized drugs is the final goal, a necessary prerequisite is the early determination of the disease status and causes. It was evident that the most acute and chronic disease states will result in subtle or dramatic changes in the relative composition of a person's blood serum.[2] This hypothesis has strong support from regular clinical tools, where simple electrophoresis of plasma leads to the identification and semiquantitative "fingerprinting" of proteins that are abundant in blood serum. The presence of specific electrophoresis patterns can interpret by physicians to diagnose a significant number of disorders.[3] Changes in protein electrophoresis patterns are diagnostic for liver and renal failure, as well to states of massive malnutrition, systemic shock or other large scale inflammatory events. Simple one-dimensional agarose electrophoresis of protein serum is an effective but slow and insensitive tool for the detection of gross protein imbalances. The reason of the difficulty for the detection of protein composition in serum is arising from its complex composition. Human blood serum contains >20,000 different proteins, some of which are present in concentrations > 50 g/L such as albumin, down to specific disease markers including cardiac troponin or natriuretic peptide that are found after a myocardial infarct or in patients with congestive heart failure respectively in concentrations of 2-9 μg/L and 0.6-1.4 μg/L respective. Besides albumin, the other proteins found in plasma at high

concentrations are prealbumin (0.2- 0.4 g/L), antitrypsin (a protease inhibitor 0.5 g/L), macroglobulin (1.5-3.5 g/L), lipoprotein (3-7 g/L), transferrin (2-4 g/L), and immunoglobulins A, D, E, G (8-17 g/L). About 20 proteins constitute 99 weight% of all of the serum protein content. Table 4.1 displays the isoelectric point, molecular weight and approximate concentrations of the 20 most common proteins in human serum. Most of the serum proteins are negatively charged, but their molecular weights vary from 28 to 900 kDa. It is important to note that some of these proteins such as transferrin display a quite significant range in concentration.

Table 4.1 Approximate Weight Content of High Abundant Proteins in Serum/Plasma. [4]

Protein	gL^{-1}	Mw^a	pI^b	***Protein***	gL^{-1}	Mw^a	pI^b	***Protein***	gL^{-1}	Mw^a	pI^b
Albumin	50	65	5.2	**α-Antitrypsin**	0.5	52	5.4	**Factor H**	0.2	139	?
IgG 1-4	10	150	7.5-7.8	**C3-Complement**	0.5	180	5.8	**Ceruloplasmin**	0.2	135	4.4
Transferrin	2-4	80	5.6	**Haptoglobin**	0.2	41	5.1-7	**C4-Complement**	0.2	200	6
Fibrinogen	2	340	5.6	**Apolipoprotein A1**	0.2	28	5.4-5.6	**Complement B**	0.2	100	5.9-6.1
IgA Total	1.5	350	4.9	**Apolipoprotein B**	0.2	515	5.0-5.3	**Prealbumin**	0.2	60	?
α-Macroglobulin	1.5	750	5.3-6.3	**α-1-acid glycoprotein**	0.2	40	2.7	**C9-Complement**	0.1	71	5.60
IgM	0.5	900	5-7	**Lipoprotein(a)**	0.1	400-700	?				

a) molecular weight in kDa. b) isoelectric point.

The plasma protein composition can change for various reasons[5] such as, i) inter- and intradaily changes in serum composition, ii) age related changes in serum composition, iii) nutritional status, iv) differences in serum composition for each individual and v) disease related changes in serum composition. The detection of the vast number of proteins acquired with proteomic techniques such as surface-enhanced laser desorption/ionization (SELDI)[6] technique allows the determination of patterns of protein distribution that in comparison with normal sera may allow to find specific protein signatures for specific diseases. But here the instrumentation is expensive, the throughput

is low and the dynamic range is limited. If specific fractions of proteins are removed from the serum, then mass spectrometry is more sensitive and a tool for the discovery of hitherto unknown serum proteins. However mass spectrometry is at the moment not well suited as a high throughput tool for the economical screening of large numbers of serum samples, and is certainly unrealistic as a tool for personalized diagnostics.

With 2-D-SDS-PAGE electrophoresis, the specific proteins identified may also be sequenced.[7] Isoelectric focusing allows separation of proteins according to their charge, while in the second dimension the proteins are separable according to their molecular weight. This technique has led to the discovery of signature protein patterns in patients with ovarian carcinomas and in patients with inflammatory bowel disease.[8] But these chromatograms are examined by eye and therefore only significant changes in serum composition are recognized. Plasma proteins that are present in much smaller amounts are specifically detected by monoclonal antibodies, with enhanced troponin or myoglobin levels being used to diagnose myocardial infarcts and increased PSA antigen used to detect prostate cancers.[9] The third group is composed of specific disease markers that are present in smallquantities to signal the early stage of a specific disease or a group of disorders. In such a case the gross plasma composition may be changed either significantly or subtly. Classic examples for such markers include those for neoplastic diseases, where the debris produced by the large number of dead and therefore lysed cells significantly increases the DNA content of the plasma.[10] While the use of monoclonal is powerful, each monoclonal antibody has to be raised and can only detect one specific protein. Moreover, the technical difficulties as regards to quantification are significant.[11] We pose the hypothesis that most disease states will leave their “fingerprint” in the

overall plasma composition, leading to an altered serum content of specific proteins or protein groups. The development of generalized and easy access "serum sensors" should give fast, reliable, and accurate readings of a person's health status. A "chemical nose/tongue" strategy[12,13] provides an alternative strategy to the above methods for protein sensing. In the "nose" approach, differential interactions of analytes with a receptor array generate a pattern that is used for identification. A variety of scaffolds have been employed for array-based sensing of proteins, including oligopeptide-functionalized resins[14], substituted porphyrins[15], polymers[16, 17] and synthetic polymer-nanoparticle systems[18, 19]. While highly effective at identifying proteins, these systems generally feature high limits of detection (generally 8-40 μM) and require a large number of detector elements relative to the number of proteins sensed. Moreover, these methods have not been applied to sensing in challenging matrices such as biofluids.

4.2 Results and Discussion

In gold nanoparticle-fluorescent conjugated polymer based array we used six different functionalized cationic nanoparticles and a fluorescent polymer to detect seven target proteins at detection limit of 4 nM for β-galactosidase (β-gal) with the accuracy of 94%.[18] To provide a more effective system suitable for protein sensing in serum, we created hybrid synthetic-biomolecular sensor elements. In the sensing process an array of green fluorescent protein (GFP)-nanoparticle (**NP**) complexes generates a signature that can be employed to identify proteins in human serum. Compared to our previous sensor array using polymers, the biocompatibility of both the nanoparticles and GFP allows us to use this system without affecting the target protein conformation during their

detection[20,21]. In addition, the GFP-**NP** conjugate mimics protein-protein surface interactions, which is instrumental in reaching much lower detection limits and thus enabling detection of biomedically relevant changes in protein concentration in undiluted human serum.

Our sensing strategy relies on the electrostatic complementarity between GFP and the **NP**s. GFP is a beta barrel shaped marker protein that is negatively charged at physiological conditions (3.0 diameter x 4.0 nm length, MW = 27 KDa, pH 7.4, pI = 5.92) [22, 23], with an excitation peak at 490 nm and emission peak at 510 nm (Figure 4.1a). Due to their positive charges, the gold **NP**s complex the anionic GFP, resulting in fluorescence quenching. We hypothesized that in the presence of analyte proteins the binding equilibrium between GFP and **NP** would be altered due to competitive binding, thus modulating the fluorescence response (Figure 4.1b). The fluorescence response can be positive or negative depending on the binding affinity of analyte proteins towards NPs and GFP. The higher affinity to NPs produces positive response and otherwise generates negative response as a result of analyte protein-GFP aggregation (Figure S17).

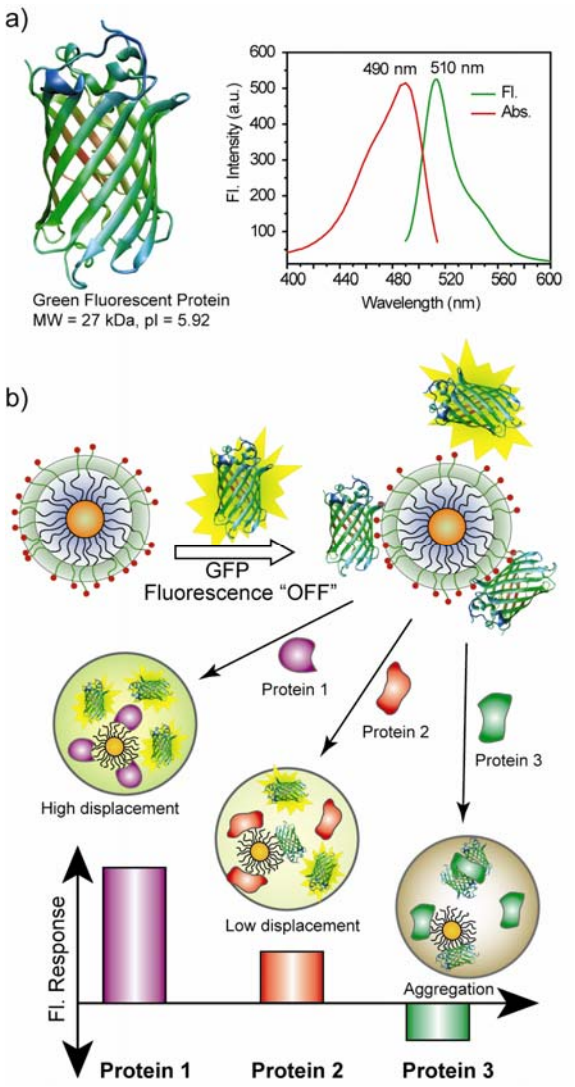

Figure 4.1 Modes of sensor response. a) Structure, absorbance and fluorescence spectra of GFP in 5 mM sodium phosphate buffer, pH 7.40. b) Schematic illustration of the competitive binding between protein and quenched nanoparticle-GFP complexes and protein aggregation leading to the fluorescence light-up or further quenching.

To confirm this hypothesis, five cationic gold NPs (**NP1**–**NP5**) were fabricated as sensor elements. In addition to their cationic charges, the ligand shells of these NPs differ in hydrophobicity, aromaticity, and hydrogen bonding ability (Figure 4.2).

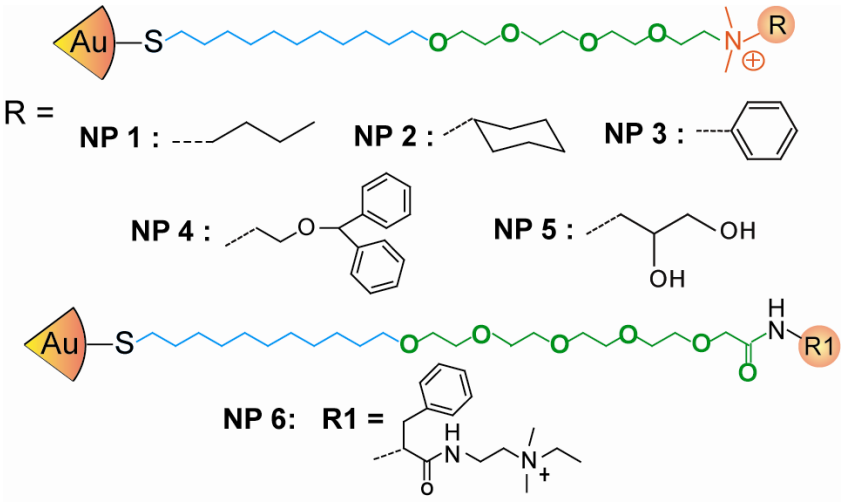

Figure 4.2 Structural features of nanoparticles . Chemical structure of cationic gold nanoparticles. **NP1** features only cationic charge, **NP2** and **NP4** feature groups capable of hydrophobic interaction, **NP3** features groups capable of hydrogen bonding and **NP5** has aromatic recognition unit capable of π-π interaction.

Roughly 20 serum proteins with different charge and molecular weights constitute 99% by mass of the serum protein content[24]. We choose five of the most abundant serum proteins for our studies: albumin, IgG, transferrin, fibrinogen and α-antitrypsin (Table 4.2).

Table 4.2 Molecular weight, isoelectric point and concentration of five analyte serum proteins[24] in human serum.

Protein	μML^{-1}	Mw^a	pI^b	$\%^c$
Albumin	769	65	5.2	70
IgG	66.7	150	7.5-7.8	14
Transferrin	25-50	80	5.6	5.7
Fibrinogen	5.9	340	5.6	2.8
α-Antitrypsin	9.6	52	5.4	0.7

a) molecular weight in kDa. b) isoelectric point. c) weight percent in human serum.

Preliminary studies were performed in buffer. We optimized the binding ratio between GFP and nanoparticles (**NP1**–**NP5**) through fluorescence titration. The fluorescence of GFP was significantly quenched for all nanoparticles and the change of fluorescence intensity against increasing nanoparticle concentrations was plotted (Figure

4.4, Figure 4.S16). The complex stability constants (K_S) and association stoichiometries (n) were obtained through nonlinear least-squares curve-fitting analysis (Table 4.S1)[25]. The variation in complex stabilities and the binding stoichiometry demonstrate the significant effect of head groups in nanoparticle-protein affinity.

Once the binding ratio that provided maximum quenching of fluorescence was determined, we tested the ability of our sensor to detect serum proteins in 5 mM sodium phosphate buffer using a solution of 100 nM of both particle and GFP. Testing at varying protein concentrations demonstrated that complete differentiation of the five analyte proteins was obtained at 25 nM (Figure 4.4a).

Linear discriminant analysis (LDA) was used to quantitatively differentiate the fluorescence response patterns of the nanoparticle-GFP conjugates with the serum proteins[26]. We generated the fluorescence responses six times for each protein against the five nanoparticle-GFP conjugates for this purpose. After the analysis, four canonical factors were generated (91.5%, 6.8%, 1.2% and 0.5%) that are linear combination of the response matrices obtained from fluorescence response pattern (5 nanoparticle-GFP conjugates × 5 proteins × 6 replicates). The 30 training cases (5 proteins × 6 replicates) are separated in five respective groups with 100% accuracy according to the jackknifed classification matrix and the most significant two factors are plotted in 2D (Figure 4.3b). This detection efficiency was validated through identification of unknowns from our training set, where a randomized set of the five proteins from the training set were identified with 97% accuracy (Table 4.S6).

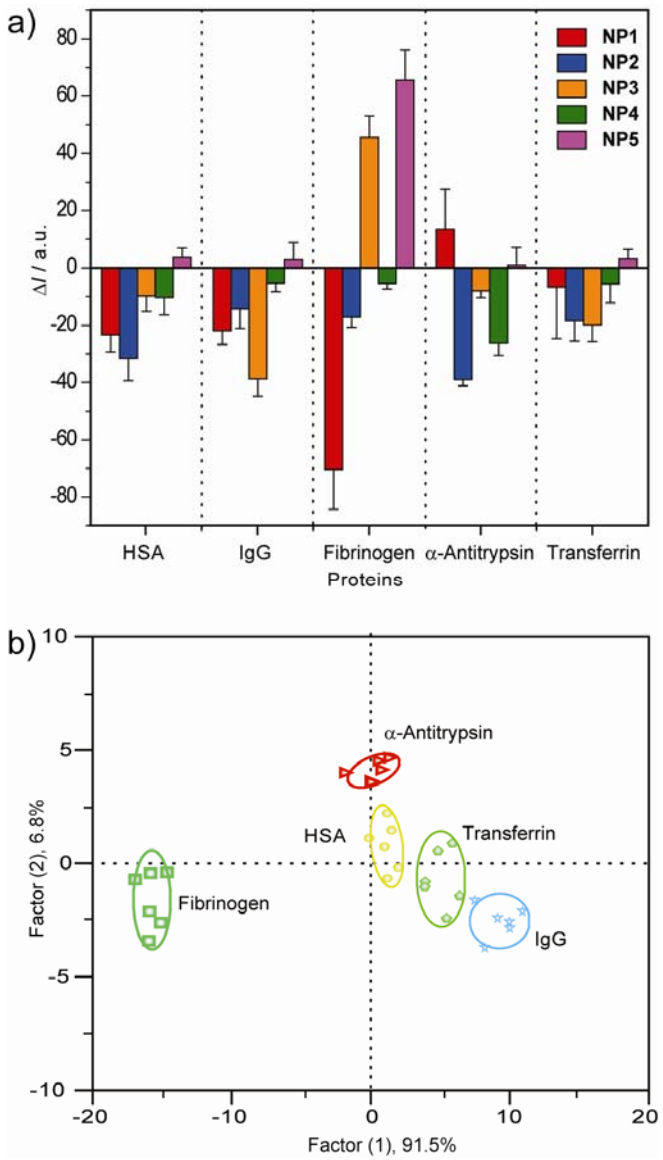

Figure 4.3 Array based sensing of five serum proteins in 5 mM sodium phosphate buffer (pH 7.40). (a) Fluorescence response (ΔI) patterns of the five nanoparticle-GFP adducts in the presence of five high abundant serum proteins at 25 nM concentration (average of six measurements). (b) Canonical score plot for the fluorescence patterns as obtained from LDA against five protein analytes at fixed concentration of 25 nM, with 95% confidence ellipses.

Protein sensing in human serum provides a far more demanding testbed than pure proteins in solution. The high overall protein content (~1 mM, 71 mg/mL) and multianalyte nature of human serum generates a complex matrix that is challenging for sensor design. To provide a controlled model for testing our methodology, we spiked

physiologically relevant concentrations of the above five proteins into commercially available human serum. We first optimized the concentration and ratio of nanoparticle-GFP conjugates. Because of the optical density of pure human serum, a higher concentration of GFP (250 nM) was required to get sufficient response. The titration data (Figure 4.4) indicates that saturation in fluorescence quenching was not observed even at a 8:1 **NP**/GFP ratio due to the presence of the other proteins in human serum that compete with GFP for nanoparticle binding. To provide reproducible quenching and a high level of sensitivity, we used a particle concentration of 500 nM, corresponding to the inflection point observed in the titration curves (Figure 4.4).

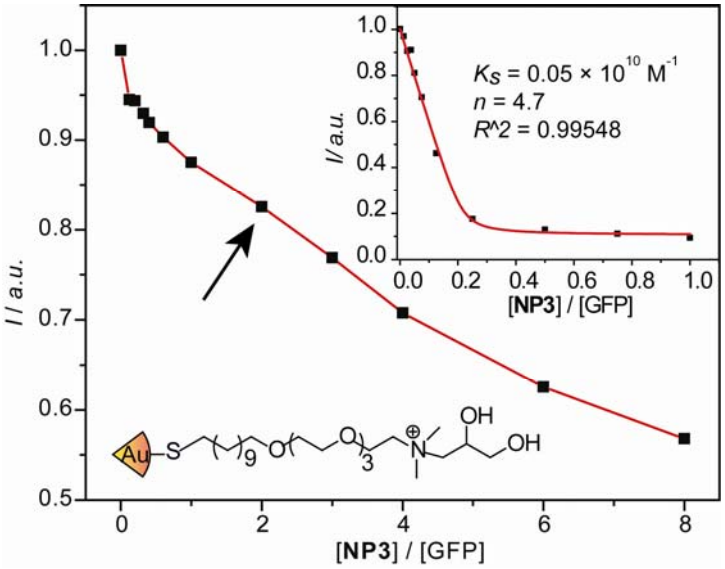

Figure 4.4 Determination of the optimum ratio of fluorophore to nanoparticle. The changes of fluorescence intensity of GFP (250 nM) at 510 nm were measured after the addition of cationic nanoparticles (0-2 μM) with an excitation wavelength of 475 nm. The absorption effect from gold core was subtracted by using non-interacting tetra(ethylene glycol)-functionalized gold nanoparticles. Inset shows the change of Fluorescence intensity of GFP (100 nM) at 510 nm upon addition of cationic **NP3** in 5 mM sodium phosphate buffer. The red solid lines represent the best curve fitting using the model of single set of identical binding sites and the arrow indicates the optimum binding ratio used for our study.

Using the conditions optimized above, 500 nM was the minimum amount of spiked analyte required for reproducible differentiation of the target proteins. We created a training matrix (5 nanoparticle-GFP conjugates × 5 proteins × 6 replicates) with GFP-

nanoparticle conjugates and each of the proteins. Similar to the buffer studies, each of the proteins generated distinct fluorescence response (Figure 4.5a). As before, these patterns were further subjected to LDA analysis, providing a 97% identification accuracy, as α-antitrypsin slightly overlaps with IgG. The four canonical factors are 76.9%, 20.3%, 2.7%, 0.1% and the plot of the first two factors with 95% confidence ellipses is presented in Figure 4.5b. We next tested the system against unknowns taken from the training set. Out of 30 samples 28 samples were correctly identified affording a 93% identification accuracy (see Table 4.S7 for original data). We identified target proteins in the complex serum matrix at physiologically relevant submicromolar concentrations. As a point of reference, we were able to detect and identify the analyte proteins between 0.06 to 8.4% (by molarity) of total serum protein concentration (Table 4.3).

Table 4.3 Change of protein concentration as a percentage of its typical concentration in normal serum detected by the sensor array.

Protein	μML^{-1}	%[a]
Albumin	769	0.06
IgG	66.7	0.75
Transferrin	25-50	1-2
Fibrinogen	5.9	8.4
α-Antitrypsin	9.6	5.2

[a] Change in protein concentrations in molarity.

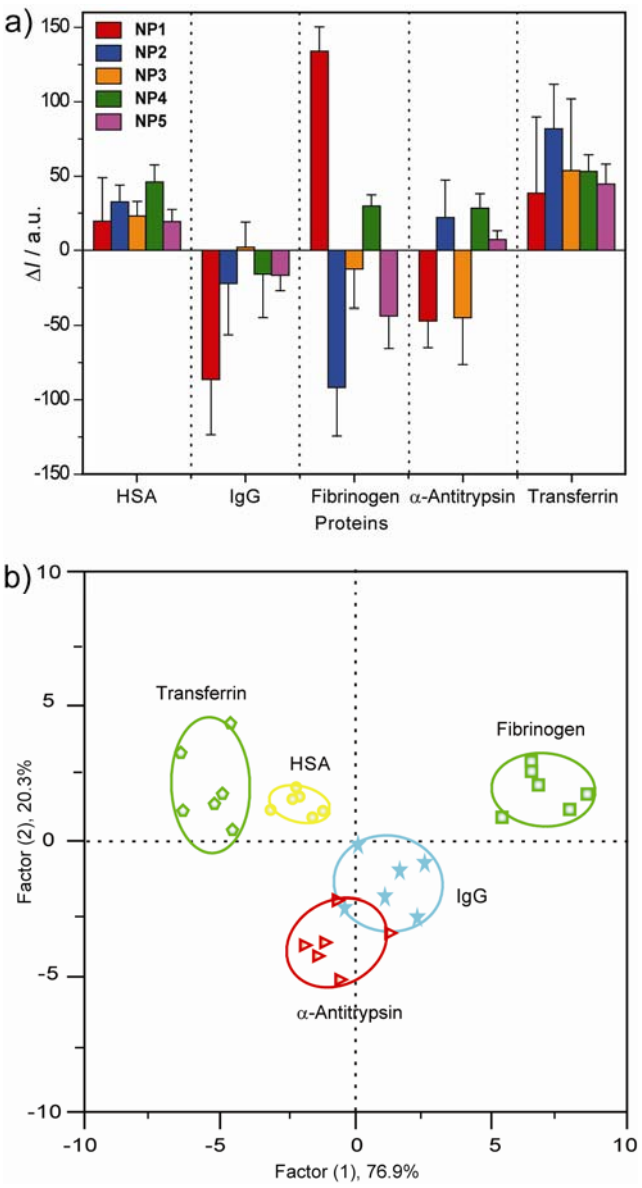

Figure 4.5 Array based sensing of five serum proteins in human serum. a) Fluorescence response (ΔI) pattern of the five nanoparticle-GFP adducts in the presence of serum proteins spiked in human serum at 500 nM concentration (responses are average of six measurements and error bars are standard deviations of the measurements from the mean). b) Canonical score plot for the fluorescence patterns as obtained from LDA against five protein analytes at fixed concentration (500 nM) with 95% confidence ellipses.

After successful detection of serum proteins in human serum, the next challenge arises from the detection of a protein at variable concentration level and in mixture with other proteins. One of the limitations of the antibody and other approaches is the

differentiation between the variable concentration levels of a single protein. To find out the ability of our system over in this regard, we performed the similar experiments with HSA and IgG at different concentrations (500 nM, 1 µM and 2 µM). It is observed that the LDA plots for various concentrations are not random rather follow certain patterns and can be differentiated from each other with certain extent (Figure 4.6a). Essentially, clusters around a common center that are distinct from each other can be observed for proteins with variable concentrations (Figure 4.6b).

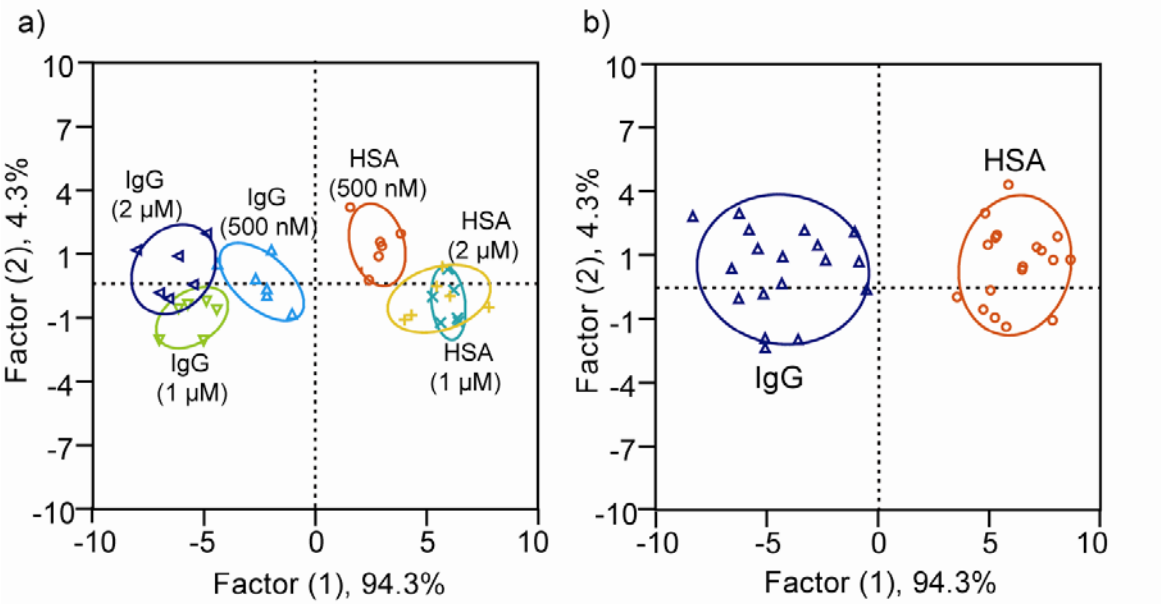

Figure 4.6 Discrimination of HSA and IgG at different concentrations and mixture of proteins. a) Canonical score plot for the fluorescence patterns as obtained from LDA for human serum albumin (HSA) and immunoglobulin G (IgG) at different concentrations (500 nM, 1 µM and 2 µM) with 95% confidence ellipses. b) Clustering of all the data for the three concentrations mentioned for each protein as obtained from LDA analysis.

After getting the differentiation at varying level of protein concentration we continued our investigation towards the detection of mixture of proteins in serum. We mixed HSA and IgG in serum at 1:1 molar ratio with 250 nM each as well as 500 nM each and compared with 500 nM of individual proteins. When subjected to the LDA analysis of the fluorescence responses, it shows that the canonical score plots revolve

around the HSA and IgG plots and clearly distinct from them (Figure 4.7). Although we can discriminate the mixture of proteins at different concentration from each other, no correlation between the plots could be drawn since the complex equilibrium among the serum proteins, GFP and NP make the system behave differently. However, a profile of mixture of proteins can be generated that could enable detection of diseased states caused by an elevated level of proteins which are being developed.

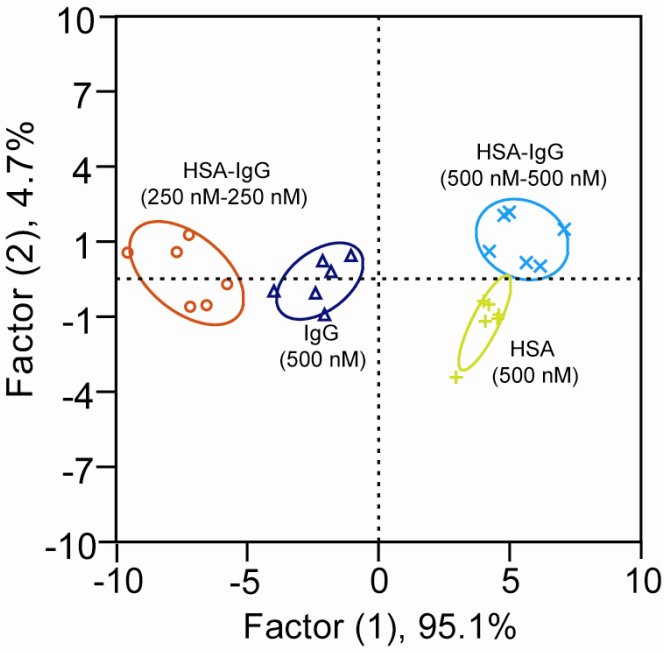

Figure 4.7 Differentiation of mixture of proteins. HSA and IgG were mixed at 1:1 molar ratio with 250 nM each and 500 nM each and added to the five GFP-**NP** complexes. The canonical score plots obtained from LDA analysis were compared with that for the 500 nM of the individual proteins.

4.3 Conclusion

In conclusion, we have demonstrated a nanoparticle-GFP array based biosensor that can effectively identify most abundant serum proteins rang at very low concentration with higher efficiency. We also successfully extend this efficiency in detection of proteins in highly complex system i.e., human serum which is composed of several proteins with variable concentrations. This result indicate that the simple nanoparticle-GFP array can

efficiently recognize biological analyst in serum simply and instantaneously with reliable fashion. In this approach the competitive complexation between GFP and analyte proteins with nanoparticles makes this system comparable to natural protein-protein interaction, providing potential for further optimization via engineering of both the synthetic and biological components. We also believe that optimization of this methodology potentially modernize the medical diagnostics, both in the clinic and as a tool for personalized diagnostics.

4.4 Experimental Section

4.4.1 Methods, Instrumentation and Materials

Green fluorescence protein (GFP) was expressed according to known procedure[27]. In brief, starter cultures from a glycerol stock of GFP in BL21(DE3) was grown overnight in 50 ml culture media at 37 ^{o}C. The following day, 5 ml of the starter cultures was added to a Fernbach flask containing 1 L culture media and shaken until the OD_{600} = 0.6 - 0.7. The culture was then induced by adding isopropyl-β-D-thiogalactopyranoside (IPTG) (1 mM final concentration) and shaken at 28 ^{o}C. After three hours, the cells were harvested by centrifugation and the pellet was then resuspended in lysis buffer. Once lysed, the solution was pelleted and the supernatant was further purified using HisPur Cobalt columns. The analyte proteins, serum albumin (HSA), immunoglobulins (IgG), transferrin, fibrinogen and α-antitrypsin all from human serum were purchased from Sigma-Aldrich and used as received. Cationic nanoparticles **NP1**, **NP2** were synthesized according to the reported procedure and **NP3**-**NP5** were prepared following the similar procedure which is elaborately described in supporting information. 5 mM sodium

phosphate buffer, pH 7.4 was used as a solvent for the experiment in buffer solution. The commercial human serum from untransfused male donors was purchased from MP Biomedicals, LLC and used without further treatment.

In the fluorescence titration between nanoparticles and GFP, the change of fluorescence intensity at 510 nm was measured with an excitation wavelength of 475 nm at various concentrations of nanoparticles from 0 to 100 nM on a Molecular Devices SpectaMax M5 microplate reader at 25 ^{o}C in 5 mM sodium phosphate buffer. The change of fluorescence intensity against increasing nanoparticle concentrations was plotted (Figure 4.S2), using a non-interacting gold nanoparticle (e.g. PEG-**NP**) as a control to compensate for particle absorption. Nonlinear least-squares curve-fitting analysis was employed to estimate the binding constant (*Ks*) and association stoichiometry (*n*) using the model in which the nanoparticle is assumed to possess *n* equivalent of independent binding sites. In case of human serum, similar procedure was followed, but the only modification was the concentration of GFP (250 nM) and the nanoparticles (0-2 μM).

To create the training matrix, GFP and nanoparticles are mixed in the ratio obtained from fluorescence titration. In case of 5 mM sodium phosphate buffer solution the final concentration of nanoparticle and GFP were 100 nM each. On the other hand, in serum solution study the final concentration of nanoparticle and GFP were 500 nM and 250 nM respectively. After 30 min of incubation 200 μL of each solution was loaded into a well on a 96-well plate (300 μL Whatman black bottom micropalte) and the fluorescence intensity at 510 nm recorded using fluorescence microplate reader (Molecular Devices SpectraMax M5). Subsequently, 10 μL of protein solution, 0.525 μM for buffer solution and 10.5 μM for serum solution, was added so that the final concentrations were 25 nM

and 500 nM in buffer and serum respectively. After incubation for 30 min the fluorescence intensity at 510 nm was recorded again. The difference between the two intensities before and after addition of proteins was considered as the fluorescence response (Table 4.S1 and 4.S3). This process was repeated for five serum proteins with five selective cationic nanoparticles in six replicates. This data was used to generate the 6 × 5 × 5 (6 replicates × 5 proteins × 5 nanoparticles) training matrix. This training matrix was used for classical linear discriminant analysis (LDA) in SYSTAT (version 11.0).

For the unknown detection, we prepared the protein solutions (0.525 μM or 10.5 μM) out of the five serum proteins according to buffer or serum study. From this prepared solution we randomly choose 30 samples for each system (buffer or serum) and the same method was followed using the nanoparticle-GFP motif. We replicated each unknown samples three times instead of six for preparing training matrix. We considered the average response of three replicates for a single unknown sample and analyzed with five known proteins in LDA analysis.

4.4.2 Experimental Data

4.4.2.1 Synthesis of Ligands and Nanoparticles.

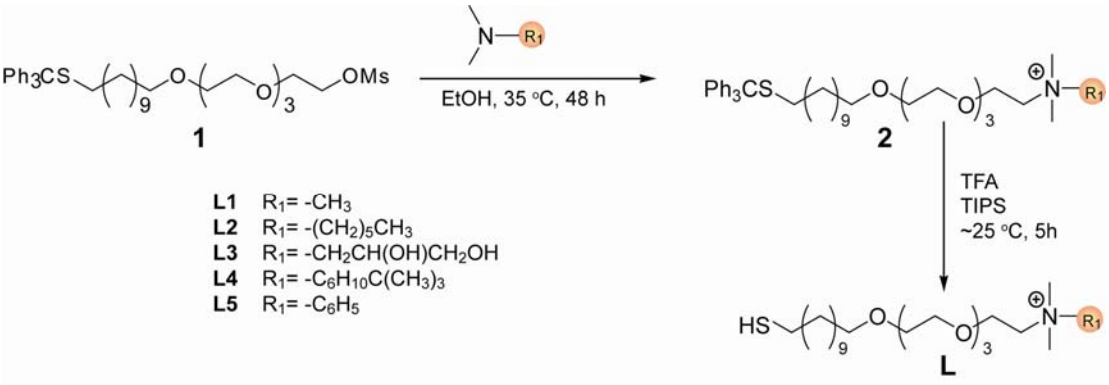

Scheme 4.S1 Synthesis of ligands.

General procedure: Compound **2** bearing ammonium end groups were synthesized by the reaction of 1,1,1-triphenyl-14,17,20,23-tetraoxa-2- thiapentacosan-25-yl methanesulphonate (**1**) with corresponding substituted N,N-dimethylamines with stirring for 48 hours at ~35 ^{o}C. The trityl protected thiol ligand **(2)** was dissolved in dry dichloromethane (Methylene Chloride, DCM) and an excess of trifluoroacetic acid (TFA, ~20 equivalents) was added. The color of the solution was turned into yellow immediately. Subsequently, triisopropylsilane (TIPS, ~1.2 equivalents) was added to the reaction mixture. The reaction mixture was stirred for ~5 h under Ar-atmosphere at room temperature. The solvent, most of the TFA and TIPS were distilled off under reduced pressure. The pale yellow residue was further dried in high vacuum. The product (**L**) formation was quantitative and their structure was confirmed by NMR and mass spectroscopy. The yields were >95%.

Compound **L1**: ^{1}H NMR (400MHz, $CDCl_3$, TMS): δ 3.95 (br, 2H, -CH_2O-), 3.70-3.58 (m, 14H, -CH_2O- + -OC$\underline{H_2}$-(CH_2N)-), 3.49 (t, 2H, -CH_2N-), 3.25 (s, 9H, -N(CH_3)$_3$-), 2.90 (s, 3H, -$CH_3SO^-_3$-), 2.52 (q, 2H, -CH_2S-), 1.64-1.51 (m, 4H, (SCH_2)C$\underline{H_2}$ + -C$\underline{H_2}$(CH_2O)-) , 1.36-1.22 (m, 15H, -SH + -CH_2-).

^{13}C NMR (400 MHz, $CDCl_3$) δ(ppm): 71.58, 70.56, 70.49, 70.34, 70.24, 70.15, 70.04, 65.13, 54.72, 39.25, 31.07, 29.76, 29.65, 29.62, 29.57, 29.53, 29.51, 29.27, 28.56, 26.10.
ESI-MS (*m/z*): calculated for $C_{22}H_{48}NO_4S^+$ [M^+], 422.33; found 421.1.

Compound **L2**: ^{1}H NMR (400MHz, $CDCl_3$, TMS): δ 3.95 (br, 2H, -CH_2O-), 3.68-3.56 (m, 14H, -CH_2O- + -OC$\underline{H}_2$-(CH_2N)-), 3.46 (t, 2H, -CH_2N-), 3.40-3.33 (m, 2H,-NCH_2-), 3.19 (s, 6H, -$(CH_3)_2$N-), 2.87 (s, 3H, -$CH_3SO^-_3$-), 2.52 (q, 2H, -CH_2S-), 1.76-1.53 (m, 6H, -(NCH_2)C$\underline{H}_2$-) + (SCH_2)C$\underline{H}_2$ + -C$\underline{H}_2$(CH_2O)-) , 1.41-1.22 (m, 21H, -SH + -(NCH_2CH_2-)C$\underline{H}_2$-) + -CH_2-), 0.89 (t, 3H, - CH_3-).
^{13}C NMR (400 MHz, $CDCl_3$) δ(ppm): 71.59, 70.54, 70.51, 70.44, 70.33, 70.15, 70.00, 66.42, 64.82, 63.50, 51.90, 34.07, 31.18, 29.59, 29.54, 29.52, 29.49, 29.09, 28.39, 26.07, 25.84, 24.68, 22.71, 22.37, 13.85.
ESI-MS (*m/z*): calculated for $C_{27}H_{58}NO_4S^+$ [M^+], 492.41; found 492.0.

Compound **L3**: ^{1}H NMR (400MHz, $CDCl_3$, TMS): δ 4.78 (br, 1H, -CHO$\underline{H}$(CH_2OH)-), 4.59 (br, 1H, -CH_2O$\underline{H}$-), 4.50-4.45 (m, 1H, -C$\underline{H}$OH(CH_2OH)-), 4.43 (d and br, 2H,-NCH_2-), 3.95 (d and br, 2H, -CH_2O-), 3.86-3.76 (d and br, 2H, -C$\underline{H}_2$-OH), 3.75-3.55 (m, 14H, -CH_2O- + -OC$\underline{H}_2$-(CH_2N)-), 3.48 (t, 2H, -CH_2N-), 3.34 (s, 6H, -$(CH_3)_2$N-), 2.99 (s, 3H, -$CH_3SO^-_3$-), 2.52 (q, 2H, -CH_2S-), 1.71-1.51 (m, 4H, + (SCH_2)C$\underline{H}_2$ + -C$\underline{H}_2$(CH_2O)-), 1.42-1.21 (m, 15H, -SH + -CH_2-).
^{13}C NMR (400 MHz, $CDCl_3$) δ(ppm): 71.65, 70.45, 70.37, 70.19, 69.97, 68.07, 66.79, 66.47, 64.89, 64.81, 64.42, 63.83, 60.42, 53.59, 53.15, 45.41, 42.76, 39.51, 34.14, 29.55, 29.30, 29.16, 29.02, 28.74, 28.59, 28.46, 26.08, 24.74, 23.54.
ESI-MS (*m/z*): calculated for $C_{24}H_{58}NO_4S^+$ [M^+], 482.35; found 482.0.

Compound **L4**: ^{1}H NMR (400MHz, $CDCl_3$, TMS): δ 3.96 (br, 2H, -CH_2O-), 3.79-3.75 (m, 1H, H_{Cyclo}), 3.66-3.57 (m, 14H, -CH_2O- + -OC$\underline{H}_2$-(CH_2N)-), 3.46 (t, 2H, -CH_2N-), 3.12 (s, 6H, -$(CH_3)_2$N-), 2.89 (s, 3H, -$CH_3SO^-_3$-), 2.52 (q, 2H, -CH_2S-), 2.28 (d, 2H, H_{Cyclo}), 2.01 (d, 2H, H_{Cyclo}), 1.64-1.54 (m, 4H, -(SCH_2)C$\underline{H}_2$ + -C$\underline{H}_2$(CH_2O)-), 1.47 (q, 2H, H_{Cyclo}), 1.33 (t, ^3J = 8.0 Hz, 1H, -SH), 1.30-1.22 (m, 14H, -CH2-), 1.16 (q, 2H, H_{Cyclo}) 1.04 (td, 1H -CHC-), 0.86 (s, 9H, -$C(CH_3)_3$-).
^{13}C NMR (400 MHz, $CDCl_3$) δ(ppm): 74.52, 71.71, 70.58, 70.54, 70.38, 70.31, 70.09, 64.90, 62.26, 49.05, 46.79, 39.61, 34.16, 32.30, 29.60, 29.34, 29.19, 28.65, 28.49, 27.49, 26.46, 26.24, 26.16, 25.73, 25.64, 24.78.
ESI-MS (*m/z*): calculated for $C_{31}H_{64}NO_4S^+$ [M^+], 546.46; found 546.0.

Compound **L5**: ^{1}H NMR (400MHz, $CDCl_3$, TMS): δ 7.82 (d, 2H, H_{Ar}), 7.66-7.51 (m, 3H, H_{Ar}), 4.24 (br, 2H, -CH_2O-), 3.78 (s, 6H, -$(CH_3)_2$N-), 3.68-3.52 (m, 14H, -CH_2O- + -OC$\underline{H}_2$-(CH_2N)-), 3.47-3.36 (m, 2H, -CH_2N-), 2.87 (s, 3H, -$CH_3SO^-_3$-), 2.52 (q, 2H, -CH_2S-), 1.70-1.46 (m, 4H, -(SCH_2)C$\underline{H}_2$ + -C$\underline{H}_2$(CH_2O)-), 1.42-1.1.16 (m, 15H, -SH + -CH_2-).
^{13}C NMR (400 MHz, $CDCl_3$) δ(ppm): 144.04, 130.89, 120.88, 116.50, 113.65, 71.71, 70.60, 70.50, 70.40, 70.19, 70.03, 69.90, 65.32, 56.47, 39.61, 34.13, 29.64, 29.60, 29.52, 29.17, 29.04, 28.69, 28.47, 26.07, 24.76.
ESI-MS (*m/z*): calculated for $C_{27}H_{50}NO_4S^+$ [M^+], 484.35; found 484.0.

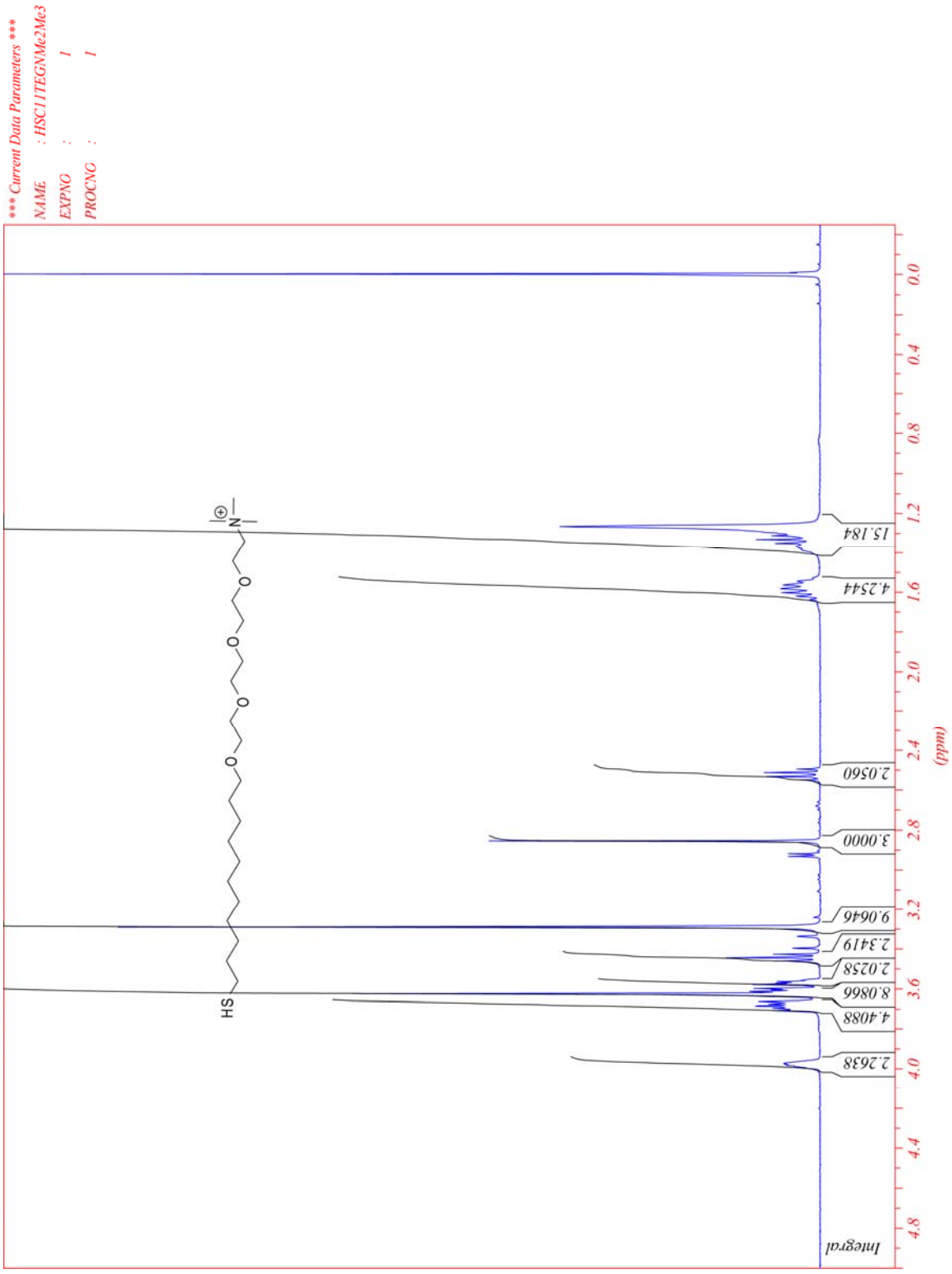

Figure 4.S1 400 MHz ^{1}H NMR spectra of **compound L1** in $CDCl_3$ (D, 99.8%).

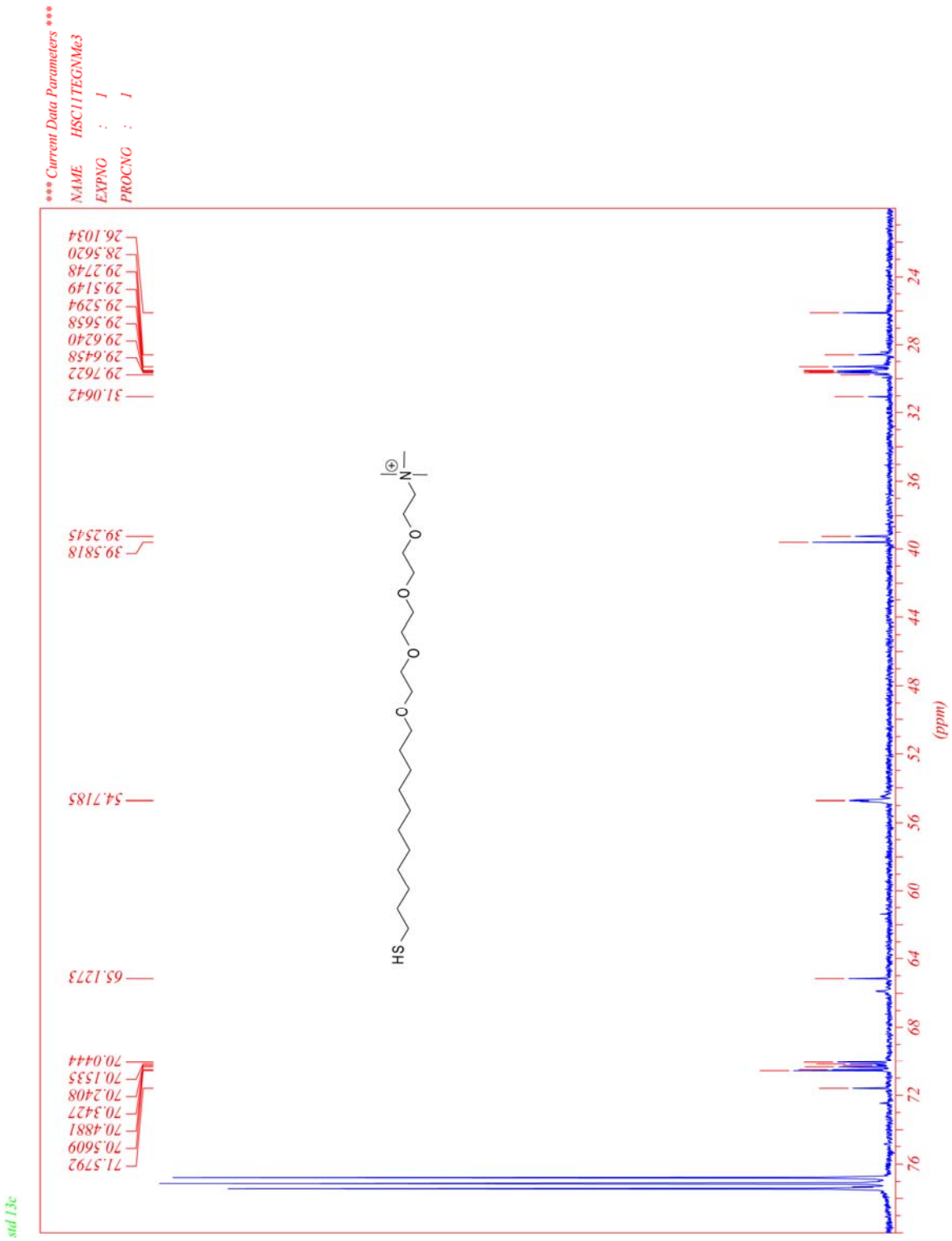

Figure 4.S2 400 MHz ^{13}C NMR spectra of **compound L1** in $CDCl_3$ (D, 99.8%).

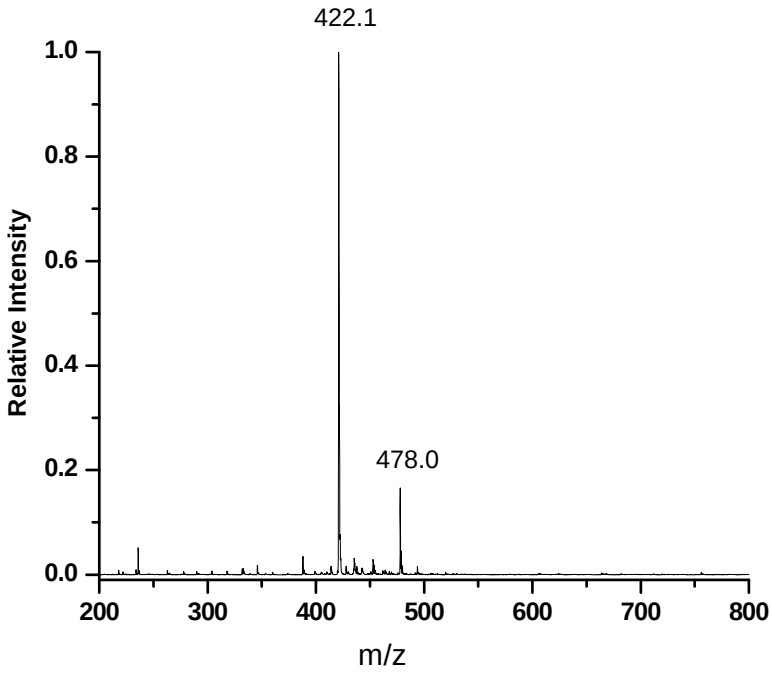

Figure 4.S3 ESI-MS spectra of **compound L1**.

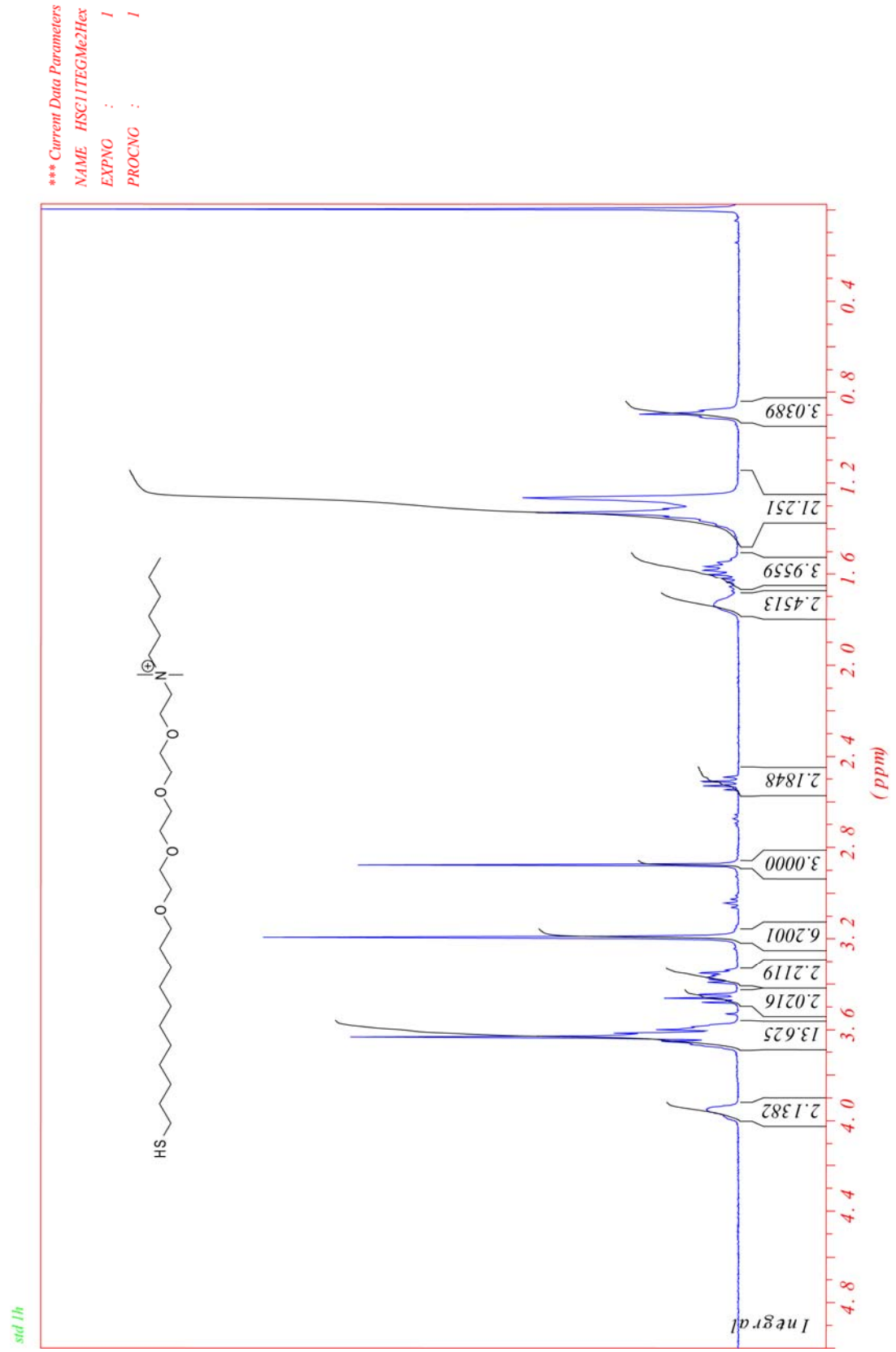

Figure 4.S4 400 MHz ^{1}H NMR spectra of **compound L2** in $CDCl_3$ (D, 99.8%).

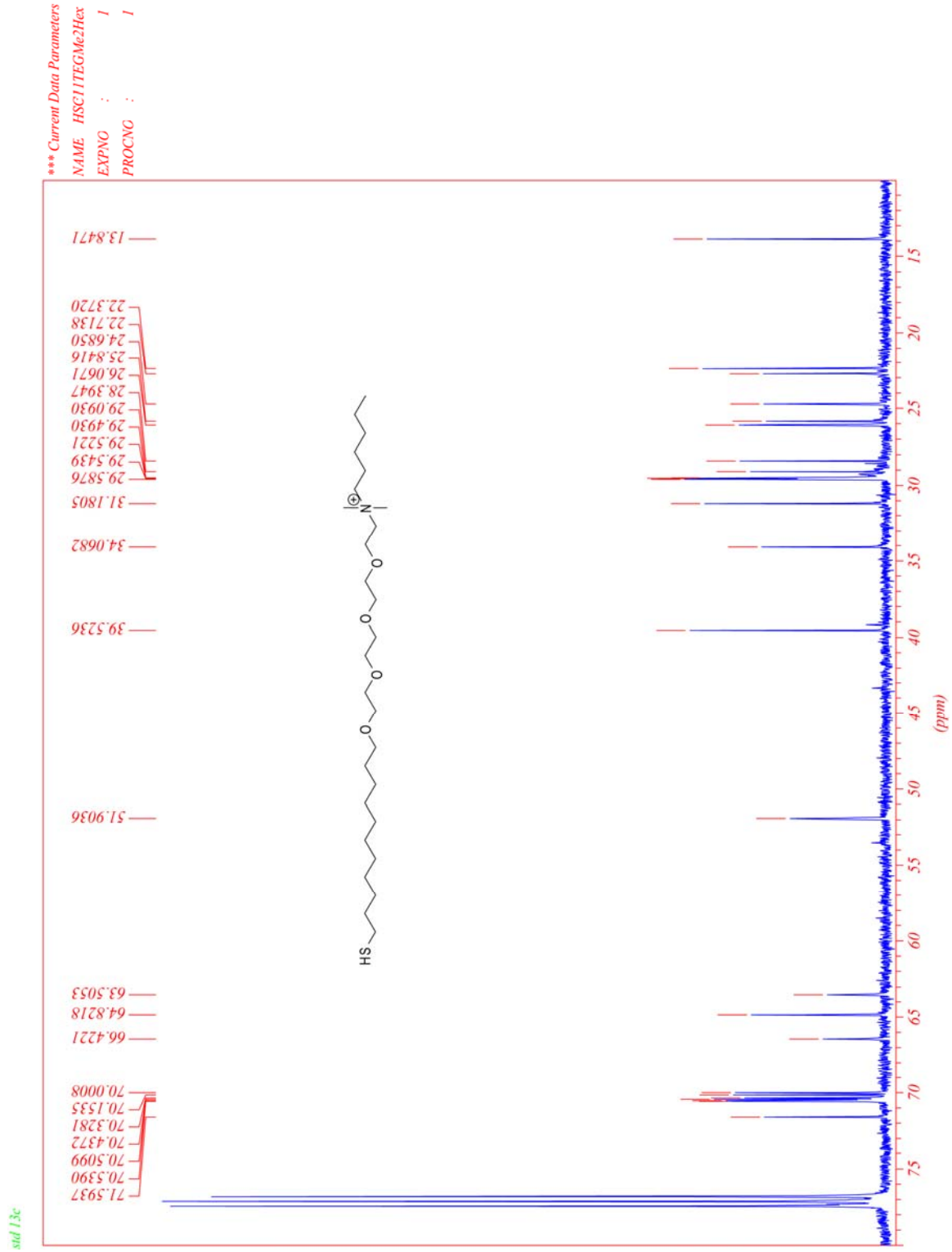

Figure 4.S5 400 MHz ^{13}C NMR spectra of **compound L2** in $CDCl_3$ (D, 99.8%).

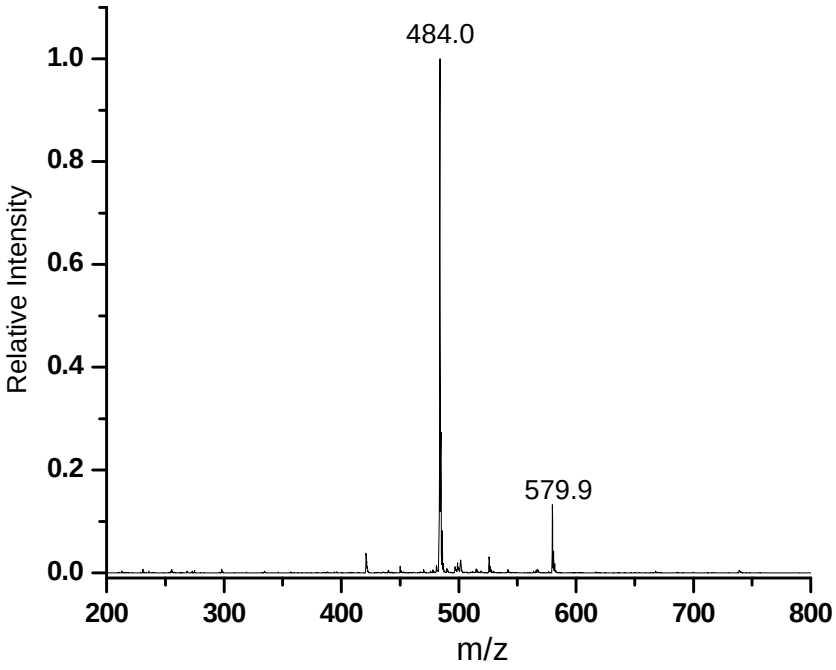

Figure 4.S6 ESI-MS spectra of **compound L2**.

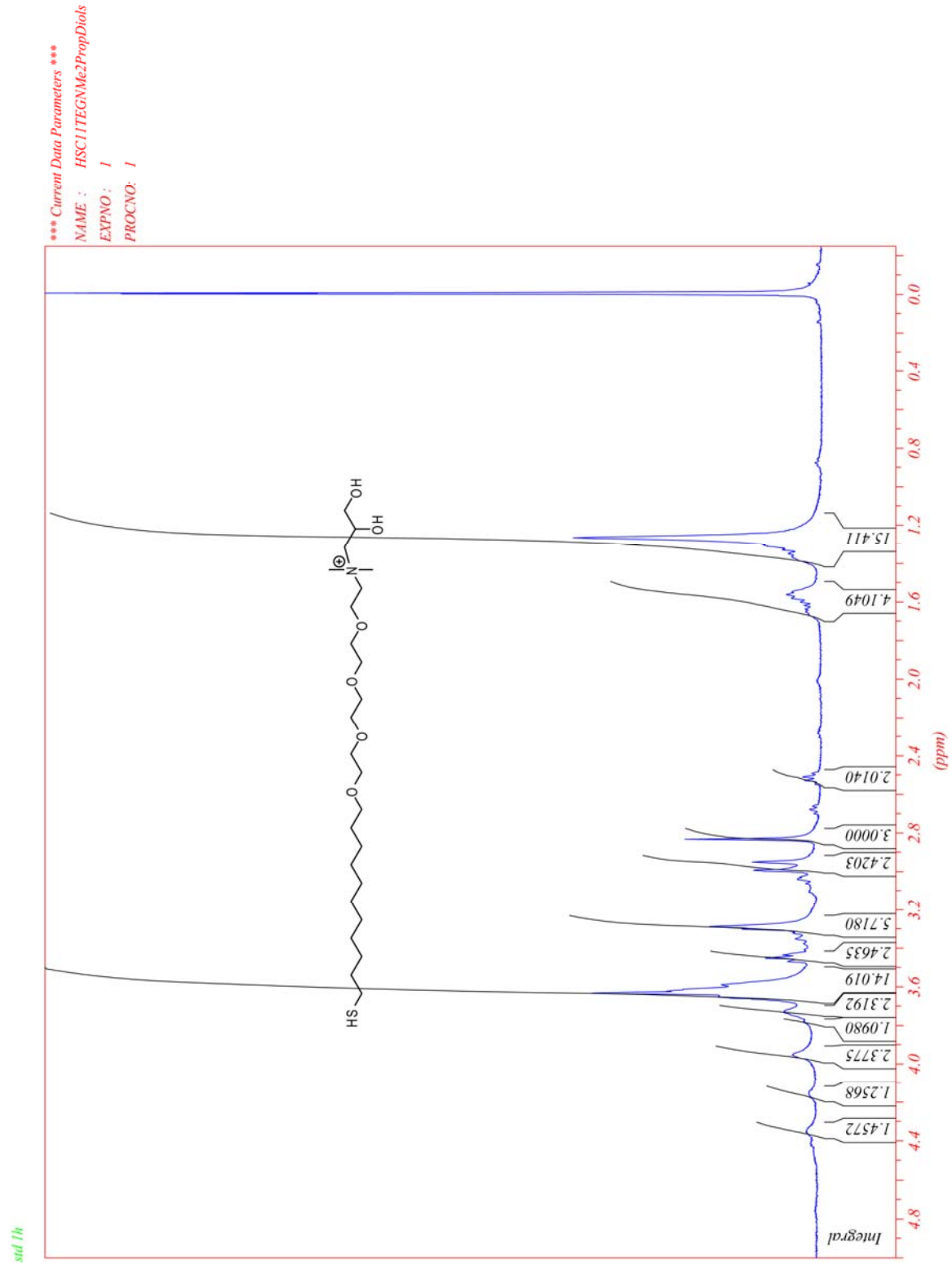

Figure 4.S7 400 MHz ^{1}H NMR spectra of **compound L3** in $CDCl_3$ (D, 99.8%).

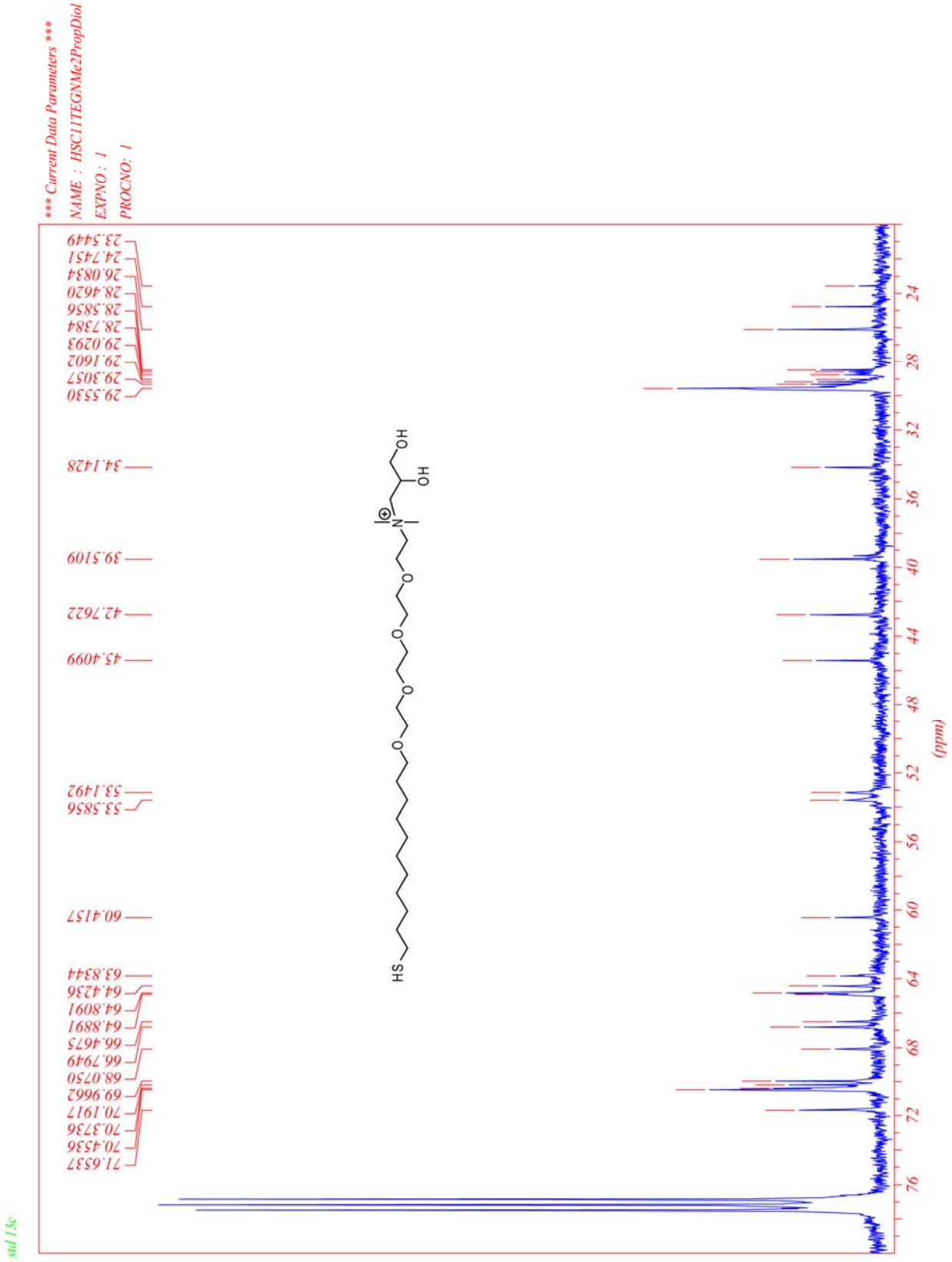

Figure 4.S8 400 MHz ^{13}C NMR spectra of **compound L3** in $CDCl_3$ (D, 99.8%).

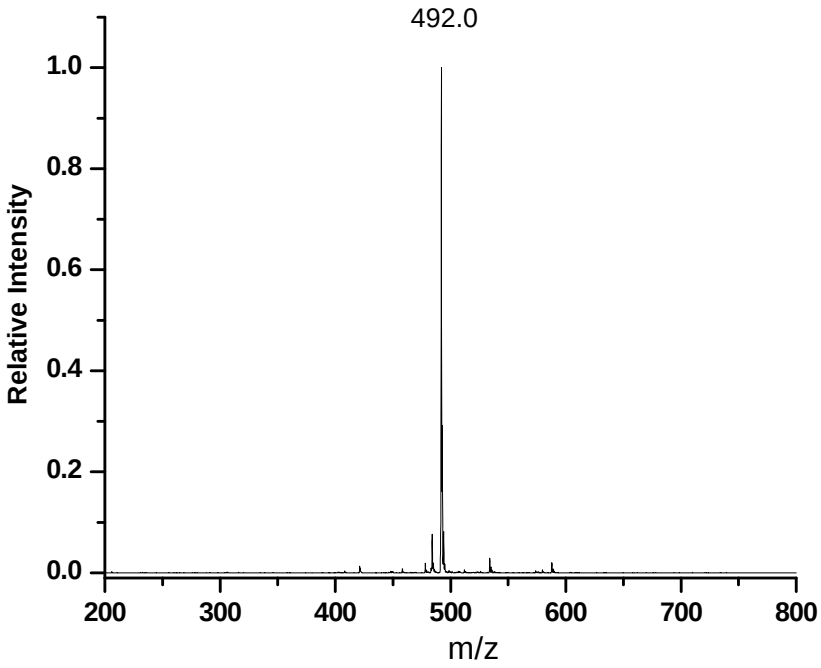

Figure 4.S9 ESI-MS spectra of **compound L3**.

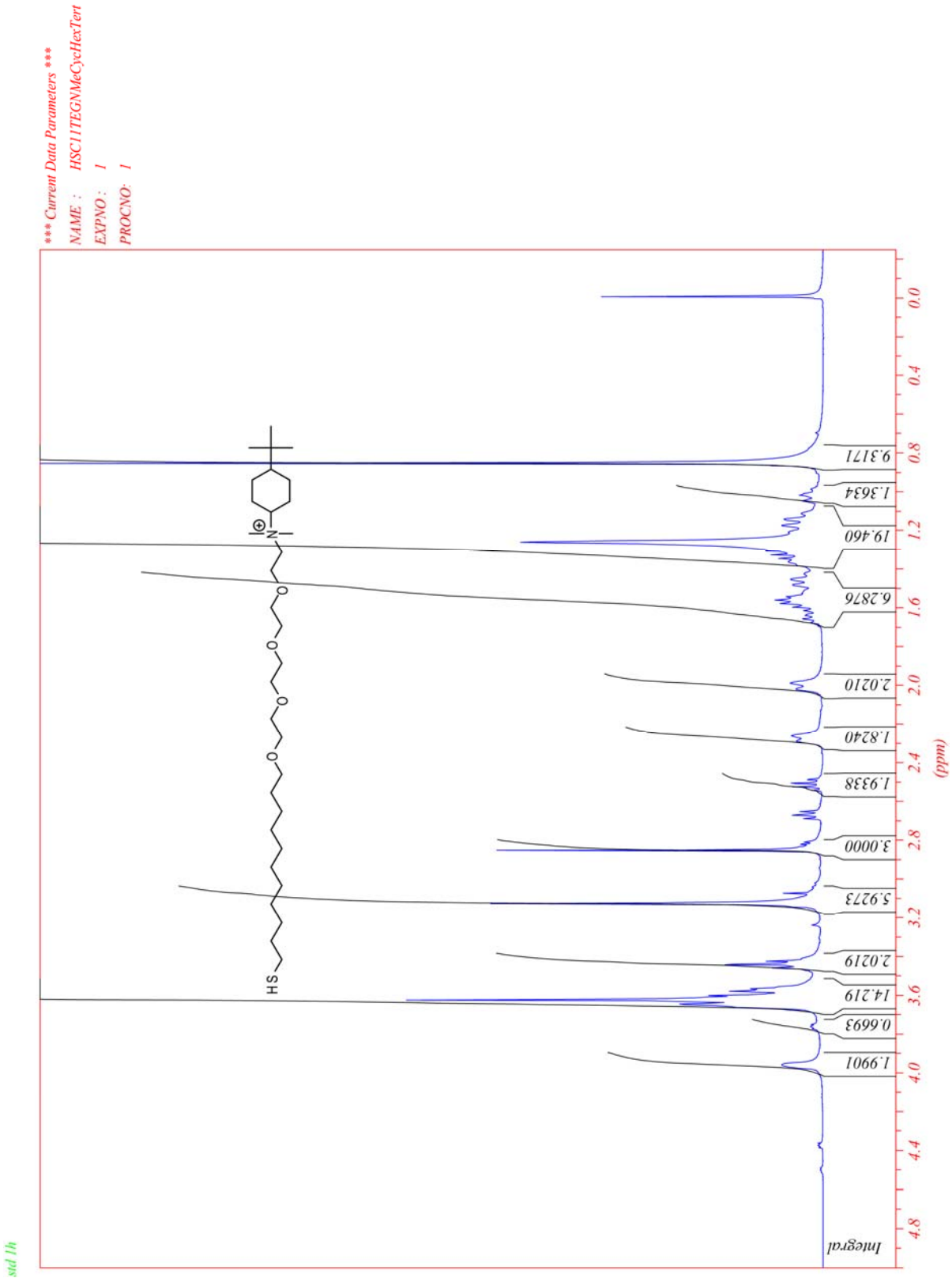

Figure 4.S10 400 MHz ^{1}H NMR spectra of **compound L4** in $CDCl_3$ (D, 99.8%).

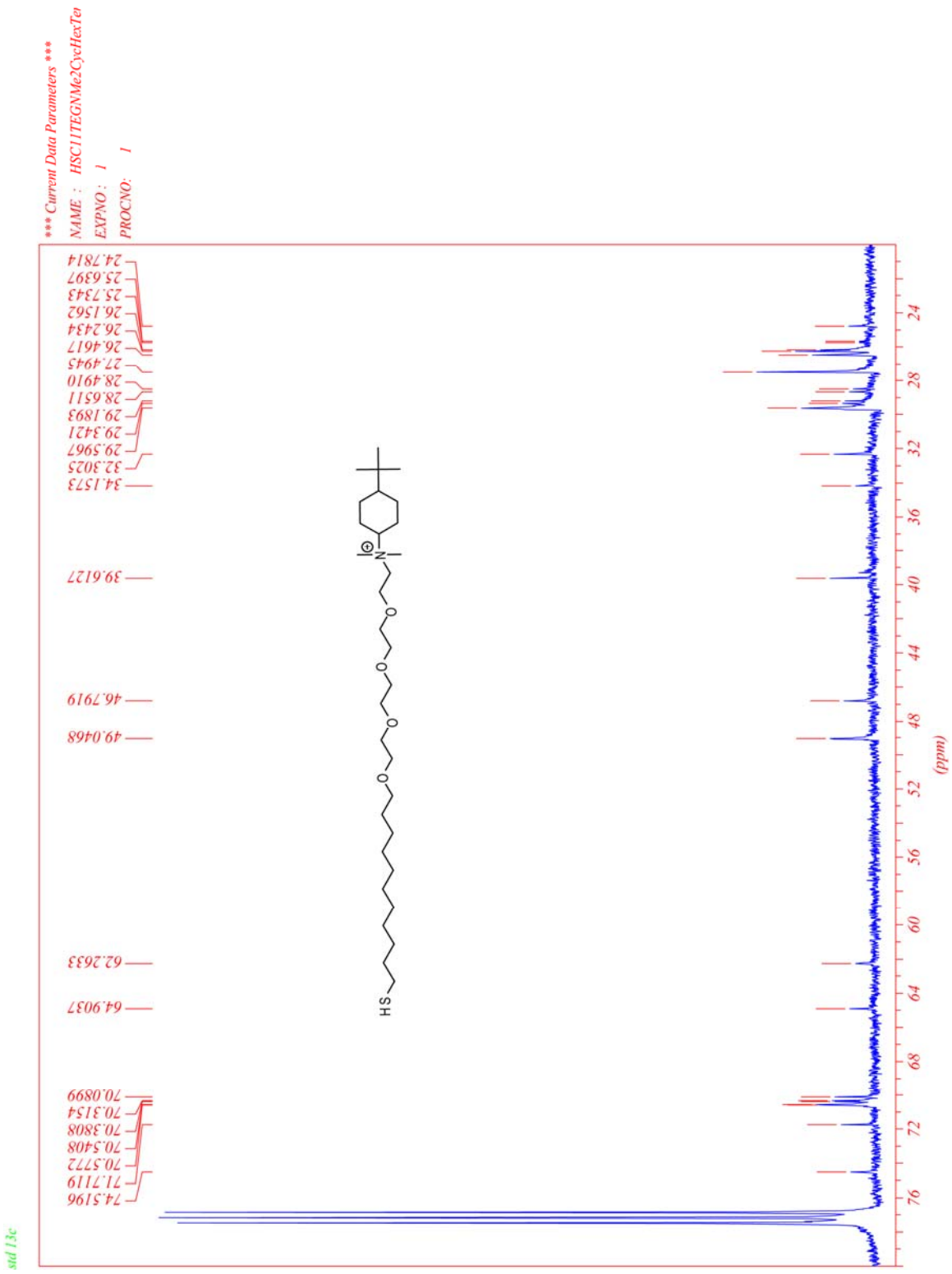

Figure4. S11 400 MHz ^{13}C NMR spectra of **compound L4** in $CDCl_3$ (D, 99.8%).

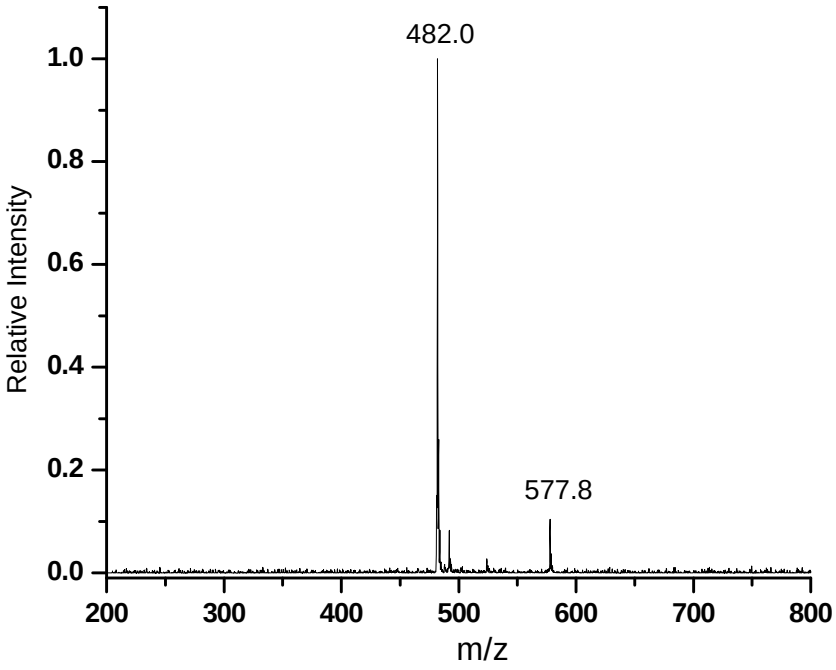

Figure 4.S12 ESI-MS spectra of **compound L4**.

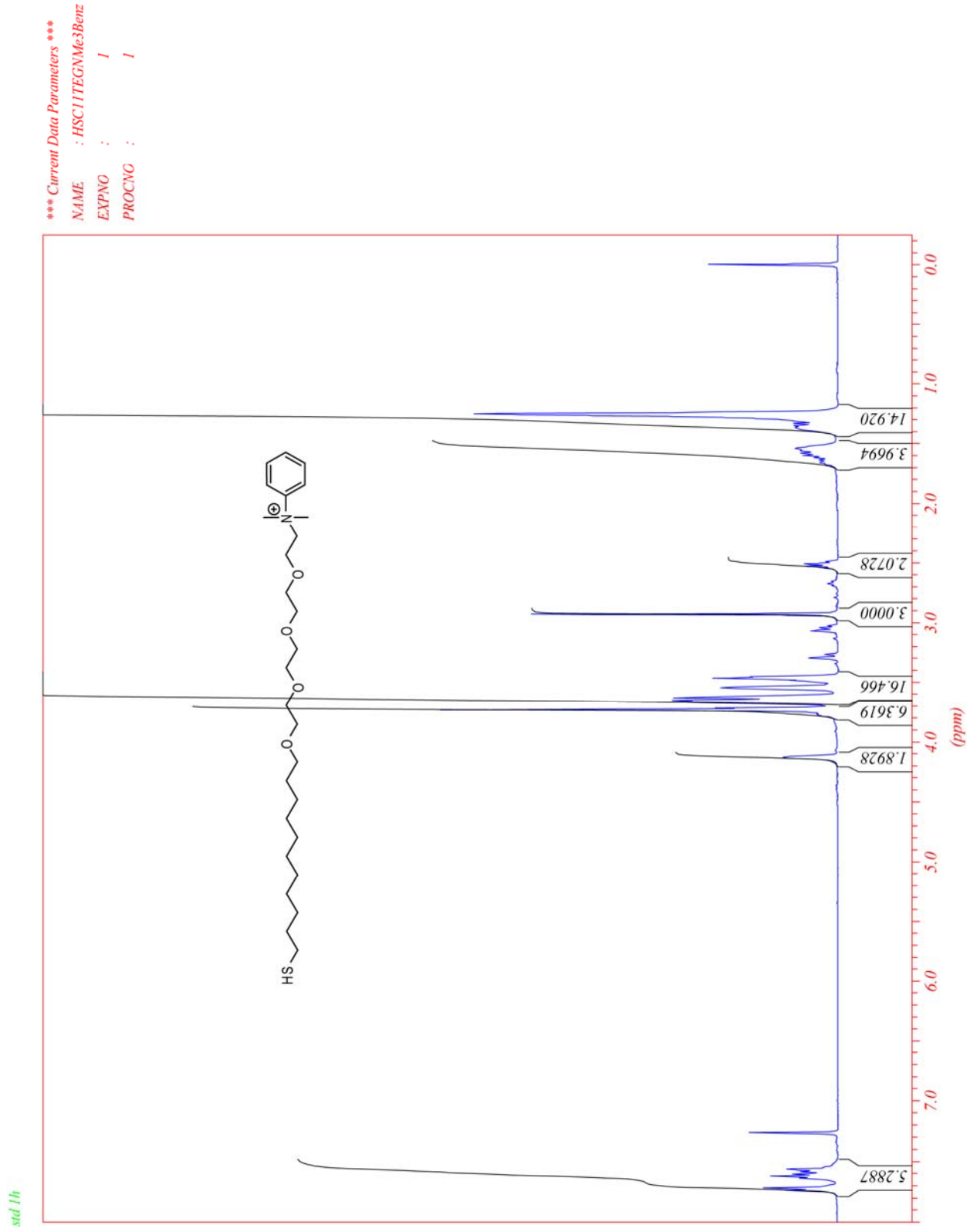

Figure 4.S13 400 MHz ^{1}H NMR spectra of **compound L5** in $CDCl_3$ (D, 99.8%).

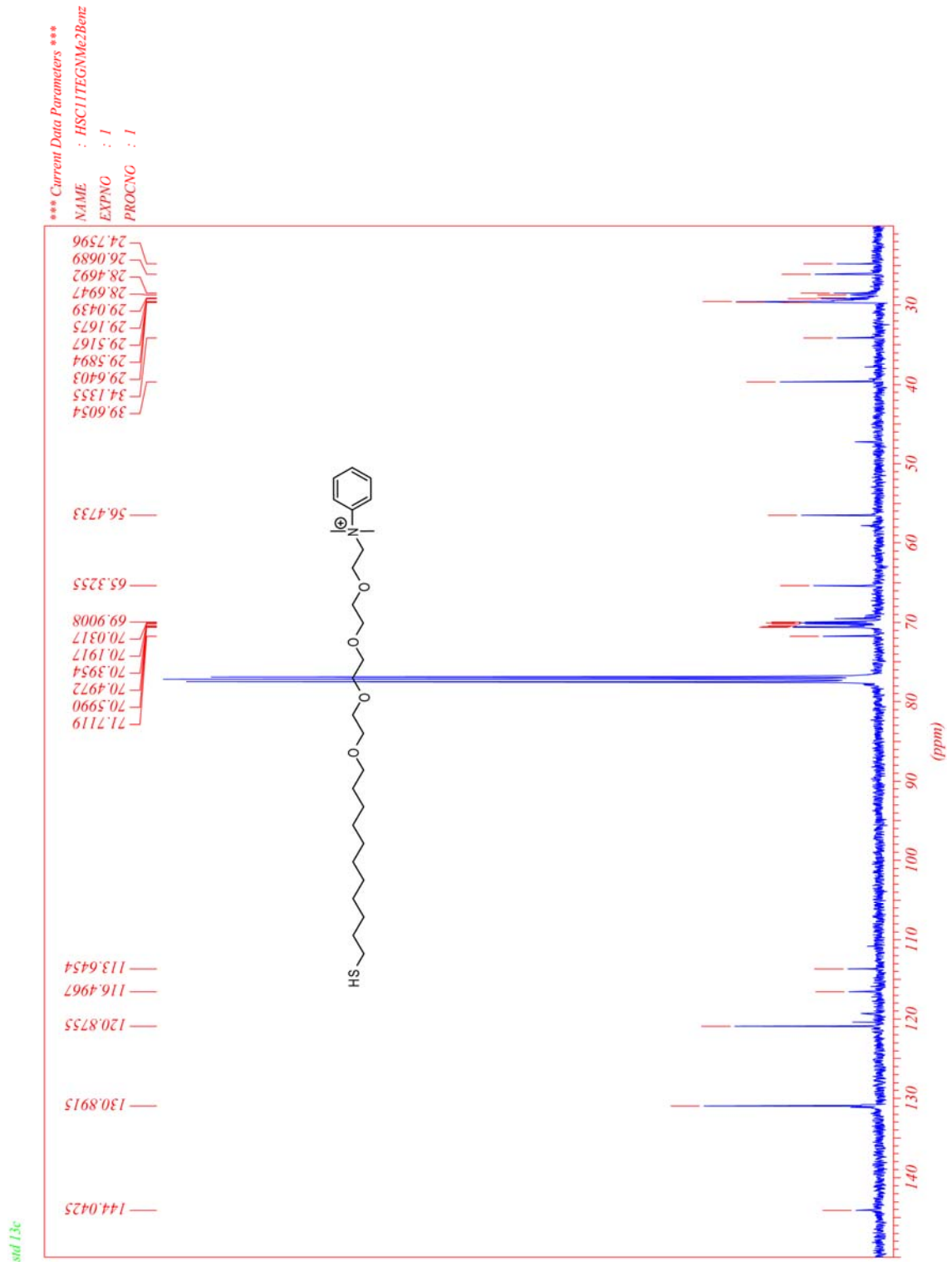

Figure 4.S14 400 MHz ^{13}C NMR spectra of **compound L5** in $CDCl_3$ (D, 99.8%).

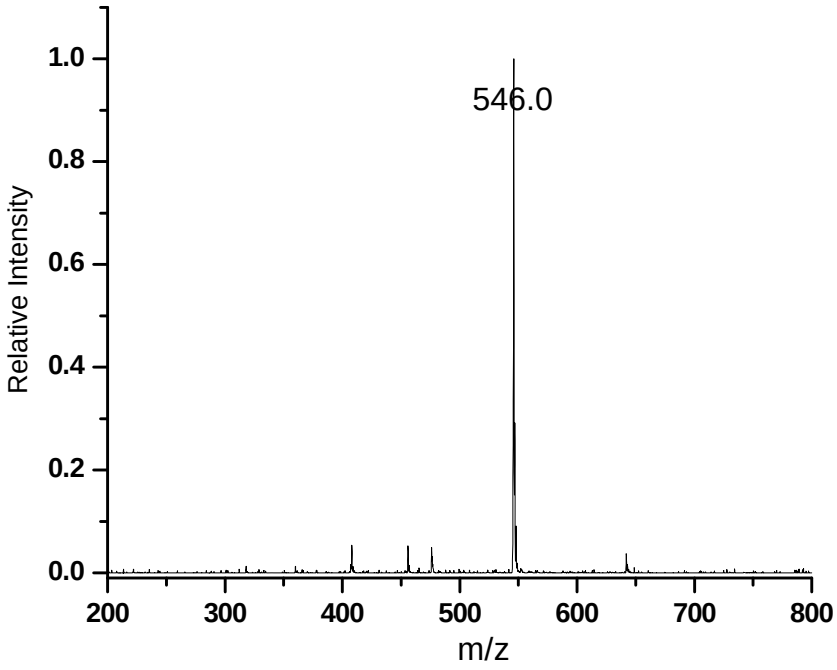

Figure 4.S15 ESI-MS spectra of **compound L5**.

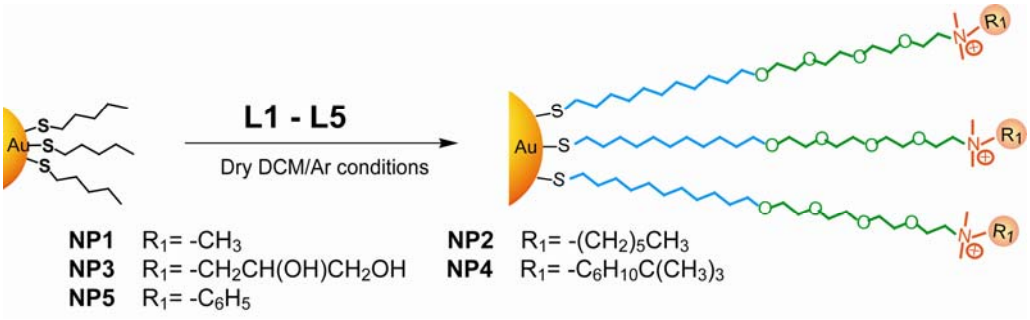

Scheme 4.S2 Fabrication of cationic gold nanoparticles.

General procedure: 1-Pentanethiol coated gold nanoparticles (*d* = ~2 nm) were prepared according to the previously reported protocol.[28] Place-exchange reaction[29] of compound **Ls** (s = 1, 2, 3, 4, 5) dissolved in DCM with pentanethiol-coated gold nanoparticles (d~2 nm) was carried out for 3 days at room temperature and the DCM was then evaporated under reduced pressure. The residue was dissolved in a small amount of distilled water and dialyzed (membrane MWCO = 1,000) to remove excess ligands, acetic acid and other salts present with the nanoparticles. After dialysis, the particles were lyophilized to afford a brownish solid. The nanoparticles are redispersed in ionized water (18 MΩ-cm). ^{1}H NMR spectra in D_2O showed substantial broadening of the proton signals and no free ligands were observed.

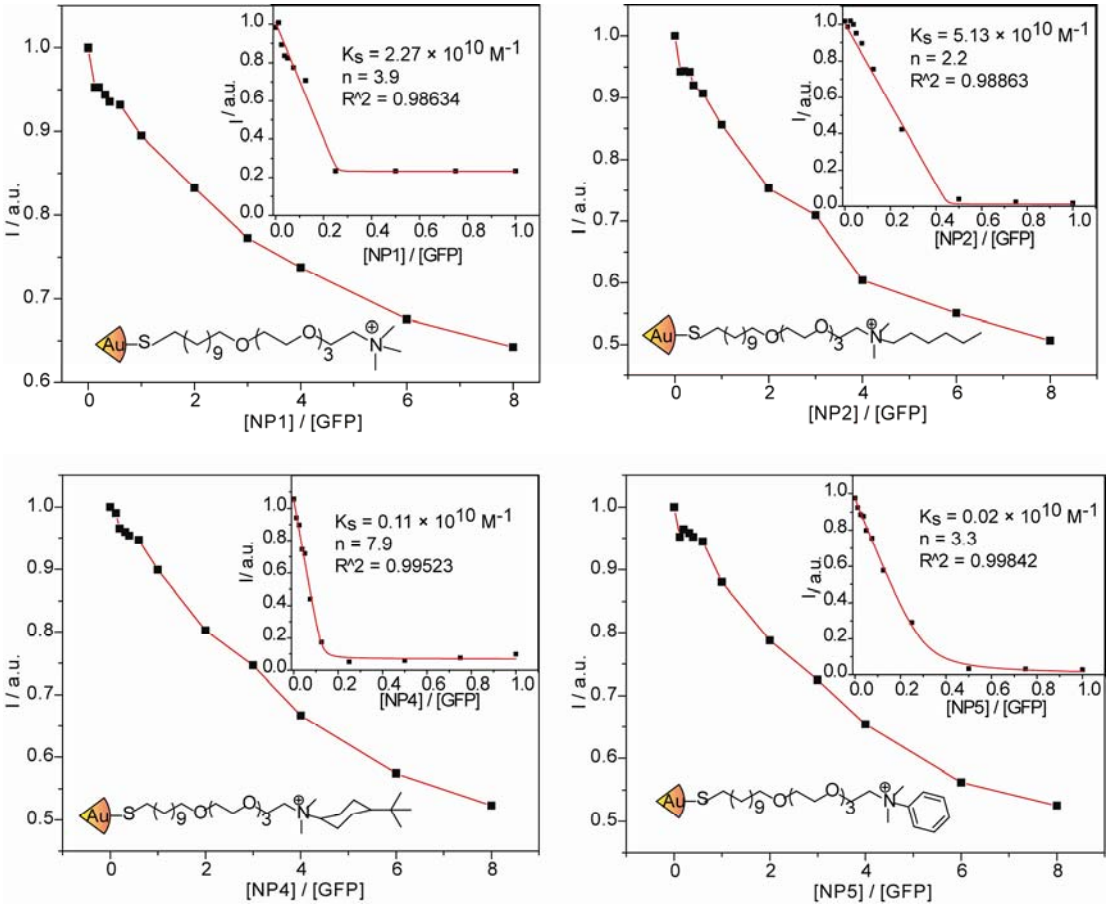

Figure 4.S16 Fluorescence titration curves for the complexation of GFP with four different cationic gold nanoparticles (**NP1**, **NP2**, **NP4**, **NP5**). The changes of fluorescence intensity at 510 nm were measured following the addition of cationic nanoparticles (0-100 nM for 5 mM sodium phosphate buffer (inset) and 0-2 μM for serum solution) with an excitation wavelength of 475 nm.

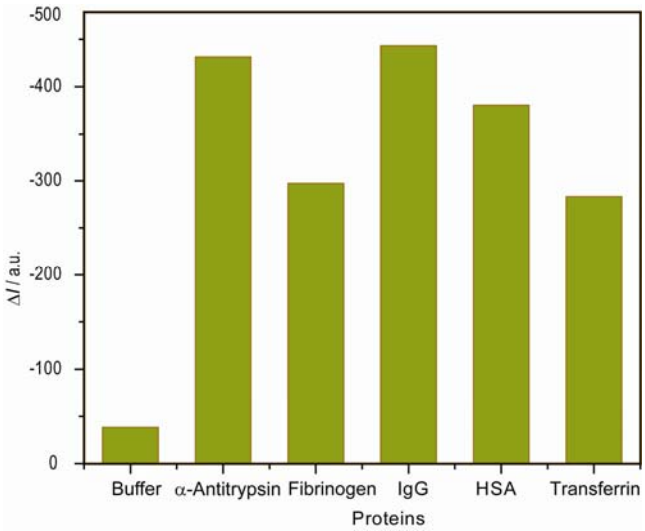

Figure 4.S17 Change in fluorescence responses (ΔI) of GFP (100 nM, 200 μL) in absence and presence of various protein solutions (25 nM). The intensities were recorded at 510 nm with an excitation wavelength of 475 nm**.** Each fluorescence response value is an average of six parallel measurements.

Table 4.S1 Binding constants (K_S), Gibbs free energy changes ($-\Delta G$) and binding stoichiometries (n) between GFP and various cationic nanoparticles (**NP1**-**NP5**) as determined from fluorescence titration.

Nanoparticle	K_S / 10^9 M^{-1}	$-\Delta G$ / kJ mol^{-1}	n
NP1	22.7	59.11	3.9
NP2	51.3	61.13	2.2
NP3	0.5	49.65	4.7
NP4	1.1	51.61	7.9
NP5	0.2	47.38	3.3

Table 4.S2 Training matrix of fluorescence response patterns of **NP**-GFP sensor array (**NP1**-**NP5**) against five serum proteins (25 nM) in 5 mM sodium phosphate buffer pH 7.4. Table continues on the next page.

Protein	**NP1**	**NP2**	**NP3**	**NP4**	**NP5**
HSA	-18.532	-45.298	-17.948	-16.819	0.972
HSA	-16.378	-29.25	-3.996	-11.575	7.191
HSA	-20.397	-36.076	-13.112	-13.901	1.021
HSA	-27.604	-24.953	-4.779	-13.927	4.034
HSA	-26.745	-25.183	-7.76	-3.6	0.781
HSA	-31.166	-28.784	-11.191	-2.124	8.168
IgG	-18.457	-20.497	-49.215	-6.814	6.723
IgG	-15.73	-12.767	-37.362	-5.608	3.726
IgG	-21.065	-5.392	-35.549	-6.856	1.957
IgG	-26.809	-7.699	-33.717	0.141	10.623
IgG	-20.746	-17.59	-42.568	-4.747	-7.43
IgG	-28.262	-21.65	-34.032	-8.2	1.772
Fibrinogen	-46.994	-20.427	44.239	-4.885	56.329
Fibrinogen	-72.301	-12.394	44.329	-8.931	73.802
Fibrinogen	-65.488	-22.13	49.268	-5.994	55.743
Fibrinogen	-78.38	-16.268	39.119	-4.24	71.327

Fibrinogen	-70.348	-15.801	58.2	-5.209	57.553
Fibrinogen	-88.654	-16.339	37.888	-3.165	79.429
α-Antitrypsin	1.832	-39.973	-8.15	-23.802	0.592
α-Antitrypsin	18.936	-40.204	-6.233	-26.518	12.63
α-Antitrypsin	15.499	-35.087	-9.344	-34.81	-2.162
α-Antitrypsin	-0.404	-37.903	-4.798	-23.846	-1.586
α-Antitrypsin	7.433	-39.452	-7.332	-25.163	-5.362
α-Antitrypsin	37.739	-41.178	-11.925	-23.795	1.874
Transferrin	-5.005	-30.502	-28.348	-14.971	-3.383
Transferrin	-12.869	-21.725	-18.571	-4.516	6.385
Transferrin	17.4	-19.154	-20.139	-11.815	4.825
Transferrin	-15.011	-14.219	-10.778	-2.678	2.904
Transferrin	-33.286	-11.069	-18.755	-2.382	5.71
Transferrin	8.789	-14.704	-23.331	2.752	2.368

Table 4.S3 LDA classification accuracy of protein analytes by using the individual GFP-nanoparticle complexes as sensor in 5 mM sodium phosphate buffer, pH 7.4. The values are considered from the Jacknifed classification matrix based on LDA analysis of the 6 replicated data listed in Table S1. The maximum classification accuracy was obtained 100% using all five GFP-nanoparticle combinations.

Proteins	**NP1**	**NP2**	**NP3**	**NP4**	**NP5**	All
HSA	67	83	67	100	67	100
IgG	100	33	100	0	100	100
Fibrinogen	50	33	33	67	17	100
α-Antitrypsin	67	50	100	0	0	100
Transferrin	33	33	83	0	0	100
Total	**63**	**47**	**77**	**33**	**37**	**100**

Table 4.S4 Training matrix of fluorescence response patterns of **NP**-GFP sensor array (**NP1**-**NP5**) against five serum proteins (500 nM) in human serum. Table continues on the next page.

Protein	**NP1**	**NP2**	**NP3**	**NP4**	**NP5**
HSA	-25.185	35.308	37.975	60.525	15.908
HSA	33.69	43.494	29.986	45.685	18.705
HSA	-34.553	33.198	11.311	54.613	10.012
HSA	79.313	26.839	15.565	49.973	28.507
HSA	14	13.784	25.269	33.235	13.216
HSA	50.658	43.361	19.192	31.82	29.904
IgG	-22.482	9.723	37.008	-2.621	-10.262
IgG	-110.788	11.703	-9.019	-7.571	-29.802
IgG	-55.84	-38.686	7.998	-74.414	-29.679
IgG	-122.045	-75.776	16.632	-2.424	-13.585
IgG	-184.384	-2.881	-14.023	-2.117	-7.345
IgG	-22.34	-36.442	-25.241	-6.95	-9.373
Fibrinogen	151.28	-119.741	-24.122	20.872	-53.202
Fibrinogen	147.351	-98.086	10.442	43.628	-32.968
Fibrinogen	133.975	-30.237	-12.07	26.133	-84.102

Fibrinogen	142.781	-112.046	-19.16	30.523	-31.204
Fibrinogen	114.114	-121.229	22.276	27.292	-28.001
Fibrinogen	113.864	-68.836	-51.75	30.508	-31.968
α-Antitrypsin	-76.466	42.259	-92.872	40.603	13.961
α-Antitrypsin	-24.938	42.652	-52.578	21.521	-0.383
α-Antitrypsin	-57.408	12.85	-16.545	29.464	6.252
α-Antitrypsin	-45.808	22.305	-67.508	13.642	10.035
α-Antitrypsin	-36.381	35.745	-20.054	30.49	12.917
α-Antitrypsin	-40.913	-23.131	-19.906	35.097	0.942
Transferrin	126.388	125.495	134.738	67.01	20.049
Transferrin	91.008	95.072	109.441	44.165	54.314
Transferrin	-34.963	54.258	-18.764	59.91	44.024
Transferrin	-60.551	101.613	71.836	45.938	41.313
Transferrin	56.279	62.391	-14.756	62.015	56.356
Transferrin	52.154	51.712	38.793	39.582	51.462

Table 4.S5 LDA classification accuracy of protein analytes by using the individual GFP-nanoparticle complexes as sensor in human serum. The values are considered from the Jacknifed classification matrix based on LDA analysis of the 6 replicated data listed in Table S3. The maximum classification accuracy was obtained 97% using all five GFP-nanoparticle combinations.

Proteins	**NP1**	**NP2**	**NP3**	**NP4**	**NP5**	All
HSA	100	83	50	33	67	100
IgG	17	67	83	17	67	100
Fibrinogen	50	50	17	100	67	100
α-Antitrypsin	33	67	67	50	83	83
Transferrin	83	33	50	0	67	100
Total	**57**	**60**	**53**	**40**	**70**	**97**

Table 4.S6 Detection and identification of unknown serum proteins in 5 mM sodium phosphate buffer, pH 7.4 using LDA. Table continues on the next page.

#	Fluorescence response pattern					Identification	Verification
	NP1	**NP2**	**NP3**	**NP4**	**NP5**		
1	4.684	-28.3937	19.506	-27.4577	11.22733	α-Antitrypsin	α-Antitrypsin
2	46.656	-29.2637	82.70033	-20.0467	113.517	Fibrinogen	Fibrinogen
3	0.349667	-29.862	-2.26733	-16.38	8.249	HSA	HSA
4	-26.234	-25.408	-33.522	-11.8157	0.307	IgG	IgG
5	-34.857	-21.2593	-23.4117	-5.48767	0.645	Transferrin	Transferrin
6	-2.04767	-34.0037	16.88767	-30.4097	17.768	α-Antitrypsin	α-Antitrypsin
7	94.439	-35.8293	104.2083	-5.826	59.99233	Fibrinogen	Fibrinogen
8	6.559667	-36.6427	-4.05033	-13.9613	6.927667	HSA	HSA
9	-33.871	-29.9463	-34.289	0.394667	0.741	IgG	IgG
10	-20.8303	-33.143	-27.1667	-10.0173	10.93633	Transferrin	Transferrin
11	-1.30033	-38.4287	10.827	-30.4497	5.354	α-Antitrypsin	α-Antitrypsin
12	66.78667	-35.138	73.21167	-4.52233	69.67133	Fibrinogen	Fibrinogen
13	1.165	-31.2983	-6.651	-11.6873	4.368	HSA	HSA
14	-17.0693	-17.9457	-23.7473	-7.08333	2.182667	IgG	IgG
15	-14.286	-25.4467	-20.7507	-4.872	-1.316	Transferrin	Transferrin

16	-8.64067	-31.4013	1.129	-22.642	8.385667	α-Antitrypsin	α-Antitrypsin
17	55.38367	-25.565	74.23333	-20.926	66.45067	Fibrinogen	Fibrinogen
18	11.715	-20.1727	2.882667	-15.2097	17.61033	HSA	HSA
19	-15.221	-37.6677	-23.318	-3.65267	1.684	Transferrin	IgG
20	-7.368	-20.7963	-13.128	-3.69333	6.640667	Transferrin	Transferrin
21	20.64133	-54.8697	50.54767	-17.1707	5.697333	α-Antitrypsin	α-Antitrypsin
22	146.8727	-43.762	111.4403	-5.83633	84.02133	Fibrinogen	Fibrinogen
23	6.840333	-48.6713	-3.30867	-7.54967	12.15967	HSA	HSA
24	-26.0133	-36.3093	-55.214	-1.13267	8.987	IgG	IgG
25	-11.3223	-16.426	-11.915	-7.36633	-0.62667	Transferrin	Transferrin
26	-6.78233	-18.0977	-13.793	-7.216	-2.137	Transferrin	Transferrin
27	3.568667	-31.5797	16.57667	-26.5613	4.504667	α-Antitrypsin	α-Antitrypsin
28	61.24267	-23.491	96.51133	-3.24867	58.63267	Fibrinogen	Fibrinogen
29	-15.2647	-29.7037	-15.109	-14.0513	4.040667	HSA	HSA
30	-11.202	-20.7027	-36.554	-3.775	2.106333	IgG	IgG

Table 4.S7 Detection and identification of unknown serum proteins in serum using LDA.

#	Fluorescence response pattern					Identification	Verification
	NP1	**NP2**	**NP3**	**NP4**	**NP5**		
1	74.75433	104.6627	52.88533	84.07	80.909	Transferrin	Transferrin
2	17.40667	44.292	33.522	4.037667	-7.886	α-Antitrypsin	α-Antitrypsin
3	-13.745	28.82867	27.56867	6.555667	8.313	α-Antitrypsin	α-Antitrypsin
4	-5.53367	56.73867	4.019333	19.02633	-94.1843	Fibrinogen	Fibrinogen
5	29.45633	28.211	41.33567	30.58633	-24.767	IgG	α-Antitrypsin
6	37.92233	-41.37	-103.575	23.30433	14.967	HSA	HSA
7	-16.582	26.09967	58.272	29.37633	38.515	HSA	HSA
8	-133.057	-23.643	7.877	-32.3313	-15.9957	IgG	IgG
9	-71.5627	-89.7873	-32.8967	-9.00367	18.158	IgG	IgG
10	62.023	38.60267	79.416	115.327	-35.331	Fibrinogen	Fibrinogen
11	122.1453	313.654	116.8473	148.417	131.8263	Transferrin	Transferrin
12	33.05733	23.643	37.877	32.33133	15.99567	HSA	HSA
13	5.293	33.464	36.257	28.801	30.66933	HSA	HSA
14	35.161	28.953	-0.567	30.251	-13.2193	α-Antitrypsin	α-Antitrypsin
15	-84.374	-90.1397	-34.6433	-75.8787	-110.12	IgG	IgG
16	48.80367	59.975	69.75367	61.452	74.422	Transferrin	Transferrin
17	54.00333	42.20967	73.615	56.78233	66.12933	Transferrin	Transferrin
18	240.9683	163.627	-28.523	-94.3863	-68.9923	IgG	IgG
19	31.52067	34.94333	43.77767	32.40133	-8.79367	α-Antitrypsin	HSA
20	60.67	48.87633	40.28167	16.78233	16.12933	HSA	HSA
21	41.82767	-32.953	-10.2337	31.91767	-39.0913	Fibrinogen	Fibrinogen
22	140.408	112.4333	-51.4157	11.00167	-97.6823	Fibrinogen	Fibrinogen
23	73.74133	45.76667	110.2757	77.66833	94.349	Transferrin	Transferrin
24	3.306	28.175	33.11667	42.325	-25.147	α-Antitrypsin	α-Antitrypsin
25	67.07967	9.277333	159.2897	32.82267	-123.864	Fibrinogen	Fibrinogen
26	87.183	43.376	157.9987	94.48633	117.043	Transferrin	Transferrin
27	-127.011	-271.885	-55.832	-204.422	58.93333	IgG	IgG
28	71.85633	32.289	16.79167	10.11067	8.785	HSA	HSA
29	-52.1673	37.82967	-31.4483	15.21	15.23333	α-Antitrypsin	α-Antitrypsin
30	115.5963	97.18933	131.6317	118.673	-99.101	Fibrinogen	Fibrinogen

Table 4.S8 Training matrix of the fluorescence responses of **NP**-GFP sensor array (**NP1**-**NP5**) against two serum proteins at different concentrations in undiluted serum.

Proteins	NP1	NP2	NP3	NP4	NP5
HSA 500 nM	36.779	93.68	35.538	21.085	47.776
HSA 500 nM	115.101	98.987	32.628	58.455	50.073
HSA 500 nM	75.371	89.106	56.712	36.143	34.554
HSA 500 nM	53.123	99.375	74.79	38.711	27.076
HSA 500 nM	79.465	88.404	55.727	51.131	25.436
HSA 500 nM	86.788	109.041	23.629	36.368	-2.934
HSA 1 µM	81.835	77.727	81.756	90.558	114.885
HSA 1 µM	48.202	94.133	100.135	55.811	102.966
HSA 1 µM	98.508	129.882	73.469	111.341	91.465
HSA 1 µM	88.247	77.25	50.121	57.31	102.692
HSA 1 µM	80.577	74.521	91.315	83.783	111.878
HSA 1 µM	103.679	119.859	86.81	63.374	91.567
HSA 2 µM	109.752	120.75	101.79	117.751	123.175
HSA 2 µM	68.678	124.737	123.571	94.761	77.74
HSA 2 µM	108.234	113.567	85.116	113.809	64.965
HSA 2 µM	91.207	88.023	84.701	114.75	66.563
HSA 2 µM	37.45	74.441	58.563	71.76	72.212
HSA 2 µM	36.984	54.034	101.945	72.592	61.694
IgG 500 nM	-20.535	-47.869	-1.231	20.578	-6.899
IgG 500 nM	-10.142	-3.756	-86.993	-51.978	0.955
IgG 500 nM	-32.613	-22.642	-90.484	-90.113	-29.181
IgG 500 nM	-17.667	-30.918	-55.741	-35.685	1.682
IgG 500 nM	10.918	-21.06	-19.7	-40.112	-22.847
IgG 500 nM	-12.79	-28.653	-39.975	19.348	-29.316
IgG 1 µM	-79.722	-18.975	-71.669	-28.268	-59.102
IgG 1 µM	-96.852	-61.204	-99.069	-27.075	-36.127
IgG 1 µM	-96.549	-34.248	-84.156	-62.283	-58.991
IgG 1 µM	-86.457	-72.164	-119.259	-69.132	-50.836
IgG 1 µM	-58.259	-54.634	-98.298	-33.522	-31.563
IgG 1 µM	-89.147	-265.236	-100.153	-35.929	-77.421
IgG 2 µM	-51.724	-83.283	-83.946	-84.5	-78.542
IgG 2 µM	-78.383	-100.504	-123.046	-65.95	-65.118
IgG 2 µM	-43.095	-65.418	-141.393	-72.145	-35.054
IgG 2 µM	-55.417	-99.826	-146.527	-47.284	-117.778
IgG 2 µM	-84.478	-60.019	-129.572	-11.872	-97.409
IgG 2 µM	-22.036	-80.941	-30.569	-61.74	-86.066

Table 4.S9 Training matrix of the fluorescence responses of NP-GFP sensor array (**NP1**-**NP5**) against mixtures of serum proteins (HSA and IgG 250 nM each; HSA and IgG 500 nM each) and individual proteins (HSA and IgG 500 nM each) in undiluted serum.

Protein(s)	NP1	NP2	NP3	NP4	NP5
HSA0.5 μM	36.779	93.68	35.538	21.085	47.776
HSA0.5 μM	115.101	98.987	32.628	58.455	50.073
HSA0.5 μM	75.371	89.106	56.712	36.143	34.554
HSA0.5 μM	53.123	99.375	74.79	38.711	27.076
HSA0.5 μM	79.465	88.404	55.727	51.131	25.436
HSA0.5 μM	86.788	109.041	23.629	36.368	-2.934
IgG0.5 μM	-20.535	-47.869	-1.231	20.578	-6.899
IgG0.5 μM	-10.142	-3.756	-86.993	-51.978	0.955
IgG0.5 μM	-32.613	-22.642	-90.484	-90.113	-29.181
IgG0.5 μM	-17.667	-30.918	-55.741	-35.685	1.682
IgG0.5 μM	10.918	-21.06	-19.7	-40.112	-22.847
IgG0.5 μM	-12.79	-28.653	-39.975	19.348	-29.316
HSA0.5-IgG0.5 μM	136.065	88.088	66.951	81.659	120.204
HSA0.5-IgG0.5 μM	24.462	33.528	69.531	77.042	56.269
HSA0.5-IgG0.5 μM	81.669	101.369	64.058	56.326	88.377
HSA0.5-IgG0.5 μM	59.897	70.35	46.265	-0.201	93.308
HSA0.5-IgG0.5 μM	103.92	50.723	74.781	34.042	79.045
HSA0.5-IgG0.5 μM	108.286	78.441	91.725	62.458	59.168
HSA0.25-IgG0.25 μM	-97.334	-184.659	-139.598	-61.371	-87.43
HSA0.25-IgG0.25 μM	-43.757	-124.828	-130.223	-91.557	-42.496
HSA0.25-IgG0.25 μM	-44.588	-80.317	-86.414	-108.216	-104.818
HSA0.25-IgG0.25 μM	-63.207	-64.866	-124.171	-97.906	-64.233
HSA0.25-IgG0.25 μM	-56.32	-137.994	-116.131	-73.141	-67.603
HSA0.25-IgG0.25 μM	-84.824	-83.432	-87.4	-63.884	-59.937

4.5 References

1. a) Capasso, C.; Rizzi, M.; Menegatti, E.; Ascenzi, P.; Bolognesi, M. *J. Mol. Recogn.* **1997**, *10*, 26. b) Caplan, A. J.; Mandal, A. K.; Theodoraki, M. A. *Trends Cell Biol.* **2007**, *17*, 87.

2. a) Castro, M. J. M.; Anderson, S. *Biochem.* **1996**, *35*, 11435. b) Cavalieri, F.; Chiessi, E.; Paradossi, G. *Soft Matter* **2007**, *3*, 718.

3. Censarek, P.; Beyermann, M.; Koch, K. W. *Biochem.* **2002**, *41*, 8598.

4. Censarek, P.; Beyermann, M.; Koch, K. W. *Febs Letters* **2004**, *577*, 465.

5. Chakrabarti, R.; Klibanov, A. M. *J. Am. Chem. Soc.* **2003**, *125*, 12531.

6. a) Chalfie, M.; KainIn, S. R. *Green Fluorescent Protein: Properties, Applications, and Protocols*. Wiley-Interscience: Hoboken, N. J. **2006**. b) Chan, W. C. W.; Nie, S. M. *Science* **1998,** *281*, 2016.

7. Chapman, E.; Farr, G. W.; Fenton, W. A.; Johnson, S. M.; Horwich, A. L. *Proc. Nat. Acad. Sci. USA* **2008**, *105*, 19205.

8. a) Chauvin, F.; Fomenkov, A.; Johnson, C. R.; Roseman, S. *Proc. Nat. Acad. Sci. USA* **1996**, *93*, 7028. b) Chen, C. P.; Hsu, C. H.; Su, N. Y.; Lin, Y. C.; Chiou, S. H.; Wu, S. H. *J. Biol. Chem.* **2001**, *276*, 45079.

9. Cheon, J.; Lee, J. H. *Acc. Chem. Res.* **2008**, *41*, 1630.

10. Chiti, F.; Dobson, C. M. *Ann. Rev. Biochem.* **2006**, *75*, 333.

11. Ciosek, P.; Wroblewski, W. *Analyst* **2007**, *132*, 963.

12. Wright, A. T.; Anslyn, E. V. *Chem. Soc. Rev.* **2006**, 35, 14.

13. Lavigne, J. J.; Anslyn, E. V. *Angew. Chem. Int. Ed.* **2001**, 40, 3119.

14. Wright, A. T.; Edwards, N. Y.; Anslyn, E. V.; McDevitt, J. T. *Angew. Chem. Int. Ed.* **2007**, 46, 8212.

15. Zhou, H. C.; Baldini, L.; Hong, J.; Wilson, A. J.; Hamilton, A. D. *J. Am. Chem. Soc.* **2006**, 128, 2421.

16. Miranda, O. R.; You, C. C. ; Phillips, R. ; Kim, I. K. ; Ghosh, P. S.; Bunz, U. H. F.; Rotello, V. M. *J. Am. Chem. Soc.* **2007**, **129**, 9856.

17. Stephenson, C. J.; Shimizu, K. D. *Polym. Int.* **2007**, **56**, 482.

18. You, C. C.; Miranda, O. R.; Gider, B.; Ghosh, P. S.; Kim, I. B.; Erdogan, B.; Krovi, S. A.; Bunz, U. H. F.; Rotello, V. M. *Nature Nanotechnol.* **2007**, *2*, 318

19. Phillips, R. L.; Miranda, O. R.; You, C. C.; Rotello, V. M.; Bunz, U. H. F. *Angew. Chem. Int. Ed.* **2008**, **47**, 2590.

20. De, M.; You, C. C.; Srivastava, S.; Rotello, V. M. *J. Am. Chem. Soc.* **2007**, 129, 10747.

21. Hong, R.; Fisher, N. O.; Verma, A.; Goodman, C. M.; Emrick, T. S.; Rotello, V. M. *J. Am. Chem. Soc.* **2004**, 126, 739.

22. Tsien, R.Y. *Annu. Rev. Biochem.* **1998**, 67, 509.

23. Chalfie M; Kain S. R. *Green Fluorescent Protein: Properties, Applications, and Protocols* pp 69 (Wiley-Interscience: Hoboken, N.J., **2006**).

24. Anderson, N. L.; Anderson, N.G. *Mol. Cell. Proteomics* **2002**, 1, 845.

25. You, C.C.; De, M.; Han; G.; Rotello, V. M. *J. Am. Chem. Soc.* **2005**, 127, 12873.

26. Jurs, P. C.; Bakken, G. A.; McClelland, H. E. *Chem. Rev.* **2000**, 100, 2649.

27. De, M.; Rana, S.; Rotello, V. M. *Macromol. Biosci.* **2009**, 9, 174.

28. Brust, M.; Walker, M.; Bethell, D.; Schiffrin, D.J.; Whyman, R. *J. Chem. Soc. Chem. Commun.*, **1994**, 801.

29. Hostetler, M. J.; Templeton, A. C.; Murray, R.W. *Langmuir* **1999**, 15, 3782.

CHAPTER 5

ENZYME AMPLIFIED ARRAY SENSING (EAAS): CHEMICAL NOSE DETECTING PROTEIN IN HUMAN URINE

5.1Introduction

Irregular protein concentration levels in biofluids, e.g. serum, urine, and saliva provide essential information for the early diagnosis of many pathological conditions such as hypoalbuminemia, cancers, Alzheimer's disease, prostatisis, HIV, and other disease states.[1] The development of strategies for monitoring protein levels remains a major issue in medical diagnostics, pathogen detection and proteomics.[2] Substantial efforts have been devoted to develop precise and efficient methods for protein sensing,[3] including enzyme-labeled immunoassays,[4] electrophoresis methods,[5] and analytical techniques.[6]

The "chemical nose/tongue" approach[7] presents a potential alternative to specific recognition and separations techniques. In this approach a sensor array is generated to provide differential interaction with analytes via *selective* receptors, generating a stimulus response pattern that can be statistically analyzed and used for the identification of individual target analytes[8,9] and also analysis of complex mixtures.[10] Over the past few years, this technology has been successfully applied for protein detection using array-based approaches, including porphyrins,[11] oligopeptide-functionalized resins,[12] and polymers.[13] In a real word example, a single functional conjugated polymer poly (thiophene) has been successfully applied as a food freshness sensor to detect biogenic amines in fish associated with food poisoning (e.g. histamine) with increasing concentrations from 22.5 μM to 4.5. Recently, we have developed nanoparticle-GFP

based “chemical nose” strategy for protein detection in biofluid that is highly sensitive (500 nM)[14] as compared to other reported similar approaches (1-350 μM).[11,12,13c,d] We have also developed a sensor array composed of gold nanoparticles and fluorescent polymers that can identify proteins through a fluorophore-displacement mechanism.[15] This sensor array achieved detection limits of 215 nM for low M_w proteins.

The increased sensitivity required for many diagnostic uses[16] presents a challenging goal for array-based sensor because the detection process generally relies on fluorescence responses that are restricted by the inherent emissivity of the fluorophores used. To overcome this limitation, we have explored the use of enzymes to provide array-based sensors with enhanced sensitivity. In this Enzyme Amplified Array Sensing (EAAS) approach, the sensitivity of the array is amplified through an enzymatic reaction. This approach couples the signal amplification process of ELISA with the versatility of the “chemical nose” approach. In this dissertation, the use of this method to sense and identify a range of biomedically relevant proteins at 1 nM in both buffer and desalted human urine is reported.

Our EAAS features three components: a) β-galactosidase (β-Gal) as the enzyme, b) 4-Methylumbelliferyl-beta-D-Galactopyranoside (MUG) as a fluorogenic substrate to provide “turn on” sensing, and c) gold nanoparticles (**AuNP**s) as the receptors to provide differential protein affinity, and hence discrimination. In practice, cationic **AuNP**s electrostatically bind the anionic β-Gal, inhibiting the enzyme without denaturation.[17] Displacement of the particle by analyte proteins restores β-Gal activity, generating a fluorescent readout signal (Figure 5.1) that is amplified through enzymatic catalysis.

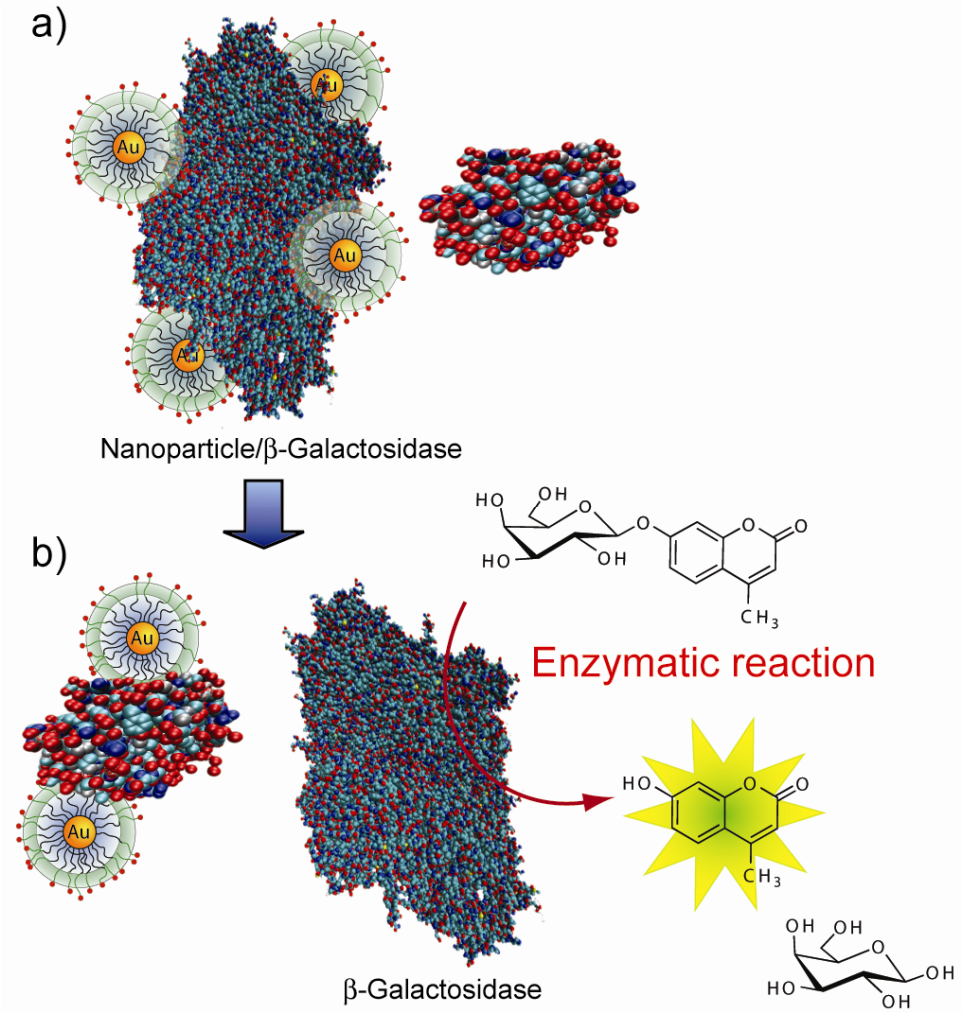

Figure 5.1 A schematic representation of sensors comprised of β-Galactosidase (β-Gal) and cationic **AuNP**s. In a) supramolecular adducts of β-Gal and **AuNP** formed through complementary electrostatic interactions, inhibiting the enzymatic activity of β-galactosidase. As shown in b) β-Galactosidase is displaced from the β-Gal/**AuNP** complex by protein analytes, restoring the catalytic activity of β-Gal towards the fluorogenic substrate 4-methylumbelliferyl-β-D-Galactopyranoside, resulting in an amplified signal for detection.

5.2 Results and Discussion

The anionic tetrameric enzyme β-Gal (17.5×13.5×9 nm, pI = 4.6, M_w = 465 kDa), was chosen as the amplifying element due its stability to a wide range of temperature, pH, and ionic strength conditions.[18,19] Gold nanoparticles (~2 nm core diameter) with a positive surface charge were used to bind efficiently to the anionic β-Gal trough electrostatic

complementary and electrostatic charge interactions (see Figures 5.S29, 5.S31, and 5.S33 for zeta potential and DLS measurements). These **AuNP**s feature a tetraethylene glycol unit in the ligand shell to minimize the denaturation of the bound enzyme/analyte protein and variable terminal functionality to generate the differential affinity required for sensing (Figure 5.2).[20]

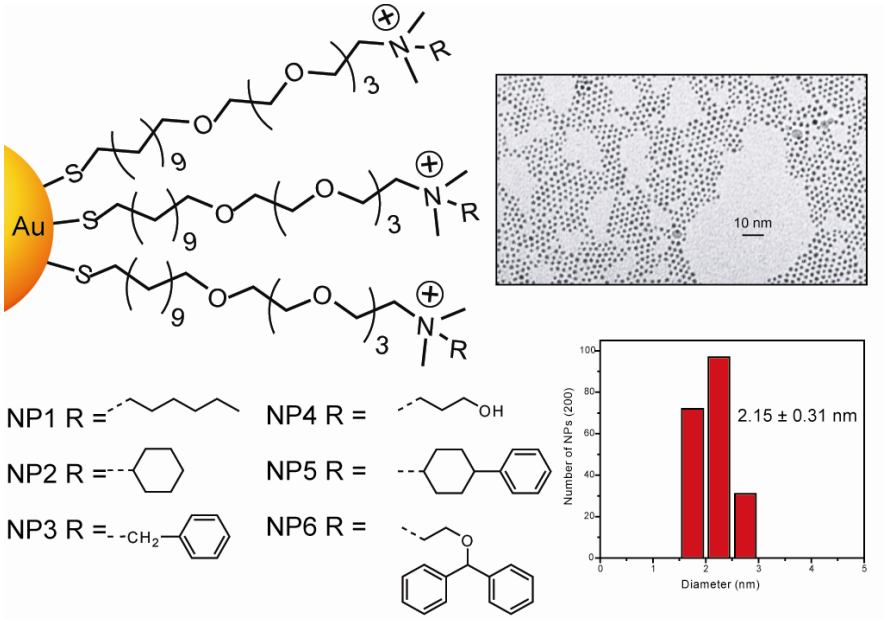

Figure 5.2 Structure features of the cationic gold nanoparticles (NP1-NP6). The transmission electron microscopy (TEM) and histogram plot show the morphology, monodispersity, and sizes of the metallic core gold nanoparticles.

As a starting point, we focused on the optimization on the binding ratio between **AuNP**s (**NP1-NP6**) and β-Gal through inhibition activities in phosphate buffer. We conducted an activity assay of β-Gal-catalyzed hydrolysis at various concentrations of nanoparticles (see Figure 5.S26). Typically, a concentration of 0.5 nM of β-Gal in phosphate buffer solution (5 mM, pH = 7.4) was incubated with various concentration of **NP1-NP6** for 30 minutes and 1 mM of the fluorogenic substrate (MUG, λ_{exc} = 455 nm)

was added to **AuNP**-enzyme complexes for the inhibition and enzyme-substrate reaction studies. As a control, the enzyme inhibition was also studied with neutral tetra(ethylene glycol) functionalized nanoparticles. The normalized first-order rate of fluorogenic substrate hydrolysis was plotted versus the ratio of nanoparticles to β-Gal, and showed a tendency to decrease upon addition of nanoparticles, as shown for **NP2** in Figure 5.3. This result clearly indicates that activity of β-Gal is inhibited by nanoparticle binding. This inhibition of β-Gal activity depends on subtle structural changes of peripheral ligands on the **AuNP**s with the linear end group (**NP1**) exhibiting less suppression than a branched isomeric structure (**NP2**).

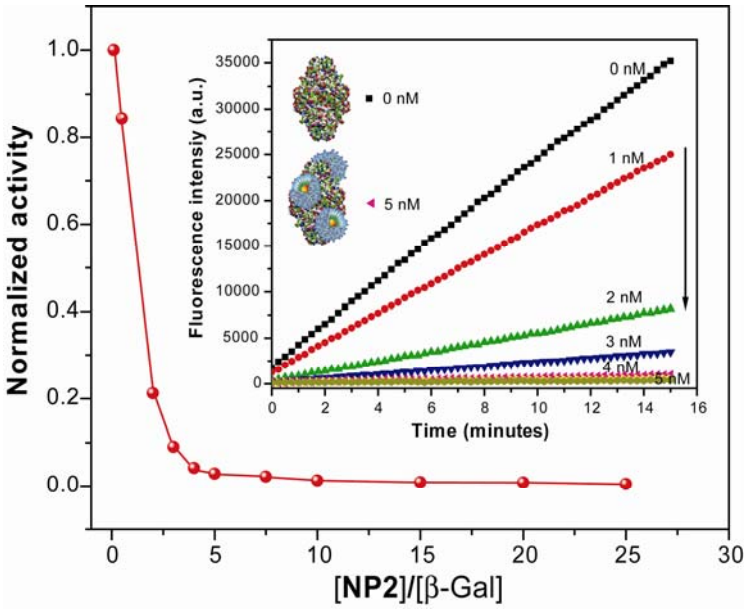

Figure 5.3 Normalized inhibition activity of β-Gal (0.5 nM) against 1 mM substrate MUG upon addition of cationic **NP2** in 5 mM phosphate buffer. The inset shows the kinetics of the fluorescence spectra before and after addition of **NP2.** The arrow in the inset indicates the direction of activity (0 nM indicates free enzyme and 5 nM indicates inhibited enzyme with **NP**s).

A total of nine proteins of various sizes, surface charges, molecular weights, and isoelectric points were chosen to test generality and limitations of our sensor, (Table 5.1, see Table 5.S6 for zeta potentials, r_h values and extinction coefficients at 280 nm of the

analyte proteins). Fluorogenic substrate hydrolysis for the β-Gal/**AuNP** conjugates against individual proteins in buffer is summarized in Figure 5.4. The individual target proteins generated distinguishable and highly reproducible rates of the fluorogenesis, indicating the potential for protein discrimination.

Table 5.1 Physical properties of the proteins used as sensing targets in phosphate buffer solution at pH 7.4.[13a]

Protein‡	**Mw (kDa)**	**pI**
α-Amylase (α-Am)	50.0	5.0
Bovine serum albumin (BSA)	66.3	4.8
Cytochrome *c* (CytC)	12.3	10.7
Ferritin (Fer)	750.0	4.5
Human serum albumin (HSA)	69.4	5.2
Lipase (Lip)	58.0	5.6
Lysozyme (Lys)	14.4	11.0
Myoglobin (Myo)	17.0	7.2
Alkaline phosphatase (PhosB)	140.0	5.7

‡ Proteins in *italics* are commonly found in human urine.

All proteins were tested using a fluorescence displacement assay of six β-Gal/**AuNP** assemblies array for six replicate measurements, providing a data set as a 6 × 6 × 9 matrix. The resulting data was analyzed through linear discrimination analysis (LDA) using SYSTAT software (version 11)[21] and transformed into five canonical factors. This statistical analysis method is used to recognize the linear combination of features that differentiate two or more classes of objects or events. The five canonical factors contain 42.2%, 34.1%, 12.1%, 5.8%, and 4.9% of the variation, respectively. The canonical

score plot of the first three factors is presented in Figure 5.5, where each dot represents the fluorescence response pattern of a single protein target to the β-Gal/**AuNP** sensor array. The canonical plot reveals nine distinct clusters corresponding to individual target proteins that give rise to a 100% classification accuracy obtained from a Jackknifed matrix in LDA. This result demonstrates that the β-Gal/**AuNP** sensor array is sensitive enough to differentiate target proteins in the 1 nM range, significantly more sensitive than prior methods, including our previous fluorescent polymer-nanoparticle conjugates systems.[11,12,13,15]

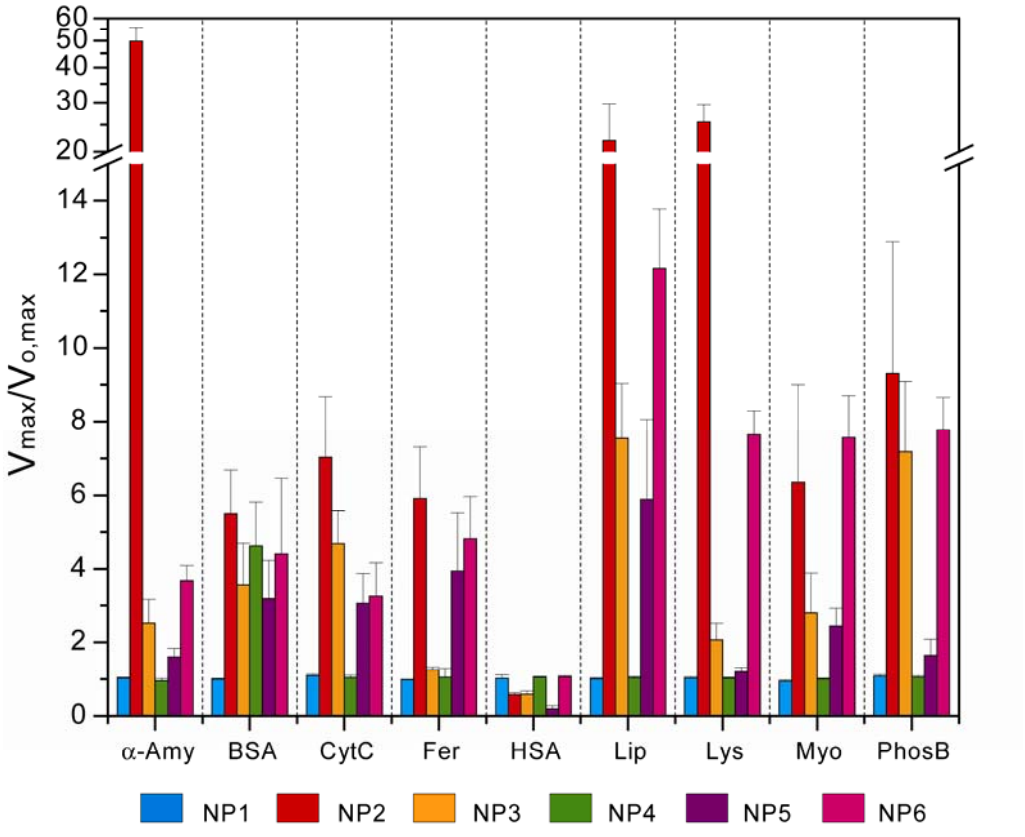

Figure 5.4 Fluorescence response patterns ratio of β-Gal and six **AuNP** adducts against various target proteins. Each value represents an average of six parallel measurements with standard deviation.

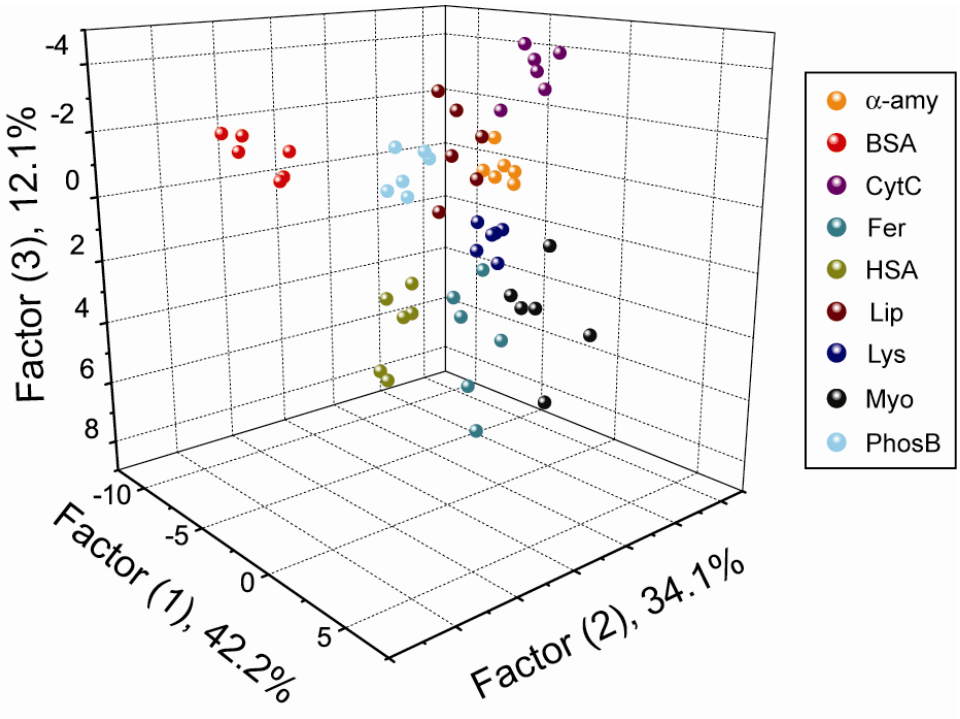

Figure 5.5 Canonical score plot of the first three factors of fluorescence response patterns obtained through β-Gal/**AuNP** sensor array against nine target proteins in 1 nM concentration.

The high sensitivity of our β-Gal/**AuNP** sensor array can be attributed to signal amplification through the enzyme-substrate reaction of β-Gal. Significantly, the same training matrix analyzed using only one nanoparticle structure gives rise to classification accuracies of 33%, 44%, 37%, 31%, 44%, and 35% for **NP1** to **NP6** respectively, indicating almost equal ability of each particle to discriminate between protein targets (Table 5.S3).

To investigate the robustness identification accuracy of the β-Gal/**AuNP** sensor array, we prepared sixty unknown protein samples at 1 nM randomly chosen from the training set for identification. The fluorescence response patterns obtained for each unknown against the sensor array were analyzed through LDA analysis. The resulting patterns were classified through the canonical score plot by the first two factors of simplified

fluorescence patterns based on the Mahalanobis distances of unknowns to the centroid of the respective protein clusters in the canonical score plot. An identification accuracy of 92% (55 correct out 60) demonstrates reproducibility of our enzyme-nanoparticle sensor system for identification.

Sensing of proteins in real world biofluids such as protein in human urine provides a far more demanding test than sensing in simple buffer solutions. The overall protein content (>1.5 μM, 0.150 g/L) and the multianalyte nature of the human urine (>1500 proteins as competing biomolecules) generate a complex matrix that is challenging for sensor design.[22] An additional complication that arises is variation in ionic strength, an issue that addressed biomedically through desalting using the standard spin column chromatography, a technique we employed in our studies that would complicate real-world analysis, human urine was used for medical analysis (see Figures 5.S27 and 5.S28). [22,23]

The complexation between β-Gal and cationic **AuNP**s in human urine (Bioreclamation Inc.) solution desalted via spin column chromatography was also determined by the hydrolysis of MUG by β-Gal in the presence of various concentrations of **AuNP**s (Figure 6, additional information see Figures 5.S34 and 5.S35). In this experiment, β-Gal was dissolved in human urine protein solution (~1.5 μM, see SI for details) buffered to pH = 7.4 using 5 mM phosphate buffer. This solution was then equilibrated with a stoichiometric amount of nanoparticles for 15 min. Then, an excess amount of the MUG solution (1 mM) was added to initiate the enzymatic reaction. The activity of β-Gal was directly correlated with the **AuNP**s concentration, indicating that the activity of β-Gal is inhibited by **AuNP**s complex formation.

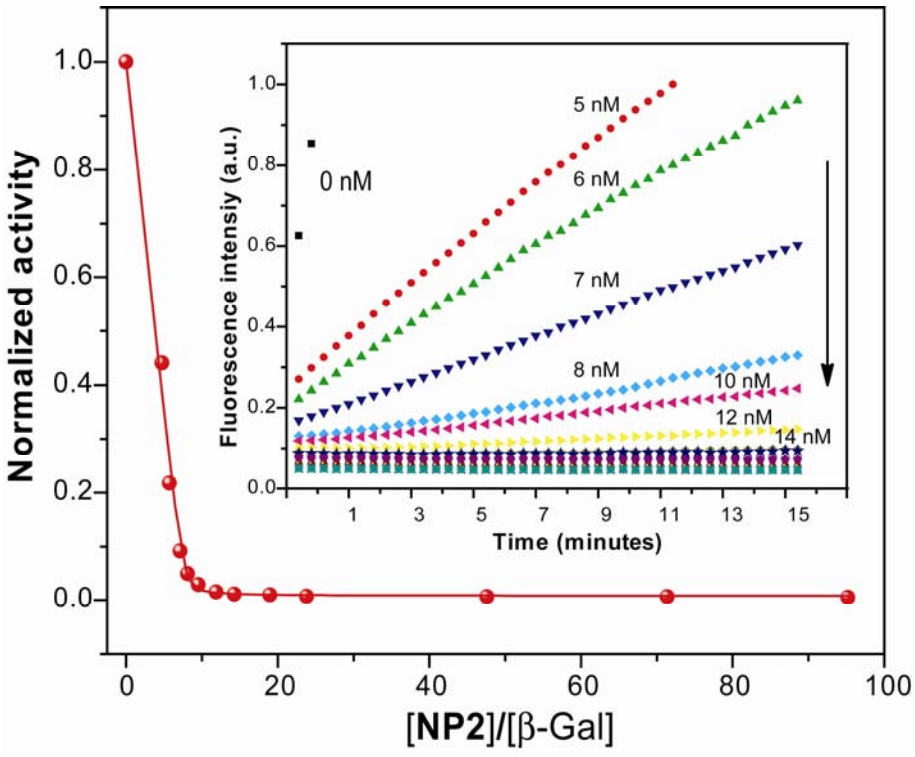

Figure 5.6 Normalized inhibition activity of β-Gal (0.5 nM) against 1 mM substrate MUG upon addition of cationic **NP2** in the presence of desalted human urinary proteins. The inset shows the kinetics of the fluorescence spectra before and after addition of **NP2**. The arrow in the inset indicates the direction of activity.

Using the conditions optimized above described, it was established that 1 nM concentration of spiked proteins was required for reproducible differentiation of the target analytes (Table 5.1). As before, we created a training matrix (six β-Gal/**AuNP** adducts × nine proteins × six replicates) with β-Gal/**AuNP** adduct and each of the proteins. Each protein in the human urine protein solution generated a distinct fluorescence response. The rates of fluorogenic substrate hydrolysis for β-Gal/**AuNP** pair in the presence of individual protein analytes are summarized in Figure 7, showing that **NP1** and **NP4** exhibit stronger affinity for β-Gal than for other proteins, producing smaller hydrolysis rates and less fluorescence response. As before, this fluorescent response pattern was subjected to further LDA analysis producing a 6 × 6 × 9 matrix.

This matrix was transformed into five canonical factors. The five canonical factors contain 62.3%, 20.7%, 9.1%, 4.3%, and 0.9% of the variation, respectively.

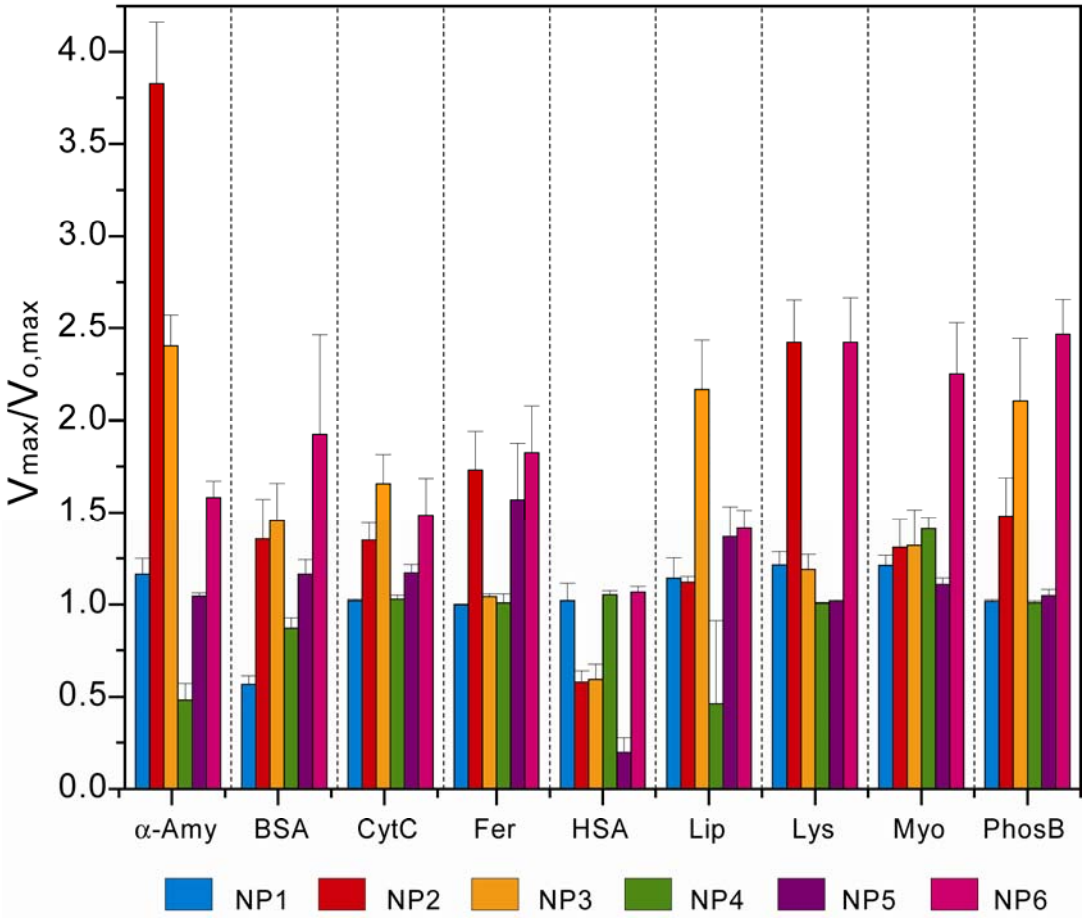

Figure 5.7 Fluorescence response patterns ratio of β-Gal and six **AuNP** adducts against various target proteins. Each value represents an average of six parallel measurements.

The canonical score plot of the first three factors is presented in Figure 5.8, where each dot represents the fluorescence response pattern of a single protein target to the β-Gal/**AuNP** sensor array. The canonical plot reveals nine distinct clusters corresponding to individual target proteins, giving rise to a 100% classification accuracy based on the

Jackknifed matrix in LDA. This result demonstrates that the β-Gal/**AuNP** sensor array is sensitive enough to differentiate each of the target proteins at 1 nM in the biofluid matrix (0.067% of the total protein content in urine), comparable with the preliminary study carried out in buffer. This sensitivity is improved as described before 4-215 fold in comparison with simple fluorophore displacement[15] and it is also comparable with the preliminary study carried out in buffer. The particles in this study are well suited for differentiation: the same training matrix analyzed using a single nanoparticle gives rise to classification accuracies of 33%, 52%, 41%, 43%, 48%, and 31% from **NP1** to **NP6**, respectively (Table 5.S10). This indicates almost an equal contribution of each particle in the discrimination of the examined protein targets.

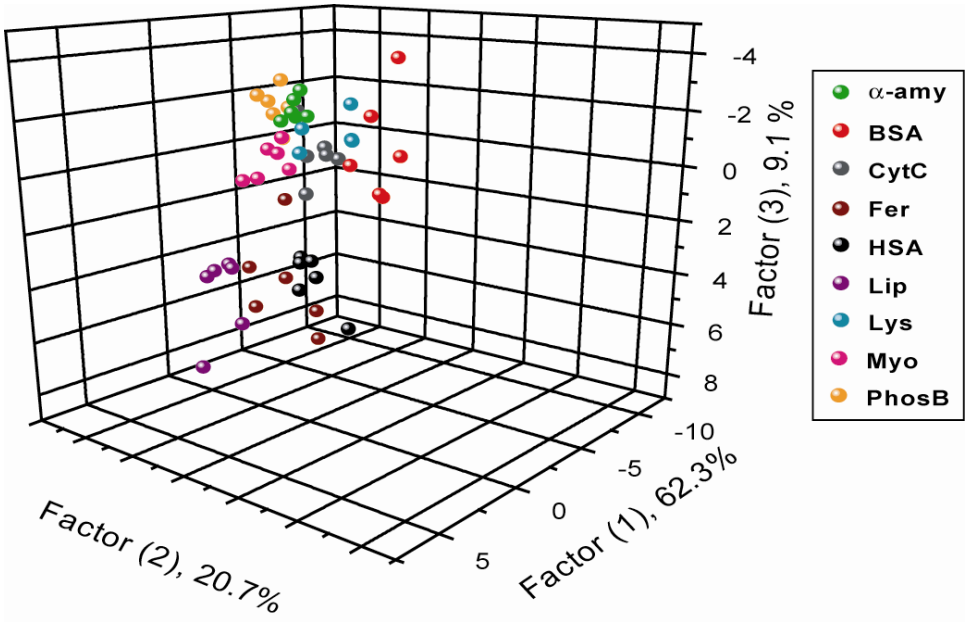

Figure 5.8 Canonical score plot of the first three factors of fluorescence response patterns ratio obtained through β-Gal/**AuNP** sensor array against nine target proteins at 1 nM in desalted human urine (~1.5 μM total protein content).

The accuracy of the β-Gal/**AuNP** sensor array was validated by identifying unknown proteins in the competitive environment of desalted human urine protein

solution. Sixty unknown protein solutions spiked at 1 nM were chosen arbitrarily from the training set. The fluorescence response patterns were newly analyzed through LDA analysis, and further classified by the Mahalanobis distances of unknowns to the centroid of the respective protein clusters in the canonical score plot. This process identified 55 out of 60 unknowns correctly, corresponding to a 92% identification accuracy, demonstrating both the feasibility and reproducibility of our enzyme-nanoparticle sensor system.

5.3 Conclusion

In this study, we have demonstrated the use of enzymatic amplification dramatically increase the sensitivity of the array-based sensing of proteins. Using this EAAS method, we were able to rapidly and reproducibly sense proteins at concentrations of 1 nM in both phosphate buffer and desalted human urine protein solution. These studies demonstrate that sensing can be achieved with high sensitivity in a complex biomatrix, providing an important first step for the creation of array-based biosensors for real-word diagnostic applications. In our ongoing studies, we are exploiting both new alternative approaches for protein detection and new data analysis strategies to apply this methodology to more complex matrices featuring a large diversity of target analytes.

5.4 Experimental Section

5.4.1 Binding of β-Gal to Cationic AuNPs 1-6. Agarose (Type-IB, Sigma Aldrich) gel electrophoresis was performed using a FisherBiotech Electrophoresis System (mini-horizontal unit FB-SB-710). β-Gal (2 μM) was incubated with cationic **AuNP**s at

different ratio in sodium phosphate buffer (5 mM, pH 7.4) for 15 minutes. 5 μL of 80% glycerol in deionized water (18 MΩ-cm) was added to 40 μL of above solutions and the samples were loaded onto the gel. A constant voltage (100 V) was applied to the system for 45 min to achieve adequate separation. The gels were then stained in a 0.5% Coomassie blue solution (40% volume methanol and 10% volume acetic acid in distilled water) for 1 h. Extensive destaining process was carried out with a 40% volume methanol and 10% volume acetic acid aqueous solution until the proteins were clearly visible.

5.4.2 Concentration of desalted human urinary proteins. The male human urine sample (Bioreclamation Inc.) was first adjusted to pH 3.5. Then, the pH-adjusted urine sample was applied on a pre-activated maxi spin column (Norgen Biotek Corporation, NBC). A buffer solution (P/N 21602) from NBC was used to wash the column. At pH 3.5, the urinary proteins are able to bind to the resin in the column based on their charges; while the salts and other related species are removed with the eluent. The purified urine proteins were finally eluted with an elution buffer solution (P/N 21605) from NBC (Figures S26 and S27). The concentrated and salt-free human urine proteins were diluted at a concentration of 120 μg/mL (~1.5 μM) in 5 mM phosphate buffer. This complex matrix was used to prepare β-Gal solutions at 0.5 nM. Experiments using these samples need to be processed as soon as possible; delays of more than 2 h might cause unreliable results.

5.4.3 Protein Sensing in Presence of Desalted Human Prinary Proteins. β-galactosidase (β-Gal) and the fluorogenic substrate (4-Methylumbelliferyl-beta-D-galactopyranoside, MUG) were purchased from Sigma-Aldrich. In the two different studies, nanoparticle and β-Gal solutions were prepared i) in sodium phosphate buffer solution (5 mM, pH 7.4) and ii) 120 μg/mL human urinary proteins in 5 mM phosphate buffer. In the activity assay studies, β-Gal (0.5 nM) was incubated with various concentrations of **NP1-NP6** for 30 minutes and 1 mM of the fluorogenic substrate (MUG) was added. As a control experiment, the enzymatic activity of β-Gal was also monitored in the presence of neutral tetraethylene glycol functionalized nanoparticles. The β-Gal stock concentration was 275 nM, while the stock concentrations of **NP1-NP6** were prepared in the range of 100 nM and 50 nM. The inhibition studies were carried out at pre-determined times by adding 5 μL of MUG (42 mM in DMSO) and 5 μL of PB buffer into 200 μL β-Gal/**AuNP** solution. The enzymatic activity was followed by monitoring product formation every 22 s for 15 minutes at 455 nm using a microplate reader (EL808 Bio-Tek Instruments, Inc.). The samples were measured in triplicate. From the activity/inhibition studies, optimal concentrations of β-Gal/**AuNP** complexes were obtained.

Once the different inhibiting characteristics of the β-Gal/**AuNP** complexes were established, stoichiometric amounts of β-Gal and **NP1-NP6** were used to sense the protein targets in two different solutions. In the first solution the analyte targets were spiked in 5 mM phosphate buffer (pH 7.4) while the second was spiked in 5 mM phosphate buffer containing 120 μg/mL human urinary proteins. As a general protocol, each solution of the β-Gal/**AuNP** complex (200 μL) was placed into a well on the 96-

well microplate. After incubation for 30 mins, 5 μL of an analyte protein solution (stock solution = 42 nM) was added to each well. After incubation for another 30 min, 5 μL of MUG (42 mM in DMSO) was added to the sample and the enzyme reaction activity was monitored for product formation every 22 s for 15 minutes at 455 nm using a microplate reader. This process was carried out for 9 proteins to generate six replicates for each, leading to a training data matrix of 6 nanoparticles × 9 proteins × 6 replicates that was subjected to a classical linear discriminant analysis (LDA) using SYSTAT (version 11.0). In the studies of unknown samples, sixty unknown protein solutions were randomly selected from nine proteins in the training set, and prepared at 42 nM concentration diluted from a stock solution with UV absorbance at 280 nm equal to 0.1. The sensing assay was conducted using the aforementioned procedure with 5 μL of unknown, affording a final protein concentration of 1 nM into the 96 wells microplate reader. Each unknown was performed twice against sensor array to obtain an average of a fluorescence response pattern. Afterward, the protein identity was detected by LDA analysis, with the system correctly determining a 92% of accuracy of the unknown samples over the span of the experiment. In the experimental setup, the solution preparation, data collection, and LDA analysis were operated by different persons to reduce bias and increase reproducibility of the unknown experiment.

5.4.4 Instrumentation. TEM samples were prepared by depositing 3 μL of a diluted aqueous solution of cationic **AuNP**s (5 μM) onto a 300 mesh carbon-coated copper grid. The samples were dried in air at room temperature. TEM images were obtained on a JEOL 100CX electron microscope operated at 100 keV and analyzed using Image J. More than 200 **AuNP**s were taken as target samples to calculate the average diameters

and size distributions. ζ-Potential (ZP) and dynamic light scattering (DLS) results were used to characterize the charge and the hydrodynamic diameter of both nanoparticles and proteins. Cationic gold nanoparticles were dissolved in sodium phosphate buffer (5 mM, pH 7.4) to make solutions at 5 μM concentrations. The samples were filtered through a Millipore syringe-driven filter (0.22 μm) and injected into a folded capillary disposable cell. In the case of the proteins, the samples were filtered through a Millipore syringe-driven filter (0.22 μm) and injected into the disposable cell. Both ZP and DLS were measured on a MALVERN Zetasizer Nano ZS instrument. Each sample was scanned six times and an average value was reported.

5.4.5 Synthesis of AuNPs 1-6. Pentanethiol-coated **AuNP**s with core diameter ~2 nm were synthesized using the Brust-Schiffrin two-phase synthesis method.[1] Murray place-exchange method[2] was used to obtain the quaternary ammonium functionalized **AuNP**s **1-6** (see Schemes 5.S1, 5.S2, and 5.S3 for synthesis and Figures 5.S1-5.S25 for characterization).[3] The cationic **AuNP**s were very stable in aqueous solution.

5.4.6 Target Proteins. α-Amylase (α-Amy, from *Bacillus licheniformis*), bovine serum albumin (BSA, from *Bovine serum*), cytochrome *c* (CytC, from equine heart), ferritin (Fer, from equine spleen), human serum albumin (HAS, from *human serum*), lipase (Lip, from *candida rugosa*, type VII), lysozyme (Lys, from chicken egg white), myoglobin (Myo, from equine heart), and alkaline phosphatase (PhosB, from bovine intestinal mucosa) were purchased from Sigma-Aldrich and used as received. The protein

---

[1] a) Kanaras, A. G.; Kamounah, F. S.; Schaumburg, K.; Kiely, C. J.; Brust, M. *Chem. Commun.* **2002**, 2294. b) Brust, M.; Walker, M.; Bethell, D.; Schiffrin, D. J.; Whyman, R. *J. Chem. Soc. Chem. Commun.* **1994**, 801.

[2] Templeton, A. C.; Wuelfing, M. P.; Murray, R. W. *Acc. Chem. Res.* **2000**, *33*, 27.

[3] You, C. C.; Miranda, O. R.; Gider, B.; Ghosh, P. S.; Kim, I. B.; Erdogan, B.; Krovi, S. A.; Bunz, U. H. F.; Rotello, V. M. *Nat. Nanotech.* **2007**, *2*, 318.

concentrations were standaridized by the absorbance at 280 nm in 5 mM phosphate buffer at pH 7.4 using a Hewlett Packard 8452A Diode Array Spectophotometer.

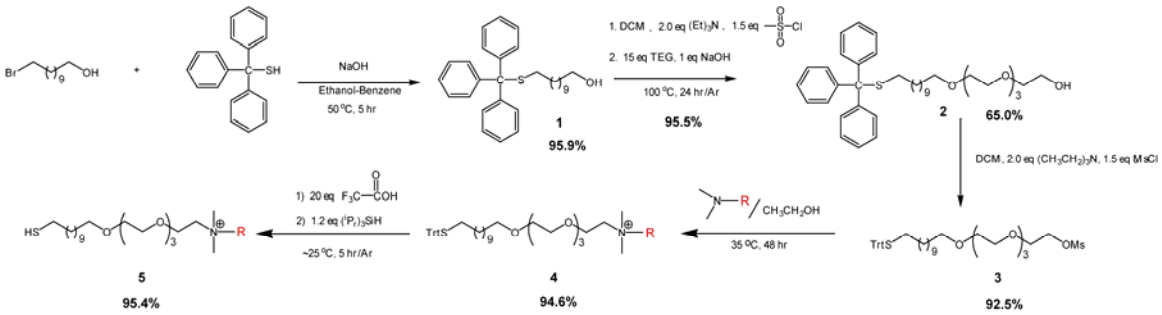

Scheme 5.S1 Synthesis of ligands **L1**, **L2**, **L3**, **L4, L5** and **L6**. [4]

General procedure:

Compound 1: Triphenylmethanethiol (7.92 g, 28.66 mmol) was dissolved in a solution of ethanol/benzene (1:1, 50 mL) and NaOH (1.43 g, 35.82 mmol) in 15 mL of H_2O was added. Then 11-bromo-1-undecanol (6 g, 23.88 mmol) was also dissolved in a solution of ethanol/benzene (1:1, 50 mL) and added to the triphenylmethanethiol mixture. The new reaction mixture was stirred overnight at room temperature. Once the reaction was completed (checked by TLC) all the mixture was poured into a saturated solution of $NaHCO_3$ and washed three times. The organic layer was separated and added into another solution saturated of NaCl and also washed for three times. Afterward the organic layer was separated, dried (Na_2SO_4), and concentrated using a rotavapor. The crude product was purified by column chromatography over silica gel using hexane/ethyl acetate (9:1, 4:1 and 1:1, v/v) as an eluent. The solvent was removed in vacuum to obtain compound **1** as a colorless oil (Yield 10.23 g, >95.9 %, see NMR Figure S1).

[4] C.-C. You, O. R. Miranda, B. Gider, P. S. Ghosh, I.-B. Kim, B. Erdogan, S. A. Krovi, U. H. F. Bunz, V. M. Rotello, *Nat. Nanotechnol*. **2007**, *2*, 318-323.

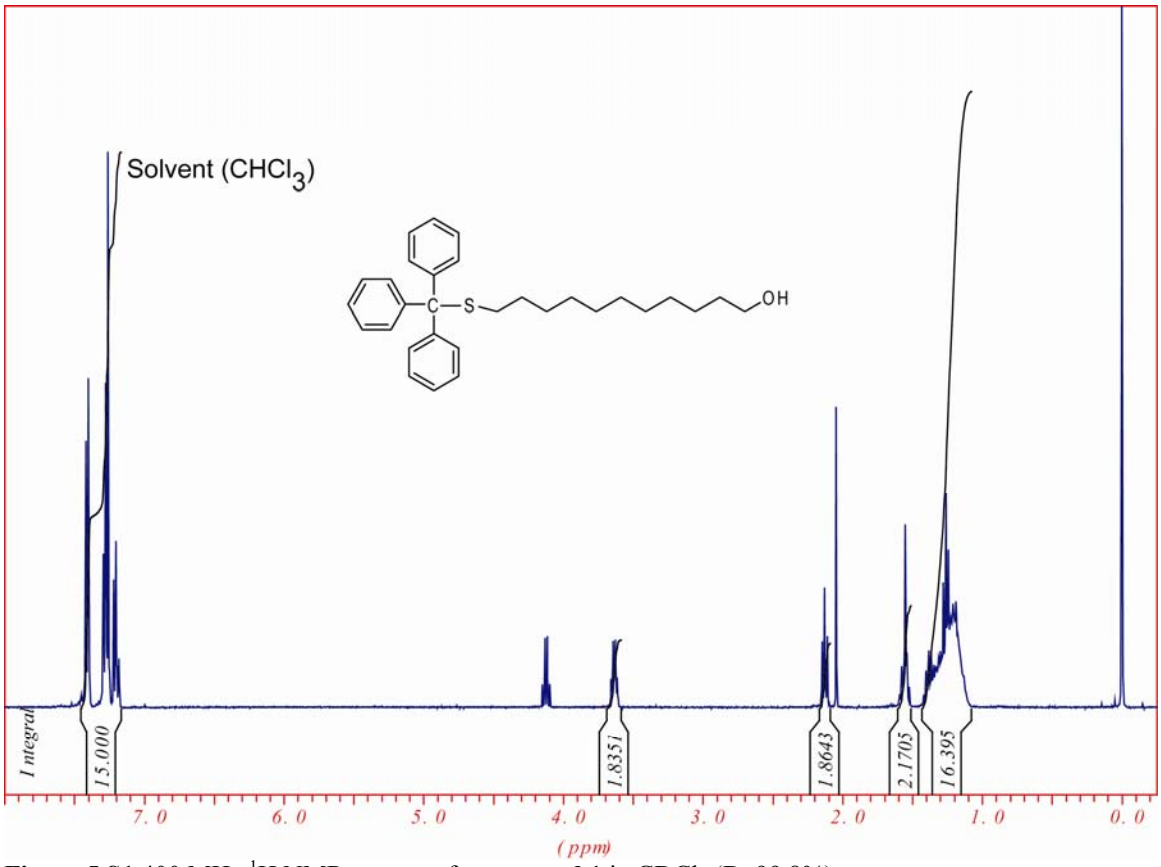

Figure 5.S1 400 MHz ^{1}H NMR spectra of **compound 1** in $CDCl_3$ (D, 99.8%).

Compound 2: To a solution of compound **1** (9 g, 20.15 mmol) in dry dichloromethane (DCM) at 4 °C, triethylamine (4.08 g, 40.3 mmol) was added. Methylsulfonyl chloride (3.46 g, 30.2 mmol) was injected drop by drop to the solution maintaining the temperature less that 5 °C. After 30 minutes the reaction mixture was warmed up to room temperature and stirred for another 30 minutes. Once the reaction was completed (according to TLC), the DCM was evaporated. The viscous compound was again diluted with DCM and poured into 0.1 M solution of HCl, and treated twice. Organic layer was poured into a saturated solution of $NaHCO_3$ and washed three times. The organic layer was separated and added into another solution saturated of NaCl and also treated three times. Afterward organic layer was separated, dried (Na_2SO_4) and concentrated at reduced pressure. The crude product was purified by column chromatography over silica gel using hexane/ethyl acetate (1:1, v/v) as an eluent. Solvent was removed in vacuum to afford compound **2** as colorless oil (Yield 10.1 g, >95.5 %). The NMR showed an additional peak on the spectra of compound **1** around 2.95 ppm confirming the synthesis of 11-(tritylthio)undecyl methanesulfonate (see Figure S2). To synthesize 1,1,1-triphenyl-14,17,20,23-tetraoxa-2-thiapentacosan-25-ol, NaOH (0.8 g, 20 mmol) in 1 ml of H_2O was added to 58.26 mL of tetraethyleneglycol (TEG: 52.3 g, 300 mmol) and stirred for 1 h at 90 °C. To this reaction mixture, 11-(tritylthio)undecyl methanesulfonate (10 g, was added (by dissolving in TEG) and stirred for 24 h. The reaction mixture once completed (according to TLC) was extracted by washing with a solution of hexane/ethyl acetate (4:1, v/v) six times (checked by TLC). Afterward, the organic layer was separated

and concentrated at reduced pressure. The crude product was purified by column chromatography over silica gel (flash running) using hexane/ethyl acetate (1:1 and 0:1, v/v) as an eluent. The solvent was removed in vacuum to obtain compound **2** as a colorless oil (Yield 7.83 g, >65.0 %, see NMR Figure 5.S3).

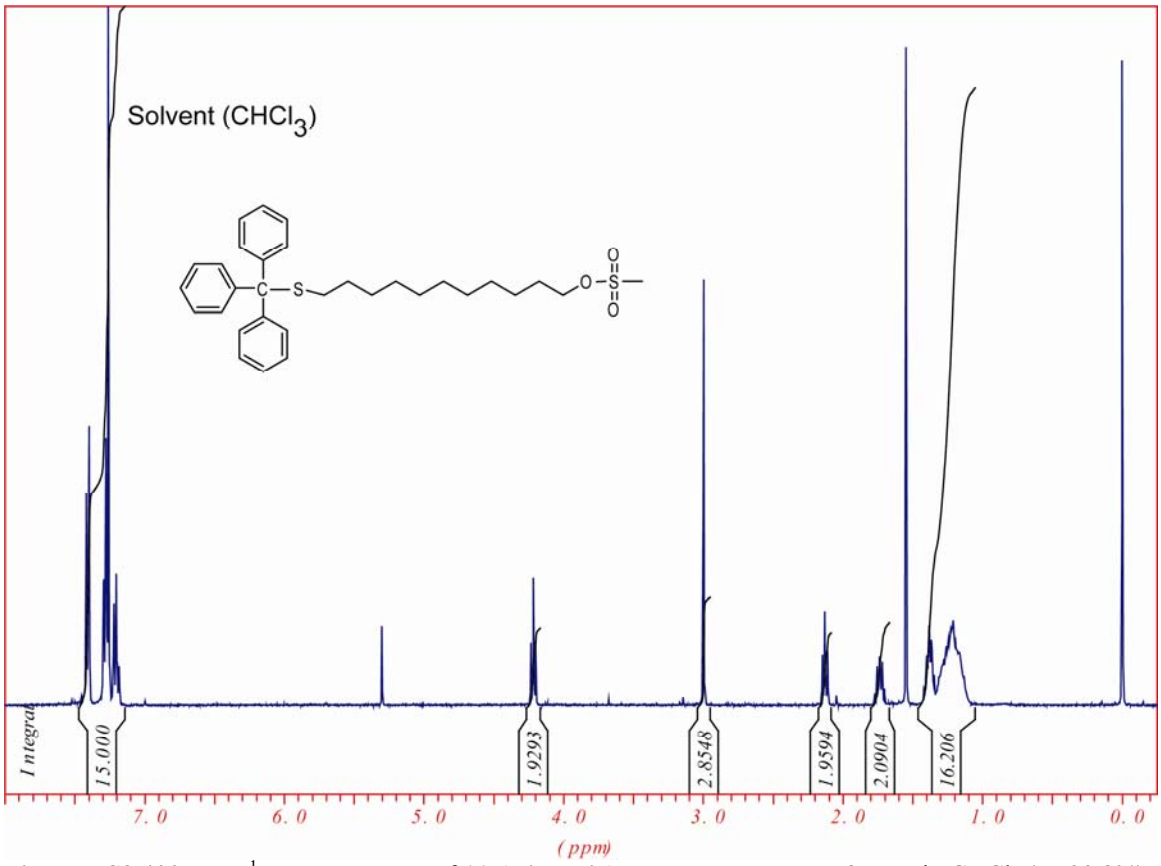

Figure 5.S2 400 MHz ^{1}H NMR spectra of **11-(tritylthio)undecyl methanesulfonate** in $CDCl_3$ (D, 99.8%).

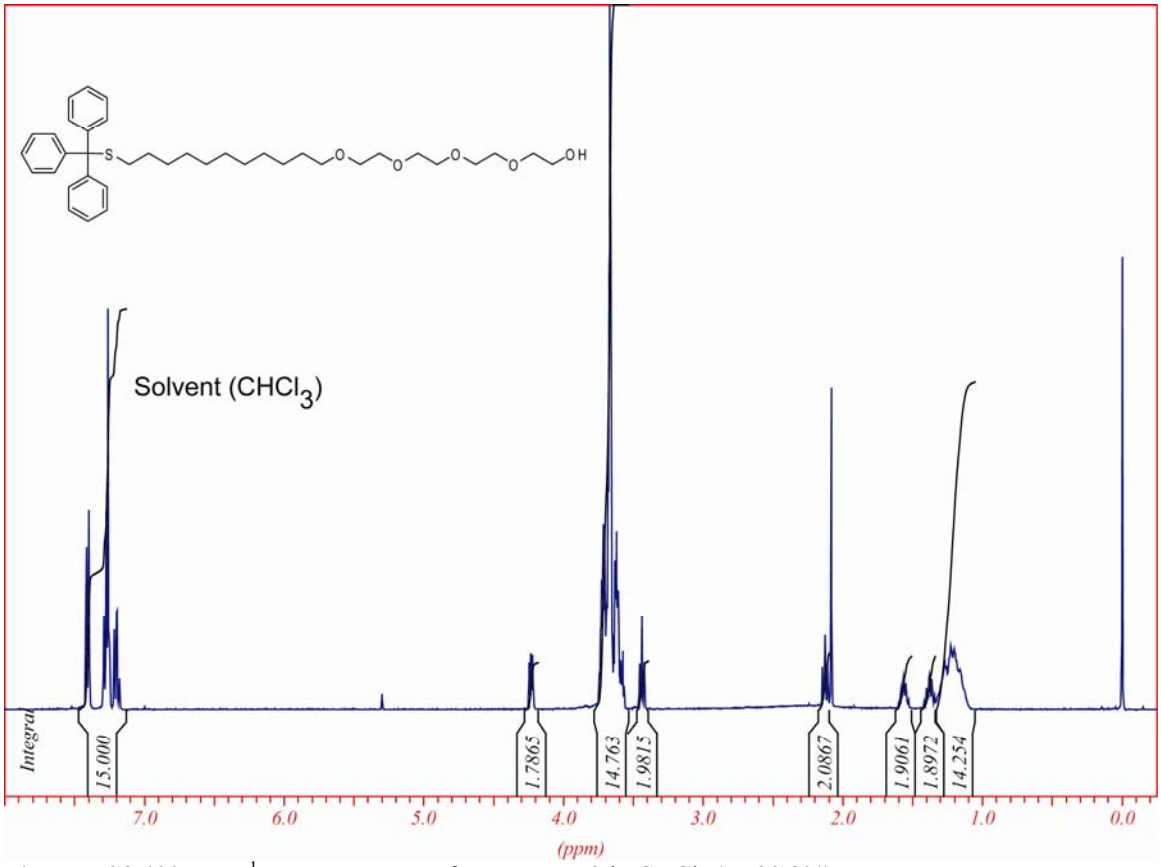

Figure 5.S3 400 MHz ^{1}H NMR spectra of **compound 2** in $CDCl_3$ (D, 99.8%).

Compound 3: Compound **2** (7 g, 11.24 mmol) was dissolved in dry dichloromethane (DCM) at 4 °C, and was followed by the addition of triethylamine (3.41 g, 33.72 mmol). Methylsulfonyl chloride (2.44 g, 16.86 mmol) was injected drop by drop to the reaction mixture maintaining the temperature less that 5 °C. After 30 minutes the reaction mixture was warmed up to room temperature and stirred for another 30 minutes. When the reaction was finally completed (according to TLC), the DCM solvent was evaporated. The viscous compound was again diluted with DCM and was poured into 0.1 M solution of HCl, and washed twice. The organic layer was poured into a saturate solution of $NaHCO_3$ and treated three times. Organic layer was separated and added into another solution saturated of NaCl and also treated for three times. Afterward, the organic layer was separated, dried (Na_2SO_4) and concentrated at reduced pressure. The crude product was purified by column chromatography over silica gel (flash running) using hexane/ethyl acetate (1:1, 1:4 and 0:1 v/v) as an eluent. Solvent was removed in vacuum to afford compound **3** as a colorless oil (Yield 7.31 g, >92.5 %). The NMR results showed an additional peak on the spectra of compound **1** around ~2.75 ppm confirming the synthesis of 1,1,1-triphenyl-14,17,20,23-tetraoxa-2-thiapentacosan-25-yl methanesulphonate (see Figure 5.S4).

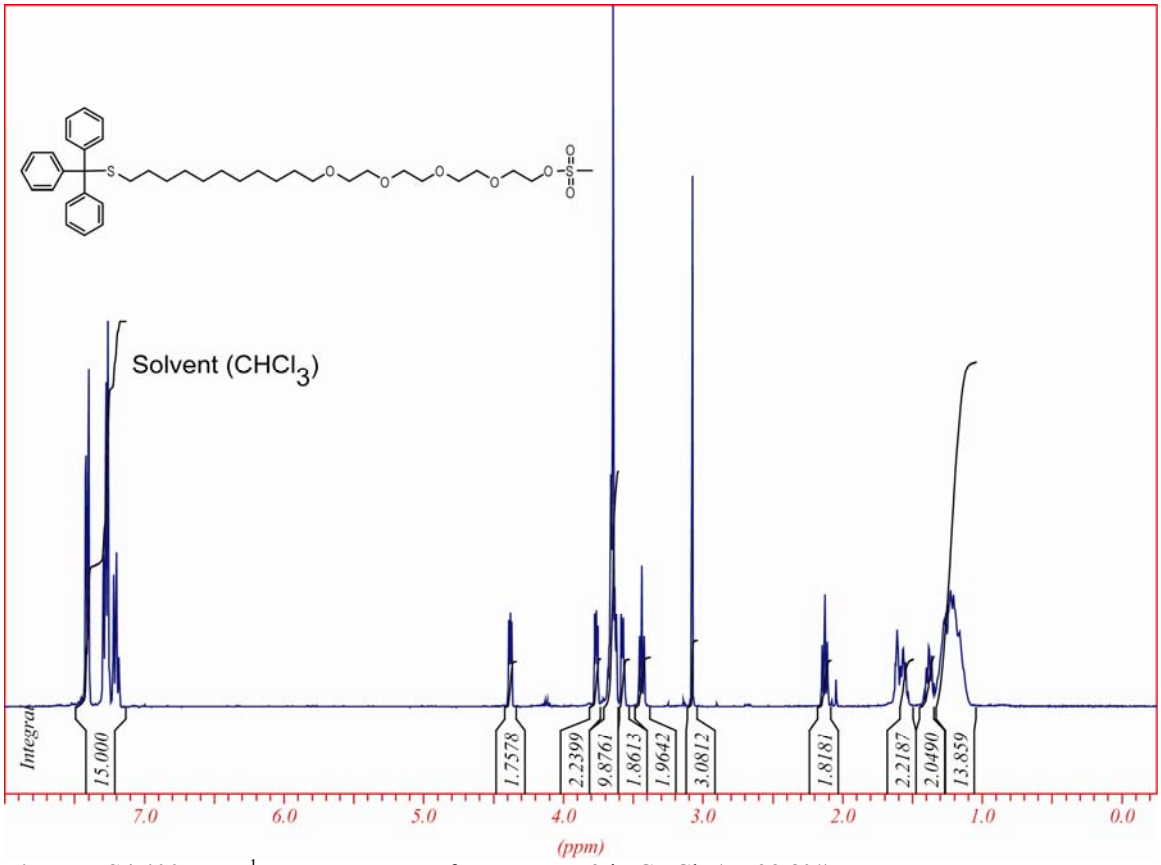

Figure 5.S4 400 MHz ^{1}H NMR spectra of **compound 2** in $CDCl_3$ (D, 99.8%).

Compound 4 (Trt L): Compound **3** (1 g, 1.43 mmol) was added to an available library of dimethylamine solutions (28.53 mmol) containing 5% of ethanol. The reaction mixtures were stirred at ~35 ^{o}C for 48 h. Crude product was checked by TLC and ethanol was eliminated at reduced pressure. The light yellow residue was purified by hexane with support of both heat and sonication and further dried in a high vacuum system. The product formation (**4**) was quantitative and their structure was confirmed by NMR. The yield was >94.6 %.

^{1}H NMR of compound 4 (Trt L)

Compound Trt L1: ^{1}H NMR (400MHz, $CDCl_3$, TMS): δ 7.43-7.38 (m, 4H, H_{Ar}), 7.31-7.24 (m, 9H, H_{Ar}), 7.23-7.17 (m, 2H, H_{Ar}), 3.98 (br, 2H, -OC$\underline{H}_2$-(CH_2N)-), 3.67-3.58 (m, 14H, -CH_2O- + -CH_2N-), 3.55 (t, 2H, -CH_2O-), 3.50-3.41 (m, 2H,-NCH_2-), 3.27 (s, 6H, -$(CH_3)_2$N-), 2.75 (s, 3H, $CH_3SO^{-}_3$-), 2.21 (t, 2H, -SCH_2-), 1.74-1.50 (m, 6H, -(NCH_2)C$\underline{H}_2$-) + (SCH_2)C$\underline{H}_2$ + -C$\underline{H}_2$(CH_2O)-), 1.42-1.11 (m, 20H, -(NCH_2CH_2-)C$\underline{H}_2$-) + -CH_2-), 0.89 (t, 3H, - CH_3-).

Compound Trt L2: ^{1}H NMR (400MHz, $CDCl_3$, TMS): δ 7.44-7.37 (m, 4H, H_{Ar}), 7.32-7.23 (m, 9H, H_{Ar}), 7.22-7.16 (m, 2H, H_{Ar}), 3.99 (br, 2H, -OC$\underline{H}_2$-(CH_2N)-), 3.67-3.58 (m, 12H, -CH_2O-), 3.57-3.54 (m, 1H, H_{Cyclo}), 3.51-3.39 (m, 4H, -CH_2O- +-CH_2N-), 3.19 (s, 6H, -$(CH_3)_2$N-), 2.75 (s, 3H, $CH_3SO^{-}_3$-), 2.12 (t, 2H, -SCH_2-), 1.77-1.65 (m, 2H, H_{Cyclo}),

1.59-1.50 (m, 2H, H_{Cyclo}), 1.48-1.07 (m, 22H, H_{Cyclo}, -(SCH_2)C<u>H_2</u> + -(SCH_2)CH_2C<u>H_2</u> + -C<u>H_2</u>(CH_2O)- + -C<u>H_2</u>(CH_2CH_2O)- + -CH2-).

Compound Trit L3: ^{1}H NMR (400MHz, $CDCl_3$, TMS): δ 7.66-7.59 (m, 2H, H_{Ar}), 7.50-7.36 (m, 7H, H_{Ar}), 7.32-7.23 (m, 9H, H_{Ar}), 7.22-7.16 (m, 2H, H_{Ar}), 4.80 (br, 2H,-NCH_2-Ar), 3.84 (br, 2H, -OC<u>H_2</u>-(CH_2N)-), 3.73-3.55 (m, 14H, -CH_2O- + -CH_2N-), 3.54-3.49 (m, 2H, -CH_2O-), 3.23 (s, 6H, -$(CH_3)_2N$-), 2.79 (s, 3H, $CH_3SO^-_3$-), 2.12 (t, 2H, -SCH_2-), 1.57-1.48 (m, 2H, -(SCH_2)C<u>H_2</u>), 1.43-1.32 (m, 2H, -C<u>H_2</u>(CH_2O)-), 1.31-1.07 (m, 12H, -CH_2-).

Compound Trit L4: ^{1}H NMR (400MHz, $CDCl_3$, TMS): δ 7.43-7.37 (m, 4H, H_{Ar}), 7.31-7.24 (m, 9H, H_{Ar}), 7.23-7.17 (m, 2H, H_{Ar}), 3.95 (br, 2H, -OC<u>H_2</u>-(CH_2N)-), 3.77 (b, 1H, OH), 3.76-3.53 (m, 16H, -CH_2O- + -CH_2N- + -C<u>H_2</u>-OH), 3.51-3.44 (m, 2H,-NCH_2-), 3.42 (m, 2H, -CH_2O-), 3.24 (s, 6H, -$(CH_3)_2N$-), 2.74 (s, 3H, $CH_3SO^-_3$-), 2.13 (t, 2H, -SCH_2-), 2.09-1.99 (m, 2H, -(NCH_2)C<u>H_2</u>-), 1.59-1.51 (m, 2H, -(SCH_2)C<u>H_2</u>), 1.42-1.33 (m, 2H, -C<u>H_2</u>(CH_2O)-), 1.33-1.10 (m, 14H, -CH_2-).

Compound Trit L5: ^{1}H NMR (400MHz, $CDCl_3$, TMS): δ 7.65-7.57 (m, 2H, H_{Ar}), 7.53-7.35 (m, 7H, H_{Ar}), 7.31-7.23 (m, 9H, H_{Ar}), 7.21-7.15 (m, 2H, H_{Ar}), 3.97 (br, 2H, -OC<u>H_2</u>-(CH_2N)-), 3.65-3.56 (m, 13H, -CH_2O- + H_{Cyclo}), 3.57-3.53 (m, 1H, H_{Cyclo}), 3.50-3.39 (m, 4H, -CH_2O- +-CH_2N-), 3.17 (s, 6H, -$(CH_3)_2N$-), 2.75 (s, 3H, $CH_3SO^-_3$-), 2.13 (t, 2H, -SCH_2-), 1.77-1.64 (m, 2H, H_{Cyclo}), 1.59-1.49 (m, 2H, H_{Cyclo}), 1.47-1.05 (m, 22H, H_{Cyclo}, -(SCH_2)C<u>H_2</u> + -(SCH_2)CH_2C<u>H_2</u> + -C<u>H_2</u>(CH_2O)- + -C<u>H_2</u>(CH_2CH_2O)- + -CH2-).

Compound Trit L6: ^{1}H NMR (400MHz, $CDCl_3$, TMS): δ 7.43-7.38 (m, 4H, H_{Ar}), 7.36-7.31 (m, 7H, H_{Ar}), 7.30-7.24 (m, 12H, H_{Ar}), 7.23-7.17 (m, 2H, H_{Ar}), 5.39 (s, 1H, CH-Ar-), 3.99-3.93 (m and br, 2H, -CH_2OCAr-), 3.92-3.87 (m and br, 2H, -OC<u>H_2</u>-(CH_2N)-), 3.65-3.55 (m, 14H, -CH_2O- + -CH_2N-), 3.54-3.51 (m, 2H, -CH_2O-), 3.49-3.44 (m, 2H, -NC<u>H_2</u>(CH_2OCAr-), 3.37 (s, 6H, -$(CH_3)_2N$-), 2.74 (s, 3H, -$CH_3SO^-_3$-), 2.13 (q, 2H, -CH_2S-), 1.59-1.50 (m, 2H, -(SCH_2)C<u>H_2</u>), 1.41-1.34 (m, 2H, -C<u>H_2</u>(CH_2O)-), 1.33-1.10 (m, 14H, -CH_2-).

Compound 5: Compound **4** was dissolved in dry dichloromethane (DCM) and an excess of trifluoroacetic acid (TFA, ~ 20 equivalents) was added. The color of the solution was turned to yellow immediately. Subsequently, triisopropylsilane (TIPS, ~ 1.2 equivalents) was added to the reaction mixture. The reaction mixture was stirred for ~5 h under Ar_2 at room temperature. The solvent and most TFA and TIPS were distilled off under reduced pressure. The pale yellow residue was purified by hexane combining both heat and sonication and further dried in a high vacuum system. The product (**L**) formation was quantitative and their structure was confirmed by NMR showing a shift of the counter ion peak on the spectra to more down field ~2.98 ppm. The yields were >95.4%.

^{1}H NMR and ^{13}C of **compound 5 (**Figures 5.S5-5.S16**)**

Compound L1: ^{1}H NMR (400MHz, $CDCl_3$, TMS): δ 3.95 (br, 2H, -OC<u>H</u>$_2$-(CH_2N)-), 3.68-3.56 (m, 14H, -CH_2O- + -CH_2N-), 3.46 (t, 2H, -CH_2O-), 3.40-3.33 (m, 2H,-NCH_2-), 3.19 (s, 6H, -(CH_3)$_2$N-), 2.87 (s, 3H, $CH_3SO^-_3$-), 2.52 (q, 2H, -CH_2S-), 1.76-1.53 (m, 6H, -(NCH_2)C<u>H</u>$_2$-) + (SCH_2)C<u>H</u>$_2$ + -C<u>H</u>$_2$(CH_2O)-), 1.41-1.22 (m, 21H, -SH + -(NCH_2CH_2-)C<u>H</u>$_2$-) + -CH_2-), 0.89 (t, 3H, - CH_3-). ^{13}C NMR(400 MHz, $CDCl_3$) δ(ppm): 71.59, 70.54, 70.51, 70.44, 70.33, 70.15, 70.00, 66.42, 64.82, 63.50, 51.90, 34.07, 31.18, 29.59, 29.54, 29.52, 29.49, 29.09, 28.39, 26.07, 25.84, 24.68, 22.71, 22.37, 13.85.

Compound L2: ^{1}H NMR (400MHz, $CDCl_3$, TMS): (3.97 (br, 2H, -OC<u>H</u>$_2$-(CH_2N)-), 3.69-3.55 (m, 14H, -CH_2O- + -CH_2N-), 3.54-3.48 (m, 1H, HCyclo), 3.44 (t, 2H, -CH_2O-), 3.13 (s, 6H, -(CH_3)$_2$N-), 2.86 (s, 3H, $CH_3SO^-_3$-), 2.52 (q, 2H, -CH_2S-), 2.25 (d, 2H, HCyclo), 1.99 (d, 2H, HCyclo), 1.73 (d, 2H, HCyclo), 1.78-1.52 (m, 4H, -(SCH_2)C<u>H</u>$_2$ + -C<u>H</u>$_2$(CH_2O)-), 1.51-1.12 (m, 19H, SH + -CH_2- + HCyclo). ^{13}C NMR(400 MHz, $CDCl_3$) δ(ppm): 73.76, 71,02, 69.85, 69.82, 69.69, 69.61, 69.37, 64.16, 61.42, 48.29, 38.89, 33.46, 28.98, 28.92, 28.87, 28.76, 28.48, 28.07, 27.94, 27.78, 25.75, 25.43, 24.68, 24.11.

Compound L3: ^{1}H NMR (400MHz, $CDCl_3$, TMS): δ 7.56-7.45 (m, 5H, H_{Ar}), 4.60 (s and br, 2H,-NC<u>H</u>$_2$-Ar), 4.03 (br, 2H, -OC<u>H</u>$_2$-(CH_2N)-), 3.75-3.50 (m, 14H, -CH_2O- + -CH_2N-), 3.48-3.41 (m, 2H, -CH_2O-), 3.14 (s, 6H, -(CH_3)$_2$N-), 2.91 (s, 3H, $CH_3SO^-_3$-), 2.52 (q, 2H, -CH_2S-), 1.72-1.46 (m, 4H, -(SCH_2)C<u>H</u>$_2$ + -C<u>H</u>$_2$(CH_2O)-), 1.44-1.15 (m, 15H, -SH + -CH_2-). ^{13}C NMR(400 MHz, $CDCl_3$) δ(ppm): 132.85, 130.97, 129.27, 126.51, 116.08, 113.24, 71.52, 70.10, 70.05, 69.97, 69.90, 69.54, 64.53, 63.42, 50.68, 39.37, 33.84, 29.33, 29.28, 29.19, 29.12, 29.01, 28.86, 28.17, 25.69, 24.46.

Compound L4: ^{1}H NMR (400MHz, $CDCl_3$, TMS): δ 4.55-4.46 (m, 2H,-C<u>H</u>$_2$-OH), 3.99 (br, 2H, -OC<u>H</u>$_2$-(CH_2N)-), 3.85 (br, 1H, -OH), 3.79-3.52 (m, 16H, -CH_2O- + -CH_2N- + -NCH_2-), 3.47 (t, 2H, -CH_2O-), 3.25 (s, 6H, -(CH_3)$_2$N-), 2.87 (s, 3H, $CH_3SO^-_3$-), 2.52 (q, 2H, -CH_2S-), 2.35-2.26 (m, 2H, -(NCH_2)C<u>H</u>$_2$-), 1.70-1.49 (m, 4H, + (SCH_2)C<u>H</u>$_2$ + -C<u>H</u>$_2$(CH_2O)-), 1.42-1.19 (m, 15H, -SH + -CH_2-). ^{13}C NMR(400 MHz, $CDCl_3$) δ(ppm): 71.12, 69.70, 69.66, 69.62, 69.58, 69.48, 69.15, 63.92, 63.15, 62.11, 51.75, 38.87, 33.46, 28.94, 28.89, 28.80, 28.73, 28.64, 28.48, 28.34, 27.79, 25.29, 24.08, 21.45.

Compound L5: ^{1}H NMR (400MHz, $CDCl_3$, TMS): δ 7.4-7.19 (m, 5H, H_{Ar}), 3.95 (br, 2H, -OC<u>H</u>$_2$-(CH_2N)-), 3.79-3.52 (m, 15H, -CH_2O- + -CH_2N- + 1H, H_{Cyclo}), 3.45 (t, 2H, -CH_2O-), 2.81 (m and br, 6H, -(CH_3)$_2$N-), 2.87 (s, 3H, $CH_3SO^-_3$-), 2.70 (q, 2H, -CH_2S-), 2.59-2.41 (m and br, 1H, H_{Cyclo}), 2.39-2.20 (m, 2H, H_{Cyclo}), 2.19-2.06 (m, 2H, H_{Cyclo}), 1.96-1.84 (m, 4H, H_{Cyclo}), 1.72-1.53 (m, 4H, -(SCH_2)C<u>H</u>$_2$ + -C<u>H</u>$_2$(CH_2O)-), 1.42-1.1.19 (m, 15H, -SH + -CH_2-). ^{13}C NMR(400 MHz, $CDCl_3$) δ(ppm): 128.76, 128.73, 127.16, 127.09, 126.72, 126.39, 71.65, 70.50, 70.41, 70.37, 70.31, 70.27, 70.00, 64.97, 62.34, 62.07, 49.15, 48.81, 40.86, 34.16, 32.49, 32.13, 29.66, 29.58, 29.30, 28.68, 28.61, 27.77, 26.79, 26.34, 26.10, 24.03.21.77.

Compound L6: ^{1}H NMR (400MHz, $CDCl_3$, TMS): δ 7.42-7.27 (m, 10H, H_{Ar}), 5.13 (s, 1H, H_{Ar}), 4.12 (br, 2H, -CH_2OCAr-), 3.96 (br, 2H, -OC$\underline{H}_2$-(CH_2N)-), 3.75-3.51 (m, 16H, -CH_2O- + -CH_2N- + -CH_2O-), 3.50-3.44 (m, 2H, -NC$\underline{H}_2$(CH_2OCAr-), 3.28 (s, 6H, -$(CH_3)_2$N-), 2.95 (s, 3H, $CH_3SO^-_3$-), 2.38 (t, 2H, -CH_2S-), 1.60-1.48 (m, 4H, -(SCH_2)C$\underline{H}_2$ + -C$\underline{H}_2$(CH_2O)-), 1.34-1.16 (m, 15H, -SH + -CH_2-). -). ^{13}C NMR(400 MHz, $CDCl_3$) δ(ppm): 141.71, 128.61, 128.67, 127.18, 116.95, 114.10, 71.61, 70.51, 70.45, 70.32, 70.19, 69.97, 67.14, 64.80, 59.91, 56.26, 55.98, 54.25, 53.09, 50.46, 43.72, 39.47, 32.43, 29.63, 29.57, 29.52, 29.24, 29.09, 28.92, 26.08.

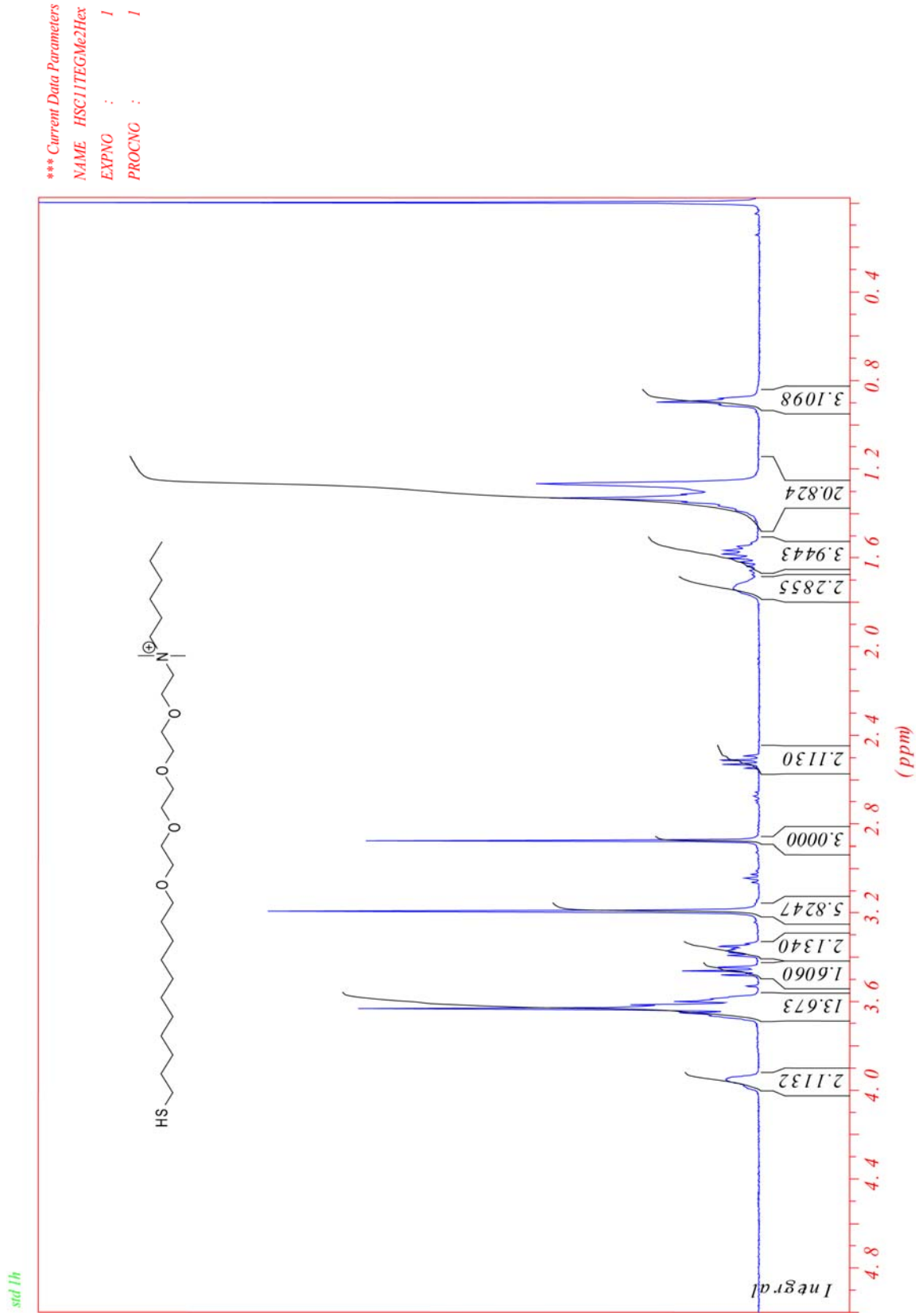

Figure 5.S5 400 MHz ^{1}H NMR spectra of **compound L1** in $CDCl_3$ (D, 99.8%).

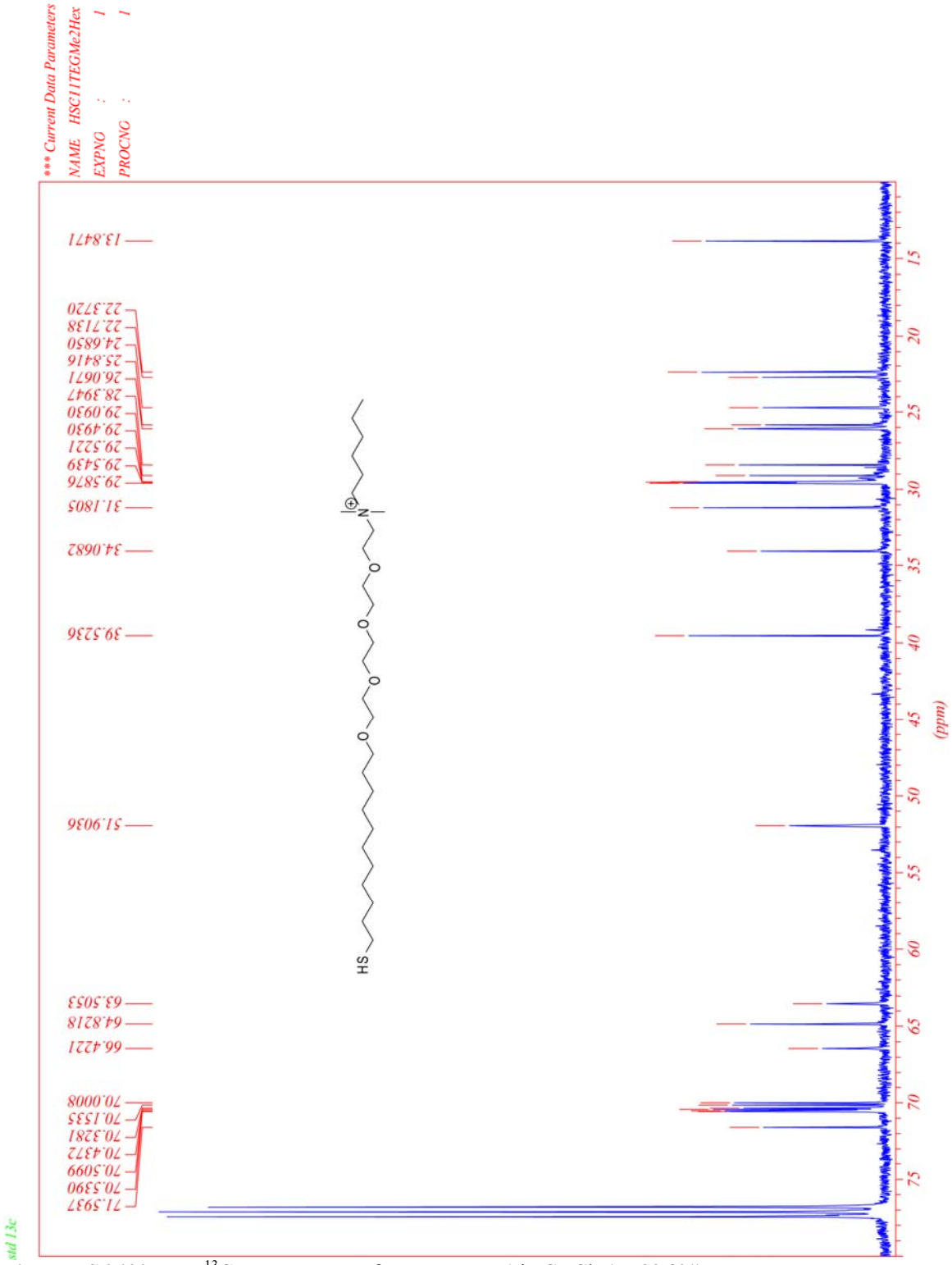

Figure 5.S6 400 MHz ^{13}C NMR spectra of **compound L1** in $CDCl_3$ (D, 99.8%).

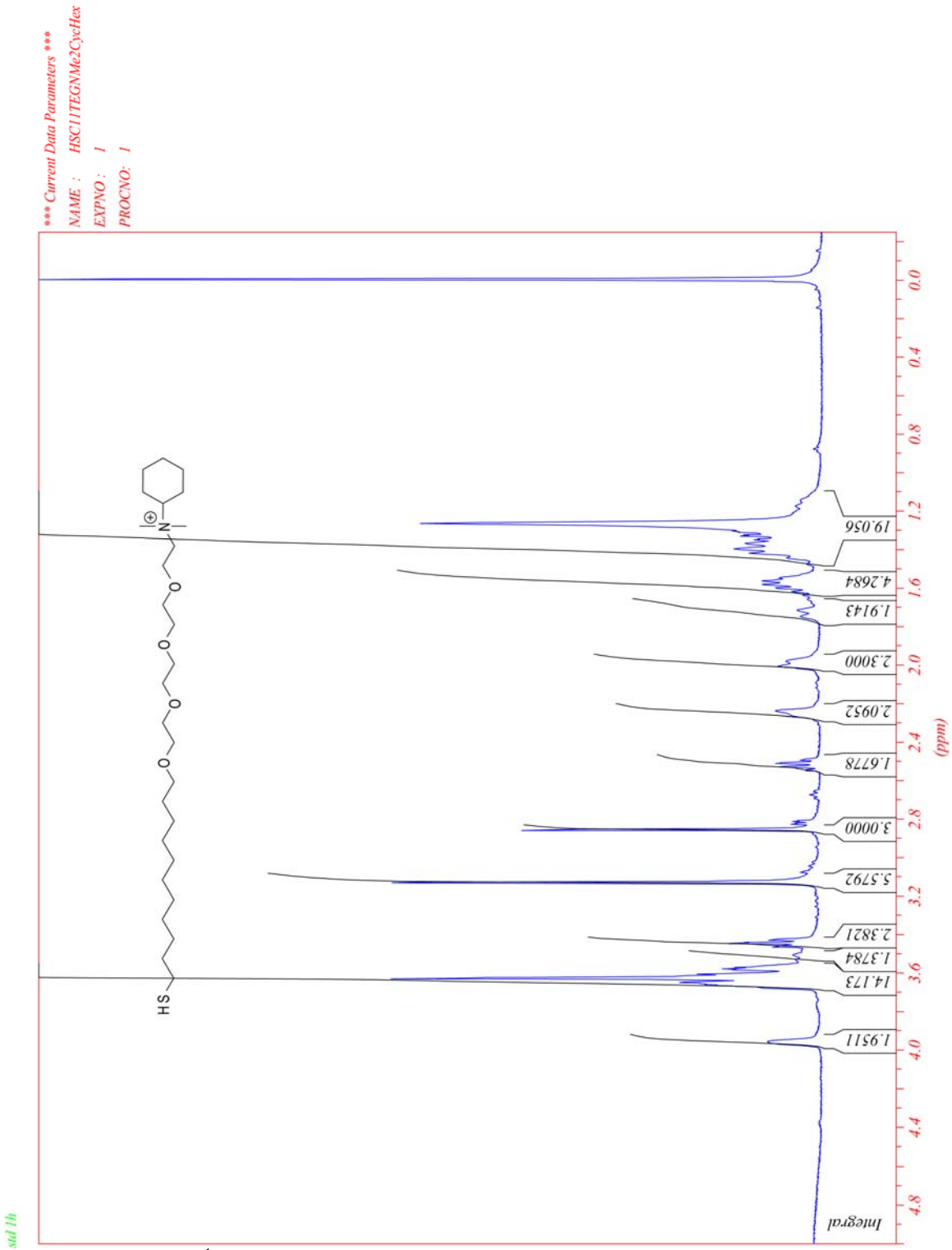

Figure 5.S7 400 MHz ^{1}H NMR spectra of **compound L2** in $CDCl_3$ (D, 99.8%).

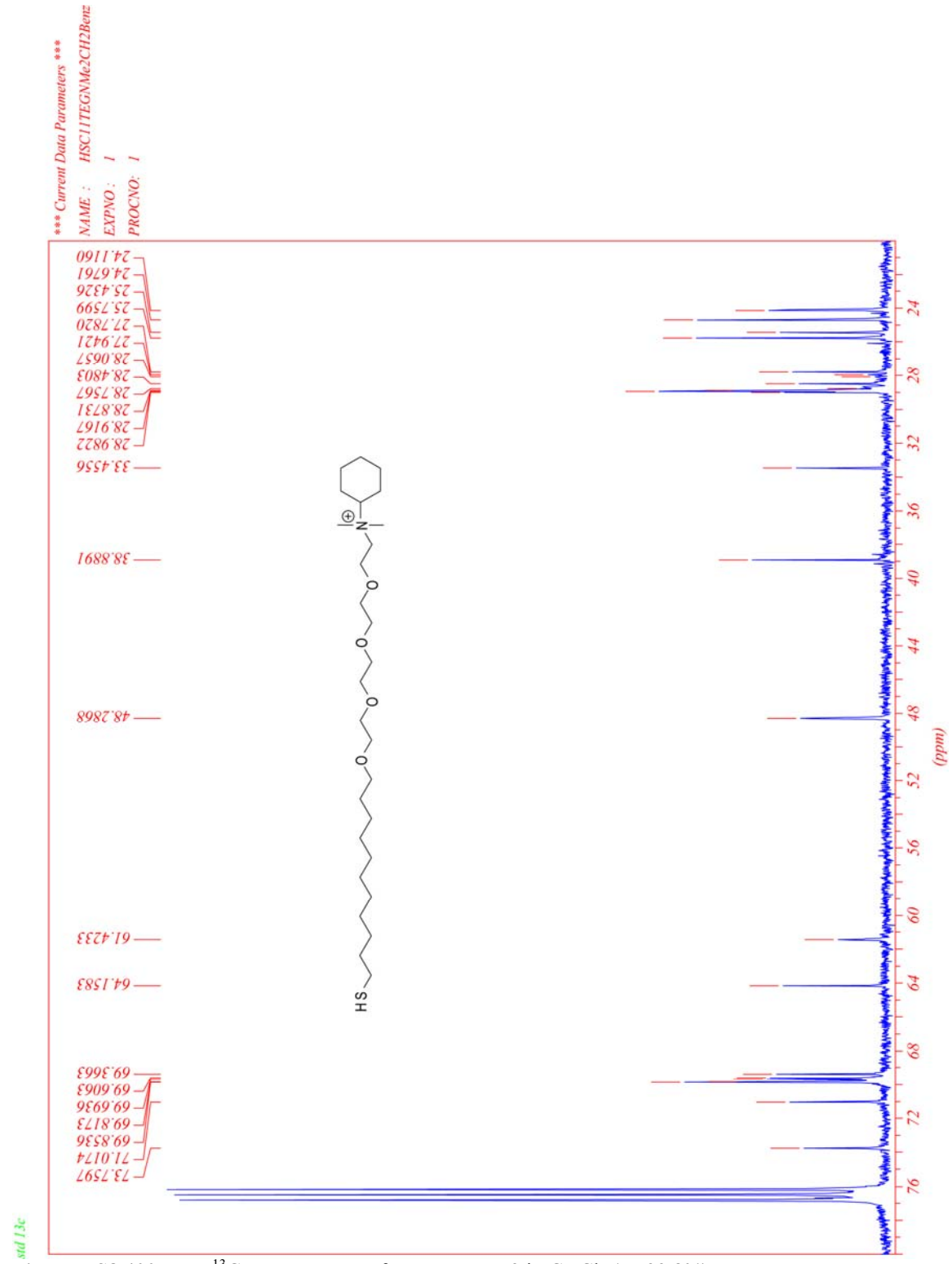

Figure 5.S8 400 MHz ^{13}C NMR spectra of **compound L2** in $CDCl_3$ (D, 99.8%).

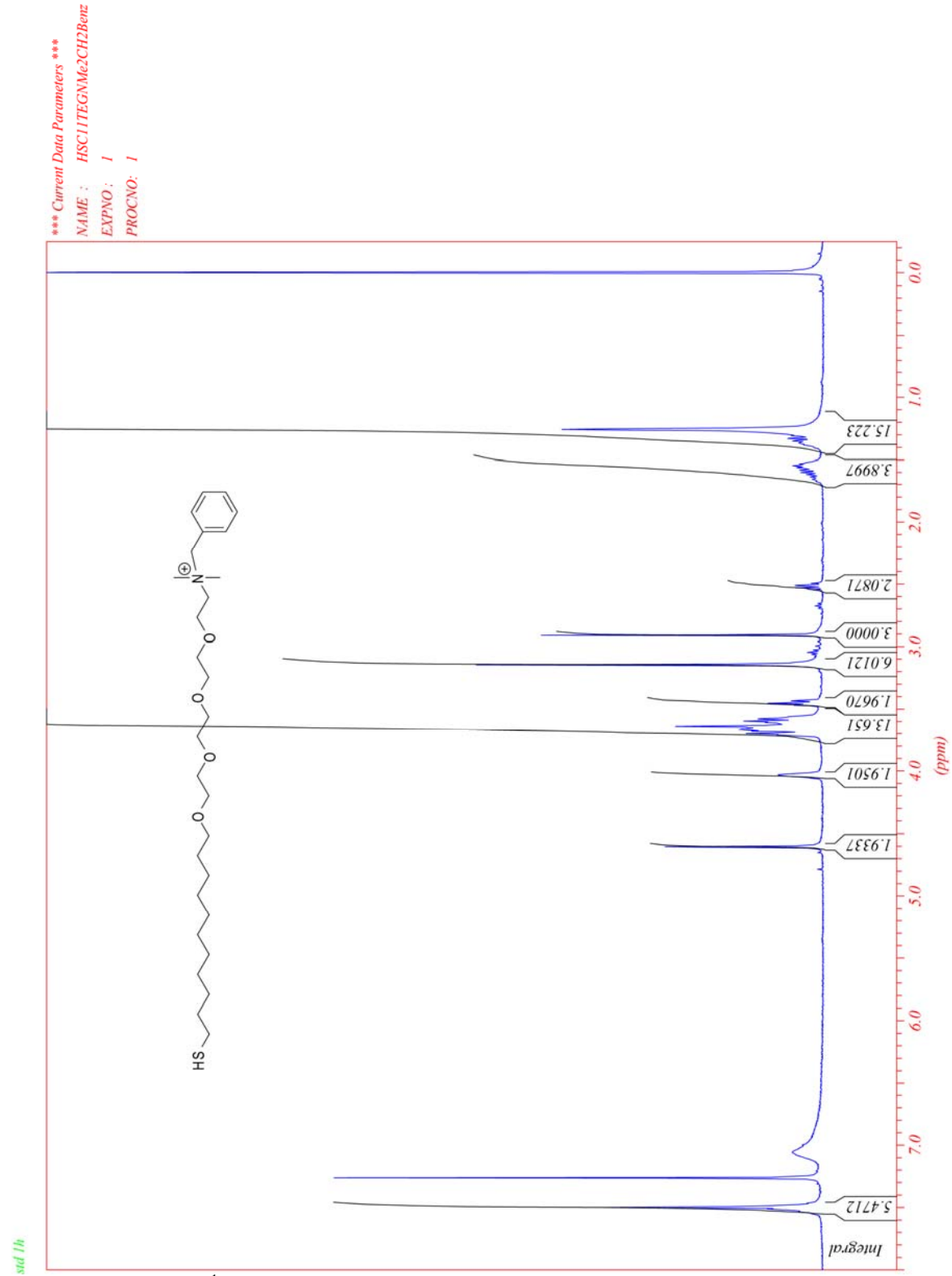

Figure 5.S9 400 MHz ^{1}H NMR spectra of **compound L3** in $CDCl_3$ (D, 99.8%).

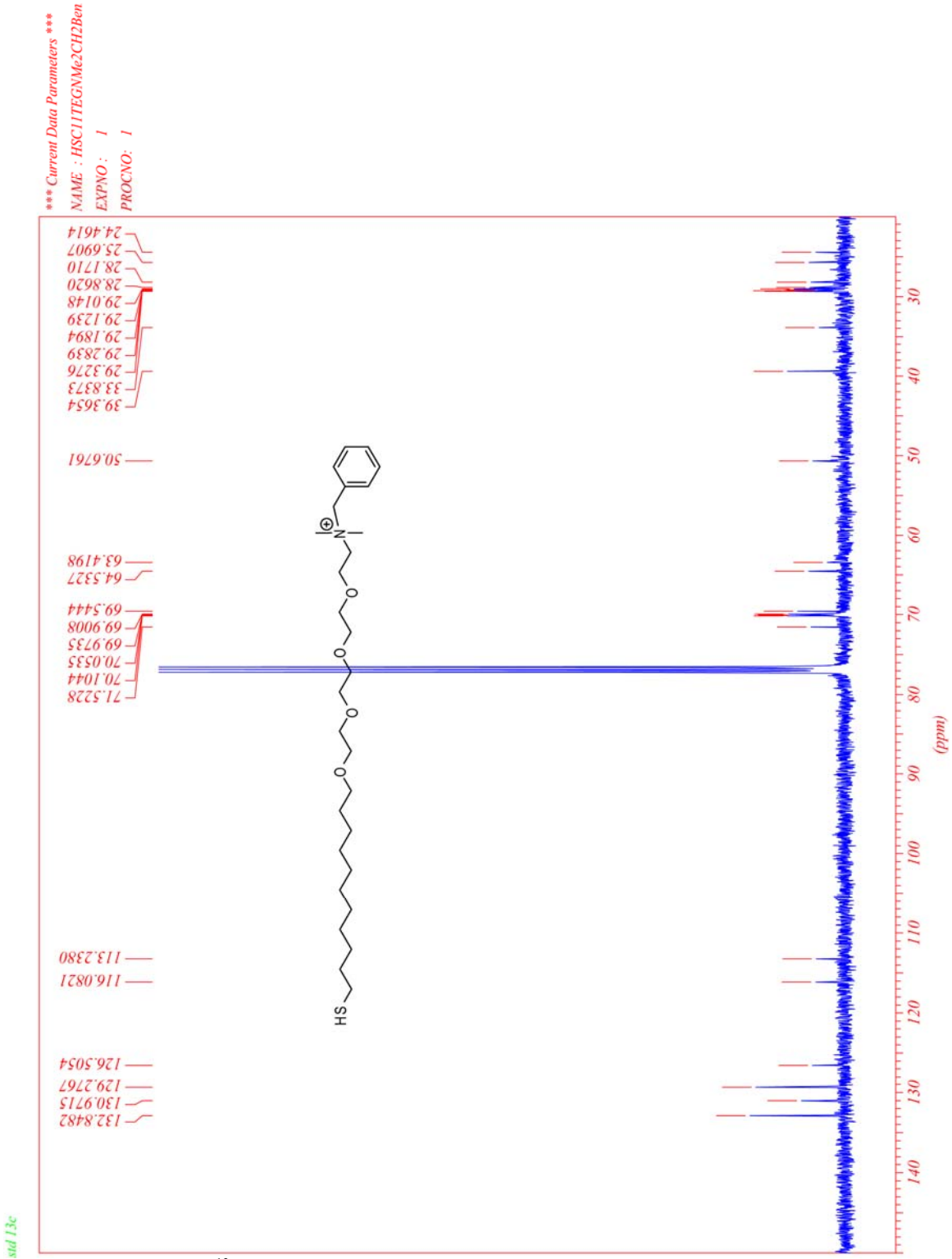

Figure 5.S10 400 MHz ^{13}C NMR spectra of **compound L3** in $CDCl_3$ (D, 99.8%).

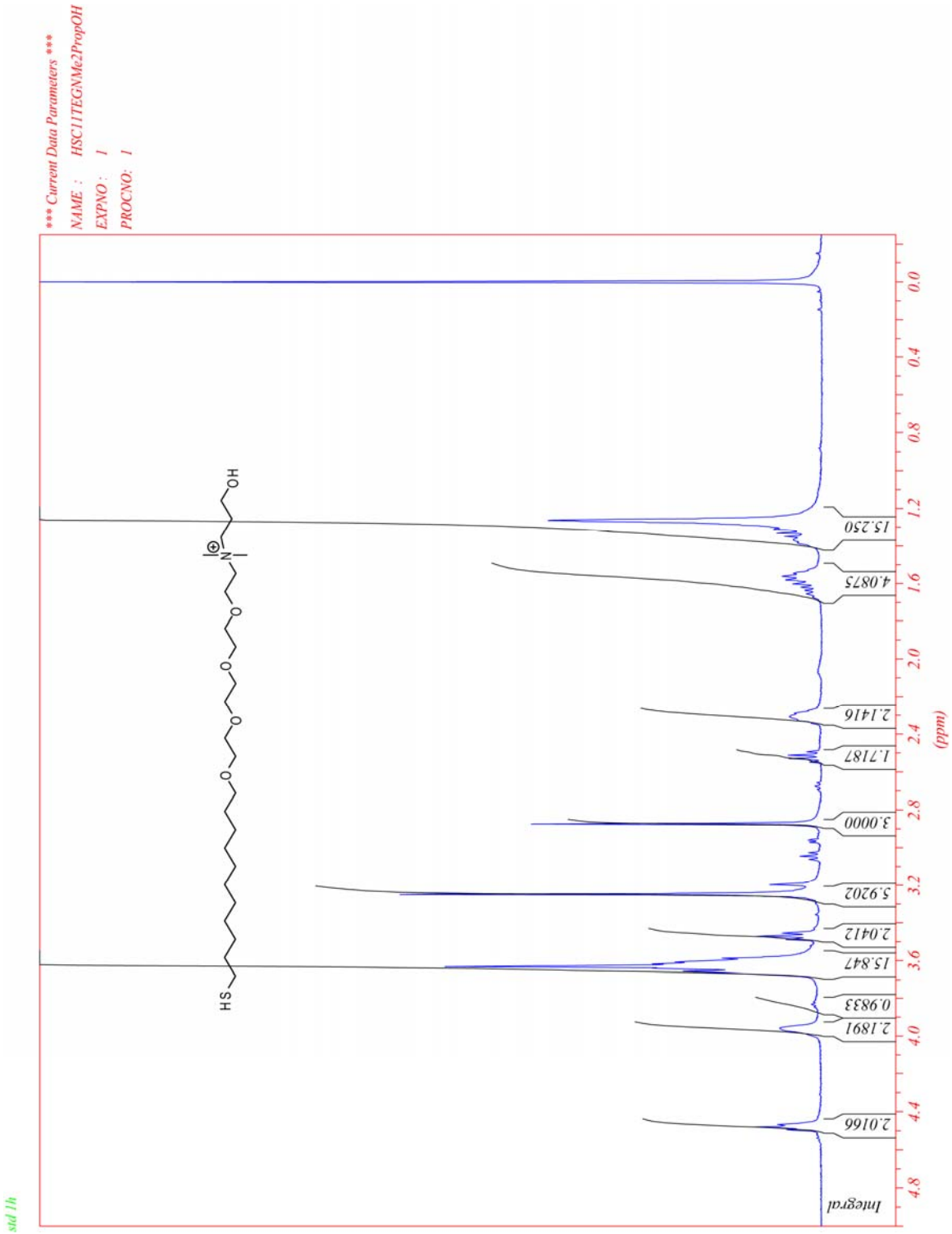

Figure 5.S11 400 MHz ^{1}H NMR spectra of **compound L4** in $CDCl_3$ (D, 99.8%).

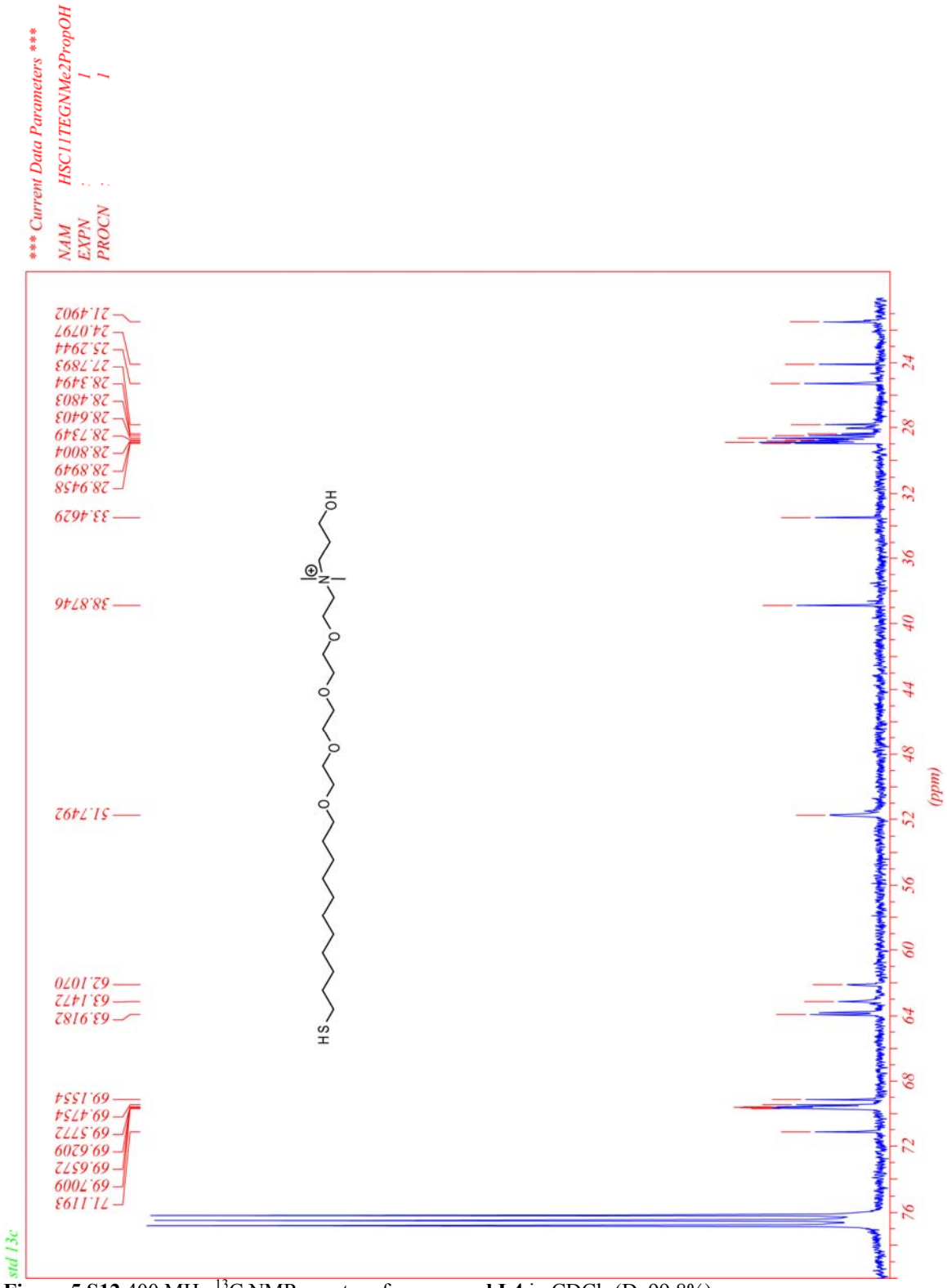

Figure 5.S12 400 MHz ^{13}C NMR spectra of **compound L4** in $CDCl_3$ (D, 99.8%).

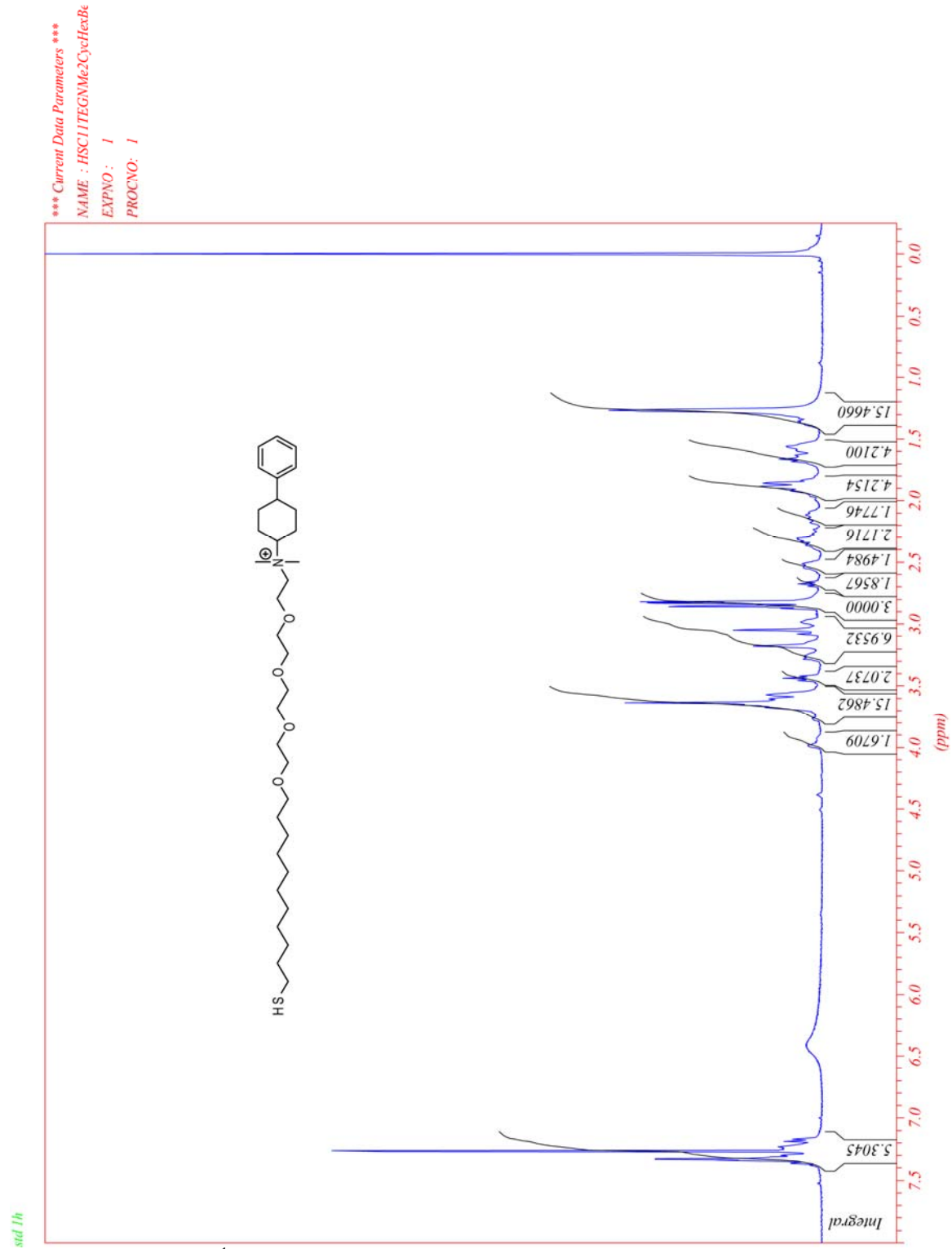

Figure 5.S13 400 MHz ^{1}H NMR spectra of **compound L5** in $CDCl_3$ (D, 99.8%).

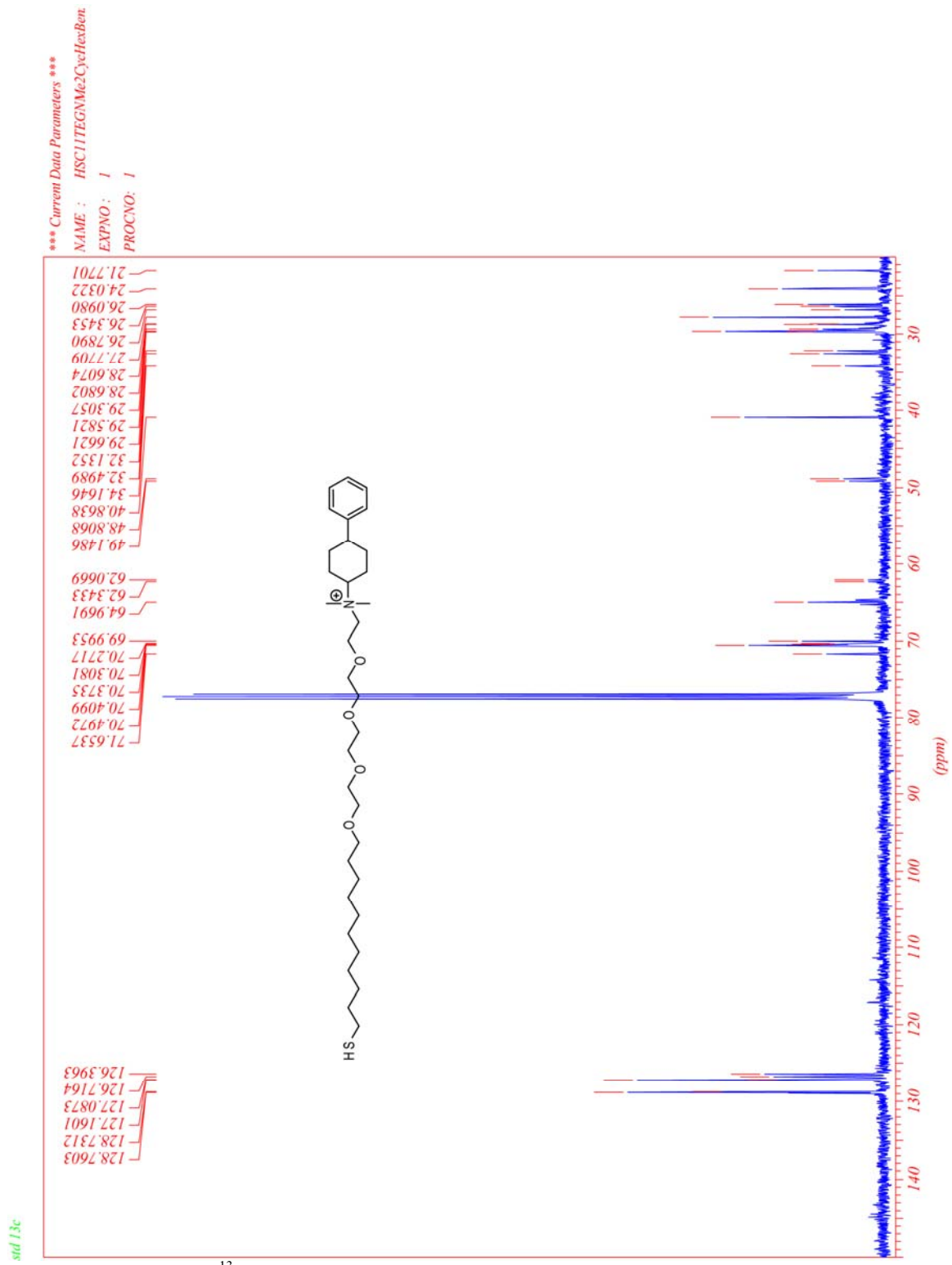

Figure 5.S14 400 MHz ^{13}C NMR spectra of **compound L5** in $CDCl_3$ (D, 99.8%).

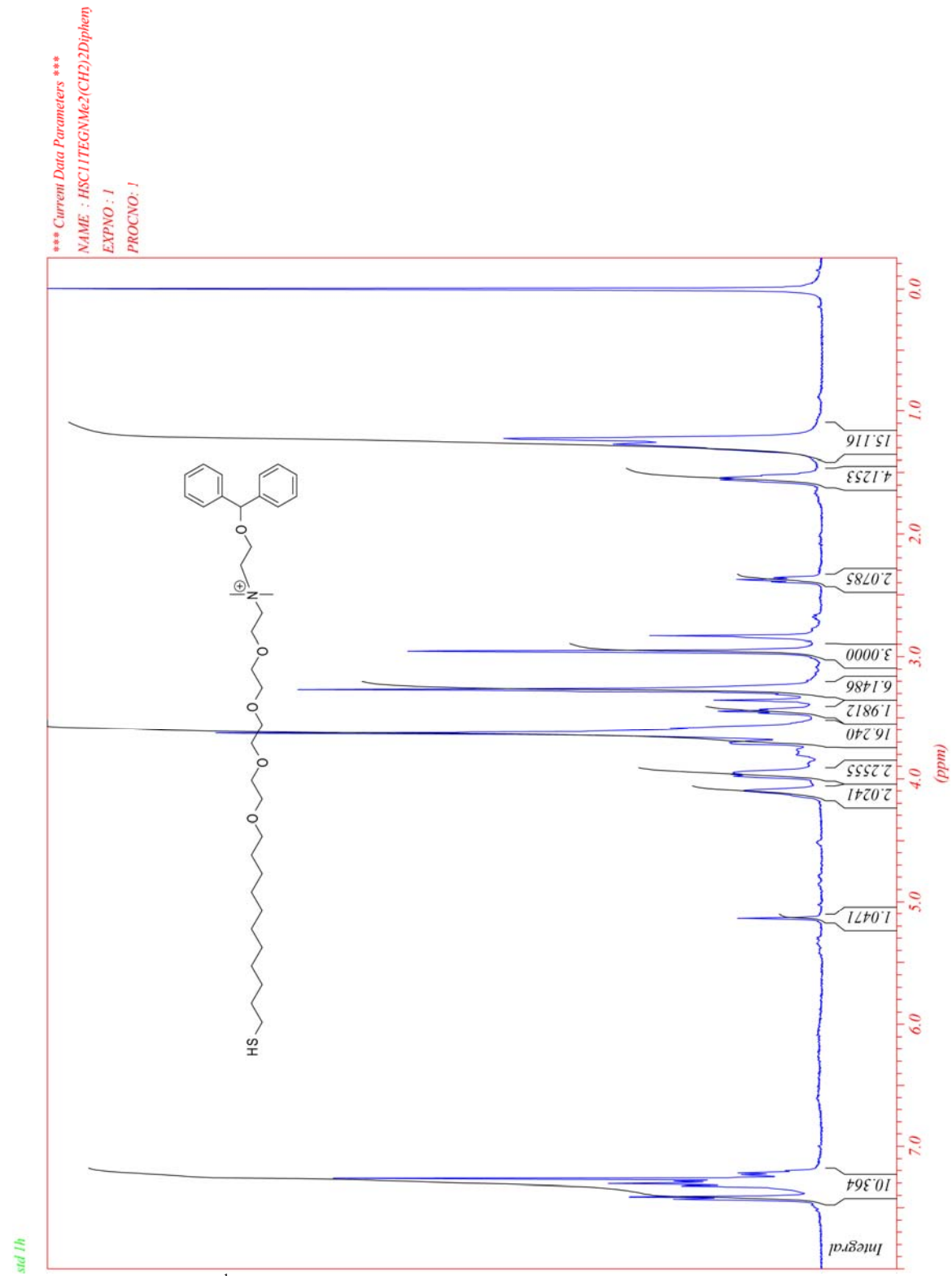

Figure 5.S15 400 MHz ^{1}H NMR spectra of **compound L6** in $CDCl_3$ (D, 99.8%).

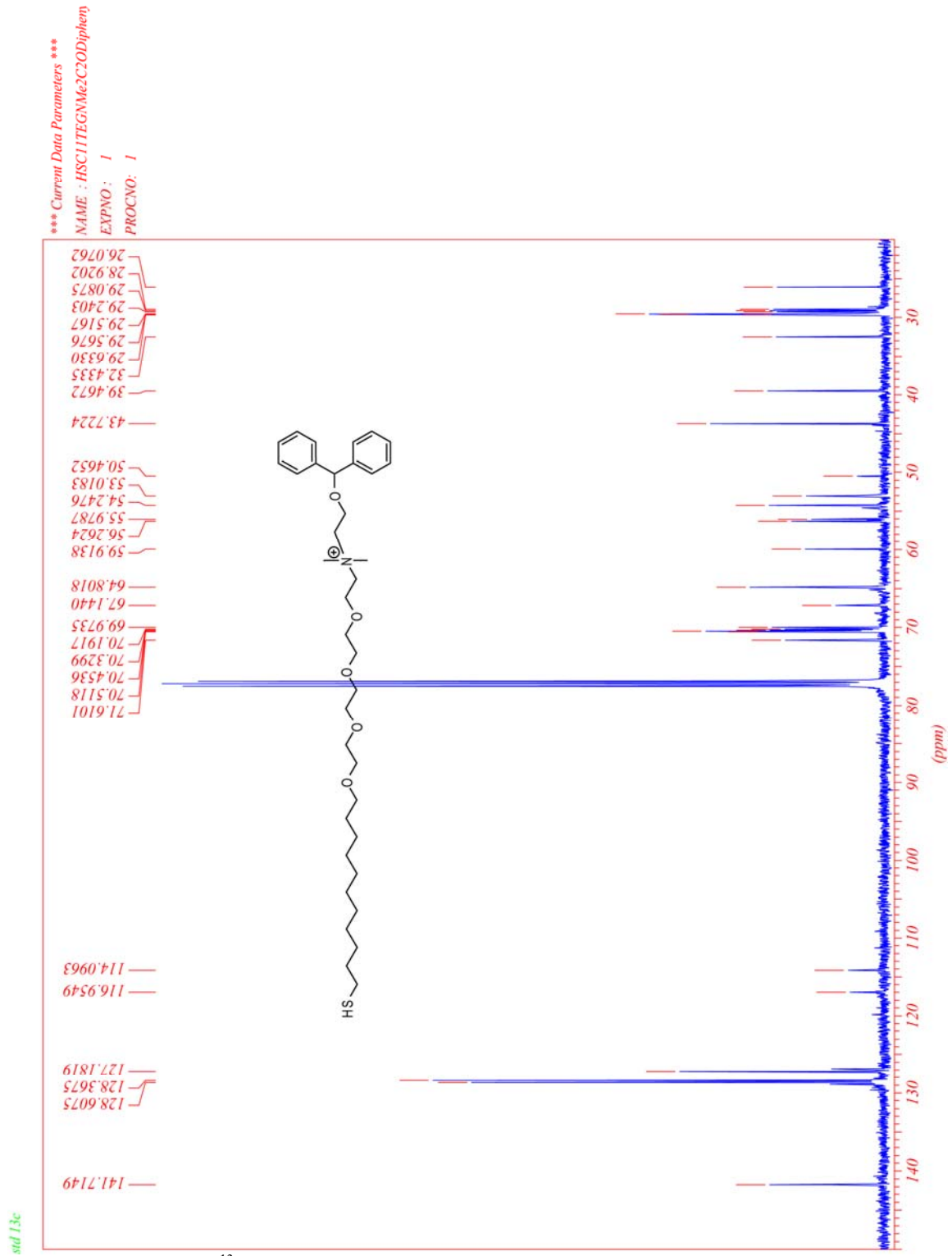

Figure 5.S16 400 MHz ^{13}C NMR spectra of **compound L6** in $CDCl_3$ (D, 99.8%).

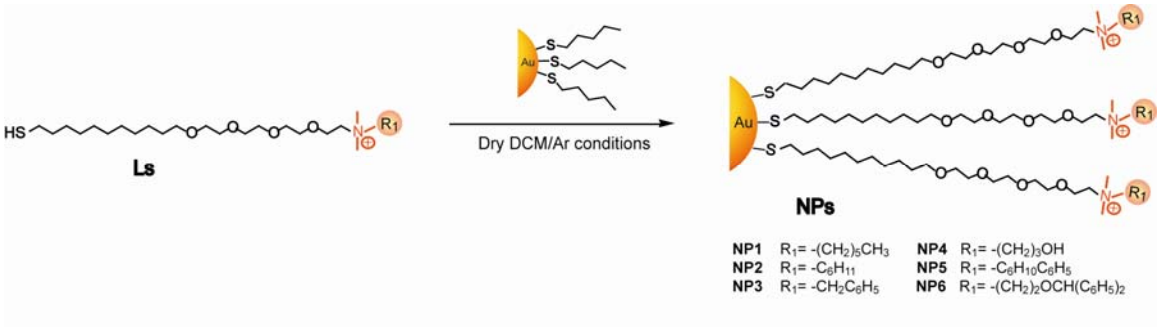

Scheme 5.S2 Synthesis of cationic gold nanoparticles **NP1-NP6.**

1-Pentanethiol coated gold nanoparticles (*d* = ~2 nm) were prepared according to the previously reported protocol (See NMR Figure 5.S17).[5] A place-exchange reaction[6] of compound **Ls** dissolved in DCM with pentanethiol-coated gold nanoparticles (d~2 nm) was carried out for 3 days at room temperature. Then, DCM was evaporated under reduced pressure. The residue was dissolved in a small amount of distilled water and dialyzed (membrane MWCO = 1,000) to remove excess ligands, acetic acid and other salts present with the nanoparticles solution. After dialysis, the particles were lyophilized to obtain a brownish solid product. The particles (**AuNPs**) are redispersed in water and/or deionized water (18 MΩ-cm). ^{1}H NMR spectra in D_2O showed substantial broadening of the proton signals and no free ligands were observed (see Figures 5.S18-5.S23).

[5] Brust, M.; Walker, M.; Bethell, D.; Schiffrin, D. J.; Whyman, R. *J. Chem. Soc., Chem. Commun.* **1994**, 801-802.

[6] Hostetler, M. J.; Templeton, A. C.; Murray, R. W. *Langmuir* **1999,** *15*, 3782-3789.

^{1}H NMR spectra of $AuS(CH_2)_4CH_3$

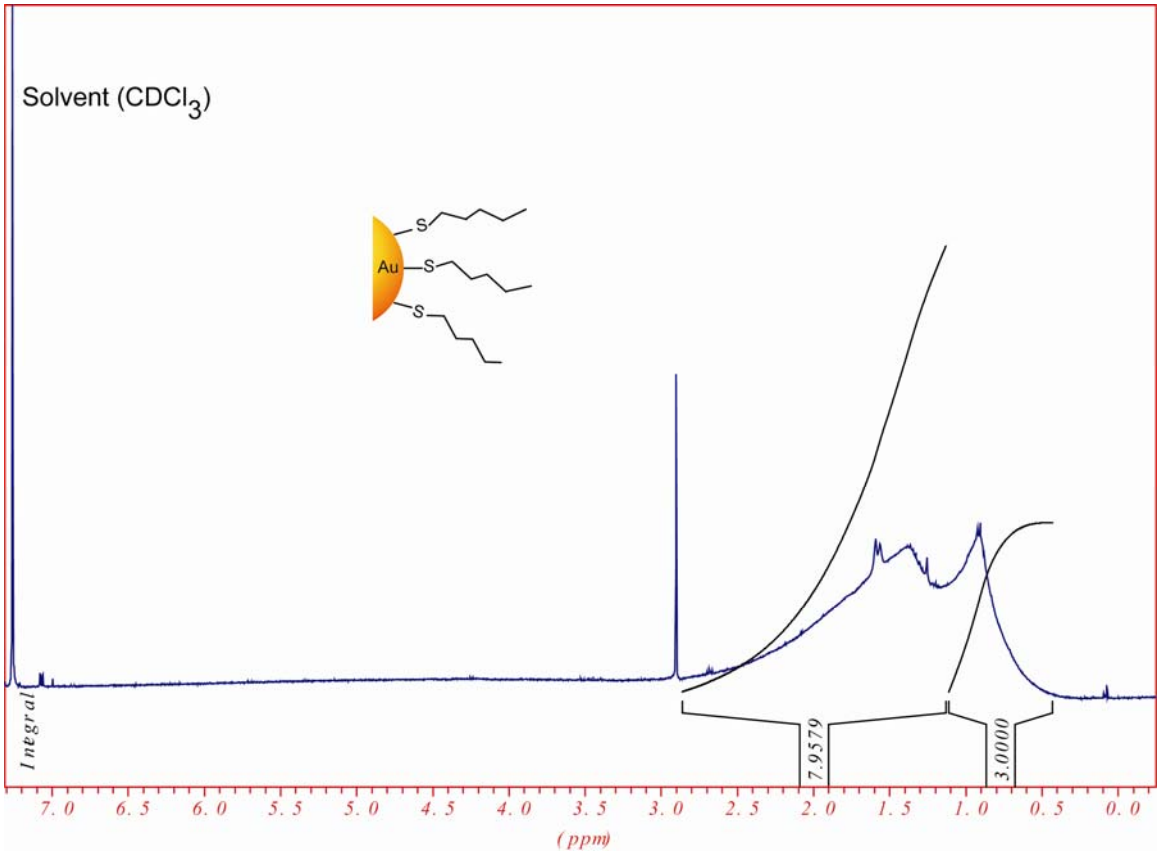

Figure 5.S17 400 MHz ^{1}H NMR of pentane-1-thiol capping the surface of the metal core gold nanoparticles. The average diameter of the metal core $AuS(CH_2)_4CH_3$ is ~ 2 nm (2.15 ± 0.31 nm).

^{1}H NMR spectra of **NP1** after place exchange with $AuS(CH_2)_4CH_3$

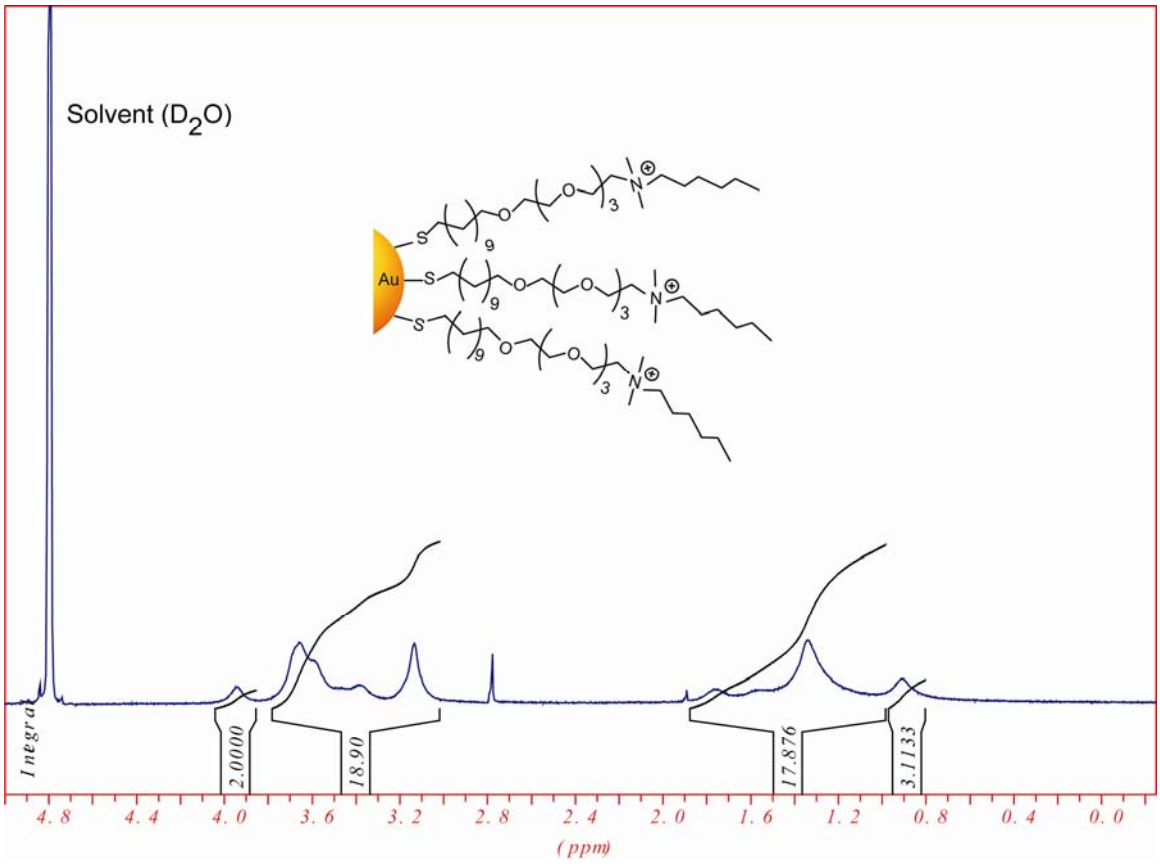

Figure 5.S18 400 MHz ^{1}H NMR of N-hexyl-23-mercapto-N,N-dimethyl-dimethyl-3,6,9, 12-tetraoxatricosan-1-aminium capping the surface of the metal core gold nanoparticles after place exchange. The average diameter of the metal core **NP1** is ~ 2 nm (2.15 ± 0.28 nm).

^{1}H NMR spectra of **NP2** after place exchange with $AuS(CH_2)_4CH_3$

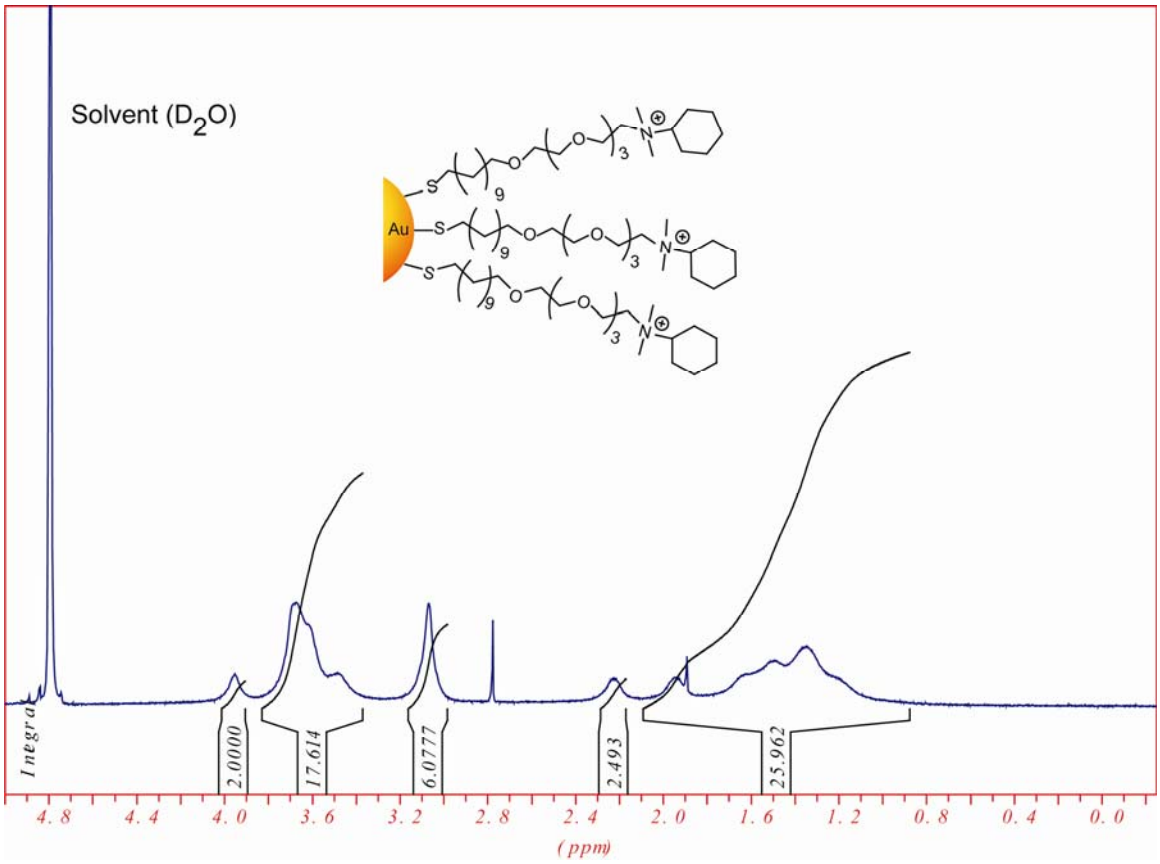

Figure 5.S19 400 MHz ^{1}H NMR of N-cyclohexyl-23-mercapto-N,N-dimethyl-3,6,9,12-tetraoxatricosan-1-aminium capping the surface of the metal core gold nanoparticles after place exchange. The average diameter of the metal core **NP2** is ~ 2 nm (2.09 ± 0.27 nm).

^{1}H NMR spectra of **NP3** after place exchange with $AuS(CH_2)_4CH_3$

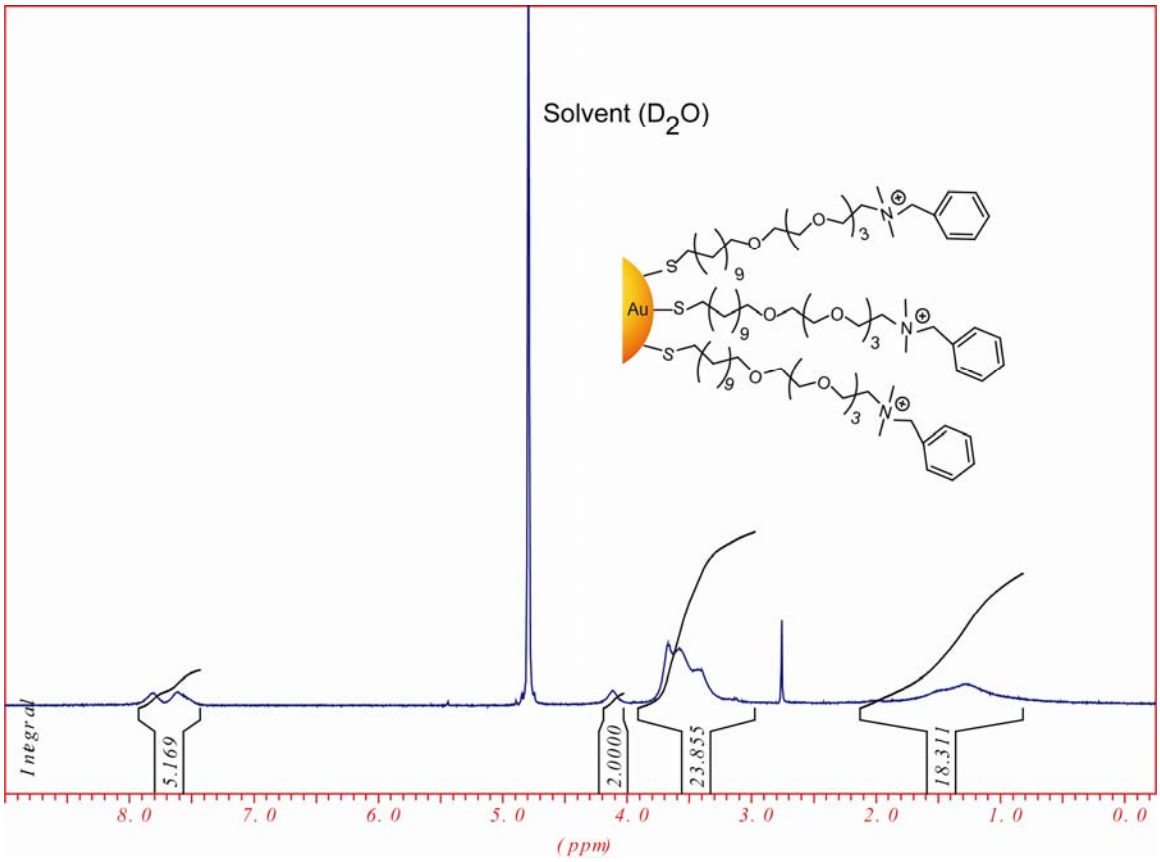

Figure 5.S20 400 MHz ^{1}H NMR of N-benzyl-23-mercapto-N,N-dimethyl-3,6,9,12-tetraoxatricosan-1-aminium capping the surface of the metal core gold nanoparticles after place exchange. The average diameter of the metal core **NP3** is ~ 2 nm (2.12 ± 0.21 nm).

^{1}H NMR spectra of **NP4** after place exchange with $AuS(CH_2)_4CH_3$

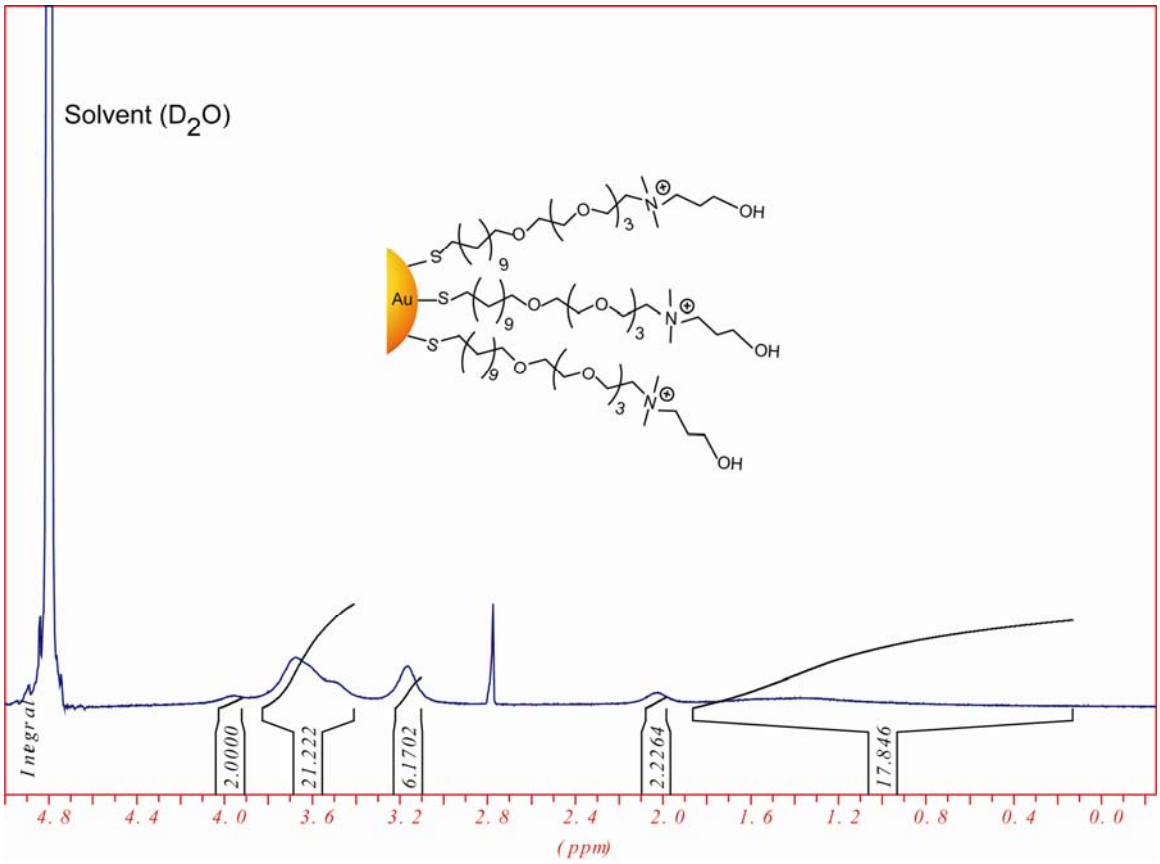

Figure 5.S21 400 MHz ^{1}H NMR of N-(3-hydroxypropyl)-23-mercapto-N,N-dimethyl-3,6,9,12-tetraoxatricosan-1-aminium capping the surface of the metal core gold nanoparticles after place exchange. The average diameter of the metal core **NP4** is ~ 2 nm (2.14 ± 0.25 nm).

^{1}H NMR spectra of **NP5** after place exchange with $AuS(CH_2)_4CH_3$

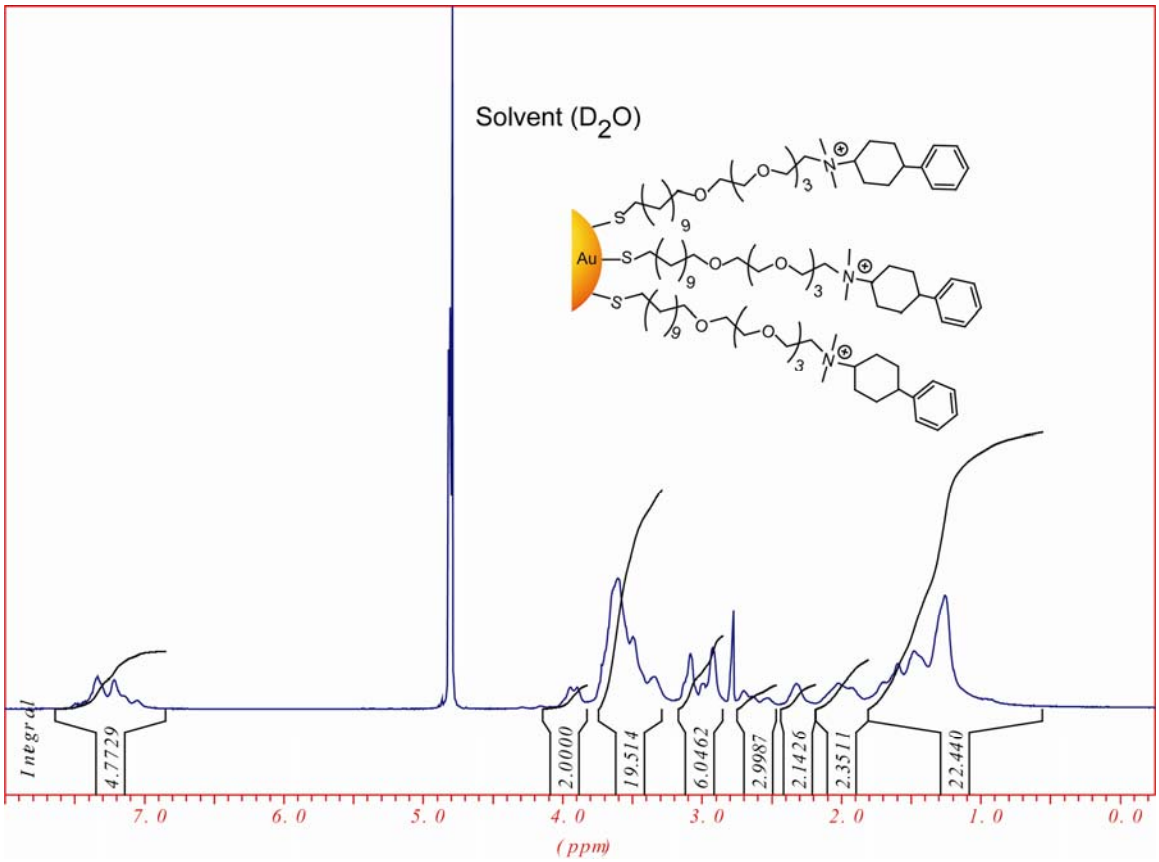

Figure 5.S22 400 MHz ^{1}H NMR of 23-mercapto-N,N-dimethyl-N-(4-phenylcyclohexyl)-3,6,9,12-tetraoxatricosan-1-aminium capping the surface of the metal core gold nanoparticles after place exchange. The average diameter of the metal core **NP5** is ~ 2 nm (2.10 ± 0.29 nm).

^{1}H NMR spectra of **NP6** after place exchange with $AuS(CH_2)_4CH_3$

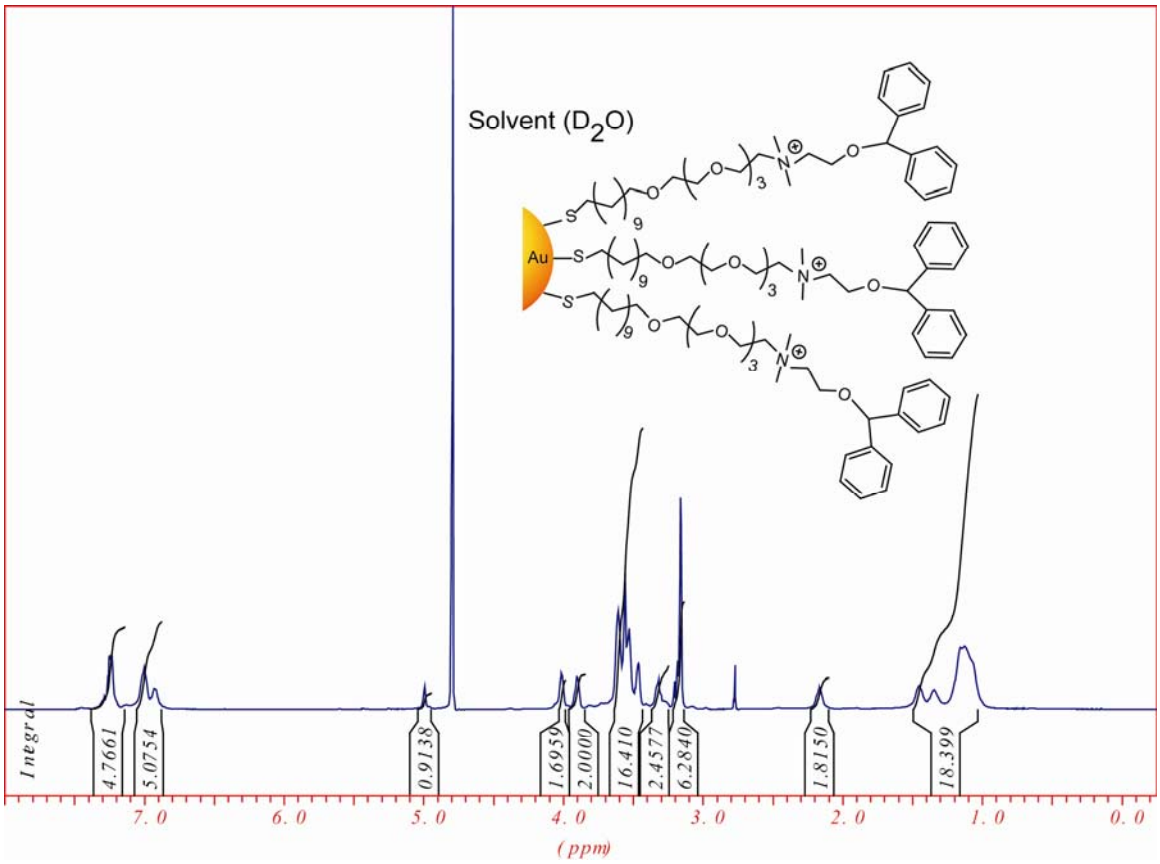

Figure 5.S23 400 MHz ^{1}H NMR of N-(2-(benzhydryloxy)ethyl)-23-mercapto-N,N-dimethyl-3,6,9,12-tetraoxatricosan-1-aminium capping the surface of the metal core gold nanoparticles after place exchange. The average diameter of the metal core **NP6** is ~ 2 nm (2.11 ± 0.22 nm).

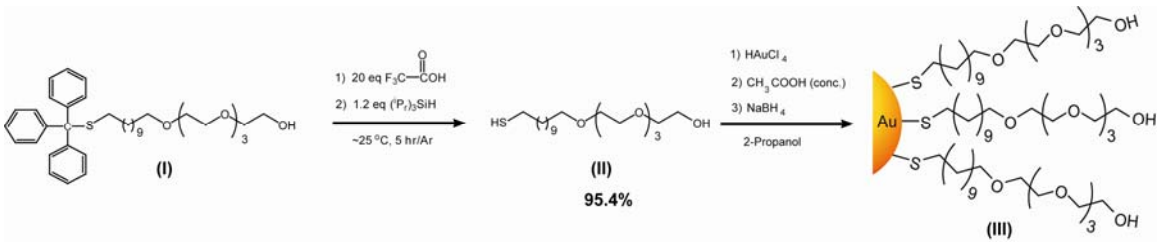

Scheme 5.S3 Synthesis of tetraethylene glycol functionalized gold nanoparticles

General procedure[7]**:** 60 mg of $HAuCl_4$ were dissolved in a mixture of 100 ml of 2-propanol and 1 ml of concentrated acetic acid (to prevent possible deprotonation of thiol molecules (**II**) after addition of excess $NaBH_4$). Compound **II** (Yield 4.57 g, >95.4%, see NMR Figure S24) bearing both thiols and hydroxyls end groups (monohydroxyl(1-mercaptounce-11-yl) was added under stirring conditions to the gold salt solution. $HAuCl_4$ was reduced by rapid addition of 10 ml of freshly prepared 0.5 M solution of $NaBH_4$ in methanol. The pale yellow gold solution turned black. After further stirring for 3 h, the volume of 2-propanol was reduced to 5-10 ml using a rotavapor. The synthesized **AuNP (III, NP_{OH})** was precipitated by pouring the reaction mixture into hexane. The tetraethylene glycol functionalized particles were cleaned several times in hexane and were separated by centrifugation. ^1H NMR spectra in D_2O showed substantial broadening of the proton signals and no free ligands were observed (See NMR Figure S25). Please notes that compound (**I**) was synthesized as shown in scheme **I** (Yield 7.83 g, >65 %, see NMR Figure S3)**.**

[7] A. G. Kanaras, F. S. Kamounah, K. Schaumburg, Ch. J. Kiely and M. Brust, *Chem. Commun.* **2002**, 2294-2295.

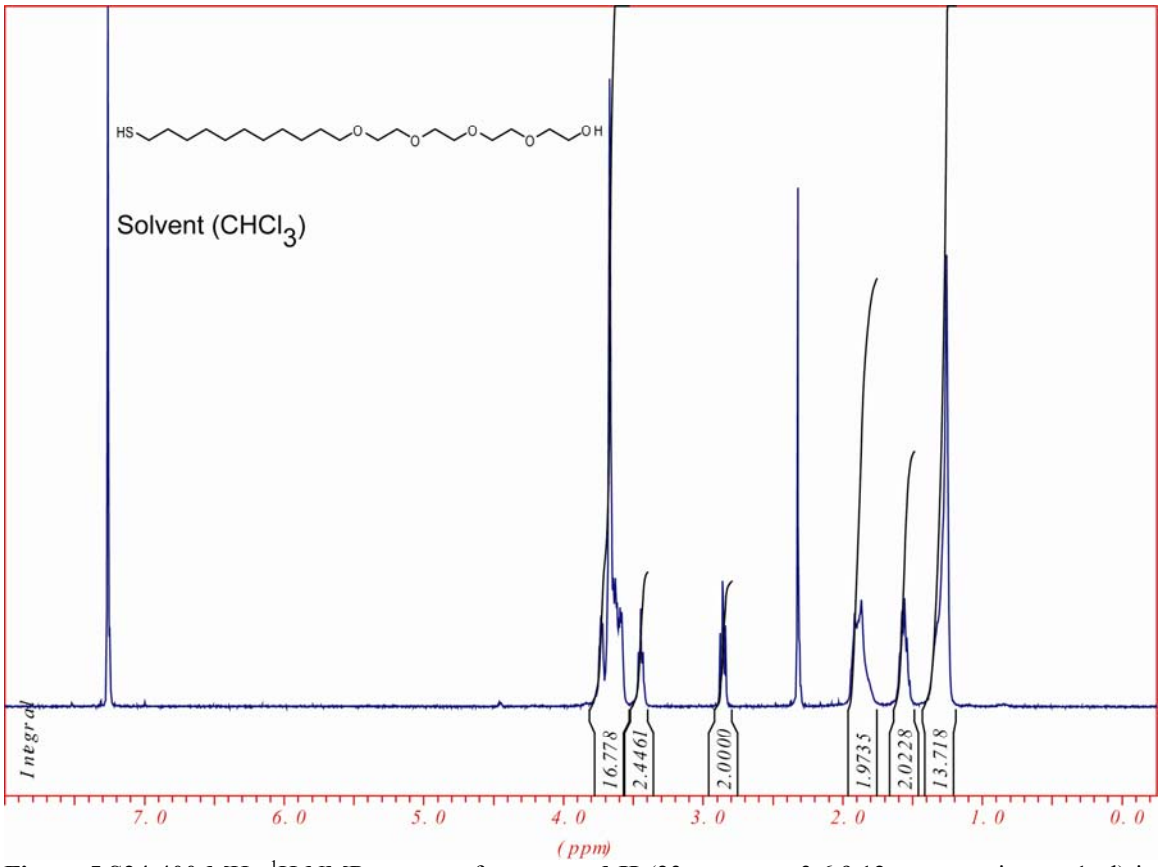

Figure 5.S24 400 MHz ^{1}H NMR spectra of **compound II** (23-mercapto-3,6,9,12-tetraoxatricosan-1-ol) in chloroform-D (D, 99.8%).

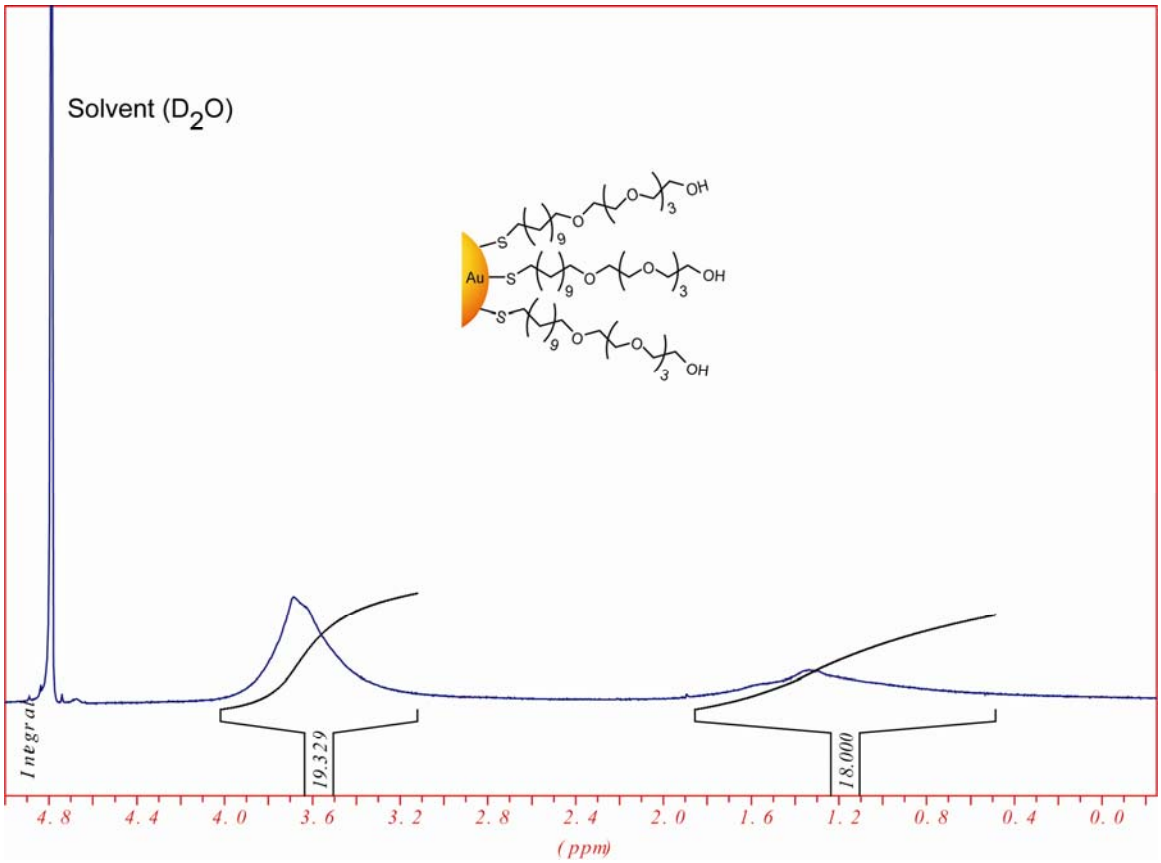

Figure 5.S25 400 MHz ^{1}H NMR of 23-mercapto-3,6,9,12-tetraoxatricosan-1-ol capping the surface of the metal core gold nanoparticles after synthesizing them. The average diameter of the metal core $\mathbf{NP_{OH}}$ is ~ 2 nm (2.40 ± 0.46 nm).

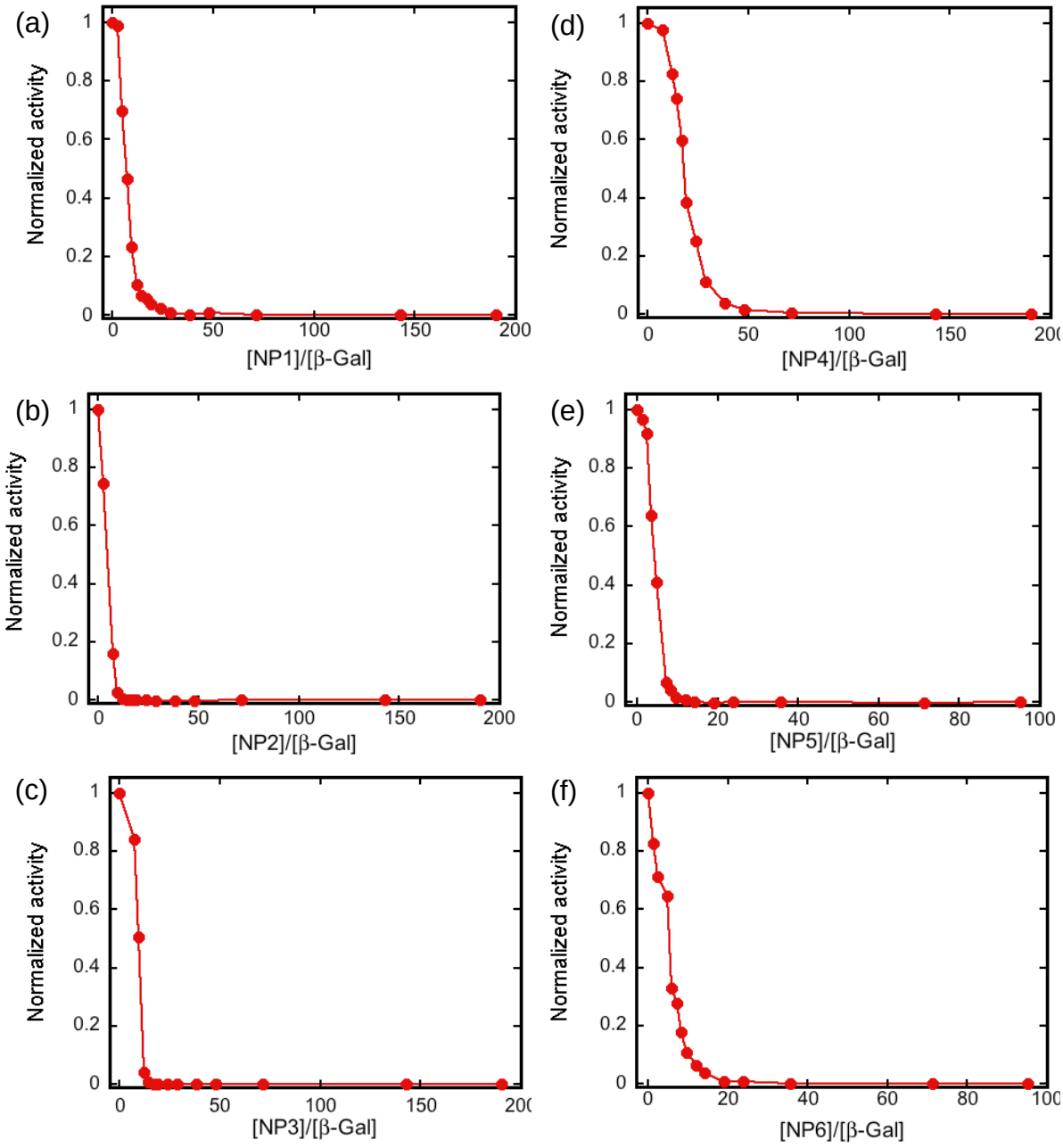

Figure 5.S26 Fluorescence titration curves for the complexation of β-Gal with cationic gold nanoparticles (**NP1-NP6**). The inhibition study was measured following the addition of cationic nanoparticles (0-100 nM) with an excitation wavelength of 455 nm. The β-Gal stock concentration was 275 nM, while the stock concentration of **NP1-NP4** and **NP5-NP6** were 100 nM and 50 nM, respectively. For the activity/inhibition studies, optimal concentrations of β-Gal/ **AuNP** complexes were obtained (β-Gal = 0.5 nM and **NP1**: 14 nM, **NP2**: 5 nM, **NP3**: 6 nM, **NP4**: 32 nM, **NP5**: 6 nM and **NP6**: 10 nM).

Table 5.S1 Final and initial kinetics ratio of the fluorescence response patterns of β-Gal and six **AuNP** (**NP1-NP6**) adducts against various target proteins ± the standard deviation (SD). Each value represents an average of six parallel measurements.

Proteins	($V_{max}/V_{o,max}$)											
	NP1	***SD***	***NP2***	***SD***	***NP3***	***SD***	***NP4***	***SD***	***NP5***	***SD***	***NP6***	***SD***
α-Amy	1.032631	0.023070	49.826124	5.782580	2.521877	0.642766	0.956224	0.065155	1.605185	0.236992	3.685843	0.410927
BSA	0.999694	0.021073	5.495259	1.192272	3.563111	1.135221	4.621077	1.189828	3.189334	1.045792	4.400572	2.060501
CytC	1.099279	0.038270	7.035717	1.641028	4.688597	0.888432	1.047342	0.056569	3.059661	0.815755	3.247085	0.923202
Fer	0.992357	0.013876	5.907556	1.403126	1.248837	0.077110	1.049945	0.240083	3.939724	1.574754	4.814340	1.156489
HSA	1.022090	0.093190	0.578550	0.061970	0.593520	0.082680	1.053750	0.020060	0.198600	0.078690	1.067530	0.030660
Lip	1.016972	0.022431	21.891588	7.816683	7.545811	1.491518	1.048292	0.028982	5.889066	2.165569	12.169190	1.601643
Lys	1.033740	0.032185	25.554471	3.995886	2.064363	0.457939	1.033634	0.024631	1.208252	0.108581	7.644296	0.648020
Myo	0.949131	0.028495	6.355809	2.647767	2.795169	1.091327	1.008620	0.023961	2.446874	0.481337	7.567806	1.130111
PhosB	1.082503	0.045996	9.308256	3.585956	7.184626	1.906531	1.051838	0.048903	1.643739	0.450590	7.773445	0.881225

Table 5.S2 Training matrix of activity response patterns generated from β-Gal/**AuNP** sensor array (**NP1**–**NP6**) and the fluorogenic substrate (4-Methylumbelliferyl-beta-D-galactopyranoside) against various types of proteins (concentration = 1 nM). Table continues on the next page.

Protein	**NP1**	**NP2**	**NP3**	**NP4**	**NP5**	**NP6**
BSA	0.044053	3.214873	1.915919	3.019801	1.508394	2.596625
BSA	0.001803	2.751742	1.862452	2.7310954	1.929778	2.125469
BSA	-0.029208	5.238646	4.532112	6.1428905	4.079058	8.703043
BSA	-0.005562	5.150131	2.309229	4.3265513	1.57304	2.363229
BSA	-0.002474	3.970872	1.487962	3.064843	3.281544	4.358388
BSA	-0.010731	5.38278	2.692894	4.6892543	1.484737	4.295396
α-Amy	0.030533	47.949173	2.694459	0.04751	0.971899	4.085935
α-Amy	0.030473	40.106219	1.095875	0.024666	0.872635	3.451511
α-Amy	0.037562	49.668787	1.225475	-0.038449	0.568434	3.20844
α-Amy	0.046226	48.437045	1.068158	-0.08928	0.49703	2.897434
α-Amy	-0.000473	53.43828	1.464148	-0.123741	0.289909	2.854269
α-Amy	0.081295	39.644225	1.239895	-0.110541	0.630381	2.807335
PhosB	0.026263	5.167704	5.097584	0.031897	0.506591	9.209252
PhosB	0.085332	8.328736	7.486119	0.129765	0.59378	7.720325
PhosB	0.091886	5.566015	8.598139	-0.00099	1.499621	8.635416
PhosB	0.170683	8.147285	3.929951	0.010107	0.340704	6.876555
PhosB	0.099291	13.73013	6.251962	0.077694	0.397096	9.220521
PhosB	0.096983	6.576261	4.349083	0.094739	0.736506	7.02314
Myo	-0.033206	8.080209	2.630773	0.021627	2.082037	6.037168
Myo	-0.027848	4.615996	1.559139	0.044039	1.226572	7.504394
Myo	-0.033647	7.094949	2.565082	0.006033	2.241766	9.31948
Myo	-0.103298	5.823526	2.629196	0.006574	1.203914	9.472293
Myo	-0.060838	4.055951	0.713224	0.015152	1.29802	7.997081
Myo	-0.09288	0.960021	0.268708	-0.036356	1.105129	6.876726
HSA	0.034241	11.695738	0.117799	0.01436	0.210229	9.729707
HSA	0.030275	16.082641	0.27824	-0.000932	0.175173	12.303557
HSA	0.030139	9.63946	0.161239	0.033209	0.13621	12.761519
HSA	0.000204	14.385132	0.165391	0.013896	0.132509	13.612848
HSA	-0.040128	14.886227	0.246951	0.035259	0.184369	11.848571
HSA	-0.070378	11.715753	0.156712	-0.001143	0.183518	11.504987
CytC	0.184217	3.334292	2.484168	0.00432	1.997726	3.585885

CytC	0.086233	6.881454	3.775898	0.058127	2.035972	3.80381
CytC	0.093745	6.705778	2.958707	0.162795	1.009177	1.514039
CytC	0.133485	4.480754	4.809584	0.022029	2.466796	2.025927
CytC	0.059278	7.360435	3.126939	0.037145	1.892558	3.668159
CytC	0.129476	5.756436	4.144335	0.029029	3.633607	1.553461
Lip	0.03489	15.975745	6.129009	0.044412	3.649662	12.760949
Lip	-0.006349	14.685047	5.771155	0.049339	4.351439	11.519174
Lip	0.059929	23.193191	7.965504	0.044512	7.374255	13.884153
Lip	0.016398	33.350164	7.693391	0.116974	2.994633	14.215449
Lip	-0.008592	18.87153	6.235977	0.033004	3.938793	11.4049
Lip	0.02107	13.406363	4.003451	0.03149	8.634694	16.495692
Fer	0.015638	3.881425	0.250667	0.594025	0.91143	4.736998
Fer	-0.025041	3.76365	0.194659	-0.079998	2.743015	5.65528
Fer	-0.012179	6.219136	0.175432	-0.055006	2.912148	5.733982
Fer	-0.001526	4.868176	0.352427	-0.020403	5.77607	5.321418
Fer	-0.026687	6.258195	0.181103	-0.036432	4.048367	3.833469
Fer	-0.003048	3.076446	0.282612	-0.071511	2.21483	2.135025
Lys	0.039216	18.908905	1.43748	0.02018	0.35339	8.155539
Lys	0.021889	25.932638	1.674801	0.087391	0.089727	8.739942
Lys	0.02705	23.321727	0.795414	0.033402	0.252776	6.517422
Lys	-0.011735	18.721133	0.953478	0.037755	0.091089	8.167482
Lys	0.058959	25.967241	0.523449	0.007717	0.198486	7.764536
Lys	0.097906	27.578963	0.761495	0.036241	0.332586	8.412007

Table 5.S3 Accuracy of LDA classification of protein analytes (Conc. = 1 nM) from the complexes of the enzyme (β-Gal) with individual cationic nanoparticles as sensors. The values are taken from the Jackknifed classification matrix based on LDA analysis of the raw data (6 replicates) listed in Table 5.S1.

Protein	**NP1-** (β-Gal)	**NP2-** (β-Gal)	**NP3-** (β-Gal)	**NP4-** (β-Gal)	**NP5-** (β-Gal)	**NP6-** (β-Gal)
α-Amy	17%	100%	17%	67%	50%	33%
BSA	17%	50%	33%	100%	0%	17%
CytC	50%	33%	50%	0%	50%	50%
Fer	50%	17%	50%	0%	33%	67%
HSA	0%	83%	67%	33%	83%	50%
Lip	33%	17%	50%	0%	50%	67%
Lys	17%	67%	50%	50%	67%	0%
Myo	50%	0%	0%	33%	50%	17%
PhosB	67%	33%	17%	0%	17%	17%
Total	33%	44%	37%	31%	44%	35%

Table 5.S4 Identification of 60 unknowns protein samples with LDA using β-Gal/**AuNP** sensor array. Table continues on the next page.

Entry	Fluorescence response pattern						Identification	Accuracy
	NP1- (β-Gal)	**NP2-** (β-Gal)	**NP3-** (β-Gal)	**NP4-** (β-Gal)	**NP5-** (β-Gal)	**NP6-** (β-Gal)	Proteins	YES/NO
1	0.0249	5.0111	7.0148	0.0265	7.7240	6.0431	PhosB	YES
2	-0.0319	7.0499	1.0191	0.0454	2.0664	7.9505	Myo	YES
3	-0.0241	4.0722	0.2621	-0.0477	3.5312	2.8284	Fer	YES
4	0.0432	19.0053	0.9033	0.0577	0.3114	6.2252	Lys	YES

5	0.0482	42.0235	2.0051	-0.1494	0.9479	2.6495	Amy	YES
6	-0.0532	20.0375	7.0020	0.0513	5.0730	14.7841	Lip	YES
7	-0.1396	4.0600	3.0306	0.0184	3.5895	2.9529	CytC	YES
8	-0.0477	10.1205	0.1779	-0.0306	0.1808	11.3290	HSA	YES
9	0.0490	22.0385	1.0080	0.0366	0.2627	7.9681	Lys	YES
10	-0.0159	3.0547	0.0240	-0.0401	2.4212	5.2937	Fer	YES
11	-0.0519	27.0321	6.0071	0.0481	5.1727	12.4804	Lip	YES
12	0.0406	6.0647	4.0280	0.0505	1.3679	7.6684	PhosB	YES
13	-0.0690	27.0339	7.0287	0.0546	4.0528	13.9802	Lip	YES
14	0.0669	25.0304	0.9457	0.0471	0.1769	8.4429	Lys	YES
15	0.0235	14.0188	0.2401	0.1601	0.1327	12.9316	HSA	YES
16	-0.0725	8.0147	1.0279	0.0063	1.6280	9.0444	Myo	YES
17	0.0947	5.0075	4.0441	0.0454	2.0443	2.8999	CytC	YES
18	0.0653	7.0399	3.1420	0.0542	1.6320	1.6501	Fer	NO
19	-0.0368	11.1823	0.1548	0.0364	0.2355	11.8070	HSA	YES
20	0.1032	4.0846	2.9033	0.0637	2.1633	1.9459	CytC	YES
21	0.0270	8.0277	4.3149	-0.0027	0.7895	7.4108	PhosB	YES
22	-0.0127	50.0125	2.0083	-0.0249	0.2990	2.6078	Amy	YES
23	0.0173	5.0105	3.0119	0.0290	2.3539	1.0394	CytC	YES
24	-0.0205	8.0175	2.0432	0.0410	1.5333	9.0862	Myo	YES
25	-0.0082	13.0109	0.2192	-0.0301	0.1516	11.8710	HSA	YES
26	0.0248	20.0153	7.0042	0.7316	5.4685	13.0649	Lip	NO
27	-0.0128	44.0447	1.8053	0.0241	4.2127	7.1356	Amy	YES
28	0.0985	8.1151	6.0505	0.1189	0.8590	6.8917	PhosB	YES
29	-0.0338	3.0126	1.0091	5.0363	1.5770	2.1641	BSA	YES
30	-0.0114	45.0051	1.0187	-0.0367	0.7776	2.5967	Amy	YES
31	-0.0702	0.0299	-0.1050	-0.0455	2.4480	2.2238	Fer	NO
32	-0.0356	13.1249	0.2015	-0.0542	0.1703	12.8905	HSA	YES
33	-0.0261	6.0661	0.3170	-0.0571	2.8549	4.5573	Fer	YES
34	-0.0291	5.1087	2.0284	-0.0303	1.6971	6.5164	Myo	YES
35	0.1081	4.4278	3.0256	0.0358	3.0605	1.9780	CytC	YES
36	-0.0332	0.2987	0.0992	-0.0133	8.2027	6.8927	Fer	YES
37	0.0514	2.8060	4.8809	6.0245	2.1747	8.1074	BSA	YES
38	0.1259	6.0918	3.9306	0.0217	1.4871	2.1888	CytC	YES
39	-0.0205	26.1369	5.5155	0.0530	4.1899	7.7610	Lys	YES
40	0.2482	21.5107	0.8112	0.0423	0.2183	14.3341	Lip	YES
41	-0.0620	7.7939	0.4299	0.0339	1.8662	6.7561	Fer	NO
42	0.3158	15.3109	0.2225	-0.0416	0.2131	14.1598	Lip	NO
43	0.0208	19.9544	6.2423	0.0622	7.4915	15.0587	Lip	YES
44	0.0391	26.8454	1.5656	0.0363	0.2279	7.7122	Lys	YES
45	0.0373	48.5690	2.0407	0.0460	0.9108	3.7984	Amy	YES
46	0.0305	3.2047	1.4620	3.0280	1.6631	2.9823	BSA	YES
47	0.0399	23.0935	1.0030	0.0393	0.3487	7.8088	Lys	YES
48	-0.0232	4.0325	0.0346	-0.0316	2.5385	5.0346	Fer	YES
49	0.0381	23.6552	7.0022	0.0383	3.0861	13.4142	Lip	YES
50	0.0367	3.2249	2.0097	4.0454	2.7286	4.4868	BSA	YES
51	0.0365	47.5912	1.0886	-0.0317	0.5385	2.8833	Amy	YES
52	-0.0249	5.3064	0.0251	-0.0541	3.0858	5.1605	Fer	YES
53	0.0265	25.0879	1.0192	0.0353	0.5735	7.2697	Lys	YES
54	-0.0217	4.1281	0.1720	-0.0463	5.0178	4.4913	Fer	YES
55	0.0197	18.1657	7.0109	0.0497	7.5318	11.8303	Lip	YES
56	0.0453	47.2604	2.0273	-0.0354	0.6315	3.3308	Amy	YES
57	-0.0195	3.7982	1.2125	4.0348	2.5901	2.6594	BSA	YES
58	-0.0167	14.0147	0.2106	-0.0469	0.1838	12.1914	HSA	YES
59	0.0454	4.0803	1.2043	5.0537	2.4238	3.1062	BSA	YES
60	0.0405	41.4076	1.1746	-0.0591	0.9762	2.8994	Amy	YES

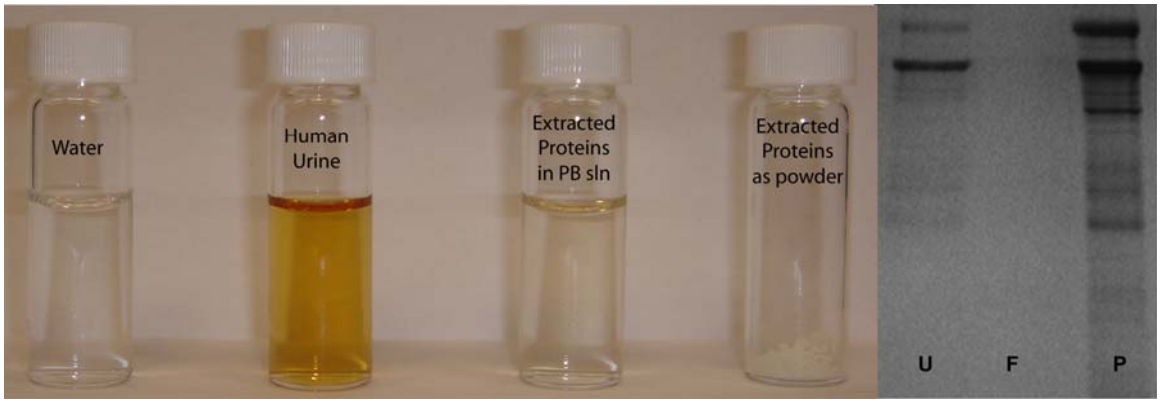

Figure 5.S27 These pictures compare the physical state and color of the concentrated human urine proteins with the original human urine samples (water is used as reference in terms of both turbidity and color). On the gel electroporesis[8], no urine proteins are lost during the binding step, as can be seen by examining the binding flowthrough. Line U is 30 µL of input human urine, line F is the binding flowthrough, and line P is 30 µL of the eluted protein.

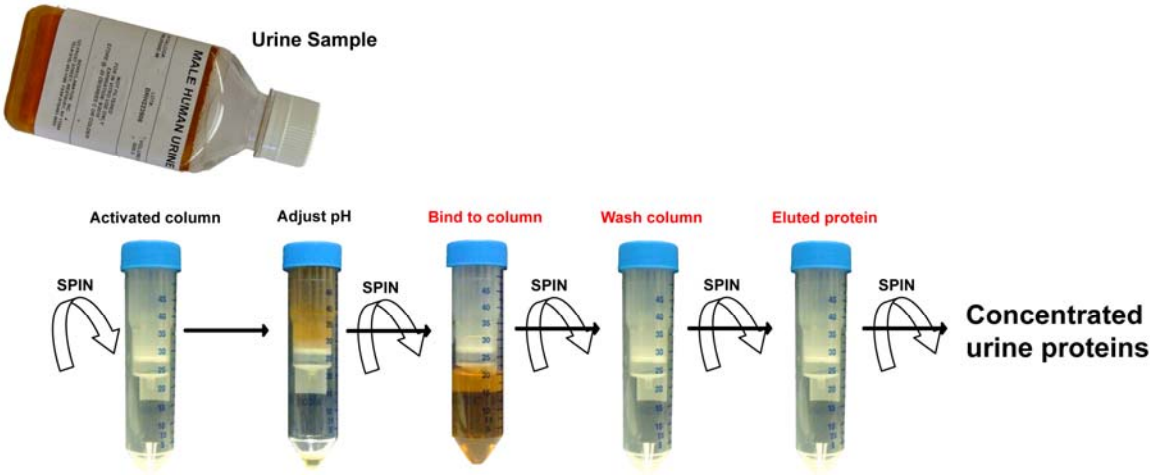

Figure 5.S28 Protein purification. Purification is based on spin column chromatography using Norgen's property resin as an ion exchanger. The resin has poor affinity for monovalent and divalent cations, making it an effective resine removal of salts. Urine proteins are preferentially purified from all other urine components including salts and other wastes.

[8] Proteospin Urine Protein Concentration Kits, Norgen Biotek Corporation.

Table 5.S5 Sources of urine proteins including soluble proteins and protein components of solid phase elements.[9]

Sources of urinary proteins	Comments
Soluble proteins	
• Glomerular filtration of plasma proteins	• Normally present (< 150 mg/day). • Defects in glomerular filter increase high molecular weight protein (e.g. albumin) excretion. • Defects in proximal tubule reabsorption or abnormal production of low molecular weight plasma proteins increase low molecular weight protein (e.g. β2-microglobulin, immunoglobulin light chains retinol-binding protein, and amino acids) excretion.
• Epithelial cell secretion of soluble proteins	• Via exocytosis (e.g. epidermal growth factor) or glycosylphosphatidyl inositol (GPI) anchored protein detachment (e.g. Tamm-Horsfall protein).
Solid phase components	
• Epithelial cells - Whole cell shedding	• Increased cell number compatible with several diseases including acute tubular necrosis (e.g. renal tubule cell shedding) and glomerular diseases (e.g. podocyte shedding).
- Plasma membrane and intracellular component shedding	• Could be due to non-specific, nephrotoxic, or apoptotic processes.
- Exosome secretion	• Normal process, see "Proteomics of Urinary Exosomes".
• Other cells	• In certain diseases, red blood cells, white blood cells, or tumor cells (e.g. bladder cancer and lymphoma) can be present in urine.

Note that epithelial cells include all epithelial cells along urinary tract starting from podocytes to urethral epithelia

[9] T. Pisitkun, R. Johnstonen, M. A. Knepper ***Molecular & Cellular Proteomics* 5:1760-1771, 2006.**

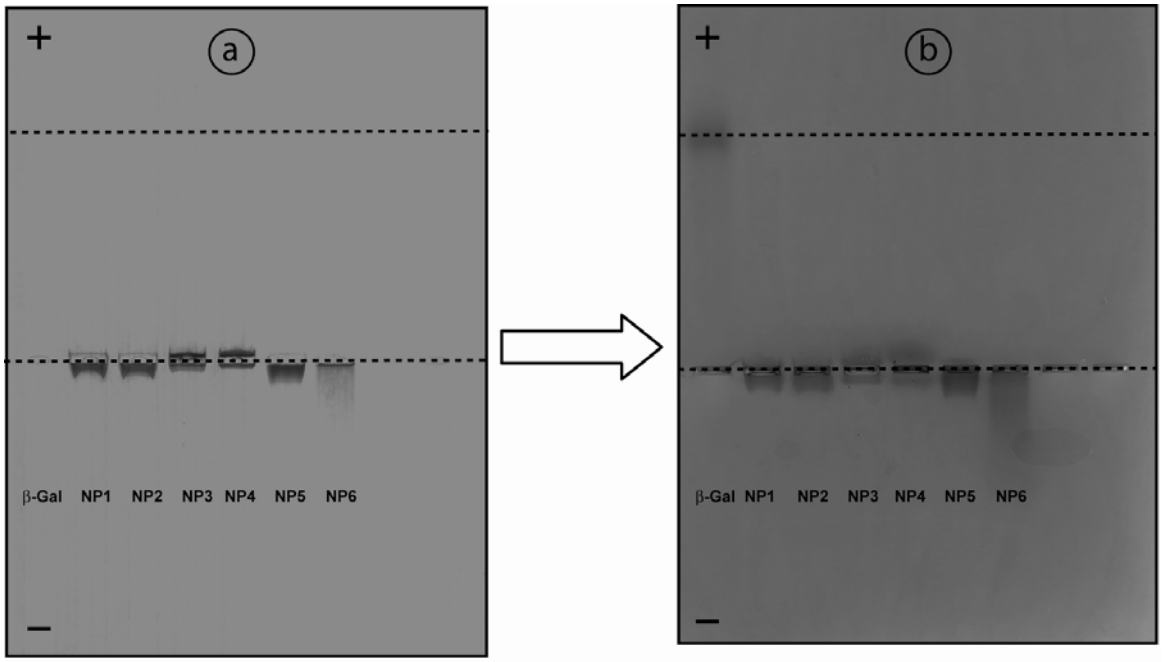

Samples (n =6)	Ligand shell composition *	Core size (nm) §	D_H (nm) †	ζ Potential (mV) ‡	Chemical structure of Ligands £
β-Gal	—	—	18.55 ± 1.71	− 22.67 ± 1.53	Large, tetrameric enzyme, Mw = 465 kDa
NP1	100% L1	2.15 ± 0.28	12.12 ± 0.10	+ 22.30 ± 0.31	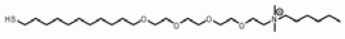
NP2	100% L2	2.09 ± 0.27	10.33 ± 0.15	+ 21.20 ± 0.10	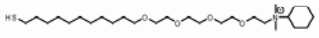
NP3	100% L3	2.12 ± 0.21	12.13 ± 0.07	+ 20.13 ± 0.57	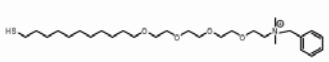
NP4	100% L4	2.14 ± 0.25	12.50 ± 0.11	+ 20.10 ± 0.22	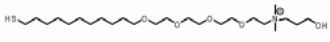
NP5	100% L5	2.10 ± 0.29	13.31 ± 0.08	+ 22.53 ± 0.19	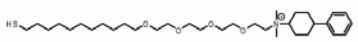
NP6	100% L6	2.11 ± 0.22	17.75 ± 0.03	+ 25.17 ± 0.03	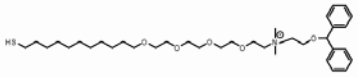

⋆ Calculated from ^{1}H NMR spectra.

§ Determined by TEM images , image J and Origin 7.0 and expressed as average diameter ± standar deviation.

† Hydrodynamic diameter (D_H) measurements are in 5 mM posphate buffer at pH 7.40.

‡ Zeta potential measurements are in 5 mM posphate buffer at pH 7.40.

£ Determined from ^{1}H NMR spectra at 400 MHz.

Figure 5.S29 Gel electrophoresis of β-gal and nanoparticles **NP1**-**NP6**: a) before staining and b) after staining. The concentration of enzyme was fixed at 8 μM as well as **NP1**-**NP6** concentrations. The average size of the core metal was determined from a population of 200 nanoparticles by both TEM and image J and expressed in average diameter ± its standard deviation between runnings. Zeta potential were measurements in 5 mM phosphate buffer, pH = 7.4.

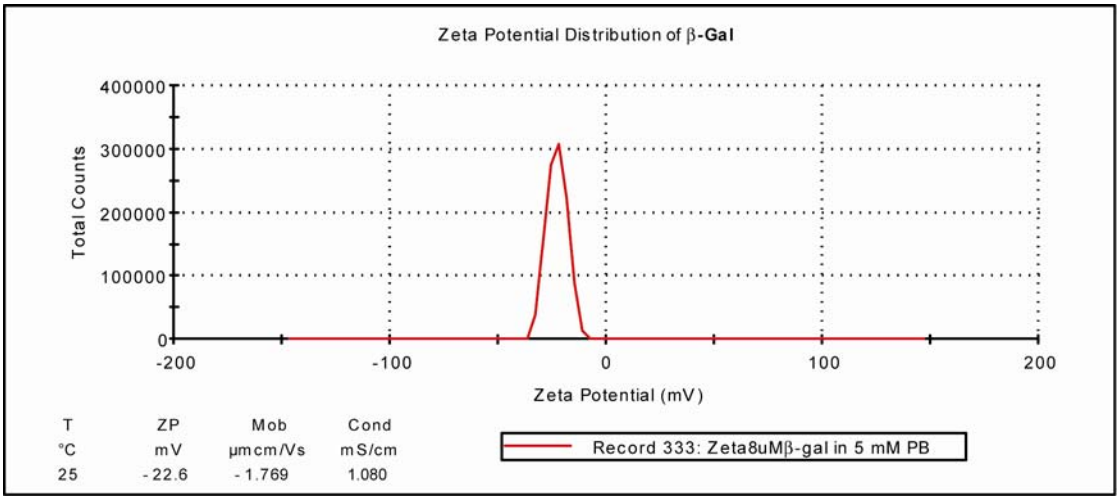

Figure 5.S30 Zeta potential of β-Gal was measured in 5 mM phosphate buffer at pH 7.4. The charge average of β-Gal was -22.67 ± 1.53 mV.

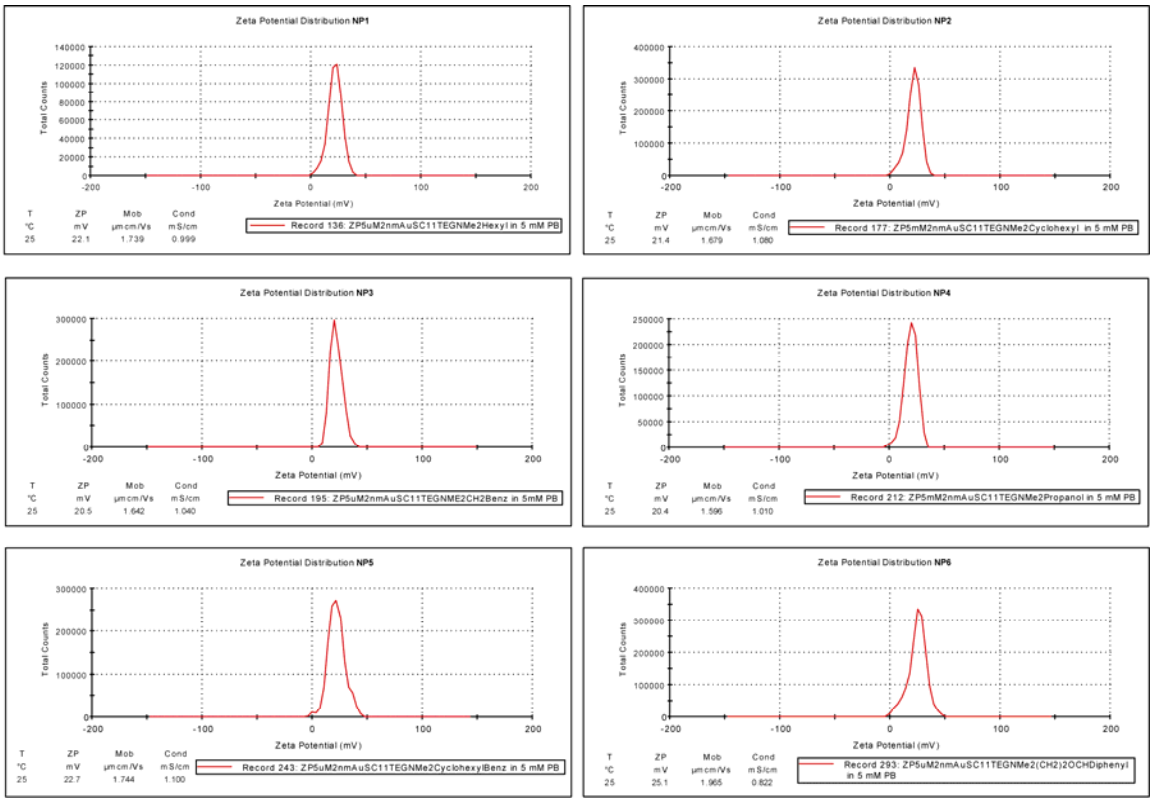

Figure 5.S31 Zeta potential of **NP1-NP6** was measured in 5 mM phosphate buffer at pH 7.4. The overall charges of these cationic **AuNP**s are on the range of + 20-25 mV.

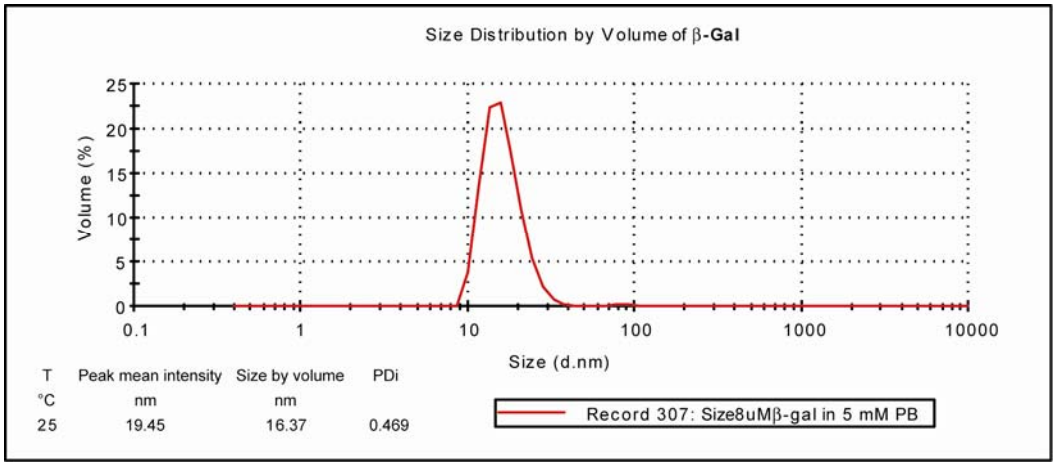

Figure 5.S32 Dynamic light scattering (DLS) of β-Gal was measured in 5 mM phosphate buffer at pH 7.4. The size average of β-Gal was 18.55 ± 1.71 nm.

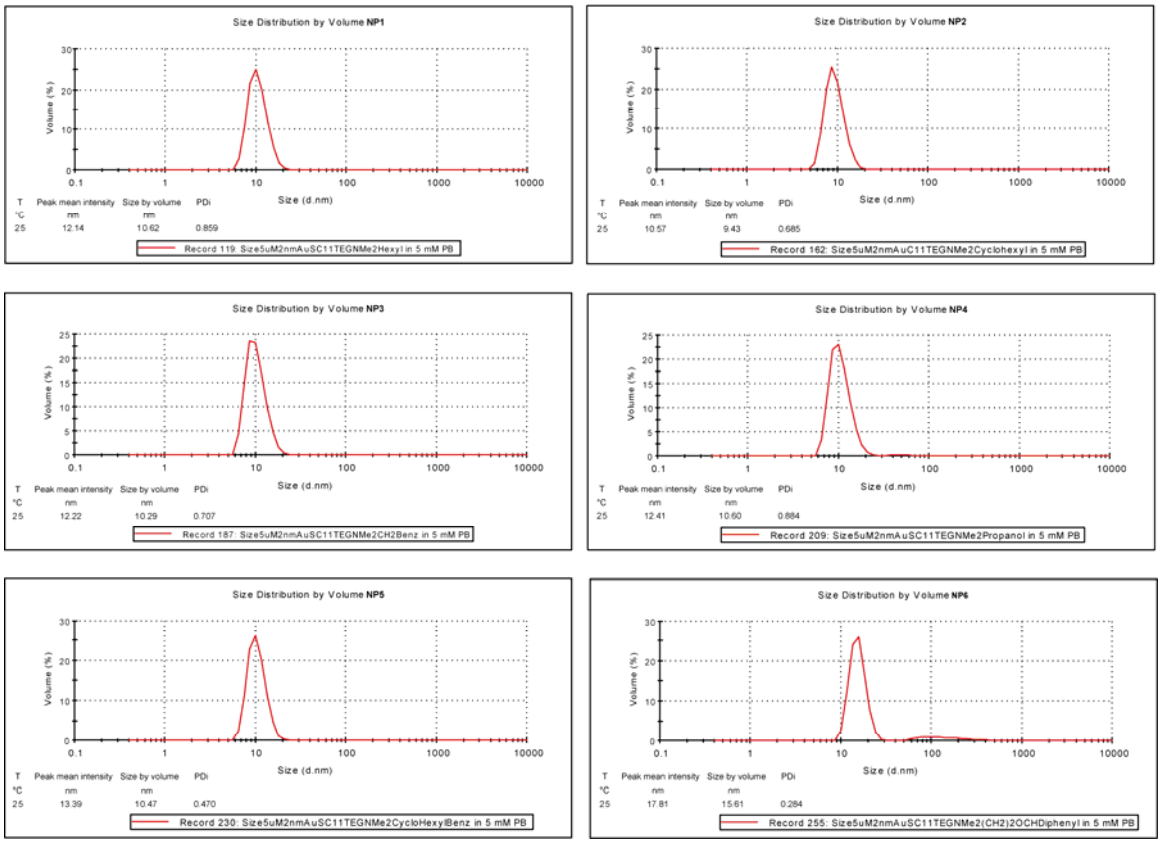

Figure 5.S33 Dynamic light scattering (DLS) of **NP1-NP6** was measured in 5 mM phosphate buffer at pH 7.4. The overall sizes of these cationic **AuNP**s are on the range of 10.57-17.81 nm.

Table 5.S6 Physical properties of the proteins used as sensing targets in phosphate buffer solution at pH 7.4.

Samples‡ (n = 6)	**D_H* (nm)**	**ζ Potential (mV)**	**ε_{280} = M^{-1} cm^{-1}**
α-Amylase (α-Am)	7.8±0.4 (0.432)	-8.6±0.9	130000
Bovine serum albumin (BSA)	8.9±0.3 (0.317)	-10.3±0.1.4	46860
Cytochrome *c* (CytC)	4.4±0.5 (0.317)	+6.29±1.5	23200
Ferritin (Fer)	27.3±0.9 (0.251)	-21.7±3.2	950000
Human serum albumin (HSA)	7.6±0.5 (0.707)	-8.8±0.1.8	37800
Lipase (Lip)	4.9±0.8 (0.493)	-12.1±0.7	54350
Lysozyme (Lys)	3.9±0.5 (0.317)	+4.5±0.5	38000
Myoglobin (Myo)	4.6±0.3 (0.668)	-12.5±0.3	13940
Alkaline phosphatase (PhosB)	13.1±0.7 (0.459)	-17.6±1.4	62780

*Note: The parenthesis adjacent to the hydrodynamic diameter (D_H) is the corresponding polydispersity index.

‡ Proteins in *italics* are found in human urine.

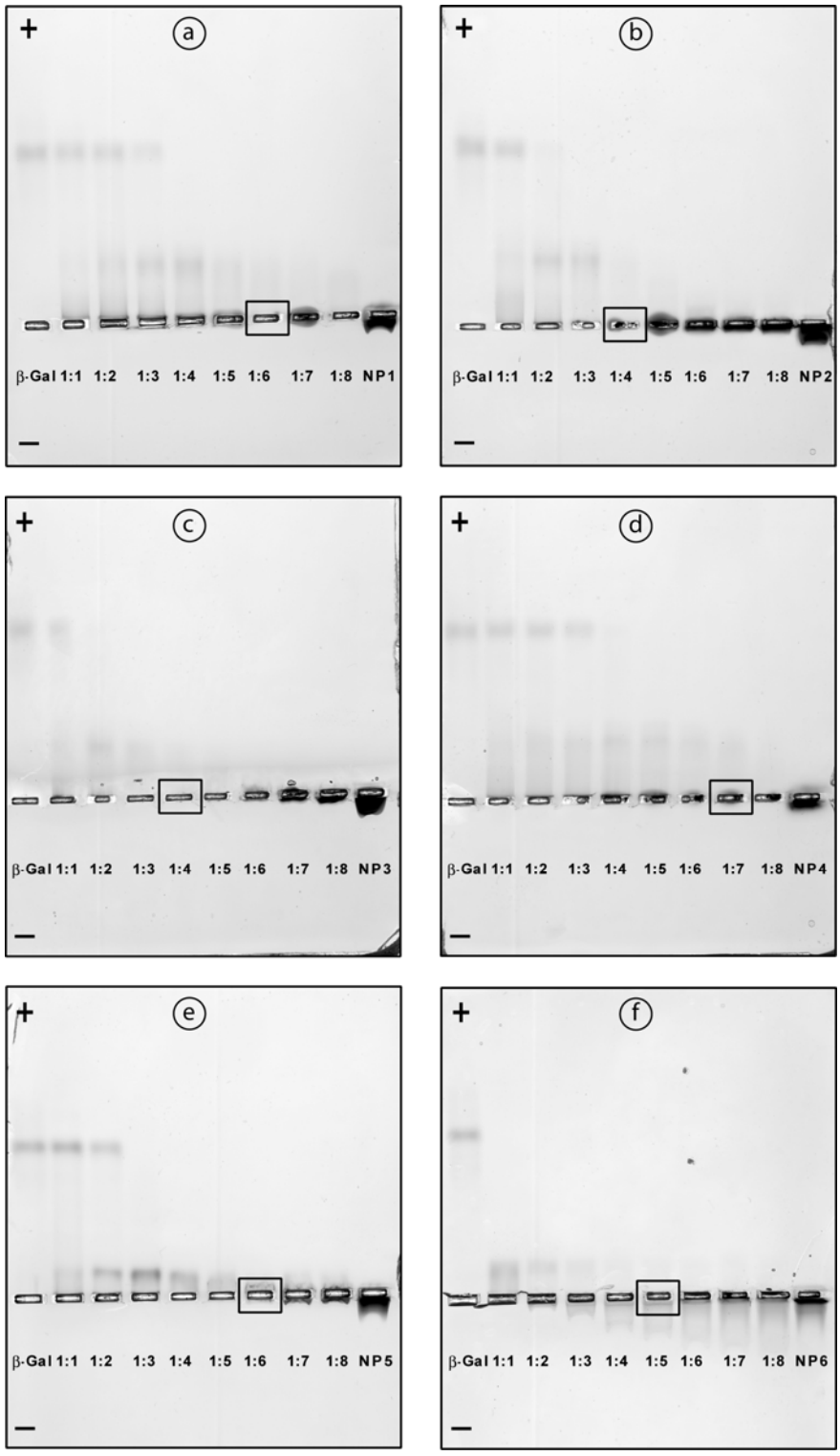

Figure 5.S34 Gel electrophoresis of β-Gal and **AuNP**s with varying molar ratios (enzyme-**AuNP** adducts) of a) **NP1**, b) **NP2**, c) **NP3**, d) **NP4**, e) **NP5**, and f) **NP6**. The concentration of the enzyme was 2 μM.

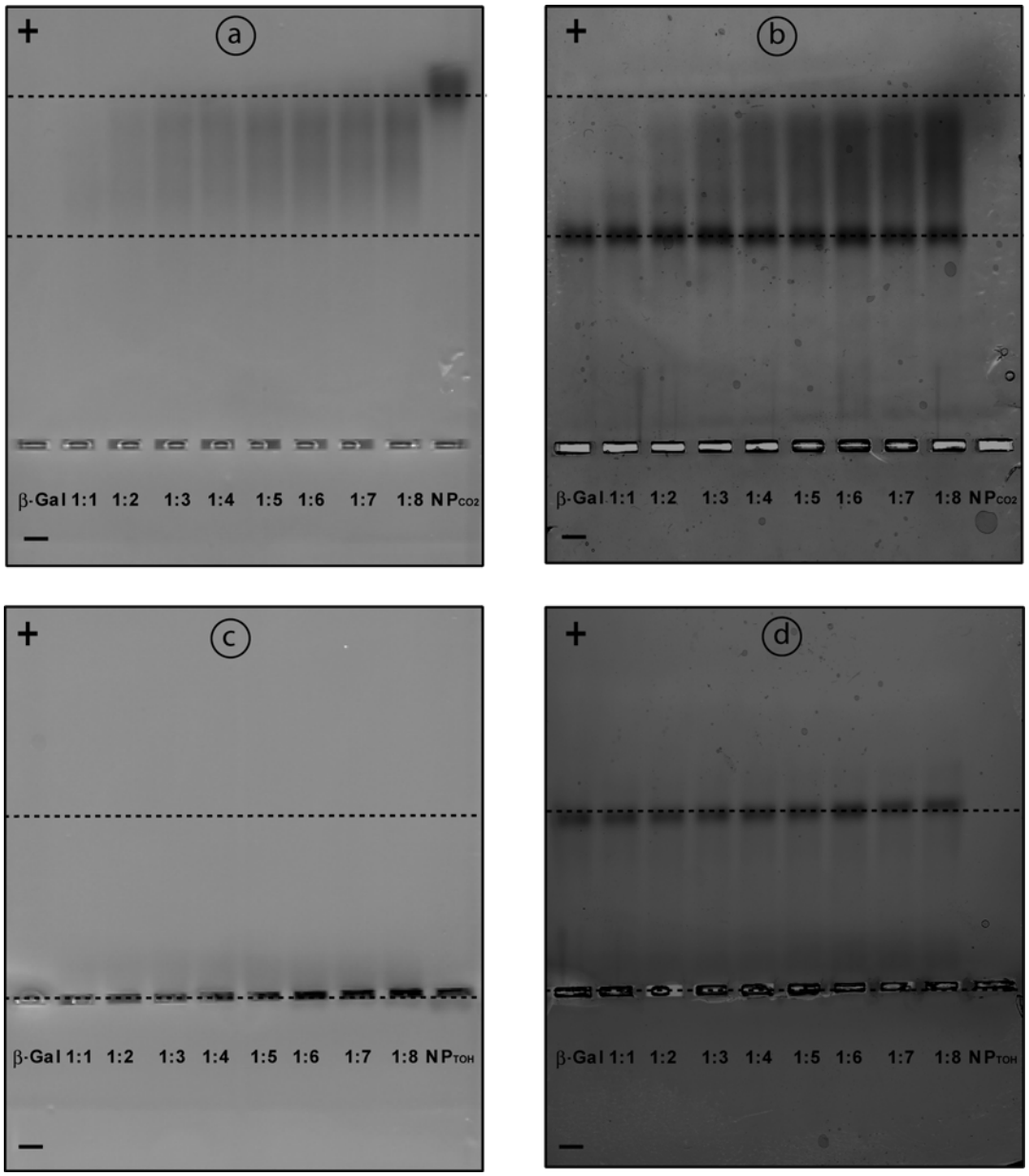

Figure 5.S35 As control experiment, gel electrophoresis of β-Gal and both negative charge $\mathbf{NP_{CO2}}$ (26-mercapto-3,6,9,12,15-pentaoxahexacosan-1-oate capping the metal core)[10] and neutral charge $\mathbf{NP_{OH}}$ **(**23-mercapto-3,6,9,12-tetraoxatricosan-1-ol capping the metal core) with varying molar ratios (enzyme: **NP**) of a) before staining $\mathbf{NP_{CO2}}$, b) after staining $\mathbf{NP_{CO2}}$, c) before staining $\mathbf{NP_{OH}}$, d) after staining $\mathbf{NP_{OH}}$. The concentration of the enzyme was 2 μM. As it can be seen on the gels b) and d) anionic **AuNP**s and neutral **AuNP**s do not interact strongly with the enzyme, β-Gal**.**

[10] R. Hong, N. O. Fischer, A. Verma, C. M. Goodman, T. Emrick, and V. M. Rotello *J. Am. Chem. Soc.*, **2004**, *126* (3), pp 739–743

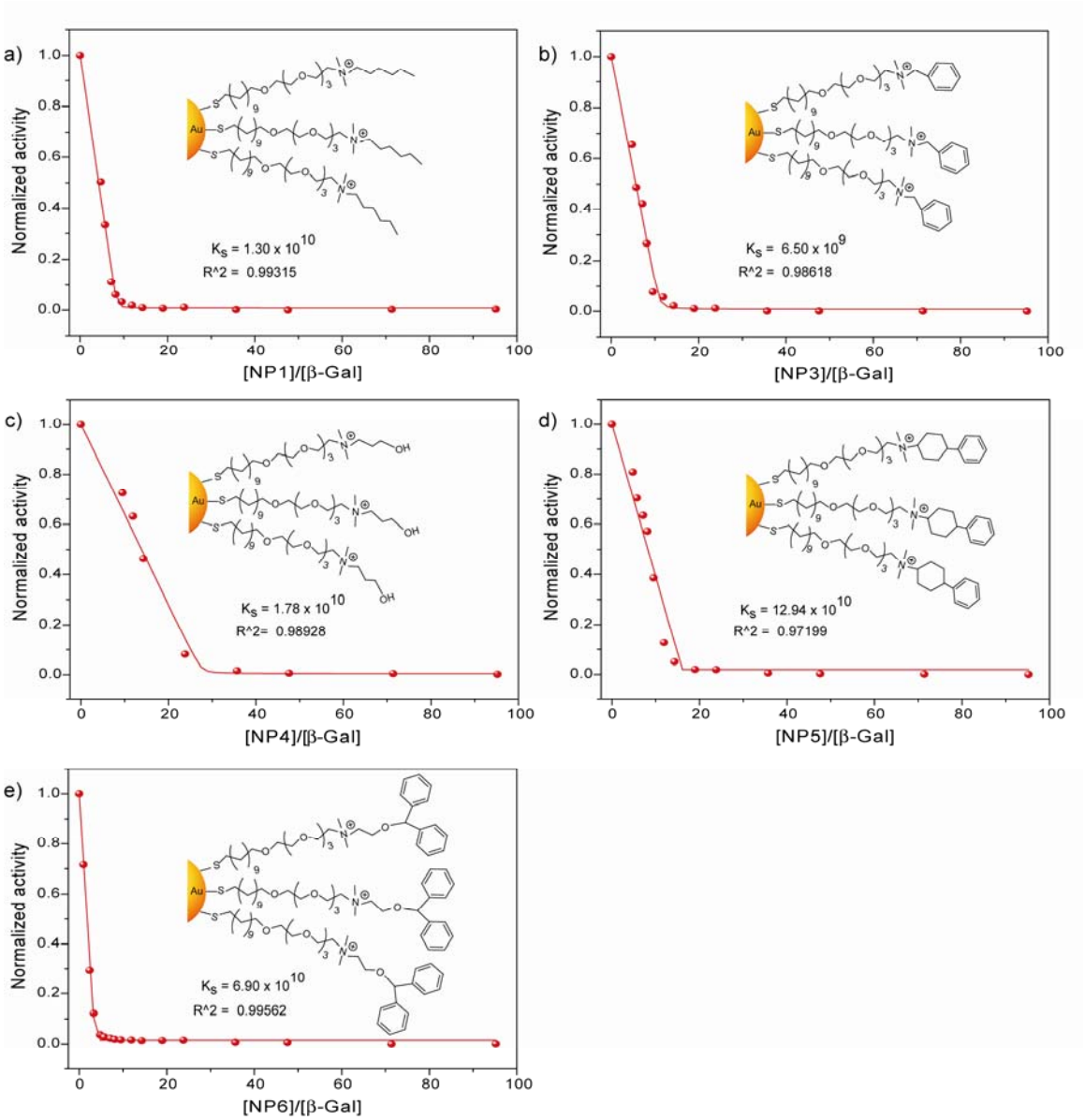

Figure 5.S36 Fluorescence titration curves for the complexation of β-Gal (0.5 nM) with cationic gold nanoparticles (**NP1-NP6**). The inhibition study was measured following the addition of cationic nanoparticles (0-100 nM) with an excitation wavelength of 455 nm.

5.4.7 Thermodynamic parameters for the enzyme-nanoparticle conjugate

Both the binding constant (Ks) and the binding ratio (n) between β-Gal and **AuNP**s could be quantified using the activity titration curves through nonlinear least-squares curve fitting analysis combined with gel electrophoresis. The experimental ratios of nanoparticles to β-Gal needed to yield ~1% enzyme activity ranged from 4.0 for **NP2-NP3** to 7.0 for **NP1** (see Table S7 and Figure S36). The inhibition of β-Gal activity strongly depends on the chemical structural changes of the peripheral ligands on the **AuNP**s, as shown in Table S7. Complex stabilities vary within approximately one order of magnitude ($\Delta\Delta G \approx 9$ KJ mol^{-1}), and the binding stoichiometry (n) between each **AuNP** and the enzyme vary from 4 to 7, since they possess different affinity. These observations indicate that the subtle structural changes of the nanoparticles end groups significantly affect the affinity for the enzyme. Under these conditions, it is estimated that >80% of **NP1-NP6** is bound to the β-Gal, based on the binding constant listed on Table S7, allowing fluorescence enhancement through both subsequent displacement enzymatic reaction.

Table 5.S7 Binding constants (K_S) and binding stoichiometries (n) between β-Gal and several cationic nanoparticles (**NP1**–**NP6**) in desalted urine as determined from both activity assays and gel.

Nanoparticles	K_S (10^{10} M^{-1})	$-\Delta G$ (kJ mol^{-1})	***n***
NP1	1.30	57.3	6
NP2	0.31	53.8	4
NP3	0.65	55.6	4
NP4	1.78	58.1	7
NP5	12.94	63.0	6
NP6	6.90	61.4	5

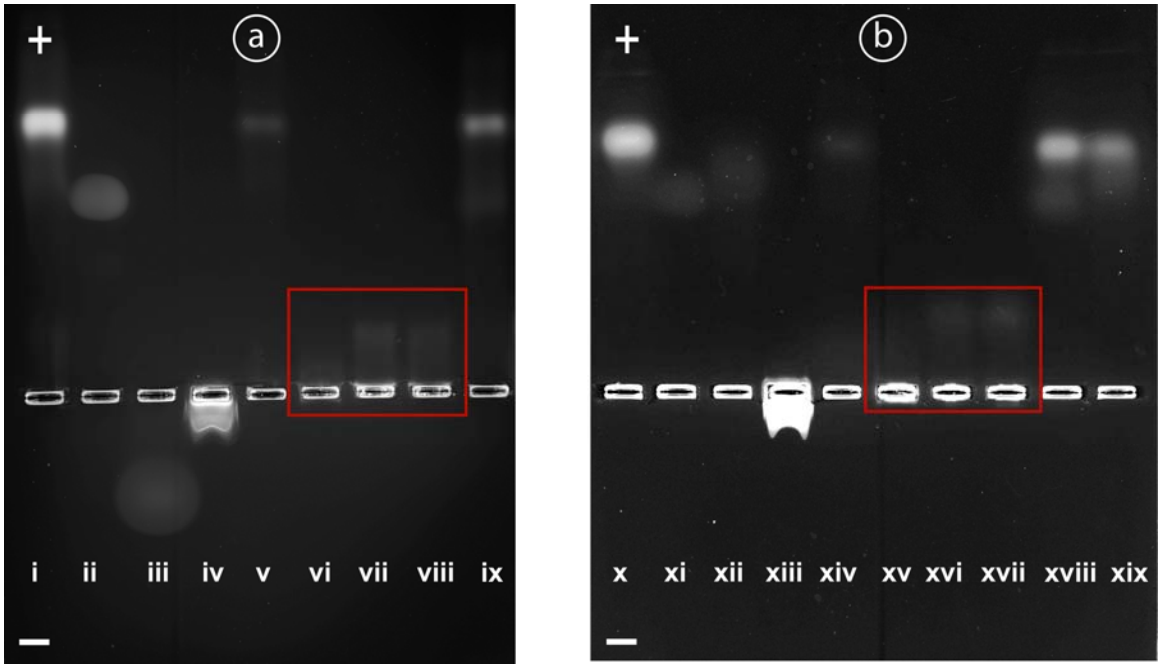

Figure 5.S37 Gel electrophoresis confirms the hypothesis that the displacement assays of the enzyme by proteins take place. **Agarose gel electrophoresis a)** shows the displacement assay of β-Gal by two proteins HSA (-) and lysozyme (+): i) 8 μM β-Gal, ii) 8 μM HSA (notes that the broad peak is probably due to high concentration of the protein), iii) Lysozyme (notes that the broad peak is probably due to high concentration of the protein), iv) 8 μM **NP2**, v) 2 μM of β-Gal and 8 μM $\mathbf{NPT_{OH}}$, vi) 1:4 molar ratio (enzyme : **NP2**), vii) 1:4 molar ratio (β-Gal : **NP2**) and 1 μM HSA, viii) 1:4 molar ratio (enzyme : **NP2**) and 1 μM lysozyme and ix) 2 μM β-Gal and 1 μM HSA confirming the no interaction between these two proteins. **Agarose gel electroporesis b)** shows the displacement assay of β-Gal by two proteins BSA (-) and Ferritin (-): x) 8 μM β-Gal, xi) 8 μM BSA (notes that the broad peak is probably due to high concentration of the protein), xii) Ferritin (notes that the broad peak is probably due to high concentration of the protein), xiii) 8 μM **NP2**, xiv) 2 μM of β-Gal and 8 μM $\mathbf{NPT_{OH}}$, xv) 1:4 molar ratio (β-Gal : **NP2**), xvi) 1:4 molar ratio (enzyme : **NP2**) and 1 μM BSA, xvii) 1:4 molar ratio (enzyme : **NP2**) and 1 μM Ferritin, xviii) 2 μM β-Gal and 1 μM BSA confirming that there is no interaction between these two proteins and xix) 2 μM β-Gal and 1 μM Ferritin confirming that there is no interaction between them.

Table 5.S8 Final and initial kinetics ratio of the fluorescence response patterns of β-Gal and six **AuNP** (**NP1-NP6**) adducts against various target proteins ± standard deviation (SD). Each value represents an average of six parallel measurements.

Proteins	**($V_{max}/V_{o,max}$)**											
	NP1	*SD*	*NP2*	*SD*	*NP3*	*SD*	*NP4*	*SD*	*NP5*	*SD*	*NP6*	*SD*
α-Amy	1.162744	0.089064	3.828086	0.335818	2.401873	0.169194	0.482782	0.089669	1.045633	0.017870	1.581139	0.088925
BSA	0.566856	0.045598	1.357927	0.215107	1.456985	0.202390	0.870069	0.056741	1.165084	0.078856	1.923542	0.538564
CytC	1.020838	0.008033	1.349411	0.095001	1.657639	0.158399	1.027977	0.021659	1.171242	0.046114	1.486211	0.199757
Fer	0.998399	0.002915	1.731210	0.209064	1.044367	0.013751	1.009791	0.047099	1.570519	0.305616	1.825326	0.250235
HSA	1.022090	0.093190	0.578550	0.061970	0.593520	0.082680	1.053750	0.020060	0.198600	0.078690	1.067530	0.030660
Lip	1.142678	0.111317	1.119827	0.032988	2.167052	0.265922	0.462804	0.448489	1.368664	0.163287	1.414100	0.097572
Lys	1.214415	0.071499	2.421471	0.231323	1.189766	0.081647	1.006598	0.004832	1.015704	0.008186	2.421105	0.244526
Myo	1.212988	0.055828	1.310051	0.153280	1.320058	0.194570	1.413432	0.059226	1.109101	0.036296	2.249909	0.278100
PhosB	1.017318	0.008850	1.480974	0.207608	2.102657	0.339915	1.010170	0.009593	1.048541	0.033976	2.465599	0.190674

Table 5.S9 Training matrix of activity response patterns generated from β-Gal/**AuNP** sensor array (**NP1**–**NP6**) and the fluorogenic substrate (4-Methylumbelliferyl-beta-D-galactopyranoside) against various proteins (concentration = 1 nM). [†] Table continues on the next page.

Protein	**NP1**	**NP2**	**NP3**	**NP4**	**NP5**	**NP6**
α-Amy	0.160975	3.393432	1.251925	-0.499563	0.072658	0.786185
α-Amy	0.119801	2.838373	1.658166	-0.359135	0.065237	0.664113
α-Amy	0.360905	3.525645	1.576092	-0.578533	0.042495	0.617349
α-Amy	0.123519	3.427957	1.378307	-0.575258	0.037157	0.557427
α-Amy	0.146484	3.781986	1.276771	-0.552547	0.021673	0.549194
α-Amy	0.119801	2.805677	1.594953	-0.614698	0.047126	0.540163
BSA	-0.524773	0.855423	0.368644	-0.042752	0.112765	1.699626
BSA	-0.407967	0.518049	0.358356	-0.212016	0.144267	0.408964
BSA	-0.435635	0.122587	0.872029	-0.177976	0.304944	1.674564
BSA	-0.425384	0.344485	0.444321	-0.122473	0.117598	0.454712
BSA	-0.440822	0.281023	0.286352	-0.129752	0.245323	0.838603
BSA	-0.510731	0.380946	0.518147	-0.113815	0.110997	0.826483
CytC	0.035445	0.235972	0.477981	0.018681	0.149347	0.689965
CytC	0.016592	0.487015	0.726525	0.010589	0.152206	0.731896
CytC	0.018037	0.474577	0.569288	0.029653	0.175445	0.291318
CytC	0.025684	0.317109	0.925419	0.040126	0.184414	0.389811
CytC	0.011405	0.520908	0.601658	0.067659	0.141485	0.705795
CytC	0.024912	0.407391	0.797416	0.005288	0.271643	0.298903
Fer	0.003009	0.706992	0.048231	0.108201	0.175369	0.911452
Fer	-0.004823	0.685545	0.037454	-0.014575	0.527787	1.088146
Fer	-0.002341	1.132817	0.033757	-0.010029	0.560338	1.103283
Fer	-0.000267	0.886735	0.067819	-0.003723	1.111381	1.023901
Fer	-0.005135	1.139926	0.034846	-0.006647	0.778952	0.737603
Fer	-0.000593	0.560372	0.054377	-0.013032	0.426158	0.410803
HSA	0.156082	-0.007475	-0.049664	0.065918	-0.173453	0.044086
HSA	0.008484	-0.068359	-0.084735	0.041808	-0.152816	0.126597
HSA	0.017289	-0.078791	0.045644	0.054551	-0.074029	0.069858
HSA	-0.050856	-1.088342	-0.127892	0.075639	-1.088317	0.034675
HSA	0.114875	-1.690797	-0.146809	0.071153	-1.556754	0.071189

HSA	-0.105869	-0.012866	-2.169627	0.021359	-1.983362	0.085226
Lip	0.146105	0.110819	1.179293	-0.316738	0.272846	0.578538
Lip	0.071871	0.119053	1.110435	-0.341516	0.325371	0.453623
Lip	0.287884	0.188278	1.532652	-0.442879	0.551288	0.268081
Lip	0.272863	0.189773	1.480295	-0.468783	0.223874	0.505244
Lip	0.145567	0.110815	1.199872	-0.258125	0.294458	0.427209
Lip	-0.019982	0.119053	0.770309	-1.474511	0.645517	0.414082
Lys	0.157841	1.338209	0.276587	0.003676	0.026419	1.161619
Lys	0.345268	1.835289	0.322254	0.015918	0.006708	1.443934
Lys	0.152547	1.650511	0.153046	0.006084	0.018897	1.793173
Lys	0.187049	1.324925	0.183459	0.006877	0.006816	1.822576
Lys	0.276511	1.837733	0.100717	0.001406	0.014839	1.538729
Lys	0.239768	1.951802	0.146523	0.006601	0.024864	1.323167
Myo	0.278681	0.571847	0.506194	0.510292	0.155658	1.569218
Myo	0.278686	0.326684	0.299995	0.391116	0.091697	0.981664
Myo	0.147753	0.502119	0.493531	0.378591	0.167591	1.254026
Myo	0.213595	0.412139	0.505887	0.457545	0.090003	1.571516
Myo	0.163881	0.287045	0.137232	0.455627	0.097038	0.993984
Myo	0.267342	0.067942	0.051702	0.348509	0.082618	1.618565
PhosB	0.005053	0.365723	0.980838	0.005815	0.037872	1.771964
PhosB	0.016418	0.589436	1.440413	0.023637	0.044395	1.485478
PhosB	0.017679	0.39391	1.654379	-0.000182	0.112109	1.661552
PhosB	0.032841	0.576594	0.756166	0.001841	0.025471	1.323127
PhosB	0.019104	0.971739	1.202948	0.014152	0.029686	1.774132
PhosB	0.018667	0.465411	0.836812	0.017257	0.05506	1.351331

† β-Gal: β-galactosidase, ε (280 nm) = 1128600 M^{-1} cm^{-1}; BSA: bovine serum albumin, ε (280 nm) = 46860 M^{-1} cm^{-1}; α-Amy: α-amylase, ε (280 nm) = 130000 M^{-1} cm^{-1}; PhosB: alkaline phosphatase, ε (280 nm) = 62780 M^{-1} cm^{-1}; Myo: myoglobin, ε (280 nm) = 13940 M^{-1} cm^{-1}; HSA: human serum albumin, ε (280 nm) = 37800 M^{-1} cm^{-1}; CytC: cytochrome *c*, ε (280 nm) = 23200 M^{-1} cm^{-1}; Lip: lipase: ε (280 nm) = 54350 M^{-1} cm^{-1}; Fer: ferritin: ε (280 nm) = 950000 M^{-1} cm^{-1}; Lys: lysozyme: ε (280 nm) = 38000 M^{-1} cm^{-1}.

Table 5.S10 Accuracy of LDA classification of protein analytes (Conc. = 1 nM) from the complexes of the enzyme (β-Gal) with individual cationic nanoparticles as sensors. The values are taken from the Jackknifed classification matrix based on LDA analysis of the raw data (6 replicates) listed in Table S2.

Protein	**NP1-** (β-Gal)	**NP2-** (β-Gal)	**NP3-** (β-Gal)	**NP4-** (β-Gal)	**NP5-** (β-Gal)	**NP6-** (β-Gal)
α-Amy	0%	100%	67%	17%	50%	33%
BSA	100%	0%	33%	83%	17%	0%
CytC	0%	17%	50%	33%	33%	0%
Fer	100%	50%	100%	0%	67%	17%
HSA	0%	33%	17%	67%	50%	100%
Lip	33%	100%	17%	0%	33%	50%
Lys	0%	100%	50%	83%	100%	17%
Myo	0%	33%	17%	100%	67%	17%
PhosB	67%	33%	17%	0%	17%	50%
Total	33%	52%	41%	43%	48%	31%

Table 5.S11 Identification of 60 unknowns protein samples with LDA using β-Gal/**AuNP** sensor array.

Entry	Fluorescence response pattern						Identification	Accuracy
	NP1- (β-Gal)	**NP2-** (β-Gal)	**NP3-** (β-Gal)	**NP4-** (β-Gal)	**NP5-** (β-Gal)	**NP6-** (β-Gal)	Proteins	YES/NO
1	0.014053	0.725769	1.387652	0.005863	0.038725	1.576353	PhosB	YES
2	0.258481	0.490884	0.268747	0.458737	0.092778	1.437691	Myo	YES
3	0.011883	0.521188	0.616283	0.059383	0.159981	0.757299	CytC	YES
4	0.014982	0.519524	0.837249	0.032874	0.198373	0.629875	CytC	YES
5	0.018655	0.578776	0.987652	0.002845	0.024236	1.654218	PhosB	YES
6	0.123629	3.417971	1.373303	-0.574268	0.031153	0.553475	Amy	YES
7	0.015273	0.435886	0.858873	0.032992	0.198745	0.498731	CytC	YES
8	0.153256	0.188375	0.476772	0.510535	0.126633	1.352787	Myo	YES
9	0.129887	-0.098539	-0.079845	0.057954	-0.398851	0.096358	HSA	YES
10	0.260995	3.124645	1.560927	-0.478231	0.062795	0.617343	Amy	YES
11	0.024187	0.693764	1.469739	0.017652	0.044163	1.678362	PhosB	YES
12	-0.498358	0.273985	0.862731	-0.182616	0.239642	0.947846	BSA	YES
13	0.136414	3.683982	1.275778	-0.392842	0.031974	0.657194	Amy	YES
14	0.028965	0.649875	0.997631	0.016238	0.054543	1.423162	PhosB	YES
15	-0.454561	0.231843	0.792837	-0.173653	0.291861	1.629482	BSA	YES
16	0.302952	1.629439	0.183849	0.006896	0.018905	1.239049	Lys	YES
17	0.150965	2.934324	1.351625	-0.593519	0.042638	0.563719	Amy	YES
18	0.017873	0.939473	1.202948	0.014322	0.032645	1.736251	PhosB	YES
19	0.184932	0.209837	0.197235	0.456526	0.153874	0.152663	Myo	YES
20	0.217752	0.146651	1.135246	-0.419791	0.257746	0.351247	Lip	NO
21	0.187493	2.965968	1.275778	-0.534757	0.057723	0.627548	Amy	YES
22	-0.503725	0.489471	0.629473	-0.122792	0.147662	0.793848	BSA	YES
23	0.009714	-0.059456	-0.048769	0.039845	-1.098469	0.118985	HSA	YES
24	0.293129	1.498453	0.307858	0.003982	0.013851	1.497034	Lys	YES
25	-0.013265	0.102732	0.936304	-1.498739	0.615528	0.317413	Lip	YES
26	0.023876	0.362539	0.918031	0.042857	0.298437	0.393148	CytC	YES
27	-0.002182	1.112349	0.039762	-0.015416	0.929874	0.577653	Fer	YES
28	-0.421627	0.497436	0.463785	-0.114537	0.182949	1.459478	BSA	YES
29	0.028768	0.470821	0.758837	0.007925	0.239754	0.621475	CytC	YES
30	0.199835	1.593782	0.153952	0.005039	0.007942	1.374757	Lys	YES
31	0.258763	0.175245	1.562535	-0.865528	0.638771	0.456171	Lip	YES
32	-0.453511	0.467336	0.518487	-0.172652	0.218672	0.635572	BSA	YES
33	0.128634	0.188264	1.329782	-0.562564	0.296625	0.498782	Lip	YES
34	-0.050942	-0.907456	-0.876578	0.079871	-1.548758	0.087461	HSA	YES
35	0.273827	1.358371	0.296496	0.014713	0.006183	1.320896	Lys	YES
36	-0.004126	1.076529	0.047659	-0.002942	0.987631	0.678657	Fer	YES
37	-0.504781	0.187457	0.638245	-0.115578	0.142746	1.538495	BSA	YES
38	-0.000318	0.981453	0.070842	-0.001639	0.887382	1.017295	Fer	NO
39	0.003155	0.936953	0.052171	-0.010561	0.176537	1.081474	Fer	YES
40	0.225627	3.383681	1.476634	-0.413654	0.042795	0.557614	Amy	YES
41	-0.000341	0.983735	0.042988	-0.018775	0.987663	0.654926	Fer	YES
42	-0.479739	0.180497	0.519372	-0.139839	0.169624	0.408965	BSA	YES
43	0.193275	0.502132	0.507256	0.377671	0.156627	1.275536	Myo	YES
44	-0.003987	0.749757	0.042145	-0.014287	0.538756	0.827541	Fer	NO
45	0.175627	0.168979	1.261547	-0.652531	0.342883	0.463789	Lip	NO
46	0.129301	2.893649	1.571664	-0.456148	0.055136	0.636467	Amy	YES
47	0.035294	0.479481	1.531231	-0.001693	0.112352	1.466216	PhosB	NO
48	0.223183	0.374849	0.372634	0.451267	0.142731	0.996628	Myo	YES
49	0.224348	0.394871	0.351719	0.376235	0.112835	1.618565	Myo	YES
50	0.179835	1.529733	0.164895	0.015324	0.008231	1.524564	Lys	YES
51	0.097657	-0.087756	-1.287873	0.048752	-1.246568	0.107367	HSA	YES
52	-0.414592	0.598458	0.628468	-0.198481	0.212453	0.683825	BSA	YES
53	0.013626	0.493882	0.721265	0.019386	0.247387	0.987563	CytC	YES
54	0.106479	-0.678467	-1.974631	0.057439	-0.74631	0.097364	HSA	YES
55	0.217583	1.712908	0.243952	0.009737	0.001754	1.684731	Lys	YES
56	0.259853	1.824312	0.168956	0.006139	0.021745	1.302892	Lys	YES
57	-0.431676	0.529435	0.618468	-0.151652	0.161652	1.605218	BSA	YES
58	0.011834	-0.087646	-1.098136	0.069973	-0.90853	0.084627	HSA	NO
59	0.115538	0.146251	1.987377	-0.252165	0.572532	0.476556	Lip	YES
60	0.118801	2.825617	1.514973	-0.615836	0.049129	0.582761	Amy	YES

5.5 References

1. a) Abdelhafiz, A. H.; Myint, M. P.; Tayek, J. A.; Wheeldon, N. M. *Clin. Thera.* **2009**, 21, 1534. b) Galic, G.; Tomic, M.; Galesic, K.; Kvesic, A.; Soljic, M.; Mozetic, V.; Loncar, Z.; Maricic, A.; Martinovic, Z. *Coll. Antropol.* **2009**, 33, 559. c) Zismam, D. A.; Kawut, S. M.; Lederer, D. J.; Belperio, J. A.; Lynch, J. P.; Schwarz, M. I.; Tayek, J. A.; Reuben, D. B.; Karlamangla, A. S. *Chest*. **2009**, 135, 929. d) Tricoli, J. V.; Schoenfeldt, M.; Conley, B. *Clin. Cancer Res.* **2004**, 10, 3943. e) Masson, J.-F.; Battaglia, T. M.; Khairallah, P.; Beaudoin, S.; Booksh, K. S. *Anal. Chem.* **2007**, 79, 612. f) Hogdall, E. V. S.; Christensen, L.; Kjaer, S. K.; Blaakaer, J.; Kjaerbye-Thygesen, A.; Gayther, S.; Jacobs, I. J.; Hogdall, C. K.; *Gynecol.Oncol.* **2007**, 104, 508. g) Couderc, R. *Ann. Biol. Clin.* **2000**, 58, 581. h) Pisitkun, T.; Johnstone, R.; Knepper, M. A.; *Mol. Cell. Proteomics* **2006**, *5*, 1760. i) Andreasson, U.; Portelius, E.; Andersson, M. E.; Blennow, K.; Zetterberg, H. *Biomarkers in Medicine* **2007**, 1, 59. j) Daniels, M. J.; Wang, Y.; Lee, M.-Y.; Venkitaraman, A. R. *Science* **2004**, 306, 876. k) Ross, J. S.; Fletcher, J. A. *Stem Cells* **1998**, 16, 413.

2. Kodadek, T. *Chem. Biol.* **2001**, 8, 105.

3. a) Soukka, T.; Paukkunen, J.; Harma, H.; Lonnberg, S.; Lindroos, H.; Lovgren, T. *Clin. Chem.* **2001**, 47, 1269. b) Acharya, G.; Chang, C.-L. Doorneweerd, D. D.; Vlashi, E.; Henne, W. A.; Hartmann, L. C.; Low, P. S.; Savran, C. A. *J. Am. Chem. Soc.* **2007**, 129, 15824. c) U. R. Muller, *Mol. Biosyst.* **2006**, 2, 470.

4. a) Engvall, E.; Perlmann, P. *J. Immunol.* **1972**, 109, 129. b) Schuurs, A. H. W. M.; Van Weemen, B. K. *J. Immunoassay* **1980**, 1, 229. c) B. B. Haab, *Curr. Opin. Biotechnol.* **2006**, 17, 415.

5. McPherson, R. A. & Pincus, M. R. Henry's Clinical Diagnosis and Management by Laboratory Methods Ch 19 (Saunders–Elsevier, **2007**).

6. a) Li, J. N.; Zhang, Z.; Rosenzweig, J.; Wang, Y. Y; Chan, D. W. *Clin. Chem.* **2002**, 48, 1296. b) Baggerly, K. A.; Morris, J. S.; Coombes, K. R. Bioinformatics **2004**, 20, 777.

7. a) Goodey, A.; Lavigne, J. J.; Savoy, S. M.; Rodriguez, M. D.; Curey, T.; Tsao, A.; Simmons, G.; Wright, J.; Yoo, S. J.; Sohn, Y.; Ansyln, E. V.; Shear, J. B.; Neikirk, D. P.; McDevitt, J. T. *J. Am. Chem. Soc*. **2001**, 123, 2559. b) Albert, K.J.; Lewis, N. S.; Schauer, C. L.; Sotzing, G. A.; Stitzel, S. E.; Vaid, T. P.; Walt, D. R. *Chem. Rev.* **2000**, 100, 2595.

8. a) Wiskur, S. L.; Floriano, P. N., Anslyn, E. V.; McDevitt, J. T. *Angew. Chem. Int. Ed*. **2003**, 42, 2070. b) Lavigne, J. J.; Savoy, S. M.; Clevenger, M. B.; Ritchie, J. E.; McDoniel, B.; Yoo, S. J.; Anslyn, E. V.; McDevitt, J. T.; Shear, J. B.; Neikirk, D. P. *J. Am. Chem. Soc*. **1998**, 120, 6429. c) Curey, T. E.; Goodey, A.; Tsao, A.; Lavigne, J. J.;

Sohn, Y.; McDevitt, J. T.; Anslyn, E. V.; Neikirk, D.; Shear, J. B. *Anal. Biochem*. **2001**, 293, 178. d) McCleskey, S. C.; Griffin, M. J.; Schneider, S. E.; McDevitt, J. T.; Anslyn, E. V. *J. Am. Chem. Soc*. **2003**, 125, 1114.

9. a) Folmer-Andersen, J. F.; Kitamura, M.; Ansly, E. V. *J. Am. Chem. Soc.* **2006**, 128, 5652. b) Buryak, A.; Severin, K. A. *J. Am. Chem. Soc.* **2005**, 127, 3700. c) Greene, N. T.; Shimizu, K. D. *J. Am. Chem. Soc.* **2005**, 127, 5695. d) Wright, A. T.; Anslyn, E. V. *Chem. Soc. Rev.* **2006**, 35, 14. e) Lee, J. W.; Lee, J.-S.; Chang, Y.-T. *Angew. Chem. Int. Ed.* **2006**, 45, 6485. f) Rakow, N. A. & Suslick, K. S. *Nature* **2000**, 406, 710.

10. a) Wright, A. T.; Edwards, N. Y.; Anslyn, E. V.; McDevitt, J. T. *Angew. Chem. Int. Ed.* **2007**, 46, 8212. b) Rakow, N. A.; Suslick, K. S. *Nature* **2000**, 406, 710. c) Lewis, N. S. *Acc. Chem. Res.* **2004**, 37, 663. d) Krantz-Rulcker, C.; Stenberg, M.; Winquist, F.; Lundstrom, I. *Anal. Chim. Acta* **2001**, 426, 217. e) Collins, B. E.; Wright, A. T.; Anslyn, E. V. *Top. Curr. Chem.* **2007**, *277*, 181. f) Buryak, A.; Pozdnoukhov, A.; Severin, K. *Chem. Commun.* **2007**, 2366. g) Phillips, R. L.; Miranda, O. R.; You, C.-C.; Rotello, V. M.; Bunz, U. F. H. *Angew. Chem. Int. Ed.* **2008**, 47, 259. h) Bajaj, A.; Miranda, O. R.; Kim, I-B.; Phillips, R. L.; Jerry, D. J.; Bunz, U. H. F.; Rotello, V. M.; *Proc. Natl. Acad. Sci. USA* **2009**, 106, 10912. i) Stephenson, C. J.; Shimizu, K. D. *Polym. Int.* 2007, 56, 482.

11. a) Baldini, L.; Wilson, A. J.; Hong, J.; Hamilton, A. D. *J. Am. Chem. Soc.* **2004**, 126, 5656. b) Zhou, H.; Baldini, L.; Hong, J.; Wilson, A. J.; Hamilton, A. D. *J. Am. Chem. Soc.* **2006**, 128, 2421.

12. c) Wright, A. T.; Griffin, M. J.; Zhong, Z. L.; McCleskey, S. C.; Anslyn, E. V.; McDevitt, J. T. *Ang. Chem. Int. Ed.* **2005**, 44, 6375.

13. a) Miranda, O. R.; You, C.-C.; Phillips, R.; Kim, I. B.; Ghosh, P. S.; Bunz, U. H. F.; Rotello, V. M. *J. Am. Chem. Soc.* **2007**, 129, 9856. b) Sandanaraj, B. S.; Demont, R.; Aathimanikandan, S. V.; Savariar, E. N.; Thayumanavan, S. *J. Am. Chem. Soc.* **2006**, *128*, 10686. c) Sandanaraj, S. B.; Demont, R.; Thayumanavan, S. *J. Am. Chem. Soc.* **2007**, 129, 3506.

14. De, M.; Rana, S.; Akpinar, H.; Miranda, O. R.; Arivizo, R.; Bunz, U. H. F.; Rotello, V. M. *Nat. Chem.* **2009**, 1, 461.

15. You, C.-C.; Miranda, O. R.; Gider, B.; Ghosh, P. S.; Kim, I. B.; Erdogan, B.; Krovi, S. A.; Bunz, U. H. F.; Rotello, V. M. *Nat. Nanotech.* **2007**, 2, 318.

16. Glijohann, D. A.; Mirkin, C. A. *Nature* **2009**, 462, 461.

17. a) De, M.; You, C.-C.; Srivastava, S.; Rotello, V. M. *J. Am. Chem. Soc.* **2007**, 129, 10147. b) Hong, R.; Fisher, N. O.; Verma, A.; Goodman, C. M.; Emrick, T.; Rotello, V. M. *J. Am. Chem. Soc.* **2004**, 126, 739. c) Jones, S.; Thornton, J. M. *Proc. Natl. Acad. Sci.*

USA, **1996**, 93, 13. d) Stites, E. W. *Chem. Rev.*, **1997**, 97, 1233. e) Conte, L. L.; Chothia, C.; Janin, J. *J. Mol. Biol.*, **1999**, 285, 2177. f) De, M.; Miranda, O. R.; Rana, S.; Rotello, V. M. *Chem. Commun.* **2009**, 16, 2157.

18. a) Jacobson, R. H.; Zhang, X. J.; Dubose, R. F.; Matthews, B. W. *Nature* **1994**, 369, 761. b) Craven, G. R.; Steers, E.; Anfinsen, C. B. *J. Biol. Chem.* **1965**, 240, 2468. c) Verma, A.; Simard, J. M.; Worrall, J. W. E.; Rotello, V. M. *J. Am. Chem. Soc.* **2004**, 126, 13987. d) Wallenfels, K.; Weil, R. *Enzymes, 3rd Ed.* **1972**, 7, 617.

19. a) Fowler, A. V.; Zabin, I. *J. Biol. Chem.* **1978**, *253*, 5521. b) Fowler, A. V.; Zabin, I. *J. Biol. Chem.* **1970**, *245*, 5032.

20. a) Hong, R.; Fischer, N. O.; Verma, A.; Goodman, C. M.; Emrick, T.; Rotello, V. M. *J. Am. Chem. Soc.* **2004**, 126, 739. b) Nikolic, M. S.; Krack, M.; Aleksandrovic, V.; Kornowski, A.; Förster, S.; Weller, H. *Angew. Chem*. **2006**, 118, 6727.

21. SYSTAT11.0 (SystatSoftware, Richmond, CA94804, USA, **2004**).

22. Adachi, J.; Kumar, C.; Zhang, Y.; Olsen, J. V.; Mann, M. *Genome Biol.* **2006**; 7: R80. b) Li, S.-J.; Peng, M.; Li, H.; Liu, B.-S.; Wang, C.; Wu, J.-R.; Li, Y.-X.; Zeng, R. *Nucl. Acids Res*. **2009**, 37, D907. c) Fliser, D.; Novak, J.; Thongboonkerd, V.; Argilés, A.; Jankowski, V.; Girolami, M. A.; Jankowski, J.; Mischa, H. *J. Am. Soc. Nephrol.,* **2007**, 18, 1057.

23. a) Magistroni, R.; Ligabue, G.; Lupo, V.; Furci, F.; Leonelli, M.; Manganelli, L.; Masellis, M.; Gatti, V.; Cavazzini, F.; Tizzanini, W.; Albertazzi, A. *Nephrol Dial Transplant,* **2009**, 24, 1672. b) Roden, A. C.; Lockington, K. S.; Trostrud, L. J.; Katzmann, J. A. *Am. J. Clin. Pathol*, **2008**, 130, 141. c) Nedelkolv, D.; Nelson, R. W. *Am. J. Kidney Dis.* **2001**, 38, 481. d) Bottini, P.; Almerinda, M.; Alves, R.; and Garlipp C. R. *Am. J. Kidney Dis.* **2002**, 39, E2.

CHAPTER 6

DETECTING PATHOGENS USING GOLD NANOPARTICLE-PPE BASED ARRAY SENSING

6.1 Introduction

Fast and efficient identification of pathogens in water and biological fluids is an important issue in medical, forensic and environmental sciences.[1] We demonstrate herein that non-covalent conjugates of gold nanoparticles[2] and a fluorescent polymer[3] identify bacteria effectively within minutes. Nanoparticle-bacteria interactions release the bound fluorescent polymer from the gold nanoparticle quencher, resulting in a "turn-on" of the polymer's fluorescence. The fluorescence responses generated by the bacterial surfaces provide an efficient means of their discrimination.[3b] We have differentiated 12 bacteria by this method. Both species of bacteria as well as strains of a single species were discerned, without the use of antibodies[3cd] or radioactive markers.[3e]

Conventional plating and culturing[4] is generally used to identify causative bacterial pathogens in clinical environments. While technologically advanced systems have been developed for specific microorganisms (Table 6.1),[5] these methods are complex or require sophisticated instrumentation. Plating and culturing is accurate, but requires >24 h.

Table 6.1 Common methods to detect bacteria.[5] Current technologies for bacterial sensing: 1) plating and culturing, biochemical tests, microscopy and luminescence, 2) immunological approaches, 3) nucleic acid probe-based methods (PCR, LCR), 4) mass spectrometry, 5) microarrays 6) biosensors. Despite sensitivity and selectivity, high cost of production, extended and complicated preparation and the often lengthy processing time by skilled operators are common disadvantages.

Method	Strength	Limitations
DNA-based methods (PCR, Nucleic acid probes, DNA microarrays, ligase chain reaction)	Fast and reliable if sequence or part of DNA sequence is known. In principle DNA from one bacterium can be identified and detected. Potentially very sensitive.	Needs specialized lab and equipment, bacteria have to be digested and DNA isolated. Expensive, sensitive to inhibitors, contamination and experimental conditions.
Immunoblotting and immunoassays	Specific and fast. Sensitivity in some cases for <100 bacteria/mL reported.	Needs specific antibody for the bacteria under consideration.
ELISA	Specific, quite sensitive and can be used not only for bacteria but as well for their toxins.	Needs antibody/enzyme system. *Direct detection:* Labeling of primary antibodies takes time and is expensive. *Indirect detection:* Cross reactivity with secondary antibody can cause non-specific signal. Additional incubation step necessary.
Immunomagnetic separations	Similar as for ELISA, allows isolation of bacteria from mixed media.	
Flow cytometry	Fast, gives number and size of bacteria determined. Sensitive. 100 cells/mL can be detected in 30 min.	Unless combined with immunological methods, type of bacteria cannot easily be determined.
Advanced microscopy combined with membrane filtration	Fast, gives results upon staining with acridine orange. Live cells fluoresce.	Gram negative bacteria are underestimated. Similar limitations as classical microscopy.
Biochemical and metabolic tests Commercial kits available	Can be made specific for some bacteria and records metabolic activity .	Relatively time consuming, not all bacteria are identified, other microorganisms can interfere.
Luminescent bacteria	Detects bacterial ATP.	Sample has to be uncontaminated by other ATP, differentiation difficult.
Mass spectrometry	Detect volatile organic compounds (VOC) from bacteria.	Can be very sensitive and quite specific but needs very sophisticated and expensive instrumentation.
Biosensing using nanoparticles using gold nanowires	Small amounts detectable can be put into microarray format.	Bacterial sensing has not yet been reported.
DNA Sensing with conjugated polymers	Fluorescence based method, high variability of structure, high sensitivity .	While powerful method has the same problems that all DNA based methods i.e. sample preparation etc.
Bacterial Sensing with conjugated polymers	Fluorescence based method, high variability of conjugated polymer structure, simplicity	Low sensitivity for bacteria, relatively low selectivity at the moment.
Electronic noses and tongues	VOC-type assay is relatively simple and arrayable.	Sensitivity unclear.
Amperometric and electrochemical detection	Can be very sensitive, claimed for 1 cell of E. coli/mL.	Electrode has to be prepared and selectivity may be difficult. Electrochemical setup necessary.
Acoustic wave biosensors	Uses antibody/cell interactions.	Same as immunoassays.
Surface plasmon resonance	Sensitive but uses antibody/cell interactions.	Same as immunoassays, expensive.
Fiber optic microsphere array	Uses very small amounts of DNA,.	Same as DNA sensors.

Point-of-care treatment decisions are therefore made *without* access to microbiological information, potentially leading to the prescription of a sub-optimal antibiotic. An example is the treatment of keflex- or methicillin-resistant *S. aureus* strains (MRSA) in community-acquired infections that require treatment with either sulfa drugs or vancomycin.[6] Reisner et al. have investigated >9000 cases of clinically reported bacterial infections[4] and found that 85-90% were due to only seven pathogens with *S. aureus* and *E. coli* being responsible for half of all infections. A simple and rapid test that could discern clinically prevalent pathogens would be of great value, increasing the

efficacy of therapy, and reducing the occurrence of drug-resistant bacteria arising from inefficient antibiotic prescription.

The detection of bacteria and pathogens plays a crucial role in food safety.[7] For example, *E. coli* O157:H7 is a world-wide cause of foodborne illness, responsible for more than 2000 hospitalizations and 60 deaths directly related to bacterial infection each year in the United States.[3d,8] Major outbreaks were associated with the contamination of unpasteurized juice, vegetables, water, etc.[9] However, testing food for contamination is difficult due to the complex and/or lengthy analysis protocols.

To address the issue of rapid identification of bacteria, we developed a protocol for bacterial sensing using an array of gold nanoparticle-conjugated polymer constructs.[10] This 'chemical nose' combines a series of analyte receptors to differentiate targets according to their unique response diagrams. An anionic conjugated polymer (Figure 6.1) is initially associated with cationic gold nanoparticles to afford fluorescence-quenched complexes. In the presence of bacteria, the negatively-charged bacterial surface[11] competitively interacts with the nanoparticles to release the semiconducting polymer, restoring fluorescence; 1.6 nm gold nanoparticles[12] seem to recognize patches of hydrophobic/functional surfaces on microorganisms and poly(L-lysine)-coated gold nanoparticles self-assemble with live bacteria through complementary electrostatic interactions.[13] The π-conjugated polymer used in this study provides both multivalency[20] and the molecular wire effect[13d] to facilitate efficient signal generation in the sensing process. As functional "patches" (*e.g.* the charged residues and hydrophobic "hot spots") are prevalent on cell and microbial exteriors,[13d] this strategy has potential applications in the identification of a wide variety of microorganisms.

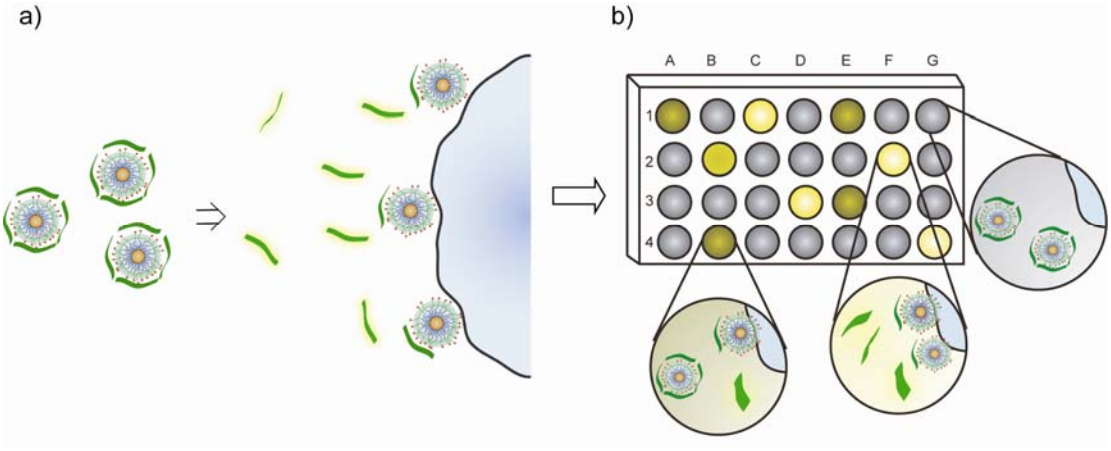

Figure 6.1 Design of the nanoparticle-conjugated polymer sensor array. a) Schematic representation of the displacement of anionic conjugated polymers from cationic nanoparticles by negatively charged bacterial surfaces. b) Schematic illustration of fluorescence pattern generation on a microplate.

6.2 Results and Discussion

For the fluorophore displacement strategy we chose **Sw-CO_2**[13d] and three hydrophobic ammonium-functionalized gold nanoparticles (**NP1**-**NP3**)[10b] as sensor elements (Figure 6.2). Fluorescence titration studies revealed that the cationic gold nanoparticles (**NP1**-**NP3**) quench the fluorescence of **Sw-CO_2** through formation of supramolecular complexes (Figure 6.3 and Table 6.2).[10a]

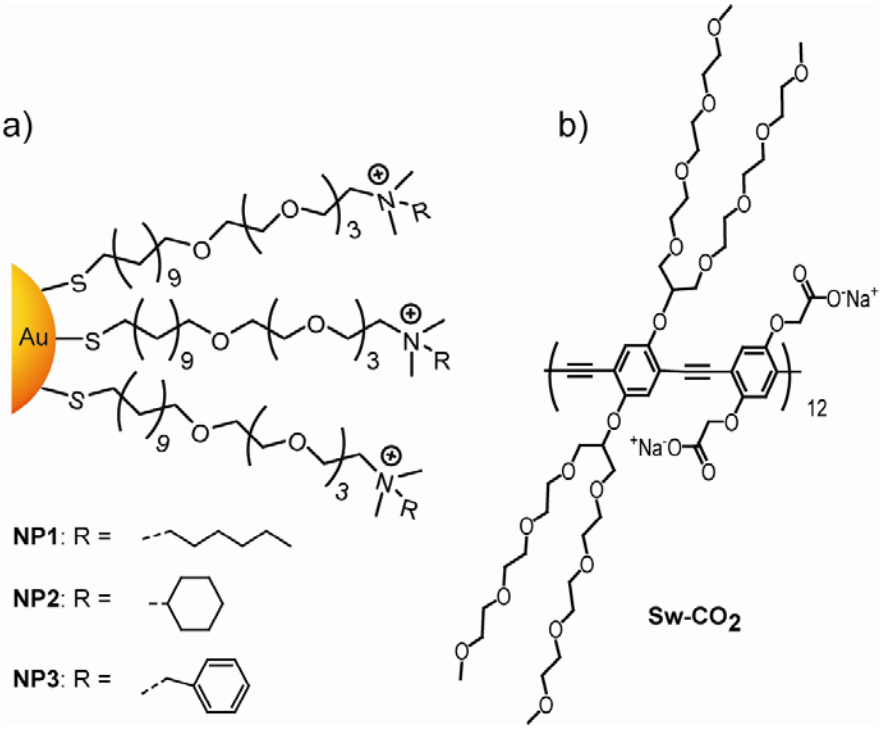

Figure 6.2. Receptor and transducer components of the bacterial sensors. a) structural representation of three cationic gold nanoparticles (**NP1-NP3**) with various hydrophobic tails. b) chemical structure of the conjugated polymer (**Sw-CO_2**) featuring a branched oligo(ethylene glycol) side chain to suppress non-specific polymer-microorganism interactions.

Quenching by the nanoparticle is efficient: typically, an aqueous solution of the polymer (100 nM, based on 12 repeat units/polymer) with a stoichiometric amount of nanoparticle displays approximately 20% of the initial fluorescence of **Sw-CO_2** (Φ = 0.33). The polymer and a stoichiometric amount of nanoparticles (**NP1-NP3**) were mixed in 5 mM phosphate buffer (pH 7.4) to yield nanoparticle-**Sw-CO_2** constructs with final polymer and nanoparticle concentrations of 100 nM and 10-40 nM, respectively.

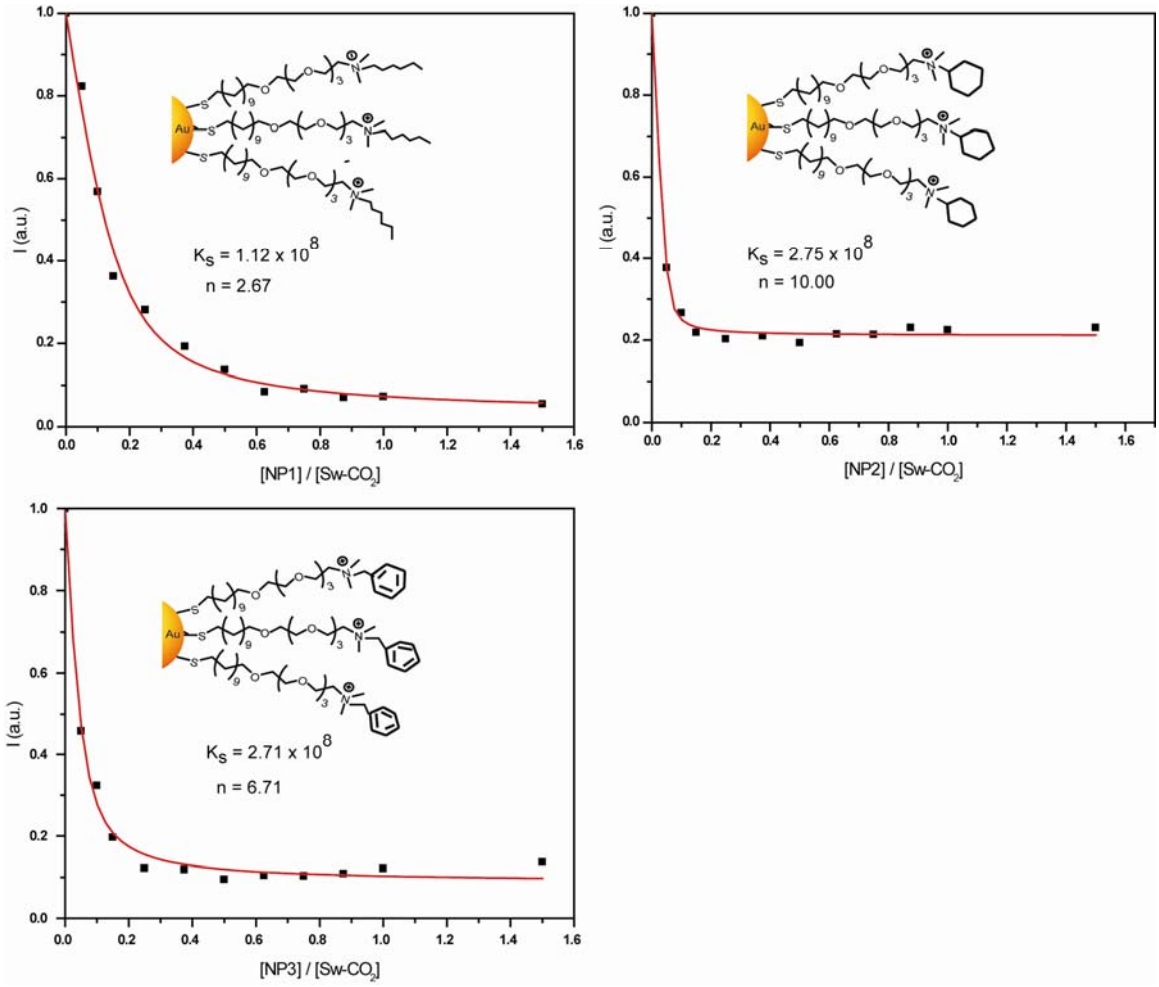

Figure 6.3 Fluorescence titration curves for the complexation of **Sw-CO_2** (100 nM) with cationic gold nanoparticles (**NP1-NP3**). The changes in fluorescence intensity at 463 nm were measured following the addition of cationic nanoparticles (0-150 nM) with an excitation wavelength of 400 nm. The solid lines represent the best curve-fitting using a calculation model of a single set of identical binding sites.

Table 6.2 Binding constants (K_S) and binding stoichiometries (n) between anionic polymer (**Sw-CO_2**) and three cationic nanoparticles (**NP1-NP3**) as determined from fluorescence titration.

Nanoparticle	K_S / 10^8 M^{-1}	$-\Delta G$ / kJ mol^{-1}	n
NP1	1.12	45.9	2.67
NP2	2.75	48.1	10.0
NP3	2.71	48.1	6.71

The exposure of these three nanoparticle-**Sw-CO_2** constructs towards bacteria (OD_{600} = 0.05) induced different levels of fluorescence changes (Figure 6.4). In most

cases, the fluorescence of the solution increases upon addition of the microorganisms. Significantly, the fluorescence changes exhibit reproducible patterns that depend upon the strains and classes of bacteria, indicating differentiation in the fluorophore displacement.

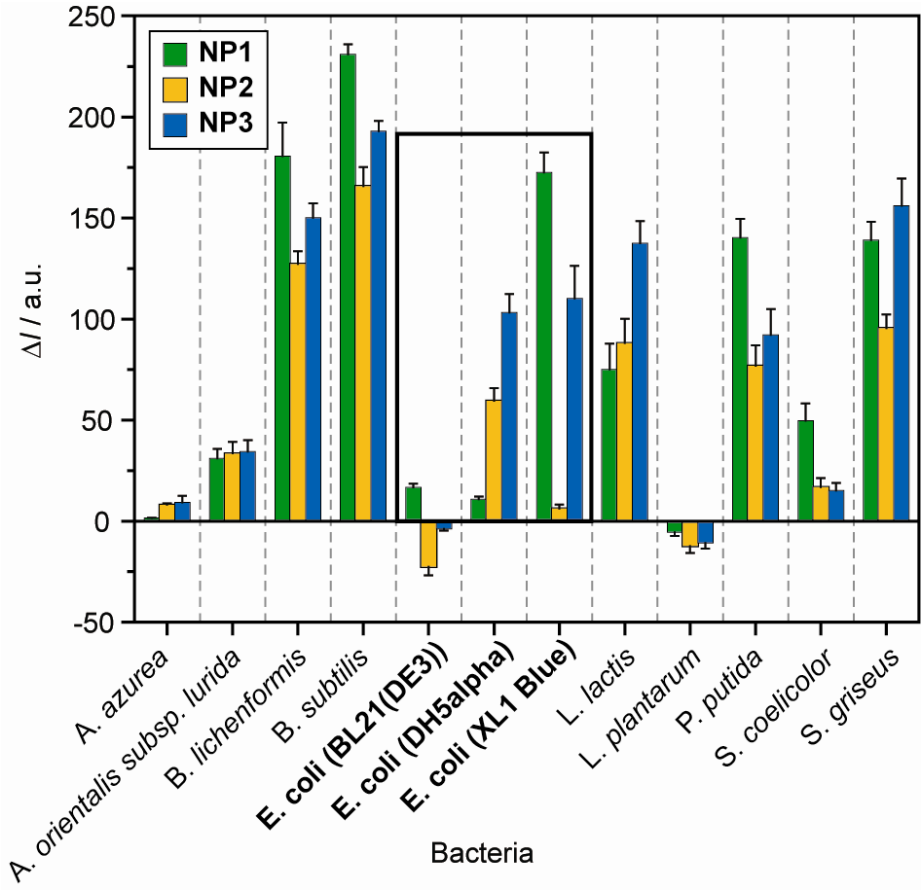

Figure 6.4 Fluorescence response patterns of nanoparticle-polymer constructs in the presence of various bacteria (OD_{600} = 0.05). Each value is an average of six parallel measurements and the error bars are shown.

The 12 different bacteria display excellent separation when the fluorescence changes were plotted in a three-dimensional graph with the fluorescence change of the

three nanoparticles (**NP1**-**NP3**) as the respective axes (Figure 6.5), explicitly demonstrating the ability of these particles to discriminate between bacteria.

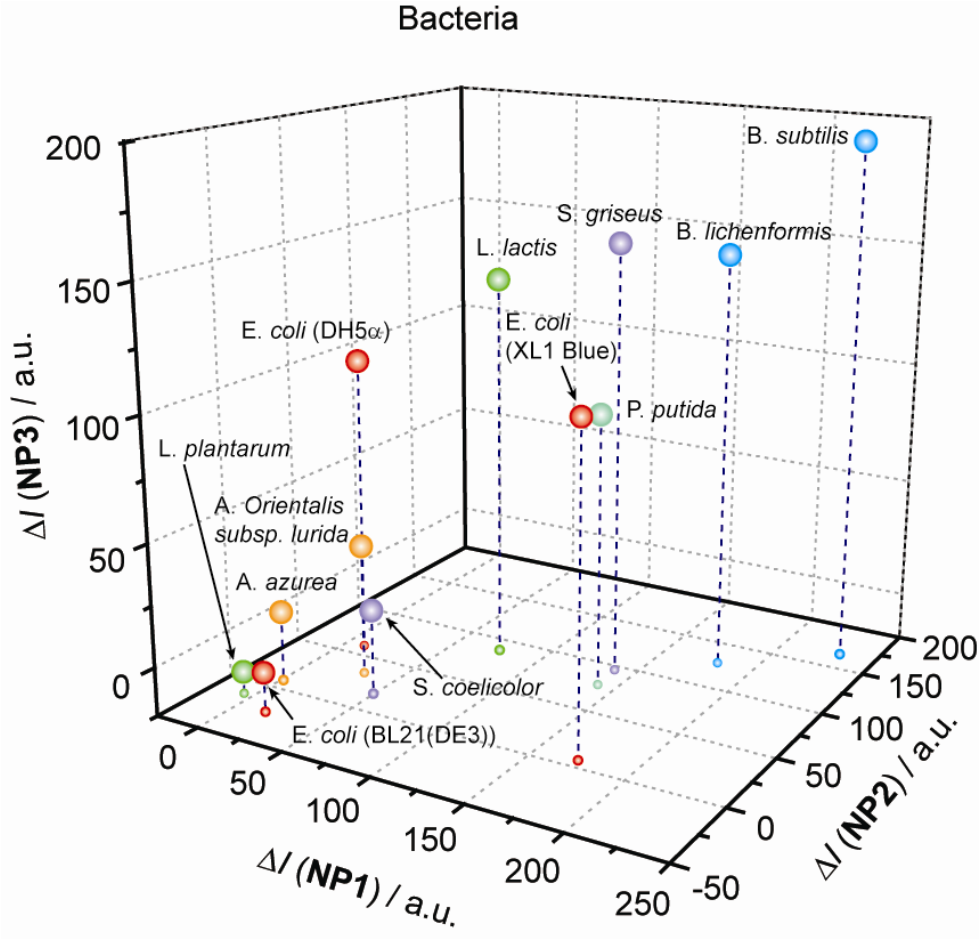

Figure 6.5 Fluorescence response patterns of nanoparticle-polymer constructs in the presence of various bacteria (OD_{600} = 0.05). Three-dimensional representation of the fluorescence intensity changes against the three nanoparticle-polymer constructs.

Initially both hydrophilic and hydrophobic nanoparticles were tested for the array. Upon incubation with bacteria, however, only the hydrophobic ones (**NP1**-**NP3**) produced significant fluorescence recovery. Since hydrophobic and hydrophilic nanoparticles exhibit comparable binding affinities to **Sw-CO_2**, the difference in the

fluorescence recovery indicates that the former strongly interact with bacteria. A plausible explanation is that the hydrophobic parts of the nanoparticles interact with hydrophobic regions on the surface of the bacteria (*e.g.* the alkyl chains in teichoic acid), enhancing the electrostatic nanoparticle-bacteria interaction and, thereby, the fluorescence regeneration. Both electrostatic and hydrophobic interactions seem to play important roles in the complexation of these particles with bacteria. We plan to engineer nanoparticles with varying size, shape and hydrophobicity to augment the diversity in the fluorescence response.

The fluorescence response patterns were analyzed through linear discriminant analysis (LDA), a quantitative statistical method extensively used in pattern recognition.[14] Discriminant functions were deduced by maximizing the separation between classes relative to the variation within classes; LDA (Figure 6.6) transformed the raw patterns to canonical scores which are clustered into 12 groups according to the individual bacteria.

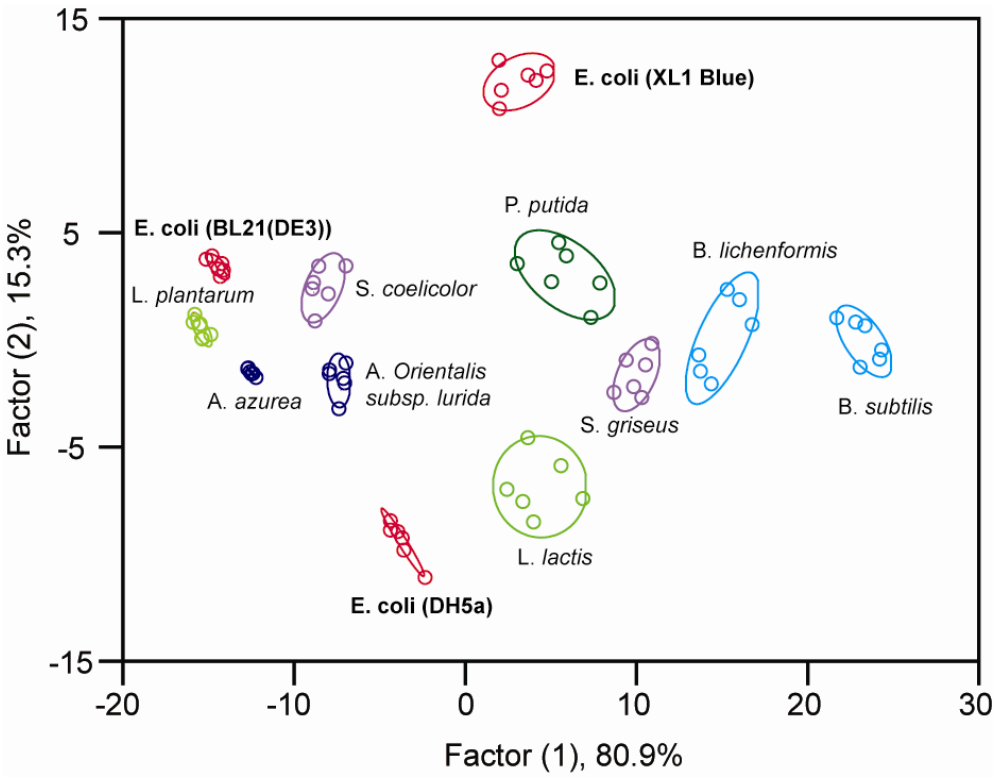

Figure 6.6 Canonical score plot for the fluorescence response patterns as determined with LDA. The first two factors consist of 96.2% variance and the 95% confidence ellipses for the individual bacteria are depicted.

The Jackknifed matrix (with cross-validation) in LDA reveals a 100% classification accuracy. We can discern all 12 microorganisms, which contain both Gram-positive (e.g. *A. azurea*, *B. subtilis*) and Gram-negative (e.g. *E. coli, P. putida*) species. The LDA plot does not place the Gram-negative bacteria into an identifiable part of the graph, suggesting that other effects are also involved in the discrimination process. Different strains of *E. coli* can be easily discerned with the current sensor array but the three *E. coli* strains are not grouped particularly close in the LDA plot, indicating that subtle differences in the bacteria generate marked changes in response. While the herein introduced concept is useful, it should be noted that the present system can merely differentiate bacteria in a clean buffered solution. Although, it is suitable to analyze

many biological samples (e.g. water), pre-separation is required for most biological fluids as the concomitant proteins may affect the analytical results. In this regard, the introduction of recognition elements specific for a bacterial surface on the nanoparticles would greatly address this problem.

With the patterns shown in Figure 6.4 as the training matrix (3 constructs × 12 bacteria × 6 replicates), we can identify unknown solutions of bacteria, randomly selected from the 12 bacterial species grown in different batches. Fluorescence response patterns generated from the three nanoparticle-polymer constructs were analyzed by LDA. After transformation of the patterns to the canonical scores using the discriminant functions established on the training samples, the Mahalanobis distances of the new case to the respective centroids of 12 groups were calculated. The closer a specific data set is to the center of one group, the more likely it belongs to that group. This assignment is based on the shortest Mahalanobis distance to the 12 bacteria in a three-dimensional space (canonical factors 1 to 3). For the 64 samples studied, 61 were correctly identified; a detection accuracy of >95% demonstrates expediency and reliability. The differentiation of the three strains of *E. coli* suggests suitable identification of pathogenic strains of normally harmless bacteria.

6.3 Conclusion

The integration of cationic gold nanoparticles with conjugated polymers provides an easily accessible yet potentially powerful biodiagnostic tool, in which the functional nanoparticles and the fluorescent polymer serve as the recognition elements and the transducer, respectively. The efficient quenching ability of gold nanoparticles coupled

with the 'molecular wire' effect of conjugated polymers compound the pronounced fluorescence response, which is dictated by the binding strength of the bacterium to the gold nanoparticle. Therefore, manipulating the surface chemistry of gold nanoparticles and the constitution of the conjugated polymer will result in constructs with expanded binding capabilities. By investigating the mechanism of binding which occurs between the hydrophobic nanoparticles and the conjugated polymer, we should be able to gain an understanding of the specific factors which govern fluorescence recovery. Based on our ability to readily differentiate 12 different bacteria using only three systems, we speculate that the detection of *any* microorganism including the differentiation of pathogenic and resistant strains will be possible with this approach.

6.4 Experimental Section

6.4.1 Instrumentation and Materials. The number average molecular weight (M_n = 25 kDa), polydispersity index (PDI = 1.8) and degree of polymerization (P_n = 12) of **Sw-CO_2** were determined by gel permeation chromatography. The cationic gold nanoparticles (**NP1**-**NP3**, $d \sim 2$ nm)[10b] were synthesized according to published procedures. The bacteria, including *Amycolatopsis azurea* (*A. azurea*), *Amycolatopsis orientalis subsp. lurida* (*A. orientalis subsp. lurida*), *Bacillus lichenformis* (*B. lichenformis*), *Bacillus subtilis* (*B. subtilis*), *Escherichia coli (BL21(DE3))* (E.*coli (BL21(DE3*)), *Escherichia coli (DH5α)* (*E.coli (DH5α)), Escherichia coli* (*XL1 Blue*) (*E.coli* (*XL1 Blue*)), *Lactococcus lactis* (*L. lactis*), *Lactococcus plantarum* (*L. plantarum*), *Pseudomonas putida* (*P. putida*), *Streptomyces coelicolor* (*S. coelicolor*), and *Streptomyces griseus* (*S. griseus*), were graciously donated by Dr. A. Bommarius

(Georgia Institute of Technology) and Dr. J. Hardy (University of Massachusetts Amherst). Fluorescence intensity changes at 463 nm were recorded in 96-well plates (300 μL Whatman® Glass Bottom microplate) on a Molecular Devices SpectraMax M5 micro plate reader with an excitation wavelength of 400 nm.

6.4.2 Bacterial Stock Preparation. Bacterial cells were grown in LB medium (3 mL) at 37 ºC to an optical density of 1.0 at 600 nm. The cultures were centrifuged (4000 rpm, 15 min) and washed with phosphate buffer (5 mM, pH 7.4) three times, resuspended in phosphate buffer and diluted to an absorbance of 1.0 at 600 nm.

6.4.3 Fluorescence Titrations. Fluorescence titration experiments determined the complexation between nanoparticles and **Sw-CO_2**. Fluorescence intensity changes at 463 nm were recorded with an excitation wavelength of 400 nm.

6.4.4 Fluorophore Displacement. Sw-CO_2 and stoichiometric amounts of **NP1**-**NP3**, as determined by the fluorescence titration study were diluted with phosphate buffer (5 mM, pH 7.4) to solutions with a final **Sw-CO_2** concentration of 100 nM. Each solution (200 μL) was placed into a well on the microplate. After incubation for 15 min, the fluorescence intensity at 463 nm was recorded with an excitation wavelength of 400 nm. Next, 10 μL of a bacterial solution (OD_{600} = 1.0) was added to each well. After incubation for another 15 min, the fluorescence intensity at 463 nm was measured again.

6.4.5 LDA Analysis. The fluorescence intensity before addition of the bacteria was subtracted from that obtained after addition of the bacteria to record the overall fluorescence response (ΔI). This process was completed for 12 bacteria to generate six replicates of each, leading to a training data matrix of 3 constructs × 12 bacteria × 6 replicates that was subjected to a classical linear discriminant analysis (LDA) using

SYSTAT (version 11.0). The Mahalanobis distances of each individual pattern to the centroid of each group in a multidimensional space were calculated and the case was assigned to the group with the shortest Mahalanobis distance. A similar procedure was also performed to identify 64 randomly selected bacterial samples based on their fluorescence response patterns. The classification of new cases was achieved by computing their shortest Mahalanobis distances to the groups generated through the training matrix (3 constructs (**NP1**-**NP3**) × 12 bacteria × 6 replicates). During the identification of unknown bacteria, the bacterial samples were randomly selected from the 12 respective bacteria and the solution preparation, data collection, and LDA analysis were each performed by different researchers, resulting in a double-blind process.

Table 6.S1 Training matrix of fluorescence response patterns generated from **NP**-(**Sw-CO_2**) sensor array (**NP1**-**NP3**) against various types of bacteria (OD = 0.05 at 600nm)

Bacteria	**NP1**	**NP2**	**NP3**
A. azurea	1.320	8.363	7.758
A. azurea	1.875	8.085	11.318
A. azurea	1.643	6.843	7.628
A. azurea	1.810	8.313	14.915
A. azurea	1.283	7.735	5.742
A. azurea	1.305	9.253	8.243
A. orientalis subsp. lurida	30.668	32.533	25.598
A. orientalis subsp. lurida	33.398	35.758	34.093
A. orientalis subsp. lurida	31.160	34.170	37.205
A. orientalis subsp. lurida	24.005	42.848	29.438
A. orientalis subsp. lurida	29.243	26.558	38.220
A. orientalis subsp. lurida	38.018	29.803	41.178
B. lichenformis	195.318	124.438	140.640
B. lichenformis	164.993	136.788	142.965
B. lichenformis	163.903	123.355	154.520
B. lichenformis	167.495	120.315	152.213
B. lichenformis	194.945	133.145	158.730
B. lichenformis	196.840	125.638	152.393
B. subtilis	235.218	174.260	196.053
B. subtilis	232.040	174.323	198.023
B. subtilis	235.505	164.763	190.720
B. subtilis	227.188	153.493	185.988
B. subtilis	222.990	172.223	189.518
B. subtilis	232.705	156.003	198.215
E. coli (BL21(DE3))	17.443	-26.578	-4.338
E. coli (BL21(DE3))	14.325	-28.983	-3.265

E. coli (BL21(DE3))	15.175	-18.655	-4.203
E. coli (BL21(DE3))	16.275	-21.973	-2.668
E. coli (BL21(DE3))	19.198	-20.328	-4.965
E. coli (BL21(DE3))	17.968	-19.300	-2.903
E. coli (DH5α)	9.335	61.068	105.800
E. coli (DH5α)	11.843	52.365	109.883
E. coli (DH5α)	12.013	60.328	100.815
E. coli (DH5α)	12.360	55.873	92.673
E. coli (DH5α)	9.893	57.170	94.078
E. coli (DH5α)	9.860	70.608	116.055
E. coli (XL1 Blue)	158.553	6.858	105.023
E. coli (XL1 Blue)	171.280	3.700	90.718
E. coli (XL1 Blue)	164.298	9.120	94.633
E. coli (XL1 Blue)	177.520	6.280	115.653
E. coli (XL1 Blue)	185.140	6.520	128.793
E. coli (XL1 Blue)	178.785	5.023	126.658
L. lactis	83.708	80.135	123.985
L. lactis	63.935	97.958	129.270
L. lactis	61.988	70.870	145.810
L. lactis	88.515	95.460	133.183
L. lactis	64.880	83.260	140.150
L. lactis	87.530	101.368	153.320
L. plantarum	-6.428	-15.945	-12.628
L. plantarum	-7.400	-10.255	-9.813
L. plantarum	-3.183	-8.055	-8.163
L. plantarum	-4.235	-11.848	-13.960
L. plantarum	-7.460	-11.235	-7.278
L. plantarum	-3.730	-16.715	-13.028
P. putida	133.883	77.358	84.243
P. putida	138.650	91.008	104.965
P. putida	126.060	62.608	77.063
P. putida	145.825	73.970	92.140
P. putida	146.658	71.735	84.733
P. putida	150.738	84.933	109.765
S. coelicolor	45.600	14.303	12.790
S. coelicolor	38.213	20.615	16.215
S. coelicolor	50.170	21.460	14.265
S. coelicolor	46.963	15.608	10.325
S. coelicolor	53.710	10.520	15.943
S. coelicolor	63.685	19.250	21.253
S. griseus	153.198	100.128	147.823
S. griseus	135.543	104.763	142.028
S. griseus	134.793	94.068	173.475
S. griseus	139.033	84.893	162.908
S. griseus	126.708	96.993	143.033
S. griseus	144.808	92.060	166.973

Table 6.S2 Accuracy of LDA classification of bacteria analytes (OD_{600} = 0.05) from the complexes of the fluorescent polymer (**Sw-CO_2**) with individual cationic nanoparticles as sensors. The values are taken from the Jackknifed classification matrix based on LDA analysis of the raw data (6 replicates) listed in Table 6.S1.

Bacteria	**NP1-(Sw-CO_2)**	**NP2-(Sw-CO_2)**	**NP3-(Sw-CO_2)**	**(NP1-NP3)-(Sw-CO_2)**
A. azurea	100	83	83	100
A. orientalis subsp. lurida	83	100	100	100
B. lichenformis	50	100	33	100
B. subtilis	100	100	100	100
E. coli (BL21(DE3))	100	100	100	100
E. coli (DH5α)	100	83	33	100
E. coli (XL1 Blue)	50	83	17	100
L. lactis	83	17	50	100
L. plantarum	100	100	83	100
P. putida	33	50	67	100
S. coelicolor	67	83	83	100
S. griseus	50	67	33	100
Total	76	81	65	100

Table 6.S3 Identification of 64 unknown bacterial samples with LDA using assemblies of **Sw-CO_2** and **NP1-NP3**. From the unknown bacterial samples, 61 out of 64 were correctly identified, resulting in an accuracy of 95.3%.

Entry	Fluorescence response pattern			LDA Identification	Correct Identification
	NP1	**NP2**	**NP3**	**Bacteria**	**Yes / NO**
1	142.533	75.388	92.108	*P. putida*	YES
2	182.858	127.943	149.733	*B. lichenformis*	YES
3	77.468	88.975	138.883	*L. lactis*	YES
4	30.539	33.934	34.990	*A. orientalis subsp. lurida*	YES
5	18.646	-23.160	-3.736	*E. coli (BL21(DE3))*	YES
6	11.639	57.813	101.611	*E.coli (DH5α)*	YES
7	49.205	16.395	15.680	*S. coelicolor*	YES
8	141.730	78.216	92.954	*P. putida*	YES
9	174.401	7.234	109.469	*E. coli (XL1 Blue)*	YES
10	31.039	32.559	33.740	*A. orientalis subsp. lurida*	YES
11	204.689	153.540	205.669	*B. subtilis*	NO
12	232.956	165.099	192.426	*B. subtilis*	YES
13	1.955	7.644	9.180	*A. azurea*	YES
14	137.791	95.444	157.609	*S. griseus*	YES
15	182.769	129.653	151.988	*B. lichenformis*	YES
16	-5.669	-12.276	-10.574	*L. plantarum*	YES
17	182.396	124.340	149.264	*B. lichenformis*	YES
18	17.094	-24.721	-4.388	*E. coli (BL21(DE3))*	YES
19	11.456	56.974	104.551	*E.coli (DH5α)*	YES
20	30.545	35.691	32.033	*A. orientalis subsp. lurida*	YES
21	174.821	6.005	113.186	*E. coli (XL1 Blue)*	YES
22	47.008	17.113	15.470	*S. coelicolor*	YES
23	232.094	165.985	191.679	*B. subtilis*	YES
24	1.936	9.194	9.234	*A. azurea*	YES

25	11.245	59.013	102.789	*E.coli (DH5α)*	YES
26	171.610	5.960	110.973	*E. coli (XL1 Blue)*	YES
27	32.531	32.886	33.358	*A. orientalis subsp. lurida*	YES
28	140.358	96.693	155.983	*S. griseus*	YES
29	204.960	155.854	174.626	*B. subtilis*	NO
30	13.996	-23.933	-3.560	*E. coli (BL21(DE3))*	YES
31	47.584	17.030	15.216	*S. coelicolor*	YES
32	-4.958	-13.494	-11.673	*L. plantarum*	YES
33	1.496	8.318	9.690	*A. azurea*	YES
34	-5.145	-11.691	-10.746	*L. plantarum*	YES
35	230.105	165.309	191.754	*B. subtilis*	YES
36	139.821	95.380	156.686	*S. griseus*	YES
37	142.581	75.099	92.426	*P. putida*	YES
38	175.360	6.960	113.460	*E. coli (XL1 Blue)*	YES
39	175.956	6.429	110.243	*E. coli (XL1 Blue)*	YES
40	177.206	131.679	153.993	*B. lichenformis*	YES
41	1.730	8.059	9.379	*A. azurea*	YES
42	143.094	77.610	91.804	*P. putida*	YES
43	176.345	7.005	109.099	*E. coli (XL1 Blue)*	YES
44	231.541	165.444	193.734	*B. subtilis*	YES
45	138.209	94.530	155.216	*S. griseus*	YES
46	179.203	126.666	151.850	*B. lichenformis*	YES
47	-5.656	-11.515	-11.946	*L. plantarum*	YES
48	48.960	17.104	17.126	*S. coelicolor*	YES
49	50.358	16.068	15.233	*S. coelicolor*	YES
50	-4.895	-12.941	-10.746	*L. plantarum*	YES
51	15.855	-23.191	-3.371	*E. coli (BL21(DE3))*	YES
52	48.326	16.870	15.005	*S. coelicolor*	YES
53	10.729	61.713	104.940	*E.coli (DH5a)*	YES
54	15.985	-23.040	-3.790	*E. coli (BL21(DE3))*	YES
55	51.345	17.133	14.724	*S. coelicolor*	YES
56	232.371	166.068	192.690	*B. subtilis*	YES
57	17.031	-24.114	-4.018	*E. coli (BL21(DE3))*	YES
58	11.475	60.711	102.038	*E.coli (DH5α)*	YES
59	1.716	8.224	8.881	*A. azurea*	YES
60	174.838	6.734	115.711	*E. coli (XL1 Blue)*	YES
61	1.920	9.241	7.370	*A. azurea*	NO
62	139.838	95.484	159.461	*S. griseus*	YES
63	17.225	-24.289	-2.963	*E. coli (BL21(DE3))*	YES
64	11.541	60.444	102.609	*E.coli (DH5α)*	YES

6.5 References

1. a) Deisingh, A.vK.; Thompson, M. *Analyst* **2002**, 127, 567. b) Berry, V.; Gole, A.; Kundu, S.; Murphy, C.vJ.; Saraf, R.F. *J. Am. Chem. Soc*. **2005**, 127, 17600.

2. Daniel, M. C.; Astruc, D. *Chem. Rev.* **2004**, 104, 293.

3. a)Thomas, S. W.; Joly, G. D.; Swager, T. M. *Chem. Rev*. **2007**, 107, 1339. b) Rosi, N. L.; Mirkin, C. A. *Chem. Rev*. **2005**, 105, 1547. c) Zhao, X.; Hilliard, L. R.; Mechery, S. J.; Wang, Y.; Bagwe, R. P.; Jin, S.; Tan, W. *Proc. Natl. Acad. Sci. U.S.A*. **2004**, 101, 15027. d) Bertozzi, C. R.; Bednarski, M. D *J. Am. Chem. Soc*. **1992**, 114, 2242. e) Amann, R. I.; Ludwig, W.; Schleifer, K. H. *Microbiol. Rev*. **1995**, 59, 143.

4. Reisner, B. S.; Woods, G. L. Reisner, B. S.; Woods, G. L. *J. Clin. Microbiol*. **1999**, 37, 2024.

5. Phillips, R. L., Miranda, O. R., You, C. C., Rotello, V. M.; Bunz, U. H. F. *Angew. Chem. Int. Ed.* **2008**, **47**, 2590.

6. Edmond, M. B.; Wallace, S. E.; McClish, D. K.; Pfaller, M. A.; Jones, R. N.; Wenzel, R. P. *Clin. Infect. Dis*. **1999**, 29, 239.

7. Batt, C. A. *Science* **2007**, 316, 1579.

8 Frenzen, P. D.; Drake, A.; Angulo, F. J. *J. Food Prot*. **2005**, 68, 2623.

9. Mead, P. S.; Slutsker, L.; Dietz, V.; McCaig, L. F.; Bresee, J.S.; Shapiro, C.; Griffin, P. M.; Tauxe, R. V. *Emerg. Infect. Dis*. **1999**, 5, 607.

10. a) Fan, C.; Plaxco, K. W.; Heeger, A. J *J. Am. Chem. Soc*. **2002**, 124, 5642. b) You, C. C.; Miranda, O. R.; Gider, B.; Ghosh, P. S.; Kim, I. B.; Erdogan, B.; Krovi, S. A.; Bunz, U. H. F.; Rotello, V. M. *Nat. Nanotechnol*. **2007**, 2, 318.

11. a)Teichoic acids and lipoteichoic acids are present on the surface of Gram- positive bacteria, while the outer membranes of Gram-negative bacteria are composed of lipopolysaccharides (LPSs). Furthermore, the membranes of most bacteria contain a large amount of anionic phospholipids (e.g. phosphatidylgylcerol), making the bacterial surface negatively charged; b) M. Kates in Handbook of Lipid Reseach: Glycolipids, Phosphoglycolipids and Sulfoglycopids, ed. M. Kates, Plenum Publishing Corporation, Springer; 1st edition, **1990**, pp. 123-234; c) Dmitriev, B.; Toukach, F.; Ehlers, S. *TRENDS in Microbiology*, **2005**, 13, 569; d) Koch, A. L. *Clinical Microbiology Reviews*, **2003**, 16, 673; e) Schaffer, C.; Messner, P. *Microbiology*, **2005**, 151, 643; f) Bos, M. P.; Tefsen, B.; Geurtsen, J.; Tommassen, J. *Proc. Natl. Acad. Sci. USA* **2004**, 101, 9417.

12. Dynamic light scattering (DLS) investigation revealed that the gold nanoparticles used in this study have a hydrodynamic diameter of 8~9 nm.

13. Niemeyer, C. M. *Angew. Chem*. **2001**, 113, 4254; *Angew. Chem. Int. Ed*. **2001**, 40, 4128. b) Kim, I. B.; Erdogan, B.; Wilson, J. N.; Bunz, U. H. F. *Chem. Eur. J*. **2004**, 10, 6247. c) Zhou, Q.; Swager, T. M. *J. Am. Chem. Soc*. **1995**, 117, 12593. d) Kim, I. B.; Phillips, R.; Bunz, U. H. F. *Macromolecules* **2007**, 40, 5290.

CHAPTER 7

COLORIMETRIC BACTERIA SENSING USING A HYBRID ENZYMATIC NANOCOMPOSITE BIOSENSOR

7.1 Introduction

Pathogenic bacteria cause 300 million cases of severe illness and many varieties of infections (e.g. cholera, syphilis, leprosy, meningitis, and pneumonia)[1] and are estimated to kill over 2 million children every year.[2] The great majority of these deaths occur in emerging nations where bacteria are present in drinking water and food.[3] Several techniques[4,5] are available in laboratories for pathogenic bacteria detection and identification, including i) plating and culturing, [6,7,8,9,10,11,12] ii) luminescence,[13] iii) immunological approaches,[7,8] iv) nucleic acid probe-based methods [9] (PCR, LCR), v) mass spectrometry,[10] vi) microarrays,[11] and vii) biosensors.[12] Despite the sensitivity and selectivity of these systems, their applications are restricted because 1) high cost of production, 2) extended and complicated preparation, 3) often lengthy processing time by skilled operators, and 4) their limited use as in-situ analysis tool. Therefore, the need to develop fast, sensitive and reliable detection methods for sensing bacteria in the field is crucial in order to safeguard public health. Recent advances in nanotechnology have enabled the development of new diagnostic platforms aimed at more sensitive and faster pathogen detection. For example, Ji *et.al*.[14] used positively charged amine-terminated polyamidoamine dendrimers on a silica surface to capture bacteria in a flow system. In this sensor, the membrane-reactive fluorophore, FAST DiA, functions as the reporter

fluorophore to transduce signals for detection and quantification of bacteria. The sensor surface was then imaged using a charge-coupled detector, reporting a detection limit of 1 x 10^4 cells/mL.[15] Gold nanoparticles (**AuNP**s) have been used to detect bacteria,[16] virus,[17] cancer cells,[18] and proteins.[19] In 2005, Murphy *et al*.[20] showed that CTAB (cetyltrimethylammonium bromide)-functionalized gold nanorods or nanospheres can conformally deposit to form monolayer on *Bacillus cereus* by strong electrostatic interaction. More recently, our group[16a] has demonstrated how this electrostatic assembly can be used for bacteria sensing through a nanoparticle-fluorescent polymer conjugate system. We were able to differentiate between 12 bacteria streams, which contain both Gram-positive (e.g. *A. azurea*, *B. subtilis*) and Gram-negative (e.g. *E. coli*, *P. putida*) species. Of particular importance was the ability to distinguish between differing *strains* of the same bacteria i.e BL21(DE3), DH5α, and XL1 Blue strains of *E. coli* at 2x10^5 cells/mL. While this nanoparticle-fluorescent polymer method was quite effective for bacterial sensing, it had three key limitations for implementation in our desired goal of point-of-use drinking water analysis. First, the limits of detection (LOD) of the fluorophore displacement assay were 10^5 bacteria/mL, far higher than is required for application in either environmental testing (≤10^2 cells/mL)[3,4a,5,15,21] or clinical applications, e.g. bacterial sepsis (<10^2cells/mL).[15,22] Secondly the method was fluorometric, dependant upon instrumentation to read-out the sensor response. Finally, sensing was done in solution, requiring handling steps that would make the method cumbersome for in-field applications. Therefore, we have designed and developed a fast and easy hybrid colorimetric enzymatic nanocomposite biosensor based on signal amplification schemes that provides high sensitivity for the detection and for the

recognition of pathogens in aqueous solutions. To test the robustness of our system, this approach is also translated to a test strip platform.

The concept of enzyme amplified colorimetric sensing provides a platform with enhanced sensitivity. Our colorimetric sensor design features three main components: a) an enzyme to provide signal amplification (*β*-Galactosidase, a tetramer 465 KDa (*β*-Gal, 17×13.5×9.0 nm) with a pI value of 4.6, Figure 7.1b),[23] b) a colorgenic substrate to provide color tuning i.e. chlorophenol-red-*β*-D-galactopyranside (CPRG), and c) a receptor to provide affinity binding with biomolecules (metal core gold nanoparticles ~2 nm of diameter). Functionalized cationic **AuNP**s electrostatically bind to the anionic enzyme *β*-Galactosidase, inhibiting the enzyme without denaturation (Figure 7.1a and Figure 7.S6 for more details). Displacement of the particle by bacteria restores *β*-Gal activity towards the colorimetric substrate (CPRG) added to the system, generating a read-out signal that is amplified through enzymatic catalysis. We hypothesized that in this activity-turn-off system, the binding equilibrium between enzyme and Au**NP**s would be affected in the presence of bacteria, resulting from the competitive binding between enzyme/**AuNP**s complexes and bacteria. Released β-Gal from the complexes recovers its activity in the enzymatic reaction with CPRG, converting the binding event into a "turn on" fashion. During this process, the initial yellow color of the substrate is converted into a red color product, giving the colorimetric effect (Figure 7.1a). Since our sensor is based on enzymatic colorimetric catalysis rather than indicator displacement assay (IDA)[24] or analyte exchange our design should provide a fast, easy and sensitive biosensor able to detect bacteria a very low concentration. Our colorimetric sensor strategy provides two key advantages for on-site sensing: a) the use of enzyme-substrate as transduction

elements will amplify the response of the sensor, providing much greater sensitivity relative to simple colorimetric methods and b) appropriate choice of substrate will enable the colorimetric assay to provide direct visual output and eliminate the need for instrumentation. We do not discard the possibility that the size of our biosensors, which has smaller dimensions than a bacteria cell, could also contribute and make it possible to detect small quantities of bacteria in relatively large samples.[23,25]

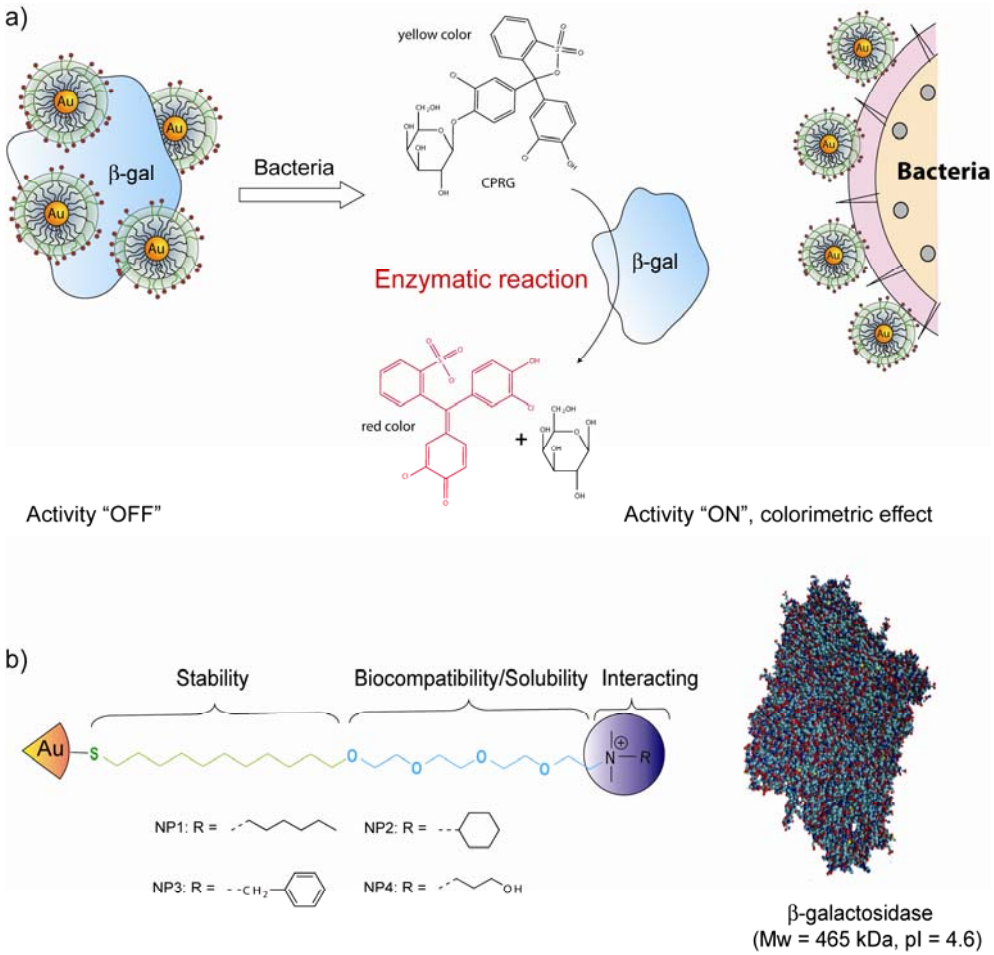

Figure 7.1 a) Design of enzyme-based sensing of bacteria: binding of nanoparticles to the bacteria surface activates the enzyme, generating a colorimetric response, b) Molecular structure of ligands attached to a 2 nm core nanoparticles and enzyme structure used in this study.

7.2 Results and Discussion

Most bacterial cell walls are negatively charged due to teichoic acids and lipopolysaccharides.[26] The negative surface charge enables bacteria to bind with positively-charged materials, which subsequently provides a potential platform for bacteria sensors. As a starting point, we conducted an activity assay of β-Gal-catalyzed hydrolysis of a colorimetric substrate at various concentrations of nanoparticles, showing a relative decrease in activity or no activity (color change) while mixed at appropriated stoichiometries (Figure. 7.2). Typically, a concentrations of 0.5 nM of β-Gal in phosphate buffer solution (5 mM, pH = 7.4) was incubated with various concentration of **NP1**-**NP4** for 15 minutes and 1.5 mM of the chromogenic substrate (CPRG, λ_{max} = 595 nm) was added to NP-enzyme complexes (Figure 7.2 and Figure 7.S6). The normalized first-order rate of chromogenic substrate hydrolysis was plotted versus the molar ratio of nanoparticles to β-Gal, and showed a tendency to decrease upon addition of nanoparticles, as shown for **NP2** in Figure 7.2. To optimize the sensor response in solution, various ligand shells composed of different functional head groups where used for the designing of the cationic particles to optimize the supramolecular interactions i.e. hydrophobic interactions, π-π interactions and hydrogen bonding.[19c] These intrinsic physical properties can vary the affinity of **NP**s to both the enzyme and bacteria, giving various responses and limits of detection (LODs). After preliminary activity studies, **NP2** was chosen as our best enzyme inhibitor from the four cationic nanoparticles used in this experiment (Figure 7.2 and Figure 7.S6), inhibiting the β-Gal activity at very low concentration.[19] **NP2** was also employed to give the lowest LOD among the **NP**s used on the bacteria detection (See Figure 7.S7). To verify this furthermore, inhibition of β-Gal

by **NP2** was carried out and monitored by spectroscopy since the product, chlorophenol red, has maximal absorbance wavelength at 595 nm. As a control, the enzyme inhibition was also studied with neutral tetraethylene glycol (**NP_{TEG}**) and carboxylate (**NP_{CO2}**) functionalized nanoparticles. In addition, α-Galactosidase (α-Gal) was also used as a control to demonstrate that CPRG is specific only for β-Gal. As seen in Figures 7.S8, only cationic particles i.e. **NP2** nanocomposite sensor gave inhibition signals while neutral and negative particles, **NP_{TEG}** and **NP_{CO2}**, failed to inhibit enzyme initially due to lack of electrostatic interactions. As a consequence they are not able to block the active sites of the enzyme (Figure (s). 7.S6, 7.S7, and 7.S8). When α-Gal was used with CPRG no activity was observed, confirming that the enzymatic colorimetric reaction is due to the specificity of CPRG to β-Gal. This result clearly indicates that activity of β-Gal is inhibited by nanoparticle binding. We observed that the inhibition depends on subtle structural changes of peripheral ligands on the **AuNP**s e.g. the linear end group (**NP1**) exhibited less suppression in activity than branched isomeric structure (**NP2**), See SI.

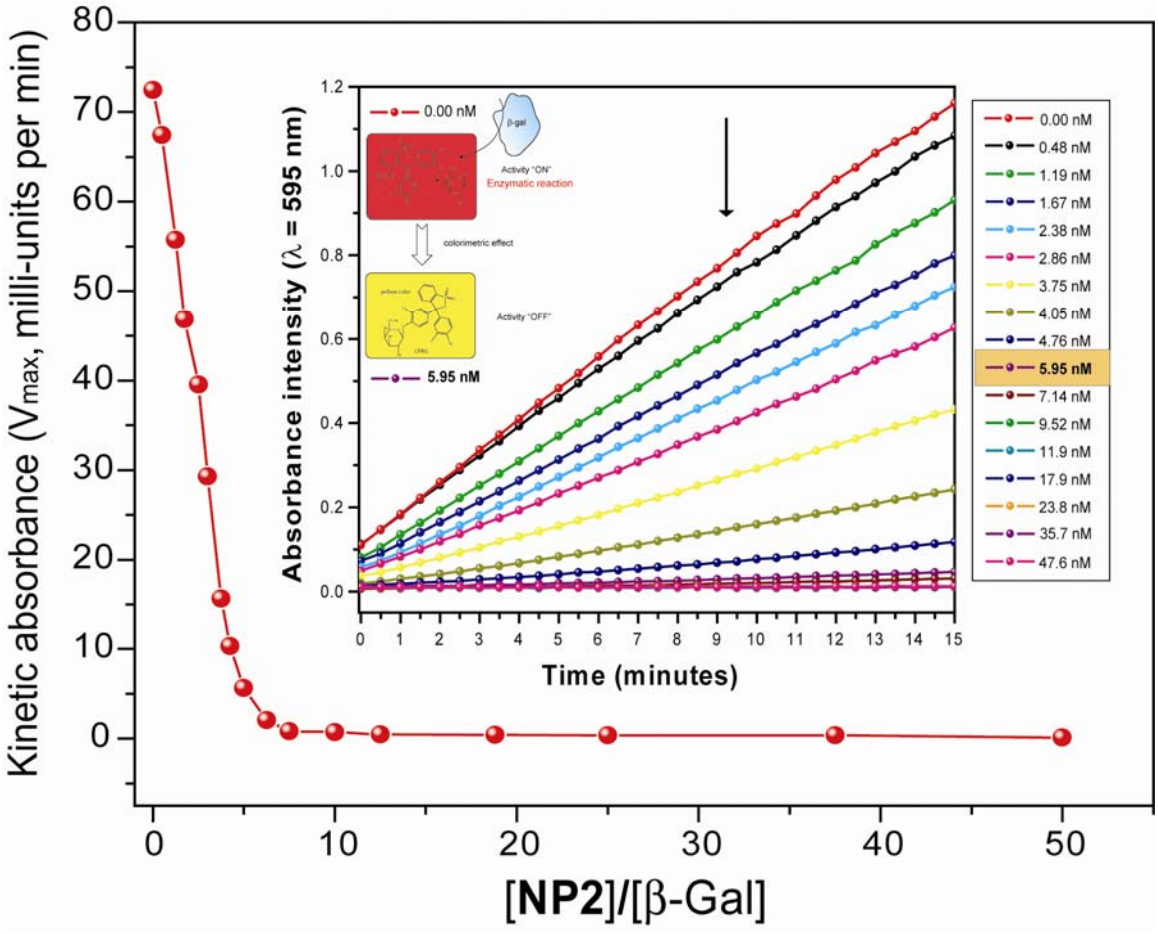

Figure 7.2 Inhibited activity assay of β-Gal (0.5 nM) against 1.5 mM substrate CPRG upon addition of cationic **NP2** in 5 mM phosphate buffer. The inset shows the kinetics of the absorption spectra before and after addition of **NP2.** The arrow in the inset indicates the direction of activity (0 nM indicates free enzyme and 5.95 nM indicates inhibited enzyme with **NP**s).

As we addressed before, most bacterial cell walls are negatively charged due to teichoic acids and lipopolysaccharides.[26] The negative surface charge enables bacteria to bind with positively-charged materials, which subsequently provides a potential platform for bacteria sensors. To address the objective of our study the negatively charged bacteria *E. coli XL1* was chosen.[32] Chromogenic substrate hydrolysis for the β-Gal/**AuNP** conjugates against individual bacteria in buffer is summarized in Figure 7.3. The individual target bacteria, *E. coli XL1*, generated distinguishable and highly reproducible rates for the colorimetric effect, indicating the potential for the differentiation of bacteria

in terms of concentration (three replicates were carried out for each sample, and each sample was also replicated three times). The color changes were analyzed following the scheme depicted in Figure 7.3. Figure 7.3 presents the changes in kinetic absorbance of β-Gal/**NP2** complex upon incubation with bacteria of different concentrations. Each concentration can be discerned not only by intensity curves and V_{max} histogram but also by a well developed trend of color changes; V_{max} is measured in units of CPRG quantity transformed per unit time related to 0.5 nM of β-Gal, see Figure 7.3a. The β-Gal/**NP2** complex was used here as a control experiment. Images were taken immediately after reading by an LCD camera to demonstrate this colorimetric effect, as well as by a fluorescence microscope to clarify a general idea of the bacteria density in solutions (Figure 7.3b).

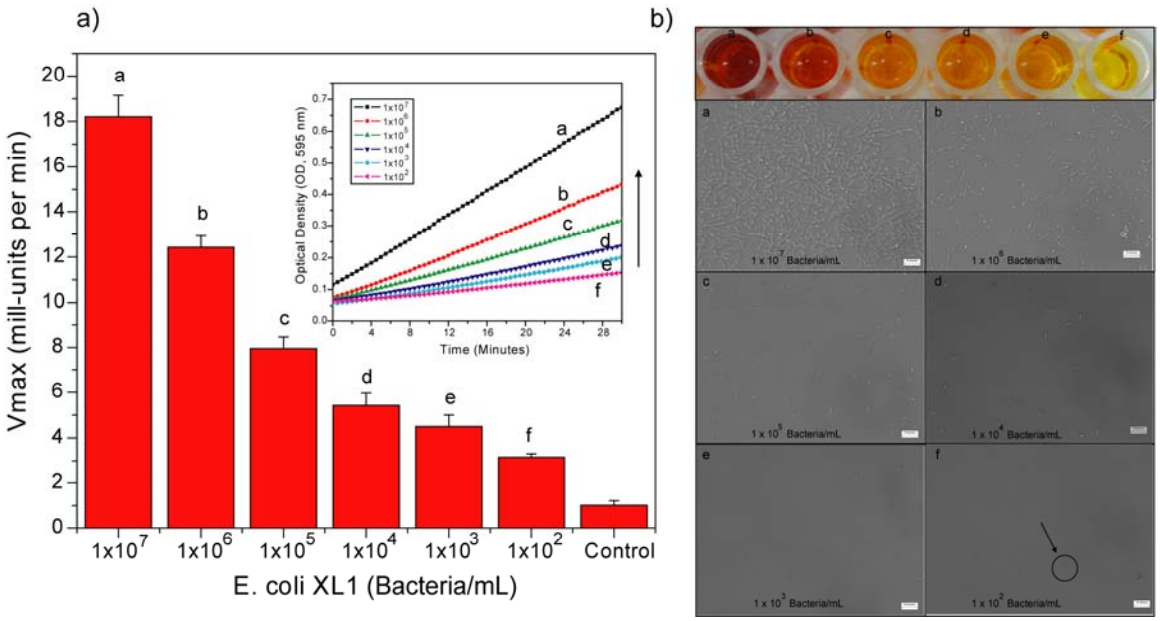

Figure 7.3 Limit of detection of *E. coli* using β-Gal/**NP2** nanocomposite. a) kinetic absorbance response upon addition of different bacteria concentrations, as control β-Gal/**NP2** nanocomposite was used without bacteria. b) microplate wells showing the color change upon variation of bacteria concentrations. Phase contrast bright-field of the *E. coli XL1* at different concentrations using fluorescence microscope at a magnification of 40X/0.55, ∞/1/FN22, using an Olympus inverted microscope at 400 nm wavelength. Note that the naked eye is extremely sensitive, able to detect concentration levels as low as $1x10^2$ bacteria/mL. Scale bar is 10 μm.

Upto this point, we have demonstrated that through appropriate choice of cationic gold nanoparticles we are able to completely inhibit β-Gal activity through binding of the particles to the enzyme surface, and that afterward addition of bacteria restored enzyme activity, generating a colorimetric response. The high sensitivity of our β-Gal/**AuNP** sensor can be attributed to signal self-amplification through the enzymatic reaction.

As the colorimetric sensing system was optimized in aqueous solution with extremely low LOD of bacteria (1×10^2 cells/mL), we investigated the application of our design to paper strips. As far as we know few colorimetric methods have been reported.[27] These can be semiquantitatively evaluated by visual read-out of the originated color in comparison to a reference color scale.[28] A key issue is the response time. Rapid bacterial penetration occurs on highly porous papers while restriction of particle/enzyme conjugates to the surface takes place on less porous materials. Considering these issues, we explored a wide range of materials available to maintain the enzyme activity and the efficiency of enzyme inhibition and activity recovery process. GF/B binder-free microfiber filter (Whatman, cat. No. 1821021) was selected as the preliminary platform due to its high wet strength, high loading capacity and mainly binding-free property. Initial composition of our strip sensor was set up with 25 mM CPRG and 15 nM β-Gal, in a way to make the reaction take place at an appropriate speed at which the color converted from yellow to dark red within 10 minutes. Then inhibition studies, similar to the solution studies, were carried out to choose the stoichiometric amount of cationic particles (i.e. **NP2**) and β-Gal to form the hybrid enzymatic nanocomposite sensor [(β-Gal/**NP2**) complex]. $\mathbf{NP_{TEG}}$ and $\mathbf{NP_{CO2}}$ were also used, as control experiment and no inhibition was observed as expected (See Figure 7.4). β-Gal/**NP2** complex was ultimately

induced by mixing β-Gal (15 nM) and **NP2** (80 nM) and incubated for 15 minutes. To test the performance of our system on a paper strip, 3 μL of CPRG (25 mM), complex solution and diverse solutions from 1×10^8 to 1×10^4 bacteria/mL of *E. coli XL1* were spiked onto GF/B filter paper at pH 7.4. Results were taken 10 minutes later by an LCD digital camera and appropriate light sources were placed at fixed positions above the strip sensors.

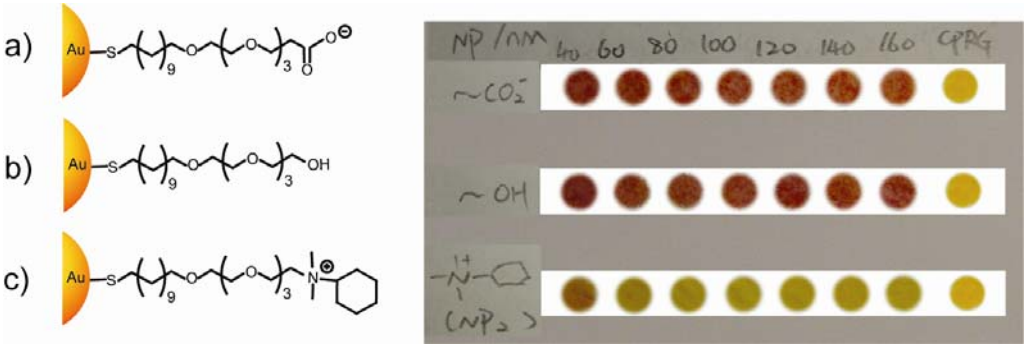

Figure 7.4 Enzymatic inhibition-colorimetric assay of β-Gal (15 nM) against 25 mM substrate CPRG upon addition of cationic, anionic and neutral nanoparticles. (a) carboxylate (**NP$_{CO2}$**), (b) hydroxyl (**NP$_{TEG}$**), and quaternary amine (**NP2**) functionalized gold on a platform testing. Inset shows total inhibition for the positive nanoparticle **NP2** at 80 nM, while no inhibition was observed for both the anionic and neutral AuNPs even at 160 nM.

The color changes on the strip platform were analyzed following the scheme depicted in Figure 7.5. The use of color imagery for sensing application has been previously reported.[28] The RGB (red, green and blue) digital image features gradual changes in color of each spot correspondingly to the specific concentrations marked above the sensors. Though differences can be observed visually, splitting of channels into red, green and blue (Figure 7.5b) reveals the way how an individual spot is composed by these three additive primary colors. Consequently, this proves that different spots are colored differently due to our sensor response to different concentrations of bacteria. The plots of RGB colorimetric channels (all values were taken at least three times and error bars are

displayed as well) in Figure 7.5c helped to monitor the effect of color tunability of the biosensor on the platform testing, observing that 1×10^4 bacteria/mL can be distinguished from control (β-Gal/**NP2** conjugate) and can be fixed as the limit of the detection of the platform testing.

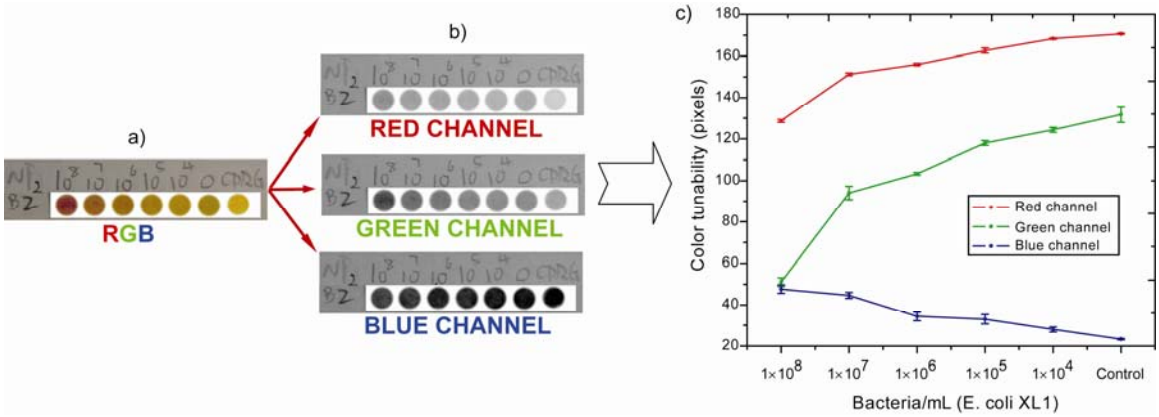

Figure 7.5 Schematic illustration of the RGB colorimetric analysis to monitor color changes on the GF/B filter paper spot at pH 7.4. a) imagine of the enzymatic activity response-colorimetric assay of the β-Gal-**NP2** complex upon addition of *E. coli XL1* at different concentration, CPRG substrate was used as a control. b) red, green, and blue channels obtained from the original sample a) to differentiate between bacteria concentration. c) the extracted values of red, green, and blue channel from the original data a). This process is repeated at least three times for each measurement in a series of images.

To further confirm this differentiation, a 3-D plot containing coordinates for each of the concentration RGB values are shown in Figure 7.6, displaying the colorimetric response that the β-Gal/**NP2** conjugate experienced upon exposure to the respective bacteria concentration. It can be seen that the four concentration of *E. coli XL1* could be readily discerned by the three RGB channel values as a resulted of the color tunability as well as the bacteria concentration. Clustering of raw RGB data of the colorimetric response allow the assessment of the discrimination capabilities of the sensor and demonstrates that the concentration of bacteria can be detected as low as 1×10^4 bacteria/mL, as shown in Figure 7.6.

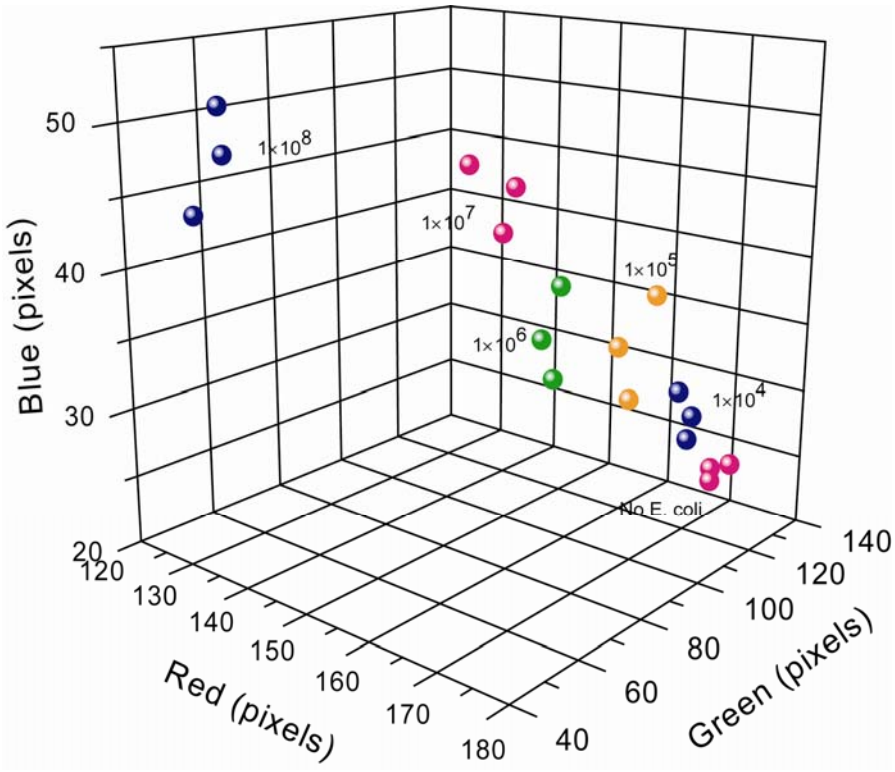

Figure 7.6 Schematic 3-D illustration of the RGB colorimetric analysis showing the limit of detection on a platform testing spot.

In order to test the generality and limitations of our sensor toward bacteria, three different bacteria strains of various sizes and surface properties (e.g. charge surface) were chosen. Gram-positive (i. e. *S. griseus* and *B. subtilis*) and Gram-negative bacteria (i. e. *E. coli XL1*) differ by their gross surface chemistries. Bacterial cell surfaces are inherently negatively charged. In Gram-negative bacteria,[29,32] the outer cell wall is composed of a lipid membrane, lipopolysaccharides, and glycoproteins, which impart negative charge to the surface. In Gram-positive bacteria,[29,32] the single-layer cell wall is comprised of a porous peptidoglycan layer[30] with attached negatively charged[31] teichoic acids, teichuronic acids, polyphosphates, and carbohydrates.[32]

Besides the relatively low LOD, our colorimetric sensing system also possesses a potential ability in discrimination of bacteria, proved in Figure 7.7. Both Streptomyces griseus (*S. griseus*) and Bacillus subtilis (*B. subtilis*), two gram-positive bacteria, are well separated from gram-negative *E. coli XL1*, no matter in more sensitive form of solution phase or on a platform testing. Our hypothesis is that Gram-negative cell contains an outer membrane composed by phospholipids and highly-charged lipopolysaccharides, resulting in a higher overall negative charge density on cell surface than that on Gram-positive cell surface, for the overall charge on Gram-positive cell is due to the presence of phosphodiester bonds between teichoic acid monomers, as a result of these unique molecular signatures among bacteria strong or weak tunability of the color can be observed.

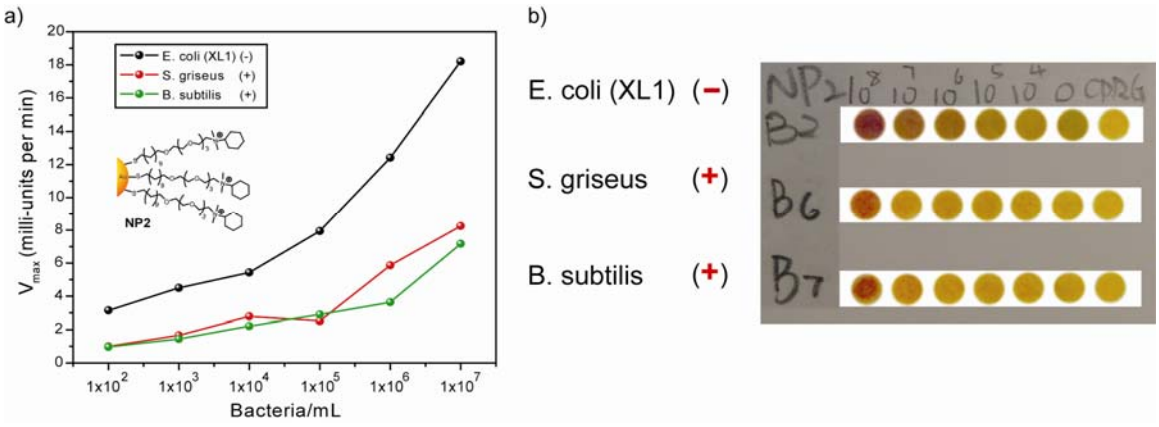

Figure 7.7 Colorimetric differentiation of Gram-negative and Gram-positive bacteria species. a) in solution phase, b) on a platform testing spot.

7.3 Conclusion

In this study, we have demonstrated that the appropriate choice of a hybrid enzymatic nanocomposite as an amplifier in a colorimetric sensor can dramatically increase the sensitivity of bacteria detection in solution as well as in a test strip platform, for example from 1×10^5 to 1×10^2 bacteria/mL (three order of magnitude in improvement), demonstrating the potential of this method for the detection of microbial contamination. Our current system changes from pale yellow to dark red color, providing highly visible response. However, the use of other substrates to optimize the read-out process can be explored. Greater sensitivity could be possible using other color combinations. We strongly believe that this colorimetric sensor with an appropriate number of receptors can generate an array that could be able to differentiate a very large number of bacteria species as well as bacteria strains. In our ongoing studies, we are exploiting both new alternative approaches for bacteria detection and new data analysis strategies to apply this methodology to more complex matrices featuring a large diversity of target analytes.

7.4 Experimental Section

7.4.1 Synthesis of Cationic Nanoparticles (AuNPs). NP1-NP4, core diameter ~2 nm, were synthesized according to References,[19] see SI for more details. The cationic **AuNP**s were very stable in aqueous solution.

7.4.2 TEM Images: These images were obtained on a JEOL 100CX electron microscope operated at 100 keV and analyzed using Image J. More than 200 **AuNP**s were taken as target samples to calculate the average diameters and size distributions (see Table 7.S1 for more details).

7.4.3 Charges and Sizes: ζ-Potential (ZP) and dynamic light scattering (DLS) were measured on a Malvern Zetasizer Nano ZS instrument. Each sample was scanned six times and an average value was reported (see Table 7.S1 for more details).

7.4.4 Activity Assays: β-galactosidase (β-Gal) and the colorgenic substrate chlorophenol-red-*β*-D-galactopyranside, CPRG were purchased from Sigma-Aldrich. In this study, nanoparticle and β-Gal solutions were prepared in sodium phosphate buffer solution (5 mM, pH 7.4). In the activity assay studies, β-Gal (0.5 nM) was incubated with various concentrations of **NP1**-**NP4** for 15 minutes and 1.5 mM of the colorgenic substrate (CPRG) was added. As a control experiments, the enzymatic activity of β-Gal was also monitored in the presence of neutral tetraethylene glycol and carboxylate functionalized nanoparticles as well as an enzymatic protein (α-Gal). The β-Gal stock concentration was 314 nM, while the stock concentrations of **NP1**-**NP4** were prepared at 100 nM. The inhibition studies in solution were carried out at pre-determined times by adding 5 μL of CPRG (1.5 mM in PB buffer) and 5 μL of PB buffer into 200 μL β-Gal/**AuNP** solution. The enzymatic activity was followed by monitoring product formation every 22 s for 15 minutes at 595 nm using a microplate reader (EL808 Bio-Tek Instruments, Inc.). The samples were measured in triplicate. From the activity/inhibition studies, optimal concentrations of β-Gal/**AuNP** complexes were obtained. Once the different inhibiting characteristics of the β-Gal/**AuNP** complexes were established, stoichiometric amounts of β-Gal and **NP1**-**NP4** were used to the bacteria detection. In the case of the test strip platform, 25 mM CPRG and 15 nM β-Gal was set up in a way to make the reaction take place at an appropriate speed for tuning the color of the substrate from yellow to dark red within a pre-determined time i.e. 10 minutes. Once the different

inhibiting characteristics of the β-Gal/**NP2** complexes were established, stoichiometric amounts of β-Gal and **NP2** was used on the bacteria detection. $\mathbf{NP_{TEG}}$ and $\mathbf{NP_{CO2}}$ were also used, as control experiment and no inhibition was observed as expected. The samples were measured in triplicate.

7.4.5 Instrumentation. Transmission Electron Microscopy (TEM) samples were prepared by depositing 3 μL of a diluted aqueous solution of cationic gold nanoparticles (**AuNP**s, 5 μM) onto a 300 mesh carbon-coated copper grid. The samples were dried in air at room temperature. TEM images were obtained on a JEOL 100CX electron microscope operated at 100 keV and analyzed using Image J. More than 200 **AuNP**s were taken as target samples to calculate the average diameters and size distributions. ζ-Potential (ZP) and dynamic light scattering (DLS) results were used to characterize the charge and the hydrodynamic diameter of both nanoparticles and proteins (Table 7.S1). Cationic gold nanoparticles were dissolved in sodium phosphate buffer (5 mM, pH 7.4) to make solutions at 5 μM concentrations. The samples were filtered through a Millipore syringe-driven filter (0.22 μm) and injected into a folded capillary disposable cell. In the case of the proteins, the samples were filtered through a Millipore syringe-driven filter (0.22 μm) and injected into the disposable cell. Both ZP and DLS were measured on a MALVERN Zetasizer Nano ZS instrument. Each sample was scanned six times and an average value was reported.

Table 7.S1 Characterization of **NP1-NP4**. The average size of the core metal was determined from a population of 200 nanoparticles by both TEM and image J and expressed in average diameter ± its standard deviation between runnings. Zeta potential were measurements in 5 mM phosphate buffer, pH = 7.4.

Samples (n =6)	Ligand shell composition *	Core size (nm) §	D_H (nm) †	ζ Potential (mV) ‡	Chemical structure of Ligands £
β-Gal	—	—	18.55 ± 1.71	– 22.67 ± 1.53	Large, tetrameric enzyme, Mw = 465 kDa
NP1	100% L1	2.15 ± 0.28	12.12 ± 0.10	+ 22.30 ± 0.31	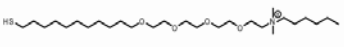
NP2	100% L2	2.09 ± 0.27	10.33 ± 0.15	+ 21.20 ± 0.10	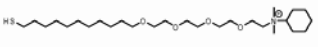
NP3	100% L3	2.12 ± 0.21	12.13 ± 0.07	+ 20.13 ± 0.57	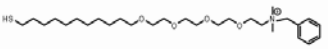
NP4	100% L4	2.14 ± 0.25	12.50 ± 0.11	+ 20.10 ± 0.22	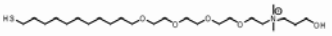

* Calculated from ^{1}H NMR spectra.
§ Determined by TEM images , image J and Origin 7.0 and expressed as average diameter ± standard deviation.
† Hydrodynamic diameter (D_H) measurements are in 5 mM phosphate buffer at pH 7.40.
‡ Zeta potential measurements are in 5 mM phosphate buffer at pH 7.40.
£ Determined from ^{1}H NMR spectra at 400 MHz.

7.4.6 Synthesis of AuNPs 1-4. Pentanethiol-coated **AuNP**s with core diameter ~2 nm were synthesized using the Brust-Schiffrin two-phase synthesis method.[1] Murray place-exchange method[2] was used to obtain the quaternary ammonium functionalized **AuNP**s **1-4** (see Figures 7.S1-7.S4 for characterization).[3] The cationic **AuNP**s were very stable in aqueous solution.

[1] a) A. G. Kanaras, F. S. Kamounah, K. Schaumburg, C. J. Kiely, M. Brust, *Chem. Commun.* **2002**, 2294. b) M. Brust, M. Walker, D. Bethell, D. J. Schiffrin, R. Whyman, *J. Chem. Soc. Chem. Commun.* **1994**, 801.

[2] A. C. Templeton, M. P. Wuelfing, R. W. Murray, *Acc. Chem. Res.* **2000**, *33*, 27.

[3] a) C. C. You, O. R. Miranda, B. Gider, P. S. Ghosh, I. B. Kim, B. Erdogan, S. A. Krovi, U. H. F. Bunz, V. M., *Nature Nanotech.* **2007,** 2, 318-323. b) O. R. Miranda, H. T. Chen, C. C. You, D. E. Mortenson, X. C, Yang, U. H. F. Bunz, V. M., *J. Am. Chem. Soc.* **2010,** 132, 5285-5289

^{1}H NMR spectra of **NP1** after place exchange with $AuS(CH_2)_4CH_3$

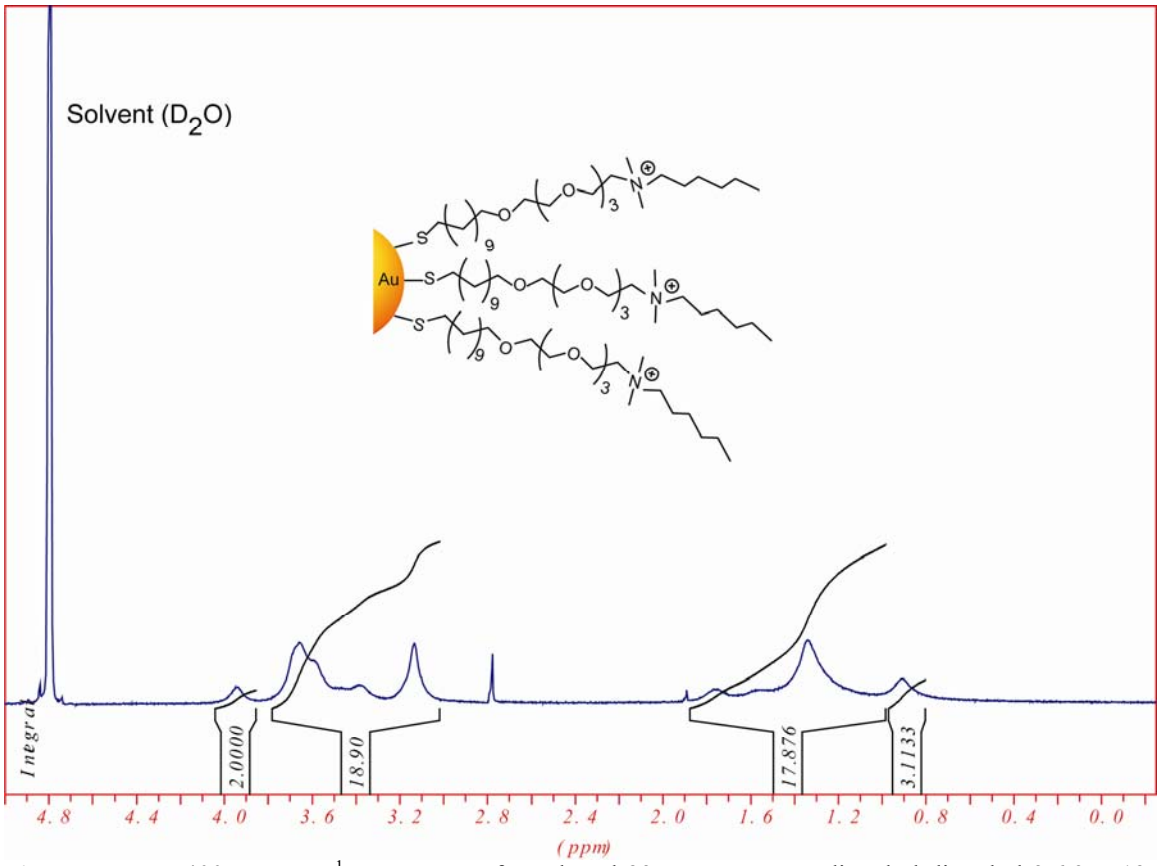

Figure 7.S1 400 MHz ^{1}H NMR of N-hexyl-23-mercapto-N,N-dimethyl-dimethyl-3,6,9, 12-tetraoxatricosan-1-aminium capping the surface of the metal core gold nanoparticles after place exchange. The average diameter of the metal core **NP1** is ~ 2 nm (2.15 ± 0.28 nm).

^{1}H NMR spectra of **NP2** after place exchange with $AuS(CH_2)_4CH_3$

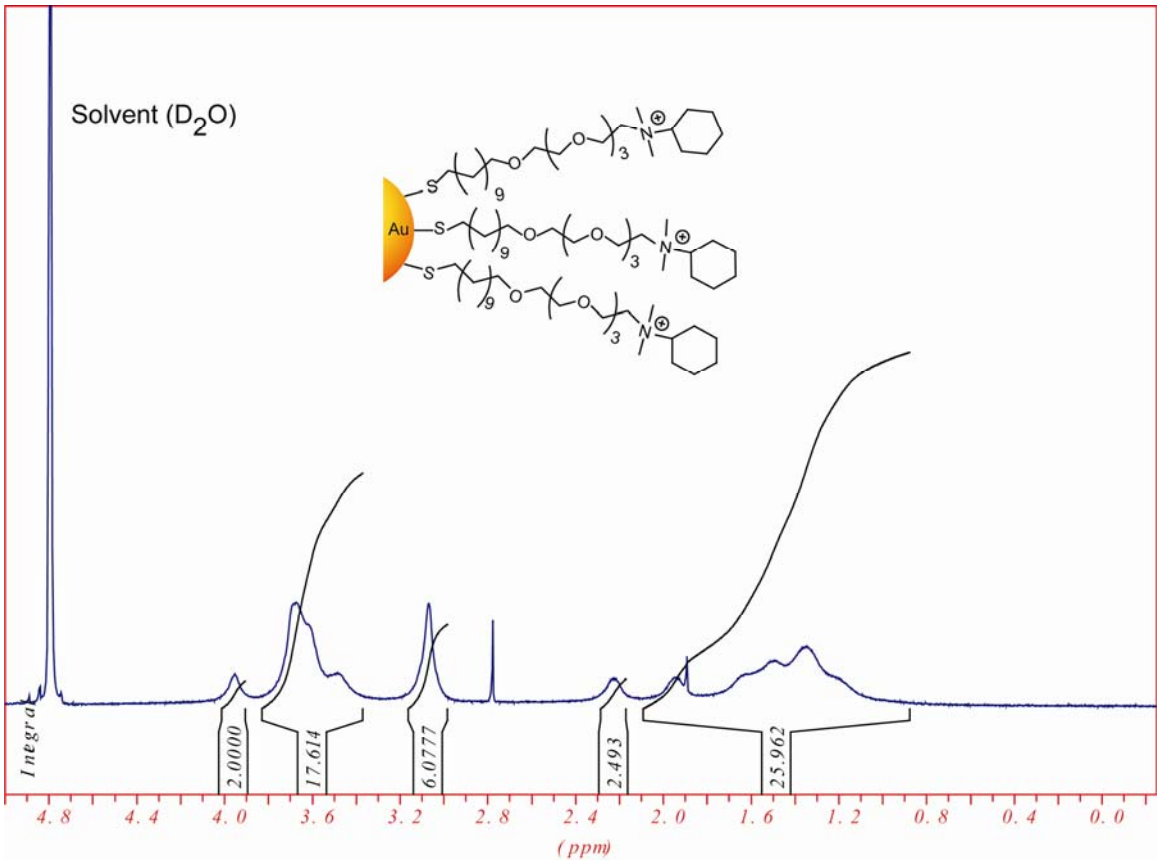

Figure 7.S2 400 MHz ^{1}H NMR of N-cyclohexyl-23-mercapto-N,N-dimethyl-3,6,9,12-tetraoxatricosan-1-aminium capping the surface of the metal core gold nanoparticles after place exchange. The average diameter of the metal core **NP2** is ~ 2 nm (2.09 ± 0.27 nm).

^{1}H NMR spectra of **NP3** after place exchange with $AuS(CH_2)_4CH_3$

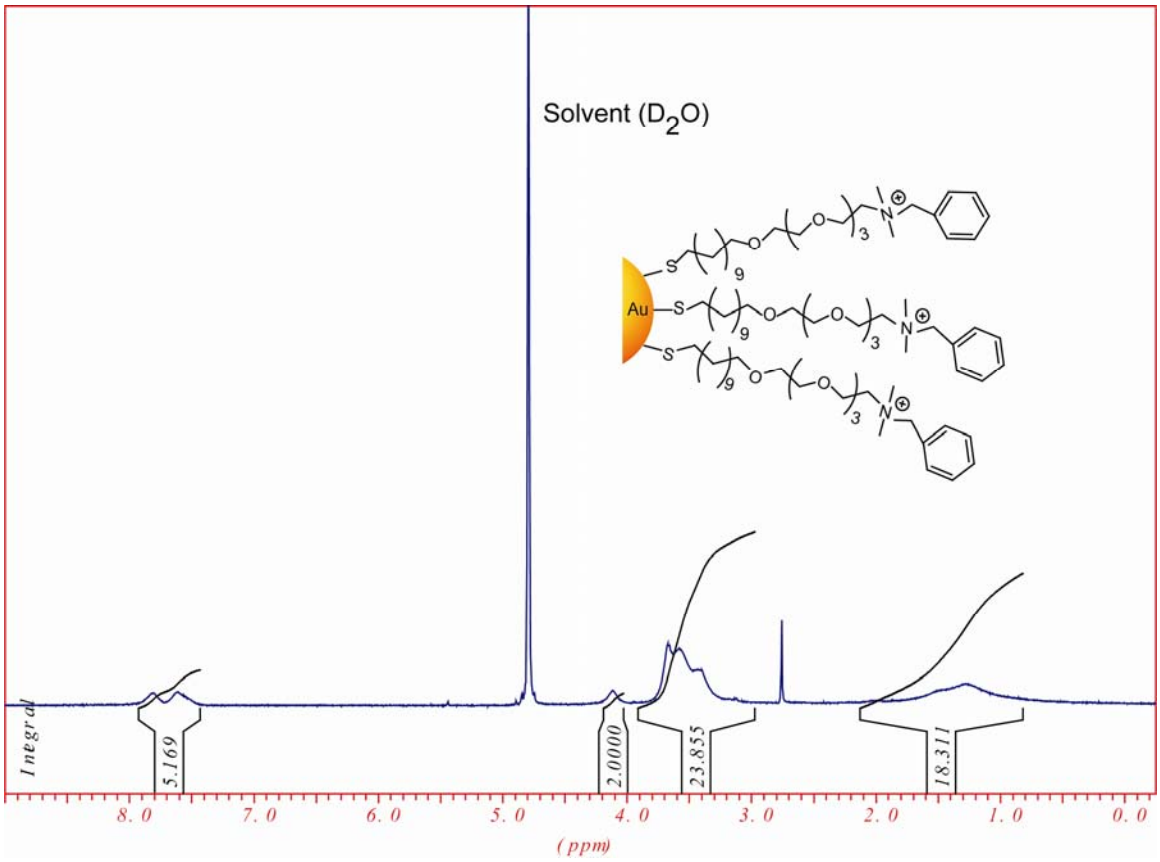

Figure 7.S3 400 MHz ^{1}H NMR of N-benzyl-23-mercapto-N,N-dimethyl-3,6,9,12-tetraoxatricosan-1-aminium capping the surface of the metal core gold nanoparticles after place exchange. The average diameter of the metal core **NP3** is ~ 2 nm (2.12 ± 0.21 nm).

^{1}H NMR spectra of **NP4** after place exchange with $AuS(CH_2)_4CH_3$

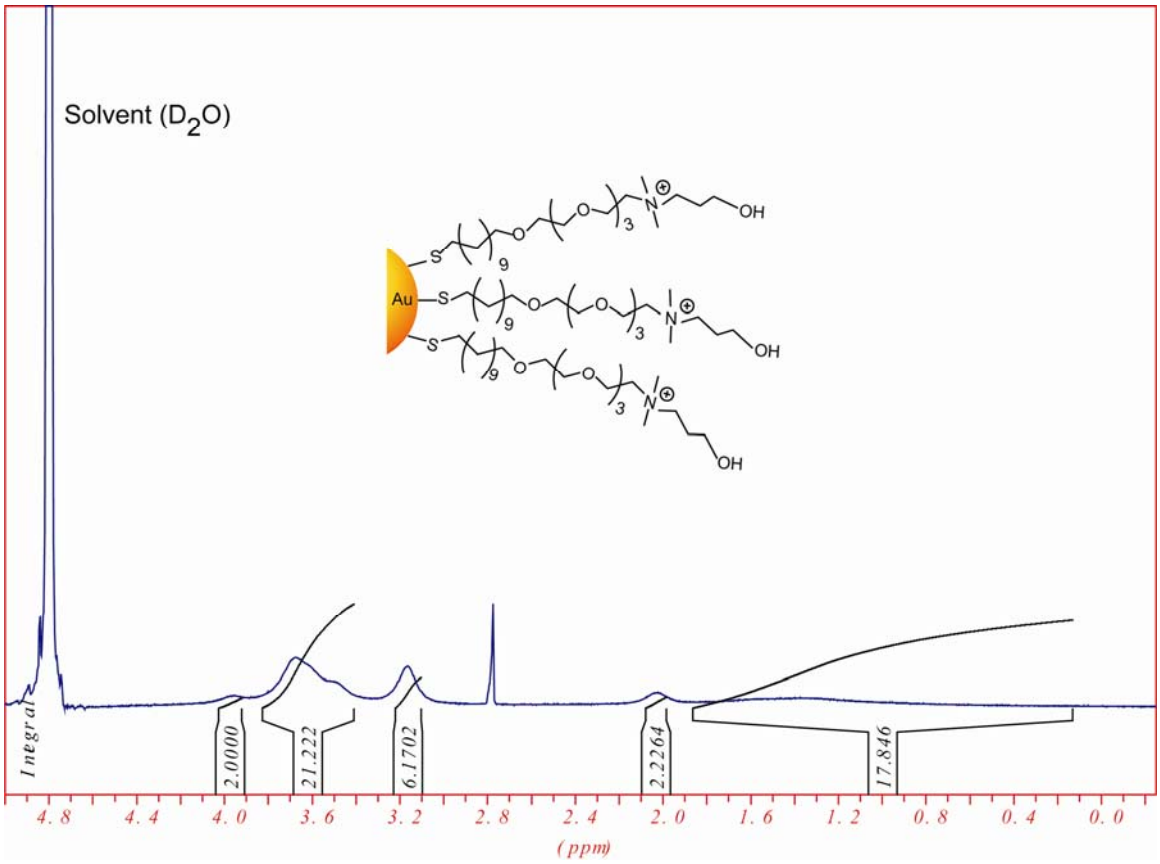

Figure 7.S4 400 MHz ^{1}H NMR of N-(3-hydroxypropyl)-23-mercapto-N,N-dimethyl-3,6,9,12-tetraoxatricosan-1-aminium capping the surface of the metal core gold nanoparticles after place exchange. The average diameter of the metal core **NP4** is ~ 2 nm (2.14 ± 0.25 nm).

7.4.7 Laser Desorption/Ionization Mass Spectrometry (LDI-MS).

The LDI-MS analyses were done on a Bruker Autoflex III time-of-flight mass spectrometer (Autoflex III; Bruker Daltonics, Germany) using a Smartbeam laser (Nd:YAG, 355 nm). All mass spectra were acquired in reflectron mode. The ion source voltage 1 and 2 were set to 19.00 kV and 16.65 kV, respectively. The reflector voltage 1 and 2 were set to 21 kV and 9.7 kV, respectively. The post ionization extraction delay was 10 ns. On this instrument, 100 laser shots were fired to acquire each spectrum, and positive ions were detected. A 2 μL of 1 μM AuNP water solution was applied to a MTP 384 ground steel sample target and allowed to air-dry before LDI-MS. The calibration was done using positively charged gold clusters (i.e., Au^+, Au_2^+, and Au_3^+). The LDI-MS results are consistent as previous reported research.[14]

[4] a) Z.-J. Zhu, P. Ghosh, O. R. Miranda, R. W. Vachet, V. M. Rotello, J. Am. Chem. Soc. 2008, 130, 14139-14143 b) B. Yan, Z. J. Zhu, O. R. Miranda, A. Chompoosor, V. M. Rotello, R. W. Vachet, *Anal. Bioanal. Chem.* **2010**, *396*, 1025-1035.

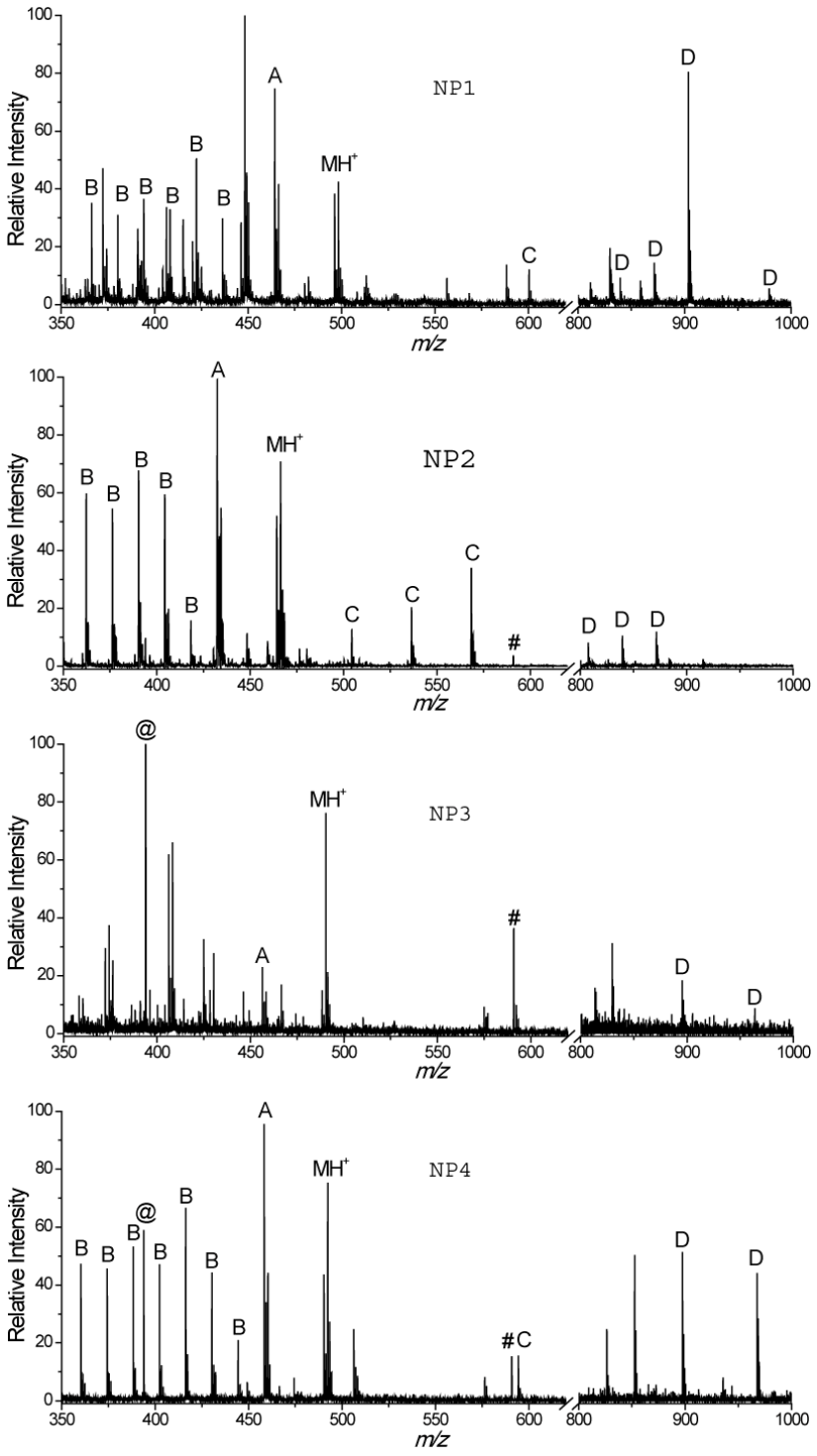

Figure 7.S5 LDI mass spectra of AuNPs **1-4**. The LDI-MS results are consistent as previous research.[1] Symbol key: @, Au_2^+ (*m/z* 393.9); #, Au_3^+ (*m/z* 590.9); MH^+, the molecular ion corresponding to surface ligand; A, a fragment ion corresponding to a loss of H_2S ($[MH\text{-}H_2S]^+$); B, ions corresponding to multiple losses of methylene groups from the alkane portion of the ligands; C, disulfide ions and their fragment ions forming from the initial pentanethiol capping group (i.e., $C_5H_{11}S$) and surface ligands; D, disulfide ions and their fragment ions forming from surface ligands.

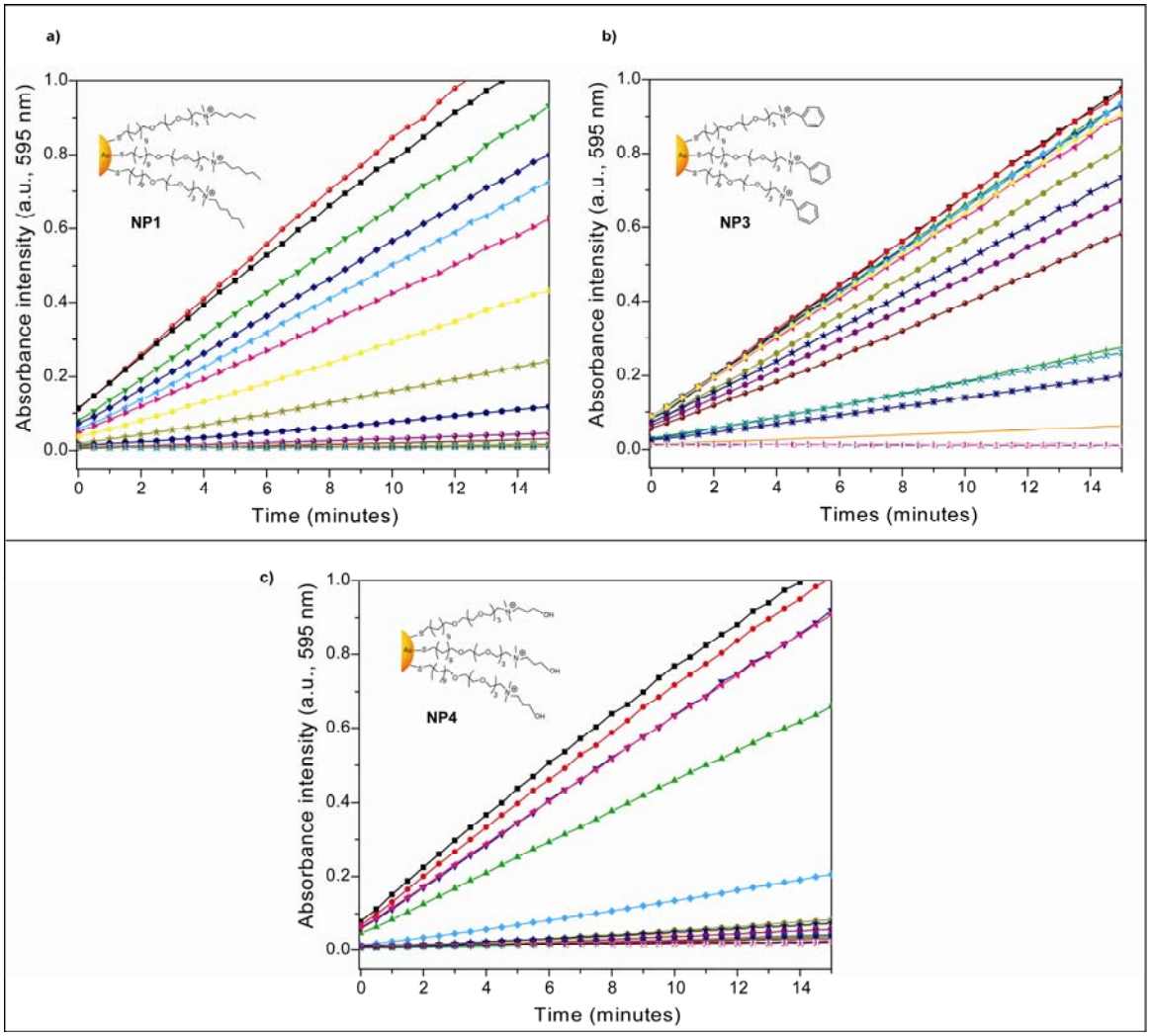

Figure 7.S6 Inhibited activity titration for the complexation of β-Gal (0.5 nM) with cationic gold nanoparticles (**NP1-NP4**). The inhibition study was measured following the addition of cationic nanoparticles (0-100 nM) with an excitation wavelength of 595 nm. The β-Gal stock concentration was 314 nM, while the stock concentration of **NP1-NP4** was 100 nM. For the activity/inhibition studies, optimal concentrations of β-Gal/ **AuNP** complexes were obtained (β-Gal = 0.5 nM and a) **NP1**: 12 nM, b) **NP3**: 9 nM, and d) **NP4**: 35 nM).

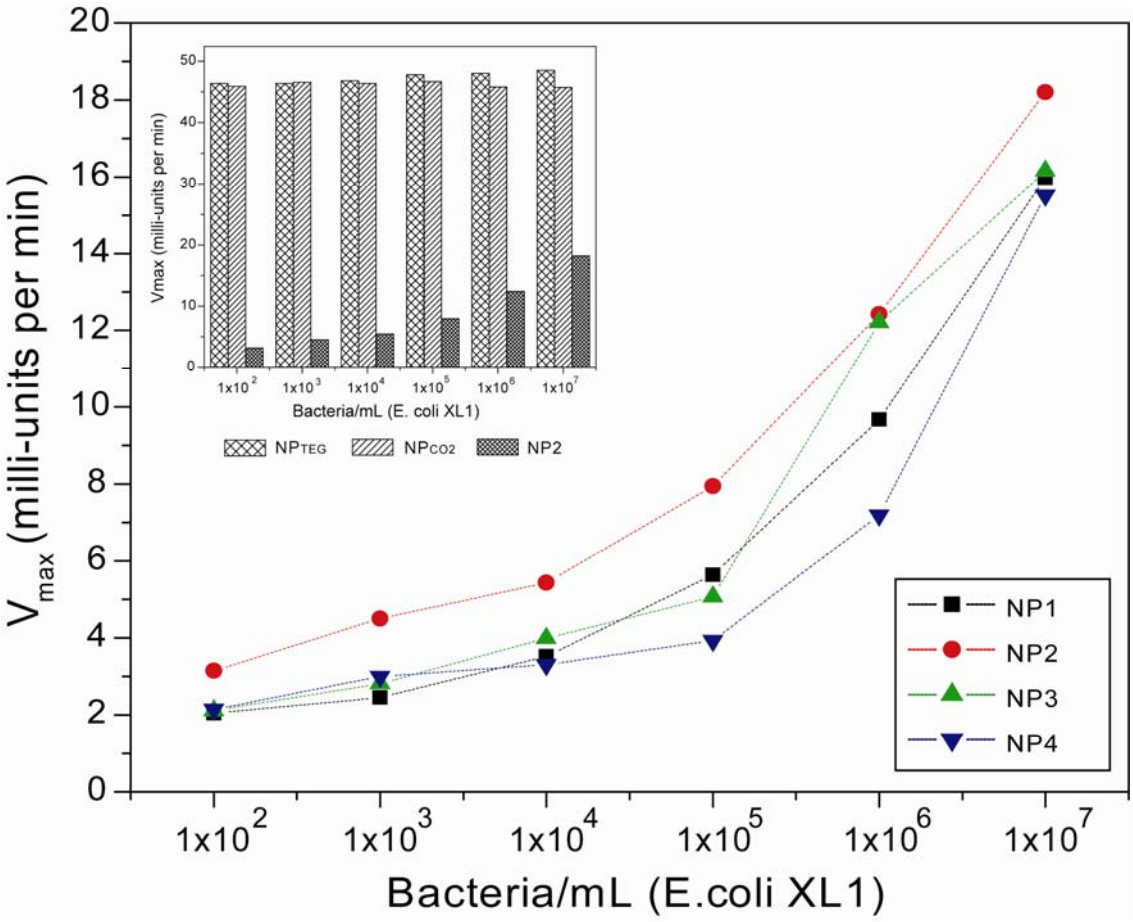

Figure 7.S7 Change of the kinetic absorbance of several enzymatic nanocomposite sensors (β-Gal and **NP1, NP2, NP3**, and **NP4**) on the incubation of different bacteria concentrations. **NP2** was employed to give the lowest limit of detection among the four nanoparticles used on the bacteria detection. In the inset, $\mathbf{NP_{CO2}}$ and $\mathbf{NP_{TEG}}$ are negative and neutral nanoparticles used as references and no interaction is observed.

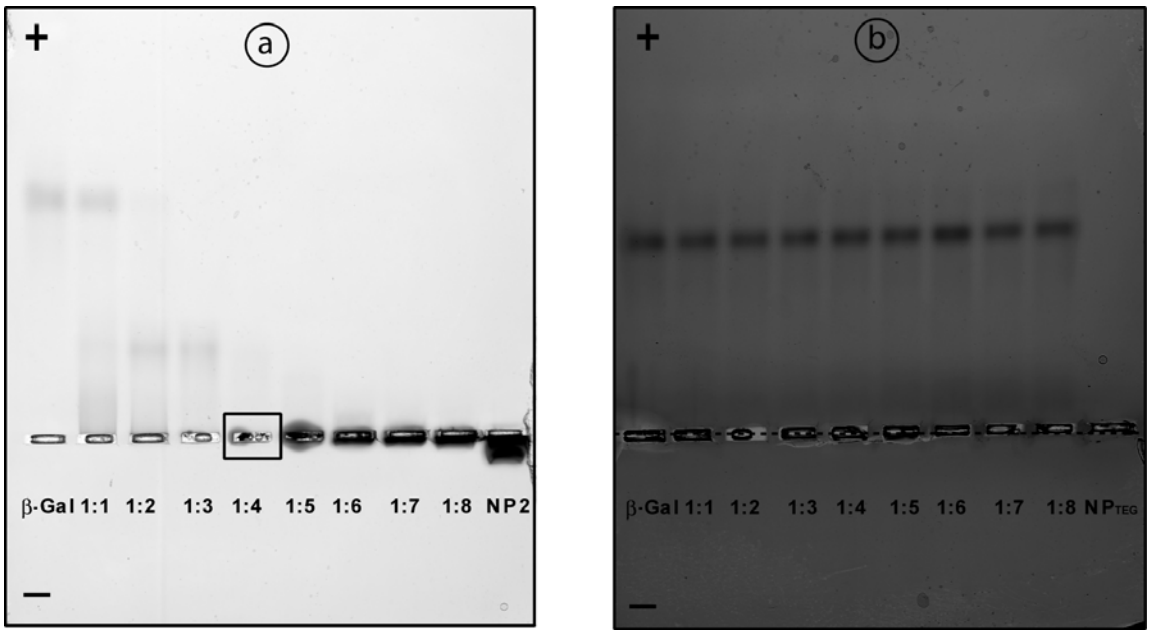

Figure 7.S8 a) Gel electrophoresis of β-Gal and **NP2** with varying molar ratios (enzyme-**NP** adducts, 1:4 optimal molar ratio) after staining. The concentration of the enzyme was 2 μM. b) As control experiment, gel electrophoresis of β-Gal and $\mathbf{NP_{TEG}}$ **(**23-mercapto-3,6,9,12-tetraoxatricosan-1-ol capping the metal core) with varying molar ratios (enzyme: **NP**) of after staining $\mathbf{NP_{TEG}}$. The concentration of the enzyme was 2 μM. As it can be seen on the gel neutral **NP**s do not interact strongly with the enzyme, β-Gal**.**

As a control, $\mathbf{NP_{CO2}}$ and $\mathbf{NP_{TEG}}$ nanoparticles, bacteria, and α-Gal in CPRG solutions were studied and no activity or colorimetric effect was observed as compared with **NP2**, confirming that the colorimetric sensing effect is only due to the hydrolysis of the substrate by the enzyme (Figure 7.4 and Figure (s). 7.S8 and 7.S9).

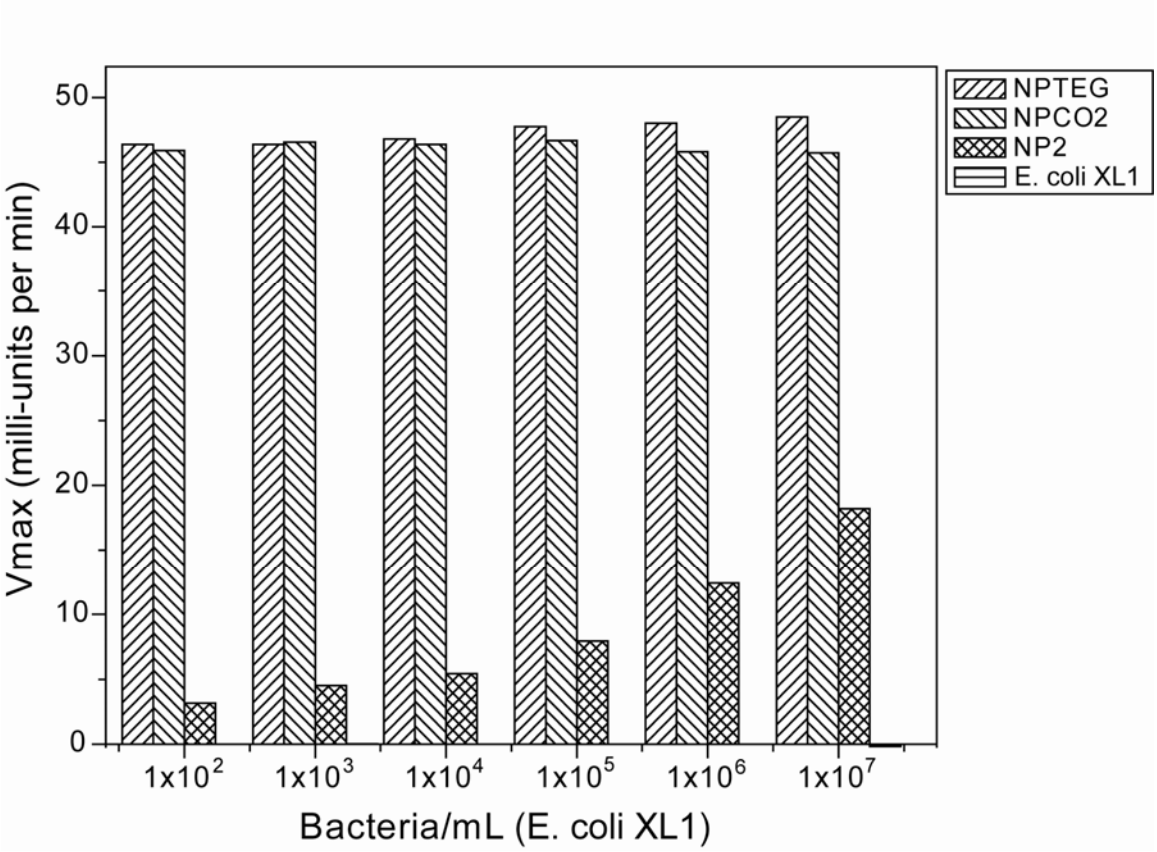

Figure 7.S9 Change of the kinetic absorbance of several enzymatic nanocomposite sensors (β-Gal/**NP2**) on the incubation of different bacteria concentrations. In the inset, $\mathbf{NP_{CO2}}$ and $\mathbf{NP_{TEG}}$ are negative and neutral nanoparticles used as references and no interaction is observed. Bacteria (E. coli XL1) and substrate as well as α-Gal and substrate were also used as control experiments and no change of color was observed in the solutions.

7.5 References

1. a) Inglesby, T. V.; O'Toole, T.; Henderson, D. A.; Bartlett, J. G.; Ascher, M. S.; Eitzen, E.; Friedlander, A. M.; Gerberding, J.; Hauer, J.; Hughes, J; McDade, J.; Osterholm, M. T.; Parker, G.; Perl, T. M.; Russell, P. K.; Tonat, K. *J. Am. Med. Assoc.* **2002**, 287, 2236. b) Brecher, M. E.; Hay, S. N. *Clin. Microbiol. Rev.* **2005**, 18, 195. c) Shorten, P. R.; Pleasants, A. B.; Soboleva, T. K. *Int. J. Food Microbiol.* **2006**, 108, 369.

2. Ford, E. E.; Colwell, R. R. A global decline in microbiological safety: a call for action. A report from The American Academy of Microbiology, Washington, D.C., **1996**, pp. 1-40.

3. Pedley, S.; Bartram, J.; Rees, G.; Dufour, A.; Cotruvo, J. A. "Pathogenic mycobacteria in Water" World Health Organization (WHO), ISBN: 92-4-156259-5, **2004**.

4. a) Deisingh, A. K.; Thompson, M. *Analyst* **2002**, 127, 567. b) Deisingh, A. M; Thompson, M. *Can. J. Microbiol.* **2004**, 50, 69. c) Cole, L. A. *Sci. Am.* **1996**, 275, 60. d) Chandler, D. P.; Straub T. M. *J. of Microbiol. Methods,* **2003**, 53, 185.

5. Straub, T.M.; Chandler, D. P. *J. Microbiol. Methods* **2003**, 53, 185.

6. a) Hugo, W. B.; Russell, A. D. "Pharmaceutical Microbiology" Blackwell, Oxford, 6th edn. **1998**. b) Adams, M. R.; Moss, M. O. "Food Microbiology" Royal Society of Chemistry, 2nd ed. **2000**.

7. Safarik, I.; Safarikova, M.; Forsythe, S. J. *J. Appl. Bacteriol.* **1995**, 78, 575.

8. Harrigan, H. F. "Laboratory Methods in Food Microbiology" 3rd ed. Academic Press, San Diego, **1998**.

9. a) Newton, C. R.; Graham, A. "PCR", 2nd ed. Bios Scientific, Oxford, **1997**. b) Eeles, R. A.; Sharp, A. C. "Polymerase Chain Reaction: The technique and its applications" Landes, R.G., Austin, TX, **1993**.

10. Strachan, N. J. C.; Nicholson, F. J.; Ogden, I. D. *Anal. Chim. Acta.* **1995**, 313, 63.

11. a) Maughan, N. J.; Lewis, F. A.; Smith, V. *J. Pathol.* **2001,** 195, 3-6. b) T. J. Aitman, *Br. Med. J.* **2001**, 323, 611.

12. a) Hall, E. A. H. "Biosensors" Open University Press, Milton Keynes, **1990**. b) Catrall, R. W. "Chemical Sensors" Oxford University Press, Oxford, **1997**. b) Ivnitski,

D.; Abdel-Hamid, I.; Atanasov, P.; Wilkins, E. *Biosensors & Bioelectronic*s **1999**, 14, 7, 599.

13. Hilpert, K.; Hancock, R. E. W. *Nature Protocols*, **2007**, 2, 1652.

14. Ji, J.; Schanzle, A.; Tabacco, M. B. *Anal. Chem.* **2004**, 76, 1411.

15. a) Heal, J. S.; Blom, A. W.; Titcomb, D.; Taylor, A.; Bowker, K.; Hardy, J. R. W. *J. Hosp. Infect.* **2003**, 53, 136. b) Perkins, S. D.; Mayfield, J.; Fraser, V.; Angenent, L. T. *Appl. Environ. Microbiol.* **2009,** 75, 5363. d) Chen, C. L.; Yu, J-C.; Holme, S.; Jacobs, M.R.; Yomtovian, R.; McDonald, C. P. *Transfusion* **2008**, 48, 1550. e) Orihuela, C.; Fillon, J. S.; Tuomanen, E. I. *Infect Immun.* **2006**, 74, 3783. f) Wu, Y-D.; Chen, L-H.; Zhao, Z-Y. *J. Clin. Microbiol.* **2008**, 46, 2613.

16. a) Phillips, R. L.; Miranda, O. R.; You, C.-C.; Rotello, V. M.; Bunz, U. H. F. *Angew. Chem. Int. Ed.* **2008**, 47, 2590 ; *Angew. Chem.* **2008**, 120, 2628. b) Lee, H.; Yoon, T. J.; Weissleder, R. *Angew. Chem. Int. Ed. Engl.* **2009**, 48, 5657. c) Grossman, H.; Myers, W.; Vreeland, V.; Bruehl, R.; Alper, M.; Bertozzi, C.; Clarke, J. *Proc. Natl. Acad. Sci. USA.* **2004**, 101, 129. d) Zhao X, Hilliard L, Mechery S, Wang Y, Bagwe R, Jin S, Tan W. *Proc. Natl. Acad. Sci. USA.* **2004**, 101, 15027.

17. a) Bruno, J. G.; Francis, K.; Ikanovic, M.; Rao, P.; Dwarakanath, S.; Rudzinski, D. E. *J. of Bionanoscience* **2007**, 1, 1. b) Yang, S. Y.; Wang, W. C.; Lan, C. B.; Chen, C. H.; Chieh, J. J.; Horng, H. E.; Hong, C. Y.; Yang, H. C.; Tsai, C. P.; Yang, C.Y.; Cheng, I. C.; Chung, W. C. *J. Virol. Methods* **2010**, 164, 14. c) Niikura, K.; Nagakawa, K.; Ohtake, N.; Suzuki, T.; Matsuo, Y.; Hirofumi Sawa, Ijiro, K. *Bioconjugate Chem.*, **2009**, 20, 1848. d) Halfpenny, K. C.; Wright, D. W. *WIREs Nanomed. Nanobiotechnol*. **2010**, 2, 277.

18. a) Bajaj, A.; Miranda, O. R.; Kim, I. B.; Phillips, R. L.; Jerry, D. J.; Bunz, U. H. F.; Rotello, V. M. *Proc. Natl. Acad. Sci. U.S.A* **2009**, 106, 10912. b) Bajaj, A.; Rana, S.; Miranda, O. R.; Yawe, J. C.; Jerry, D. J.; Bunz, U. H. F.; Rotello, V. M. *Chem. Sci.* **2010**, 1, 134.

19. a) You, C. C.; Miranda, O. R.; Gider, B.; Ghosh, P. S.; Kim, I. B.; Erdogan, B.; Krovi, S. A.; Bunz, U. H. F., Rotello, V. M. *Nature Nanotech*. **2007**, 2, 318. b) De, M.; Rana, S.; Akpinar, H.; Miranda, O. R.; Arvizo, R. R.; Bunz, U. H. F.; Rotello, V. M. *Nature Chem.* **2009**, 1, 461. c) Miranda, O. R.; Chen, H. T.; You, C. C.; Mortenson, D. E.; Yang, X. C.; Bunz, U. H. F.; Rotello, V. M. *J. Am. Chem. Soc.* **2010**, 132, 5285.

20. Berry, V.; Gole, A.; Murphy, J.; Saraf, R. F. *J. Am. Chem. Soc.* **2005**, 127, 17600.

21. a) Guidelines for Drinking Water, Third Edition, Volume 1 (Recommendations), World Health Organization (WHO), ISBN: 92-4-154638-7, **2004**. b) C. P. Gerba, "Pathogens in the environment" Gerba, C. P.; Brusseau, M. L. Pollution Science.

Academic press, New York, **1996**, 279. c) McFeters, G. A. Drinking water microbiology, Springer-Verlag, ISBN: 0-387-97162-9, **1990**.

22. a) Holme, S.; McAlister, M. B.; Ortolano, G. A.; Chong, C.; Cortus, M. A.; Jacobs, M. R.; Yomtovian, R.; Freundlich, L. F.; Wenz, B. *Transfusion* **2005**, 45, 984. b) Hoffmann, O.; Keilwerth, N.; Bastholm Bille, M.; Reuter, U.; Angstwurm, K.; Schumann, R. R.; Dirnagl, U.; Weber, J. R. *J. Cereb. Blood Flow. Metab.* **2002**, 22, 988. c) Wagner, S. J. *Vox Sanguinis* **2004**, 86, 157. d) Wu, Y-D.; Chen, L-H.; Wu, X-J.; Shang, S-Q.; Lou, J-T.; Du, L-Z.; Zhao, Z-Y. *J. Clin. Microbio*l. **2008**, 46, 2613.

23. a) Jacobson, R. H.; Zhang, X. J.; Dubose, R. F.; Matthews, B. W. *Nature* **1994**, *369*, 761. b) Verma, A.; Simard, J. M.; Worrall, J. W. E.; Rotello, V. M. *J. Am. Chem. Soc.* **2004**, *126*, 13987. c) Fowler, A. V.; Zabin, I. *J. Biol. Chem.* **1978**, *253*, 5521. d) Fowler, A. V.; Zabin, I. *J. Biol. Chem.* **1970**, *245*, 5032.

24**.** Nguyen, B. T.; Wiskur, S. L.; Anslyn, E. V. *Org. Lett.* **2004**, 6, 2499.

25. a) Rosi, N. L.; Mirkin, C. A. *Chem. Rev.* **2005**, 105, 1547. b) Alivisatos, A. P.; Gu, W.; Larabell, C. *Annu. Rev. Biomed. Eng.* **2005**, 7, 55. c) Bruchez Jr., M.; Moronne, M.; Gin, P.; Weiss, S.; Alivisatos, A. P. *Science* **1998**, 281, 2013. d) Ferrari, M. *Nat. Rev. Cancer* **2005**, 5, 161.

26. a) Kates, M. in Handbook of Lipid Research: Glycolipids, Phosphoglycolipids and Sulfoglycopids (Ed.: M. Kates), Plenum, Oxford, **1990**, 123. b) Dmitriev, B.; Toukach, F.; Ehlers, S. *Trends Microbiol.* **2005**, 13, 569. c) Koch, A. L. *Clin. Microbiol. Rev.* **2003**, 16, 673. d) Schaffer, C.; Messner, P. *Microbiology* **2005**, 151, 643. e) Bos, M. P.; Tefsen, B.; Geurtsen, J.; Tommassen, J. *Proc. Natl. Acad. Sci. USA* **2004**, 101, 9417.

27 a) Hall, M.; Eldridge, D. B.; Saunders, R. D.; Fairclough, D. L.; Bateman, R. C. Jr. *Food Biotech.* **1995**, 9, 39. b) Patange, S. B.; Mukundan, M. K.; Ashok Kumar, K. *Food Control* **2005**, 16, 465.

28. Steiner, M. S.; Meier, R. J.; Duerkop, A.; Wolfbeis, O. S. *Anal. Chem.* **2010**, AC102029J, Articles ASAP a) Bonifacio, L. D.; Puzzo, D. P.; Breslav, S.; Ozin, G. A. *Adv. Mater.* **2010**, 22, 1351. b) Janzen, M. C.; Ponder, J. B.; Bailey, D. P.; Ingison, C. K.; Suslick, K.S. *Anal. Chem.* **2006**, 78, 3591. c) Filippini, D.; Gatto, E.; Alimelli, A.; Malik, M. A.; Di Natale, C.; Paolesse, R.; Damico, A. ; Lundstron, I. *J. Porphyrins Phthalocyanines* **2009**, 13, 77.

29. a) Bos, M. P.; Robert, V.; Tommassen, J. *Annu. Rev. Microbiol.* **2007**, 61, 191. b) Duong, F.; Eichler, J.; Price, A.; Leonard, M. R.; Wickner, W. *Cell* **1997**, 91, 567.

30. Sutcliffe, I. C. *Syst. Appl. Microbiol.* **1995**, 17, 467.

31. a) Baddiley, J. *Bioessays* **1989**, 10, 207. b) Armstrong, J. J.; Baddiley, J.; Buchanan, J. G.; Carss, B.; Greenberg, G. R. *J. Am. Chem. Soc.* **1958**, 4344.

32. Navarre, W. W.; Schneewind, O. *Microbiol. Mol. Biol. Rev.* **1999**, 63, 174.

CHAPTER 8

SNIFFING CHANGES ON CELL SURFACES: DETECTION AND DIFFERENTIATION OF NORMAL, CANCEROUS, AND METASTATIC CELLS USING NANOPARTICLE-POLYMER SENSOR ARRAY

8.1 Introduction

Each cell type has unique molecular signatures that distinguish between healthy and diseased tissues.[1] In the case of cancers, the distinctions between normal *vs.* tumor and benign *vs.* metastatic cells are often subtle. The identification of cellular signatures for early cancer cell detection is a major hurdle for cancer therapy; the earlier these signatures can be established, the more effectively they can be treated.[2] Cancerous cells are differentiated from non-cancerous ones on the basis of intracellular or extra cellular (cell surface) biomarkers. Detection methods based on intracellular biomarkers (e.g. DNA/RNA/Proteins) require the previous knowledge of specific mutations in DNA/RNA[3] or changes in the regulation of protein expression inside the cells. Similarly, detection methods based on specific recognition of extracellular (cell surface) biomarkers such as histopathology,[4] bioimaging,[5] antibody arrays require previous knowledge of biomarkers on cell surfaces. Observation of over expressed antigens[6] on tumor cells using antibody-based platforms have been explored using enzyme-linked immunosorbent assay (ELISA)[7], surface plasmon resonance,[8] nanoparticles,[9] microcantilevers,[10] carbon nanotubes,[11] and expression microarrays.[12] Antibody arrays provide an effective but complex approach for cancer detection, diagnosis and prognosis,[13] however there is no single marker or a combination of biomarkers that has sufficient sensitivity and

specificity to differentiate between normal, cancerous, and metastatic cell types.[14] Here we describe a detection system that is based on selective noncovalent interactions between cell surface components and nanoparticles-based sensor elements that does not require any previous knowledge of intracellular or extracellular biomarkers.

The cell membrane surfaces consist primarily of a thin layer of amphipathic phospholipids, carbohydrates and many integral membrane proteins. The amount and types of which differ between species and according to function of cells.[15,16] This results into distinct cell membrane composition in different cell types. Therefore, one can predict, however, that there will be physicochemical (i.e., charge, hydrophobicity etc.) differences between cell types and between healthy and cancerous cells. Such physicochemical differences could potentially be detected by an array-based "chemical nose" approach that relies on selective interactions between multiple reporter elements and the target cell.

In chemical nose approach, an array of different sensors is used where every element in the sensor array responds to a number of different chemicals or analytes.[17] A distinct pattern of responses produced from a set of sensors in the array provide a fingerprint that allows classification and identification of the analyte.[18] The collection of sensors contains maximum chemical diversity as possible, so that array responds to largest possible cross section of analytes. The specific interactions involved between the reporter elements and the analyte are noncovalent and reversible. This approach provides an alternative to "lock–key" specific recognition[19] and has been used to detect metal ions,[20] volatile agents,[21] aromatic amines,[22] amino acids,[23] and carbohydrates.[24] In recent research we have demonstrated that the displacement of fluorescent polymers from differentially

functionalized gold nanoparticles with concomitant restoration of fluorescence provides an effective array-based method for the identification of proteins (Chapter 3).[25] More recently, we have shown that this methodology can be used to differentiate between bacterial species, and even between different strains of the same species (Chapter 6).[26] We report here a particle-polymer array that distinguishes between healthy, cancerous and metastatic human breast cells, and differentiates *isogenic* healthy and transformed cells.

8.2 Results and Discussion

Our detection system is based on conjugates between three structurally related cationic gold nanoparticles (**NP1**–**NP3**, Figure 8.1a and Figure 8.S4) and the poly(*para*-phenyleneethynylene) (PPE) polymer **PPE-CO_2** featuring charge multivalency[27] and molecular wire properties[28] (Figure 8.1a). In these noncovalent conjugates, the particle quenches the fluorescence of the polymer. In these non-covalent conjugates, the nanoparticle quenches the fluorescence of the polymer. The interactions between nanoparticles and anionic polymers are noncovalent, and predominantly electrostatic.

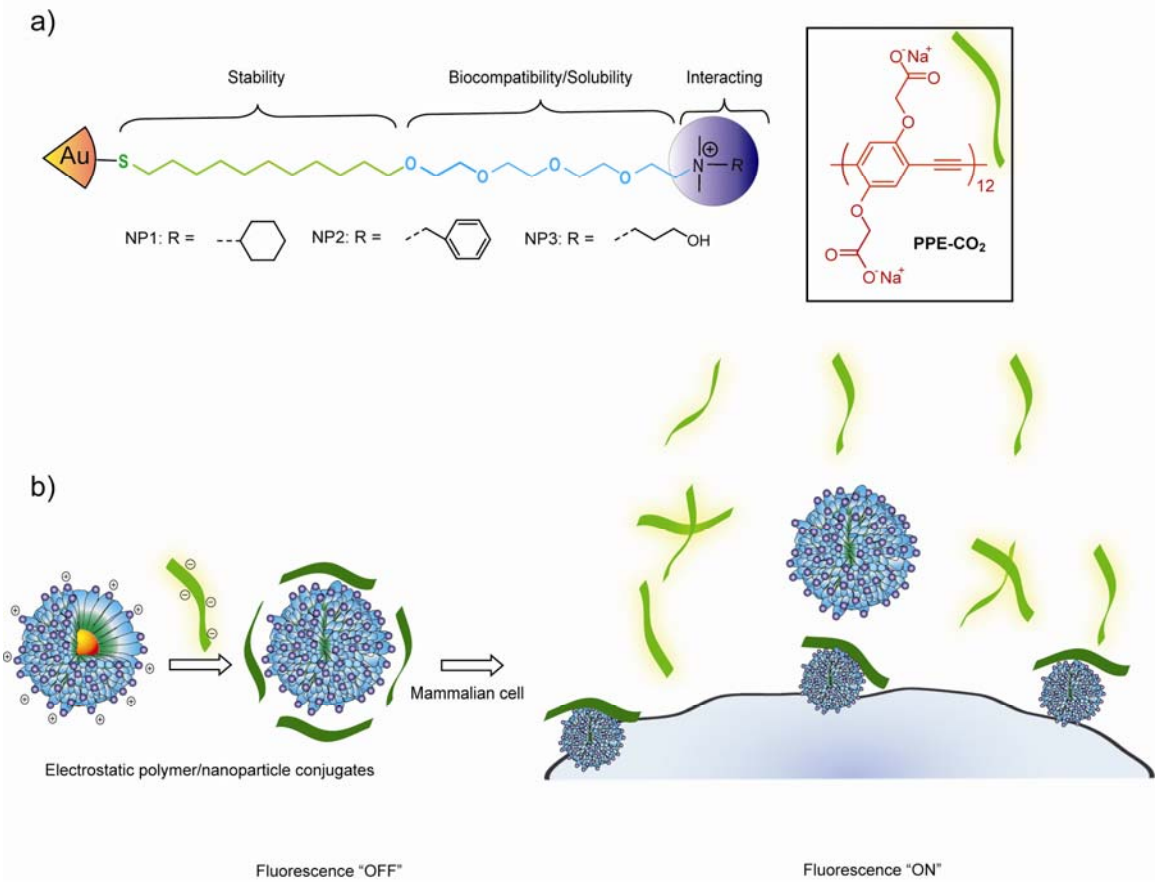

Figure 8.1 Molecular structures of nanoparticles and polymers, and schematic of fluorophore displacement cell detection array. a) molecular structures of the cationic gold nanoparticles (**NP1-NP3**) and the fluorescent polymer (**PPECO$_2$**). b) displacement of quenched fluorescent polymer (dark green strips, fluorescence off; light green strips, fluorescence on) by cell (in blue) with concomitant.

When mammalian cells were incubated with these nanoparticle-polymer complexes, there is competitive binding between nanoparticle-polymer complexes and cell types (Figure 8.1b). Because of their cationic surface, nanoparticles are expected to interact with phospholipids, membrane proteins and carbohydrates of the cell surface through both electrostatic and hydrophobic interactions. These interactions are responsible for displacement of the fluorophore polymer from the nanoparticle-polymer complexes generating a fluorescence response. The nanoparticles are expected to possess different

affinities for dissimilar cell surfaces depending on cell membrane composition and surface of nanoparticles. Selective displacement of the polymer from the particle by the cell surface regenerates fluorescence, transducing the binding event in a "turn on" fashion.

The complex stability constants (K_S) and association stoichiometries (n) for the particle-polymer dyads were obtained through nonlinear least-squares curve-fitting analysis.[29] Complex stabilities vary within 1 order of magnitude ($\Delta\Delta G \approx 4.5$ kJ mol^{-1}), and the binding stoichiometry ranges from 2.5 for **NP2** to 0.9 for **NP3** (Figure 8.S3). After determining the saturation point for fluorescence quenching, (Figure 8.S3), the appropriate stoichiometries of particle and polymer were mixed in 5 mM phosphate buffer (pH = 7.4) to yield nanoparticle- **$PPECO_2$**complexes with a final concentration of polymer of 100 nM and of nanoparticles 10-40 nM. The complexes of **$PPECO_2$** and **NP1-3** were then incubated with different cell types to determine changes in fluorescence intensities. We observed increases and decreases in fluorescence intensities depending on the cell type and the nature of nanoparticle-polymer complexes. Increased fluorescence intensities are due to the displacement of the **$PPECO_2$** polymer from the **NP-$PPECO_2$** complexes by cell surfaces (Figure 8.1b), whereas decreases in the fluorescence intensities are due to the quenching of the residual **$PPECO_2$** fluorescence by the cell surfaces. These differences in the fluorescence patterns depend on the cell type and are reproducible. We have performed array-based s sensing using 9 gold nanoparticles that possess different head groups and interact differently with polymers (Figure 8.S4a). We studied their interactions with the different cell types listed in Table 8.1, focusing on which particle set can best differentiate between different particles (see below). From

studies, we have observed the maximum differentiation grouping using 3 nanoparticles **NP1-NP3**, as established through Jackknifed analysis (Figure 8.S4b).

Table 8.1 Origin and nature of the normal, cancerous and metastatic cell lines used in this study (Color is only used to differentiate cell lines).

Human cell lines	Liver	HepG2	Cancerous
	Cervix	HeLa	Cancerous
	Testis	NT2	Cancerous
	Breast	MCF10A	Normal Immortalized
		MCF-7	Cancerous
		MDA-MB-231	Metastatic
Mouse cell lines	BALB/c mice (Breast)	CDBgo	Normal Immortalized
		TD	Cancerous

8.2.1 Detection of Differences in Cell Types. As an initial test of our method we used 4 different types of human cancer cells: HeLa (Cervical), HepG2 (Liver), NT2 (Testis) and MCF-7 (Breast). Fig. 8.2a presents the change in the fluorescence response for the nanoparticle-polymer supramolecular complexes upon addition of the different cancer cell types. Linear Discriminant Analysis (LDA) was used to statistically characterize the fluorescence changes. This analysis reduced the size of the training matrix (3 nanoparticles x 4 cell types x 6 replicates) and transformed them into canonical factors that are linear combinations of the response patterns (3 factors x 4 cell types x 6 replicates). The two canonical factors contain 96.6% and 3.3% of the variation, respectively as shown in Figure 8.2b. In this plot, each point represents the response pattern for a single cell type to the **NP-PPECO$_2$** sensor array. In the canonical fluorescence response patterns, the different cell types are clustered into four non-overlapping groups (95% level confidence ellipses, Figure 8.2b) with standard deviation of <5%. These initial results validate our ability to differentiate cancer cell types phenotypically based on their surface properties.

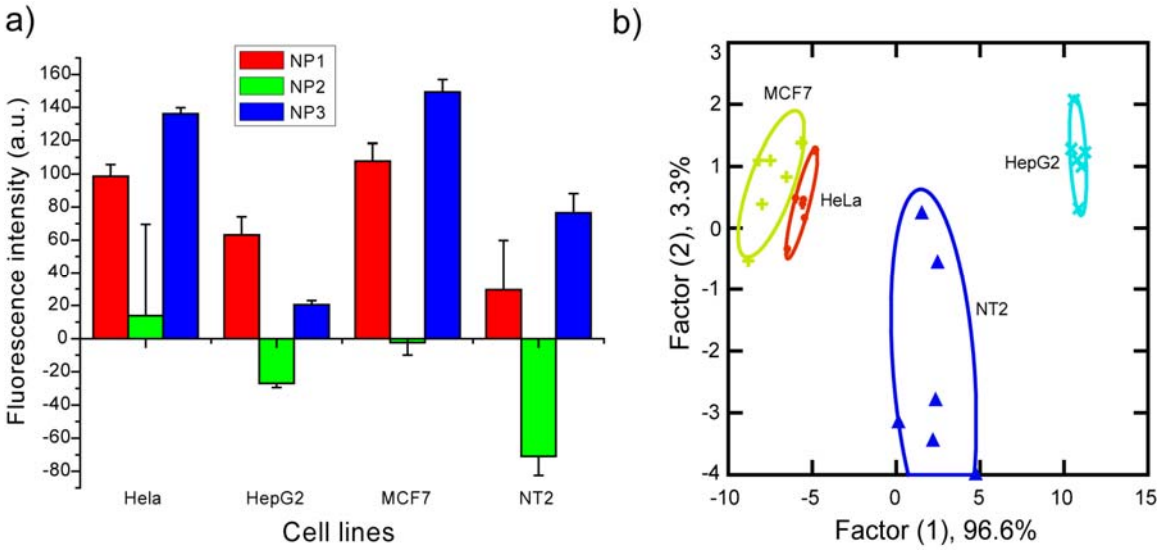

Figure 8.2 Detection of human cancerous cell lines. a) Change in fluorescence intensities ($F - F_0$) for 4 different cancer cell lines HeLa (Cervical), MCF7 (Breast), HepG2 (Liver) and NT2 (Testes) using nanoparticle-polymer supramolecular complexes. Each value is average of 6 parallel measurements. b) Canonical score plot for the two factors of simplified fluorescence response patterns obtained with **NP**–$PPECO_2$ assembly arrays against different mammalian cell types. The canonical scores were calculated by LDA for the identification of 4 cell lines.

8.2.2 Detection of Normal/Cancerous and Metastatic Cells. An important issue in cancer therapy is assessing whether tissue/cells are healthy, or either benign or metastatic tumors. We chose three different human breast cell lines to test our sensor array in this application: MCF10A a normal breast cell line, MCF7 a cancerous but non-metastatic cell line, while MDA-MB-231 is a metastatic cancer cell line. The three cell lines show differential fluorescence patterns (Figure 8.3a); LDA of their response indicates a 100% accuracy of detection (Figure 8.3b).

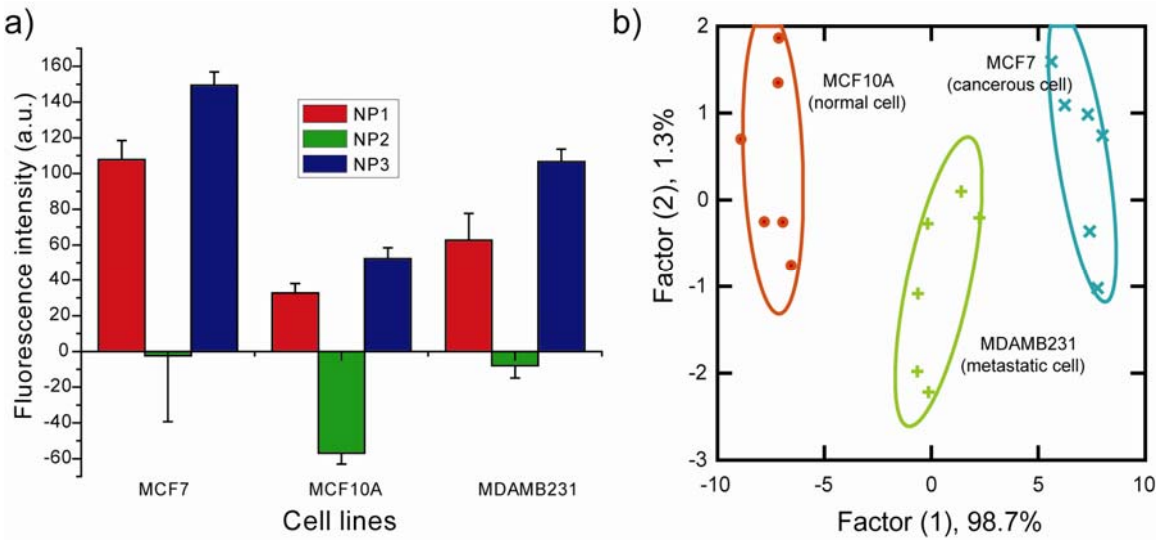

Figure 8.3 Detection of normal, cancerous and metastatic human breast cells. a) Change influorescence intensities ($F - F_0$) for 3 breast cell lines of different nature MCF10A (normal), MCF-7 (cancer) and MDA-MB231 (metastatic) using nanoparticle-polymer supramolecular complexes. Each value is average of 6 parallel measurements. b) Canonical score plot for the first two factors of simplified fluorescence response patterns obtained with **NP–PPECO$_2$** assembly arrays against different mammalian cell types.

8.2.3 Detection of Isogenic Cell Types. The above studies suggest that we can differentiate normal, cancerous and metastatic cell types with our sensor array. Each of the three cell lines, however, came from different individuals. To provide a test bed where individual-to-individual variation is not present, we used three isogenic cell lines, CDBgeo, TD, and V14 cells. Each of these isogenic cells was developed from BALB/c mice, and therefore possesses the same genotypic background. CDBgeo cells were prepared by retroviral infection with a marker gene encoding the fusion of β-galactosidase and neomycin resistance. These cells exhibit normal outgrowths when transplanted into mammary fat pads.[30] The TD cells were prepared by treating CDBgeo-cells with 10 ng/mL TGF-β for 14 days. Withdrawal for five passages resulted in a persistent epithelial to mesenchymal transformation: Tumorogenic growth resulted when transplanted. The V14 cell line was established from a primary mammary tumor arising in BALB/c-*Trp53*+/- mice. The cells lack p53 protein and form aggressive tumors that are locally

invasive in mice.[31] Figure 8.4a presents the change in fluorescence intensities of three isogenic cell types towards nanoparticle-polymer complexes. The differential response indicates that these supramolecular complexes can effectively differentiate isogenic cell types. LDA classifies the cell types into three distinct clusters with two canonical factors containing 83.0% and 17.0% of the variation, with 100% identification accuracy among these isogenic cell types (Figure 8.4b). Taken together, these studies indicate that our method rapidly and effectively differentiates cell lines based on cell type and disease state.

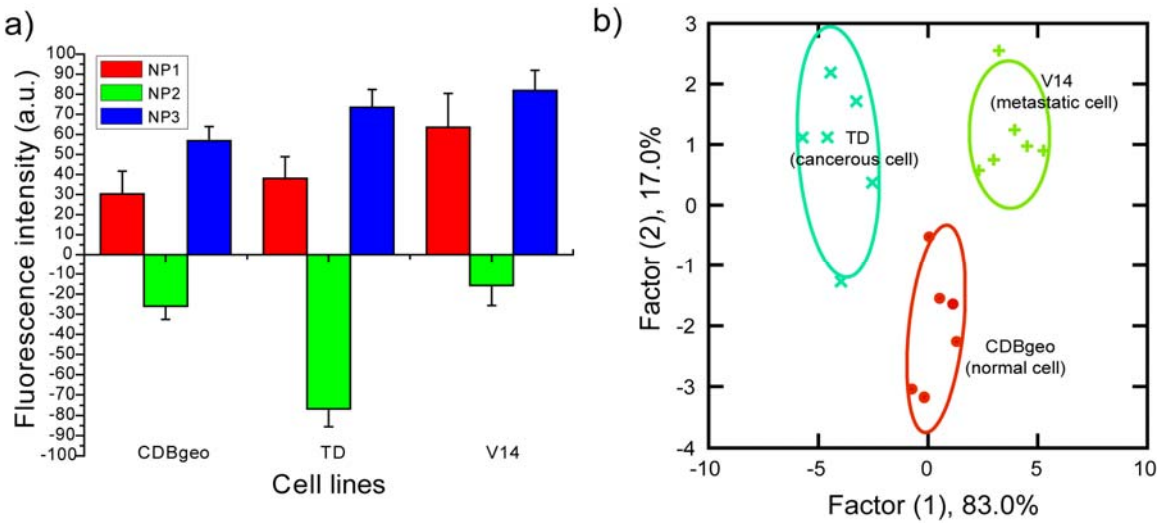

Figure 8.4 Detection of Isogenic cell types. a) Change in fluorescence intensities ($F - F_0$) for 3 cell lines of same genotype CDBgeo, TD cell and V14 using nanoparticle-polymer supramolecular complexes. Each value is average of 6 parallel measurements. b) Canonical score plot for the first two factors of simplified fluorescence response patterns obtained with **NP–PPECO$_2$** assembly arrays against different mammalian cell types.

The efficacy of our approach indicates that there are distinct phenotypic differences in the physicochemical properties of cells. One question that arises is whether there is a response that is generally indicative of whether a cell is normal or cancerous. Meta-analysis of our studies using LDA indicates that normal epithelial cell lines CDBgeo and

MCF10A were overlapping (Figure 8.5) even though both of these cell lines were isolated from mouse and human respectively. Likewise the metastatic murine (V14) and human MDMBA-231 metastatic cell lines were clustered, indicating a potential correlation between cell surface properties and disease states of cells.

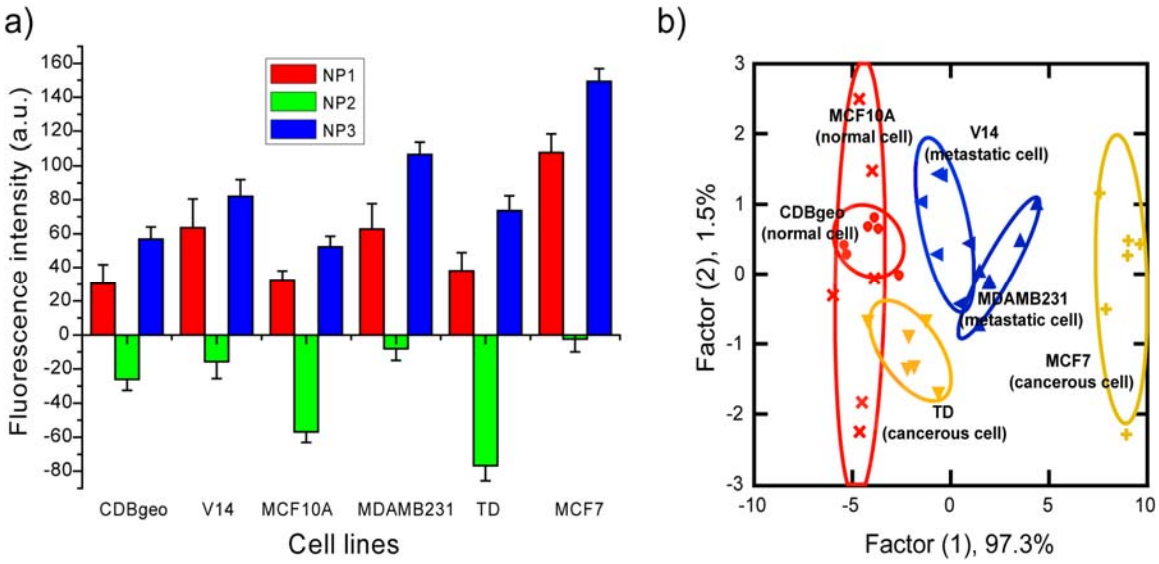

Figure 8.5 Detection of normal and cancerous cell lines. a) Changes in fluorescence intensities ($F - F_0$) of noncancerous and cancerous cell types using nanoparticle-polymer supramolecular complexes. Each value is average of 6 parallel measurements. b) Canonical score plot for the first two factors of simplified fluorescence response patterns obtained with **NP–PPECO$_2$** assembly arrays against different normal and cancerous cell types. Further differentiation was observed in the third dimension, allowing discrimination each of the species.

8.3 Conclusion

In conclusion, we have developed a rapid and effective array-based approach to differentiate between normal and cancerous cell lines. Significantly, full differentiation was achieved using only three nanoparticle-polymer dyads, indicating that a simple sensor array has ample diagnostic capacity when exposed to mammalian cells. These systems have the potential to help us understand the physical changes that occur on the surfaces of cells in various disease states. Taken together, “nose” based sensor systems

are a fundamentally new way of looking into biodiagnostic and biophysical and surface science processes involving cell surfaces.

8.4 Experimental Section

Nanoparticles[20,32] and polymers[33] were synthesized as reported previously. All the cells except MCF10A, CDBgeo, TD and V14 were grown in DMEM media supplemented with 10% FBS and 1% antibiotics in T75 flasks. NT2 cell line was obtained from Prof. R. Thomas Zoeller. CDBgeo, TD and V14 cells were grown in DMEM-F12 media supplemented with 2% ABS, 25mM HEPES, 10μg/mL insulin, 5ng/mL EGF, 15μg/mL gentamycin. Cells were washed with DPBS buffer, trypsinized with 1X trypsin and collected in the DMEM media. Fluorescence titration experiments determined the complexation between nanoparticles and PPE. Fluorescence intensity changes at 465 nm were recorded with an excitation wavelength of 430 nm. Polymer and stoichiometric amounts of **NP1-NP3**, as determined by the fluorescence titration study were diluted with phosphate buffer (5 mm, pH 7.4) to solutions with a final polymer concentration of 100 nM. Each solution (200 μL) was placed into a well on the micro plate. After incubation for 30 min, the fluorescence intensity at 465 nm was recorded with an excitation wavelength of 430 nm. Next, 100 μL of cell suspension (20,000 cells) was added to each well. After incubation for another 30 min, the fluorescence intensity at 465 nm was measured again. The fluorescence intensity before addition of the cells was subtracted from that obtained after addition of the cells to record the overall fluorescence response (DI). This process was completed for all cell lines to generate six replicates of each that was subjected to a classical linear discriminant analysis (LDA) using SYSTAT (version

11.0). The training matrix of fluorescence response patterns of NP-PPE sensor array (**NP1-NP3** = Predictors) was generated from the addition of several normal and cancerous cell lines aliquots (Cell$ = Group variable) with identical cell numbers (6 replicates) coupled with **Mahal statistics method using SYSTAT Program (version 11)**. As a result of running this program, statistical information was obtained,[34] e.g. Group frequencies and group means, discriminat functions, classification matrix such as Jackknifed classification matrix, cumulative proportion of total dispersion, canonical scores of group means, etc. The Mahalanobis distance is the distance of a case to the centroid of a group in a multidimensional space (in the current case it is two-dimension). In a blind experiment, the rates of fluorescence patterns of new case were first converted to canonical scores using discriminate functions established on training samples. Then, Mahalanobis distances of the new case to the centroid of respective groups (Normal or cancerous or metastatic cells) of training samples were calculated. The new case was assigned to the group with shortest Mahalanobis distance. This processing protocol could be automatically performed on SYSTAT 11 program. In this way, we have tested the cells blindly and have been able to assign them to specific groups.

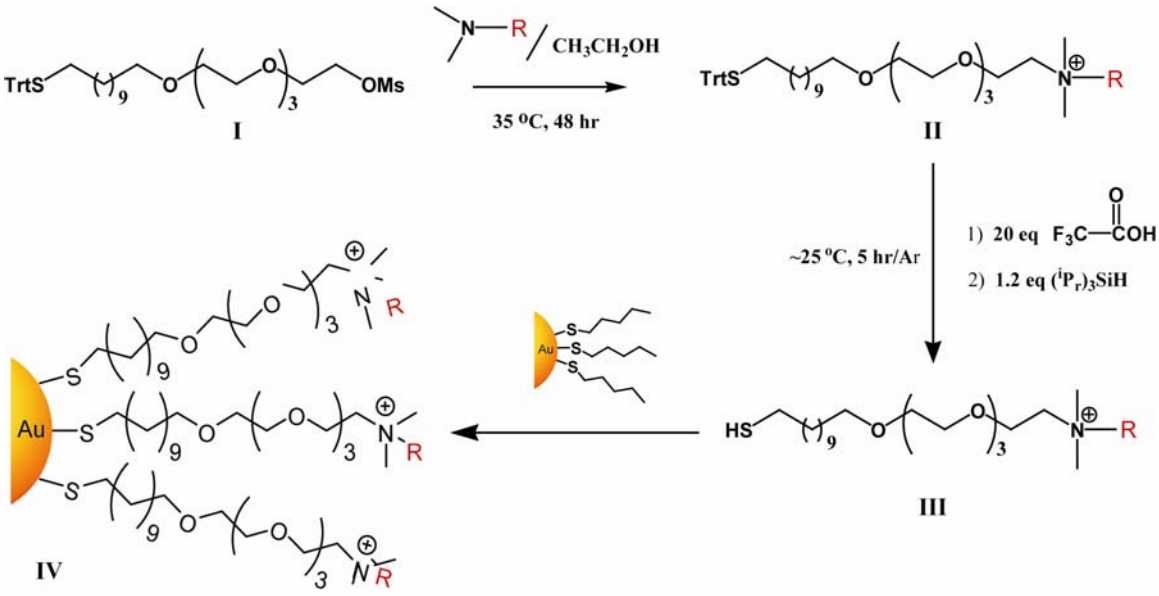

Scheme 8.S1 Synthesis of ligands[1,2,3]

General procedure: Compound **II** bearing ammonium end groups were synthesized through the reaction of 1,1,1-triphenyl-14,17,20,23-tetraoxa-2- thiapentacosan-25-yl methanesulphonate (**I**) with corresponding substituted N,N-dimethylamines during 48 h at ~35 ^{o}C. The trityl protected thiol ligand **(II)** was dissolved in dry DiChloroMethane (Methylene Chloride, DCM) and an excess of trifluoroacetic acid (TFA, ~ 20 equivalents) was added. The color of the solution was turned to yellow immediately. Subsequently, triisopropylsilane (TIPS, ~ 1.2 equivalents) was added to the reaction mixture. The reaction mixture was stirred for ~5 h under Ar condition at room temperature. The solvent and most TFA and TIPS were distilled off under reduced pressure. The pale yellow residue was further dried in high vacuum. The product (**L**) formation was quantitative and their structure was confirmed by NMR. The yields were >95%.

Compound L1: ^{1}H NMR (400MHz, $CDCl_3$, TMS): δ 3.95 (br, 2H, -OC$\underline{H_2}$-(CH_2N)-), 3.81-3.72 (m, 1H, H_{Cyclo}), 3.69-3.53 (m, 14H, -CH_2O- + -CH_2N-), 3.49 (t, 2H, -CH_2O-), 3.11 (s, 6H, -(CH_3)$_2$N-), 2.91 (s, 3H, $CH_3SO^-_3$-), 2.52 (q, 2H, -CH_2S-), 2.23 (d, 2H, H_{Cyclo}), 1.99 (d, 2H, H_{Cyclo}), 1.78-1.52 (m, 4H, -(SCH_2)C$\underline{H_2}$ + -C$\underline{H_2}$(CH_2O)-), 1.51-1.12 (m, 21H, SH + -CH2- + H_{Cyclo}).

Compound L2: ^{1}H NMR (400MHz, $CDCl_3$, TMS): δ 8.37 (d, 1H, H_{Ar}), 7.98 (d, 1H, Ar-), 7.69-7.61 (m, 3H, H_{Ar}), 7.59-7.48 (m, 1H, H_{Ar}), 4.38 (br, 2H,-NC$\underline{H_2}$-Ar), 3.76 (br, 2H, -OC$\underline{H_2}$-(CH_2N)-), 3.72-3.62 (m, 14H, -CH_2O- + -CH_2N-), 3.61-3.55 (m, 2H, -CH_2O-), 3.23 (s, 6H, -(CH_3)$_2$N-), 3.07 (s, 3H, $CH_3SO^-_3$-), 2.52 (q, 2H, -CH_2S-), 1.67-1.51 (m, 4H, -(SCH_2)C$\underline{H_2}$ + -C$\underline{H_2}$(CH_2O)-), 1.35-1.21 (m, 15H, -SH + -CH_2-).

[1] Brust, M.; Walker, M.; Bethell, D.; Schiffrin, D. J.; Whyman, R. *J. Chem. Soc., Chem. Commun.* **1994**, 801-802.
[2] Hostetler, M. J.; Templeton, A. C.; Murray, R. W. *Langmuir* **1999,** *15*, 3782-3789.
[3] C.-C. You, O. R. Miranda, B. Gider, P. S. Ghosh, I.-B. Kim, B. Erdogan, S. A. Krovi, U. H. F. Bunz, V. M. Rotello, *Nat. Nanotechnol*. **2007**, *2*, 318-323.

Compound L3: ^{1}H NMR (400MHz, $CDCl_3$, TMS): δ 3.94 (br, 2H, -OC<u>H</u>$_2$-(CH_2N)-), 3.78 (br, 1H, -OH), 3.75-3.52 (m, 16H, -CH_2O- + -CH_2N- + -C<u>H</u>$_2$-OH), 3.48 (t, 2H, -CH_2O-), 3.39-3.31 (m, 2H,-NCH_2-), 3.25 (s, 6H, -(CH_3)$_2$N-), 2.89 (s, 3H, $CH_3SO^-_3$-), 2.52 (q, 2H, -CH_2S-), 2.35-2.26 (m, 2H, -(NCH_2)C<u>H</u>$_2$-), 1.70-1.52 (m, 4H, + (SCH_2)C<u>H</u>$_2$ + -C<u>H</u>$_2$(CH_2O)-), 1.36-1.21 (m, 15H, -SH + -CH_2-).

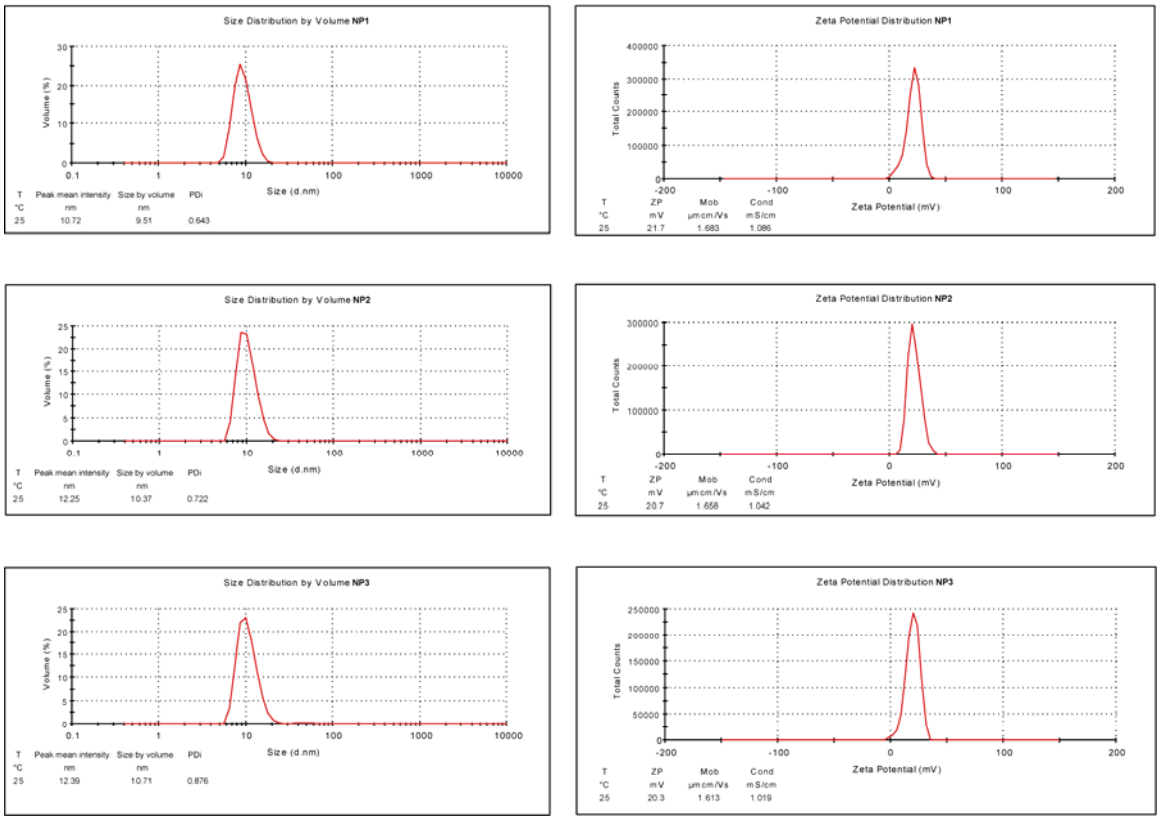

Figure 8.S1 Dynamic light scattering (DLS) and zeta potential (ZP) of **NP1**-**NP3** were measured in 5 mM phosphate buffer at pH 7.4. The overall size and charge of these cationic **NP**s were on the range of 10-12 nm and ~21 mV respectively.

Nanoparticle	Ks (10^8 M^{-1})	ΔG (KJ mol^{-1})	n
NP1	2.3	-53.1	1.9
NP2	3.7	-48.6	2.5
NP3	2.2	-53.0	0.9

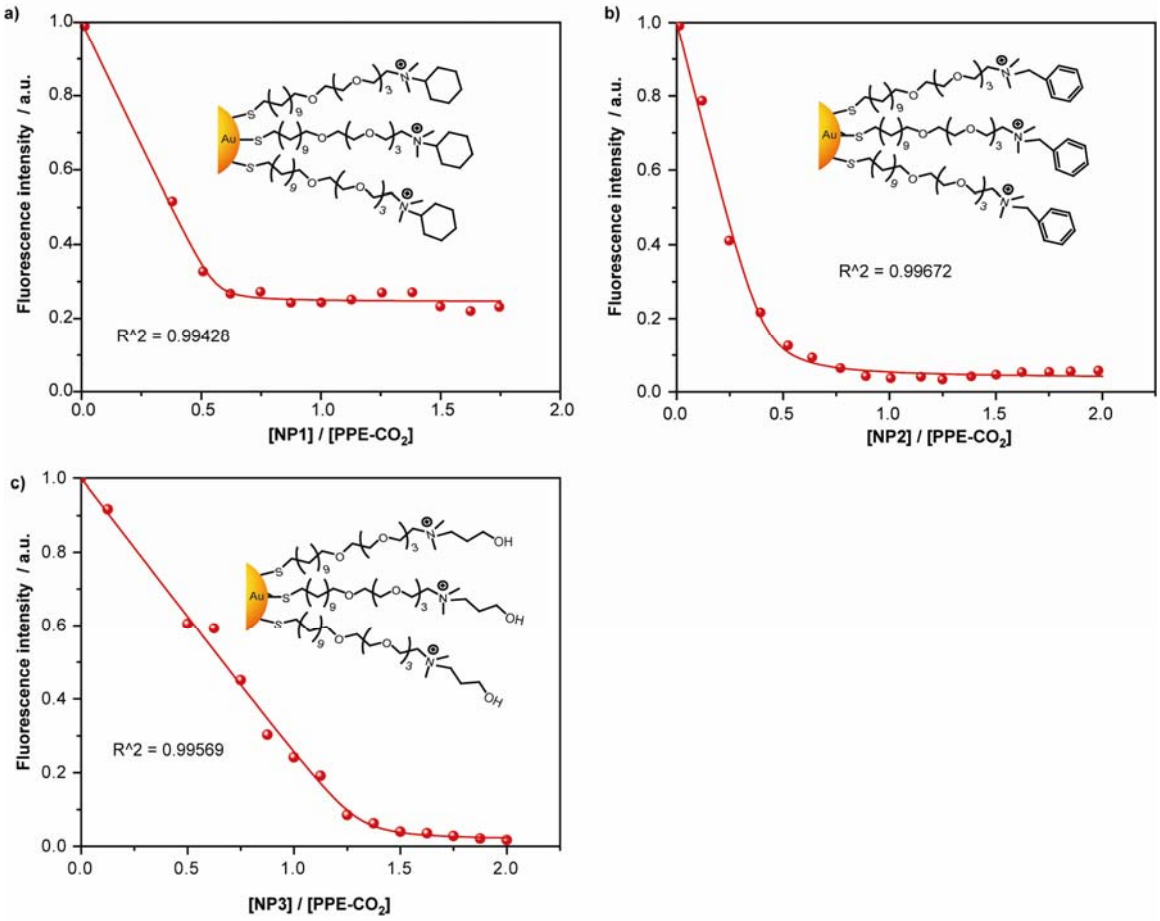

Figure 8.S2 Binding constants (log K_S), binding stoichiometries (n) between polymer **PPE-CO$_2$** and fluorescence titration curves for the complexation of **PPE-CO$_2$** (100 nM) with various cationic gold nanoparticles as showed. The intensity changes at 465 nm were followed by adding several concentrations of **NP**s with an excitation wavelength of 430 nm. The red solid lines represent the best curve-fitting.

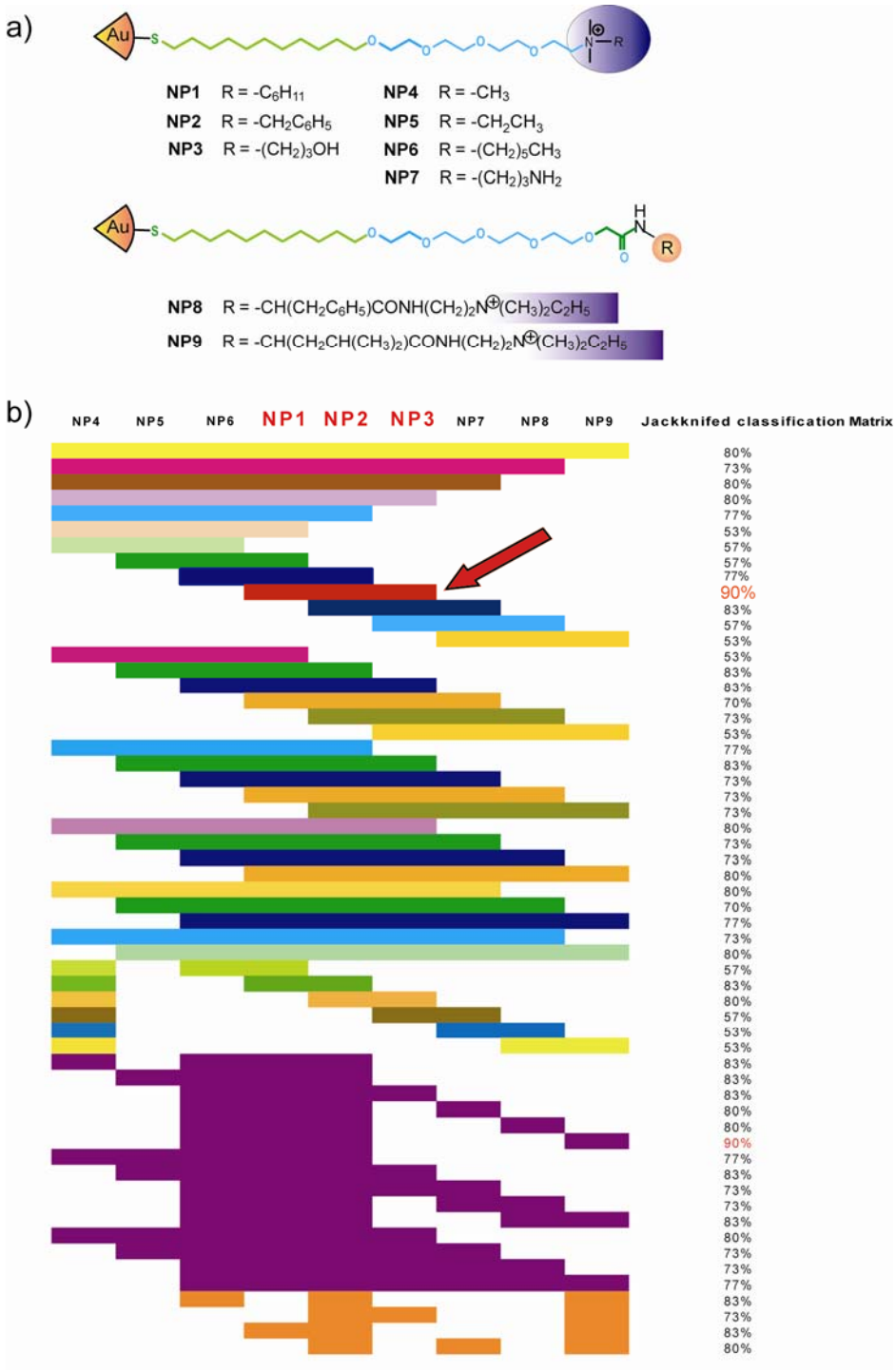

Figure 8.S3 a) Chemical structures of the nine nanoparticles screened for cell sensing. B) Jacknifed classification matrix obtained through LDA analysis for nine nanoparticles for all cell sensing studies.

Table 8.S1 Training matrix of fluorescence response patterns of **NP**-PPE sensor array (**NP1**-**NP6**) against several normal and cancerous cell lines with identical cell numbers.

Cell lines	**NP1**	**NP2**	**NP3**
HeLa	108.437	-22.619	131.272
HeLa	96.849	-32.549	135.131
HeLa	89.927	33.928	141.366
HeLa	101.968	36.883	138.971
HeLa	102.661	105.368	136.431
HeLa	91.654	-38.012	134.211
MCF7	88.523	-65.715	156.947
MCF7	114.97	26.743	137.731
MCF7	105.638	27.744	153.065
MCF7	105.96	-26.903	142.949
MCF7	117.061	17.557	155.298
MCF7	114.596	6.609	150.304
HepG2	47.544	-64.227	18.799
HepG2	66.327	-21.701	23.522
HepG2	80.899	26.59	23.866
HepG2	64.620	7.153	17.854
HepG2	62.46	26.967	19.176
HepG2	56.912	-136.285	19.934
NT2	19.087	-109.73	74.753
NT2	8.361	-123.024	74.926
NT2	73.837	-32.683	85.101
NT2	58.277	-34.835	77.39
NT2	22.529	-48.185	90.413
NT2	-5.155	-77.017	56.566

Table 8.S2 Training matrix of fluorescence response patterns of **NP**-PPE sensor array (**NP1**-**NP6**) against several normal and cancerous cell lines with identical cell numbers.

Cell lines	**NP1**	**NP2**	**NP3**
CDBgo	13.861	-24.620	51.592
CDBgo	37.105	-21.639	59.431
CDBgo	36.536	-36.333	68.922
CDBgo	44.061	-26.607	55.739
CDBgo	30.166	-17.268	56.664
CDBgo	20.477	-29.478	48.557
V14	35.127	-15.553	96.790
V14	74.667	-26.552	90.021
V14	77.513	-7.651	75.153
V14	69.386	-23.164	69.885
V14	73.883	-1.544	77.78
V14	50.385	-19.679	82.247
TD	39.278	-86.639	85.797
TD	39.432	-90.846	71.702
TD	36.815	-82.081	75.508
TD	56.404	-74.041	75.384
TD	32.872	-62.026	74.187
TD	23.431	-64.688	58.341

Table 8.S3 Training matrix of fluorescence response patterns of **NP**-PPE sensor array (**NP1**-**NP6**) against several normal and cancerous cell lines with identical cell numbers.

Cell lines	**NP1**	**NP2**	**NP3**
MCF7	88.523	-65.715	156.947
MCF7	114.97	26.743	137.731
MCF7	105.638	27.744	153.065
MCF7	105.96	-26.903	142.949
MCF7	117.061	17.557	155.298
MCF7	114.596	6.609	150.304
MCF10A	36.403	-133.662	52.088
MCF10A	38.125	42.26	50.506
MCF10A	27.901	-41.355	60.088
MCF10A	37.498	8.538	56.473
MCF10A	25.869	-73.426	41.947
MCF10A	30.117	-144.145	52.737
MDMB231	49.212	-3.683	101.597
MDMB231	78.188	0.156	111.938
MDMB231	52.489	-40.314	100.431
MDMB231	49.228	-5.52	105.549
MDMB231	64.227	-23.985	102.052

Table 8.S4 Training matrix of fluorescence response patterns of NP-PPE sensor array (**NP1**-**NP6**) against several normal and cancerous cell lines with identical cell numbers.

Cell lines	**NP1**	**NP2**	**NP3**
CDBgo	13.861	-24.620	51.592
CDBgo	37.105	-21.639	59.431
CDBgo	36.536	-36.333	68.922
CDBgo	44.061	-26.607	55.739
CDBgo	30.166	-17.268	56.664
CDBgo	20.477	-29.478	48.557
V14	35.127	-15.553	96.790
V14	74.667	-26.552	90.021
V14	77.513	-7.651	75.153
V14	69.386	-23.164	69.885
V14	73.883	-1.544	77.78
V14	50.385	-19.679	82.247
MCF10A	36.403	-133.662	52.088
MCF10A	38.125	42.26	50.506
MCF10A	27.901	-41.355	60.088
MCF10A	37.498	8.538	56.473
MCF10A	25.869	-73.426	41.947
MCF10A	30.117	-144.145	52.737
MDMB231	49.212	-3.683	101.597
MDMB231	78.1889	0.156	111.938
MDMB231	52.489	-40.314	100.431
MDMB231	49.228	-5.52	105.549
MDMB231	64.227	-23.985	102.052
MDMB231	82.855	25.657	118.102
TD	39.278	-86.639	85.797
TD	39.432	-90.846	71.702
TD	36.815	-82.081	75.508
TD	56.404	-74.041	75.384
TD	32.872	-62.026	74.187
TD	23.431	-64.688	58.341
MCF7	88.523	-65.715	156.947
MCF7	114.97	26.743	137.731
MCF7	105.638	27.744	153.065
MCF7	105.96	-26.903	142.949
MCF7	117.061	17.557	155.298
MCF7	114.596	6.609	150.304
CDBgo	13.861	-24.62	51.592
CDBgo	37.105	-21.639	59.431
CDBgo	36.536	-36.333	68.922
CDBgo	44.061	-26.607	55.739
CDBgo	30.166	-17.268	56.664
CDBgo	20.477	-29.478	48.557

8.5 References

1. Srinivas, P. R.; Kramer, B. S.; Srivastava, S. *Lancet Oncol.* **2001**, 2, 698.

2. Pantel, K.; Brakenhoff, R. H.; Brandt, B. *Nat. Rev. Cancer* **2008**, 8, 329.

3. Jen, J.; Wu, L.; Sidransky, D. *Ann N Y Acad Sci.* **2000**, 906, 8.

4. Skvara, H.; Teban, L.; Fiebiger, M.; Binder, M.; Kittler, H. *Arch Dermatol*. 2005, **141**, 155.

5. Gao, X.; Cui, Y.; Levenson, R. M.; Chung, L. W. K.; Nie, S. *Nat. Biotechnol.* **2004**, 22, 969.

6. Borrebaeck, C. *Expert Opin. Biol. Ther.* **2006**, 6, 838.

7. Ward, A .M.; Catto, J. W. F.; Hamdy, F. C. *Ann. Clin. Biochem.* **2001**, 38, 633.

8. a) Chou, S. F.; Hsu, W.L.; Hwang, J. M.; Chen, C. Y. *Biosens. Bioelectron.* **2004**, 19, 999. b) Alivisatos, P. *Nat. Biotechnol.* **2004**, 22, 47.

9. a) Soukka, T.; Paukkunen, J.; Harma, H.; Lonnberg, S.; Lindroos, H.; Lovgren, T. *Clin. Chem.* **2001**, 47, 1269. b) Nam, J. M.; Thaxton, C. S.; Mirkin, C. A. *Science* **2003**, 301, 1884. c) Wu, G.; Datar, R. H.; Hansen, K. M.; Thundat, T.; Cote, R. J.; Majumdar, A. *Nat. Biotechnol.* **2001**, 19, 856. d) Chen, R. J.; Bangsaruntip, S.; Drouvalakis, K. A.; Kam, N. W. S.; Shim, M.; Li, Y.; Kim, W.; Utz, P. J.; Dai, H. *Proc. Natl. Acad. Sci. USA* **2003**, 100, 4984.

10. Chen, R. J.; Choi, H. C.; Bangsaruntip, S.; Yenilmez, E.; Tang, X.; Wang, Q.; Chang, Y. L.; Dai, H. *J. Am. Chem. Soc.* **2004**, 126, 1563.

11. a) Wang, W. U.; Chen, C.; Lin, K. H.; Fang, Y.; Lieber, C. M. *Proc. Natl. Acad. Sci. USA* **2005**, 102, 3208. b) Cui, Y.; Wei, Q.; Park, H.; Lieber, C. M. *Science* **2001**, 293, 1289.

12. Campagnolo, C.; Meyers, K. J.; Ryan, T.; Atkinson, R. C.; Chen, Y. T.; Scanlan, M. J.; Ritter, G.; Old, L. J.; Batt, C. A. *J. Biochem. Biophys.* **2004**, 61, 283.

13. Wingren, C.; Borrebaeck, C. A. *Curr. Opin. Biotech.* **2008**, 18, 55.

14. Sanchez-Carbayo, M. *Clin. Chem.* **2006**, 52, 1651.

15. Singer, S. J.; Nicolson, G. L. *Science* **1972**, 175, 720.

16. Alberts, B.; Johnson, A.; Lewis, J. (**2002**) in *Molecular Biology of the Cell* (4th ed.).

17. Lavigne, J. L.; Anslyn, E. V. *Angew. Chem. Int. Ed.* **2001**, 40, 3118.

18. Albert, K. J.; Lewis, N. S.; Schauer, C. L.; Sotzing, G. A.; Stitzel, S. E.; Vaid, T. P.; Walt, D. R. *Chem. Rev.* **2000**, 100, 2595.

25. Wright, A. T.; Anslyn, E. V. *Chem. Soc. Rev.* **2006**, 35, 14.

20. Lee, J. W.; Lee, J. S.; Chang, Y. T. *Angew. Chem. Int. Ed.* **2006**, 45, 6485.

21. Rakow, N. A.; Suslick, K. S. *Nature* **2000**, 406, 710.

22. Greene, N. T.; Shimizu, K. D. *J. Am. Chem. Soc.* **2005**, 127, 5695.

23. a) Folmer-Andersen, J. F.; Kitamura, M.; Anslyn, E. V. *J. Am. Chem. Soc.* **2006**, 128, 5652. b) Buryak, A.; Severin, K. *J. Am. Chem. Soc.* **2005**, 127, 3700.

24. Lee, J. W.; Lee, J. S.; Chang, Y. T. *Angew. Chem., Int. Ed.* **2006**, 45, 6485.

25. You, C. C.; Miranda, O. R.; Gider, B.; Ghosh, P. S.; Kim, I. B.; Erdogan, B.; Krovi, S.A.;, Bunz, U. F. H.; Rotello, V. M. *Nat Nanotechnol* **2007**, 2, 318.

26. Phillips, R. L.; Miranda, O. R.; You, C. C.; Rotello, V. M.; Bunz, U. H. *Angew. Chem. Int. Ed. Engl.* **2008**, 47, 2590.

27. Kim, I.B.; Erdogan, B.; Wilson, J. N.; Bunz, U. H. F. *Chem. Eur. J.* **2004**. 10, 6247.

28. Zhou, Q.; Swager, T. M. *J. Am. Chem. Soc.* **1995**, 117, 12593.

29. Phillips, R. L.; Miranda, O. R.; Mortenson, D. E.; Subramani, C.; Rotello, V. M.; Bunz, U. H. F. *Soft Matter* **2009,** 5, 607.

30. Deugnier, M. A.; Faraldo, M. M.; Teuliere, J.; Thiery, J. P.; Medina, D.; Glukhova, M.A. *Dev Biol* **2006**, 293, 414.

31. Blackburn, A. C.; McLary, S. C.; Naeem, R.; Luszcz, J.; Stockton, D. W.; Donehower, L. A.; Mohammed, M.; Mailhes, J. B.; Soferr, T.; Naber, S. P.; Otis, C. N.; Jerry, D. J. *Cancer Res* **2004**, 64, 5140.

32. a) Brust, M.; Walker, M.; Bethell, D.; Schiffrin, D. J.; Whyman, R. *J. Chem. Soc., Chem. Commun.* **1994**, 801. b) Hostetler, M. J.; Templeton, A. C.; Murray, R. W. *Langmuir* **1998**, 15, 3782.

33. Kim, I. B.; Dunkhorst, A.; Gilbert, J.; Bunz, U. H. F. *Macromolecules* **2005**, 38, 4560.

34. Engelman, L. (**2004**) Discriminant Analysis. In Systat 11.0, Statistics, SYSTAT Software, Inc., i301-i358.

BIBLIOGRAPHY

1. McPherson, R. A.; Pincus, M. R. Henry's Clinical Diagnosis and Management by Laboratory Methods, *21st Edition, Elsevier*, Philadelphia, **2007**.

2. Laure, F.; Rouzioux, C.; Veber, F.; Jacomet, C.; Courgnaud, V.; Blanche, S.; Burgard,M.; Griscelli, C.; Brechot, C. *Lancet* **1988**, 332, 538.

3. Deisingh, A. K.; Thompson, M. *Analyst* **2002**, 127, 567.

4. Peer, D.; Karp, J.; Hong, S.; Farokhzad, O.; Margalit, R.; Langer, R. *Nature Nanotech.* **2007**, *2*, 751.

5. Gao, X.; Cui, Y.; Levenson, R. M.; Chung, L. W. K.; Nie, S. *Nat. Biotechnol.* **2004**, *22*, 969.

6. Verma, A.; Rotello, V. M. *Chem. Commun.* **2005**, 303.

7. Ferrari, M. *Nat. Rev. Cancer* **2005**, *5*, 161.

8. De, M.; Ghosh, P. S.; Rotello, V. M. *Adv. Mater.* **2008**, *20*, 4225.

9. Euliss, L. E.; DuPont, J. A.; Gratton, S.; DeSimone, J. *Chem. Soc. Rev.* **2006,** *35*, 1095.

10. Brust, M.; Walker, M.; Bethell, D.; Schiffrin, D. J.; Whyman, R. *J. Chem. Soc. Chem. Commun.* **1994**, 801.

11. Hostetler, M. J.; Wingate, J. E.; Zhong, C. -J.; Harris, E.; Vachet, R. W.; Clark, M. R.; Londono, J. D.; Green, S. J.; Stokes, J. J.; Wignall, G. D.; Glish, G. L.; Porter, M. D.; Evans, N. D.; Murray, R. W. *Langmuir* **1998**, 14, 17.

12. Kanaras, A. G.; Kamounah, F. S.; Schaumburg, K.; Kiely, C. J.; Brust, M. *Chem. Commun.* **2002**, 2294.

13. Fink, J.; Kiely, C. J.; Bethell D.; Schiffrin, D. J. *Chem. Mater.* **1998**, 10, 922.

14. Templeton, A. C.; Wuelfing, M. P.; Murray, R. W. *Acc. Chem. Res.* **2000**, *33*, 27.

15. Rothrock, A. R.; Donkers, R. L.; Schoenfisch, M. H. *J. Am. Chem. Soc.* **2005**, *127*, 9362.

16. Fan, H. Y.; Chen, Z.; Brinker, C. J.; Clawson, J.; Alam, T., *J. Am. Chem. Soc.* **2005**, *127*, 13746.

17. Fan, H. Y.; Leve, E. W.; Scullin, C.; Gabaldon, J.; Tallant, D.; Bunge, S.; Boyle, T.; Wilson, M. C.; Brinker, C. J., *Nano Lett.* **2005**, *5*, 645.

18. Jain, P. K.; Lee, K. S.; El-Sayed I. H.; El-Sayed, M. A. *J. Phys. Chem. B* **2006**, 110, 7238.

19. Mie, G. *Ann. Phys.* **1908**, 25, 377.

20. Kelly, K. L.; Coronado, E.; Zhao, E. L.; Schatz, G. C. *J. Phys. Chem. B* **2003**, 107, 668.

21. El-Sayed, E.; El-Sayed, M A. *Chem. Soc. Rev.* **2006**, 35, 209.

22. Su, K.-H.; Wei, Q.-H.; Zhang, X.; Mock, J. J.; Smith, D. R.; Schultz, S. *Nano Lett.* **2003**, 3, 1087.

23. Link, S.; Wang, Z. L.; El-Sayed, M. A. *J. Phys. Chem. B* **1999**, 103, 3529.

24. Liu, X.; Atwater, M.; Wang, J.; Huo, Q. *Colloid Surf. B: Biointerfaces* **2006**, 58, 3.

25. Jain, P. K.; El-Sayed, I. H.; El-Sayed, M. A. *Today* **2007**, 2, 18.

26. Zheng, J.; Zhang C.; Dickson, R. M. *Phys. Rev. Lett.* **2004**, 93, 077402.

27. van Dijk, M. A.; Lippitz M.; Orrit, M. *Acc. Chem. Res.* **2005**, 38, 594.

28. Lakowicz, J. R. *Anal. Biochem.* **2005**, 337, 171.

29. Sapsford, K. E.; Berti, L.; Medintz, I. L. *Angew. Chem. Int. Ed.* **2006**, 45, 4562.

30. Dulkeith, E.; Morteani, A. C.; Niedereichholz, T.; Klar, T. A.; Feldmann, J.; Levi, S. A.; van Veggel, F. C. J. M.; Reinhoudt, D. N.; Möller, M.; Gittins, D. I. *Phys. Rev. Lett.* **2002**, 89, 203002.

31. Thomas, K. G.; Kamat, P. V. *Acc. Chem. Res.* **2003**, 36, 888.

32. Kamat, P. V.; Barazzouk, S.; Hotchandani, S. *Angew. Chem. Int. Ed.* **2002**, 41, 2764.

33. Quinn, B. M.; Liljeroth, P.; Ruiz, V.; Laaksonen, T.; Kontturi, K. *J. Am. Chem. Soc.* 2003, **125**, 6644-6645

34. Antonello, S.; Holm, A. H.; Instuli, E.; Maran, F. *J. Am. Chem. Soc.* **2007**, 129, 9836.

35. Schmid, G.; Simon, U. *Chem. Commun.* **2005**, 697.

36. Niemeyer, C. M. *Angew. Chem., Int. Ed.* **2001**, *40*, 4128.

37. Sastry, M.; Rao, M.; Ganesh, K. N. *Acc. Chem. Res.* **2002**, *35*, 847.

38. Katz, E.; Willner, I. *Angew. Chem., Int. Ed.* **2004**, *43*, 6042.

39. Pellegrino, T.; Kudera, S.; Liedl, T.; Javier, A. M.; Manna, L.; Parak, W. J. *Small* **2005**, *1*, 48.

40. You, C. C.; De, M.; Rotello, V. M. *Curr. Opin. Chem. Biol.* **2005**, *9*, 639.

41. Caruso, F. *Adv. Matter.* **2001,** *13*, 11.

42. Naka, K.; Itoh, H.; Tampo, Y.; Chujo, Y. *Langmuir* **2003,** *19*, 5546.

43. Ghosh, S. S.; Kao, P. M.; McCue, A.W.; Chappelle, H. L. *Bioconjugate Chem.* **1990**, *1*, 71.

44. Droz, E.; Taborelli, M.; Descouts, P.; Wells, T. N. C.; Werlen, R. C. *J. Vac. Sci. Technol. B* **1996**, *14*, 1422.

45. Wang, J. *Anal. Chim. Acta* **2003**, *500*, 247.

46. McIntosh, C. M.; Esposito, E. A.; Boal, A. K.; Simard, J. M.; Martin, C. T.; Rotello, V. M. *J. Am. Chem. Soc.* **2001**, *123*, 7626.

47. Mirkin, C. A.; Letsinger, R. L.; Mucic, R. C.; Storhoff, J. J. *Nature* **1996**, *382*, 607.

48. Verma, A.; Simard, J.M.; Worrall, J.W.E.; Rotello, V.M. *J. Am. Chem. Soc.* **2004**, 126, 13987.

49. Ghosh, P. S.; Verma, A.; Rotello, V. M. *Chem. Commun.* **2007**, 2796.

50. Zhou, Q.; Swager, T. M. *J. Am. Chem. Soc*. **1995**, *117*, 12593.

51. Swager, T. M. *Acc. Chem. Res.* **1998**, *31*, 201.

52. Erdogan, B.; Wilson, J. N.; Bunz, U. H. F. *Macromolecules* **2002**; *35*, 7863.

53. Disney, M. D.; Zheng, J.; Swager, T. M., Seeberger, P. H. *J. Am. Chem. Soc*. **2004**, *126*, 13343.

54. Kim, I. B.; Dunkhorst, A.; Bunz, U. H. F. *Langmuir* **2005**, *21*, 7985.

55. Wilson, J. N.; Wang, Y.; Lavigne, J. J.; Bunz, U. H. F. *Chem. Comm*. **2003**, 1626.

56. Thomas, S. W.; Joly, G. D.; Swager, T. M. *Chem. Rev*. **2007,** *107*, 1339.

57. Chen, L.; McBranch D. W.; Wang, H. L.; Helgeson, R.; Wudl, F.; Whitten, D. G. *Proc. Natl. Acad. Sci, U. S. A*. **1999**, *96*, 12287.

58. Achutyan, K. E.; Bergstedt, T. S.; Jones, R. M.; Chen, L.; Kumaraswamy, S.; Kushon, S. A.; Lu, L.; Ley, K. D.; McBranch, D.; Mukundan, H.; Rininsland, F.; Shi, X.; Xia, W.; Whitten, D. G. *J. Mater. Chem.* **2005**, *15*, 2648.

59. Liu, B.; Bazan, G. C. *Proc. Natl. Acad. Sci, U. S. A*. **2005**, *102*, 589.

60. Song, X.; Wang, H. L.; Shi, J.; Park, J. W.; Swanson, B. I. *Chem. Mater*. **2002**, *14*, 2342.

61. Liu, B.; Bazan, G. C. *Chem. Mater.* **2004**, *16*, 4467.

62. Wang, D.; Gong, X.; Heeger, P. S.; Rininsland, F.; Bazan, G. C.; Heeger, A. J. *Proc. Natl. Acad. Sci, U. S. A.* **2002**, *99*, 49.

63. Pinto, M. T.; Schanze, K. S. *Proc. Natl. Acad. Sci, U. S. A.* **2004**, *101*, 7505.

64. Kumaraswamy, S.; Bergstedt, T.; Shi, X.; Rininsland, F.; Kushon, S. A.; Xia, W.; Ley, K. D.; Achyuthan, K.; McBranch, D.; Whitten, D. *Proc. Natl. Acad. Sci. U. S. A.* **2004**, *101*, 7511.

65. Wosnick, J. H.; Mello, C. M.; Swager, T. M. *J. Am. Chem. Soc*. **2005**, *127*, 3400.

66. Kushon, S. A.; Ley, K. D.; Bradford, K.; Jones, R. M.; McBranch, D.; Whitten, D. *Langmuir* **2002**, *18*, 7246.

67. Gaylord, B. S.; Heeger, A. J.; Bazan, G. C. *J. Am. Chem. Soc*. **2003**, *125*, 896.

68. Rininsland, F.; Stankewicz, C.; Weatherford, W.; McBranch, D. *BMC Biotech*. **2005**, *5*, 1.

69. Rininsland, F.; Xia, W.; Whittenburg, S.; Shi, X.; Stankewicz, C.; Achyuthan, K.; McBranch, D.; Whitten, D. *Proc. Natl. Acad. Sci, U. S. A.* **2004**, *101*, 15295.

70. Nilsson, K. P.; Inganas, O. *Macromolecules*, **2004**, *37*, 9109.

71. Nilsson, K. P.; Herland, A.; Hammarstrom, P.; Inganas, O. *Biochemistry* **2005**, *44*, 3718.

72. Gaylord, B. S.; Heeger, A. J.; Bazan, G. C. *Proc. Natl. Acad. Sci, U. S. A.* **2002**, *99*, 10954.

73. Wang, S.; Liu, B.; Gaylord, B. S.; Bazan, G. C. *Adv. Func. Mat*. **2003**,*13*, 463.

74. Bera-Aberam, M.; Ho, H. A.; Leclerc, M. *Tetrahedron* **2004**, *60*, 11169.

75. Dore, K.; Dubus, S.; Ho, H. A.; Levesque, I.; Brunette, M.; Corbeil, G.; Boissinot, M. ; Boivin, G. ; Bergeron, M. G. ; Boudreau, D.; Leclerc, M. *J. Am. Chem. Soc*. **2004**, *126*, 4240.

76. Fan, C.; Plaxco, K. W.; Heeger, A. J. *J. Am. Chem. Soc*. **2002**, *124*, 5642.

77. Mammen, M.; Choi, S. K.; Whitesides, G. M. *Angew. Chem. Int. Ed*. **1998**, *37*, 2755.

78. Kiessling, L. L.; Pohl N. L. *Chemistry & Biology* **1996**, *3*, 71.

79. Kiessling, L. L.; Gestwicki, J. E.; Strong, L. E. *Current Opinion Chem. Biol.* **2000**, *4*, 696.

80. Dieck, H. A.; Heck, R. F. *J. Organomet. Chem.* **1975**, 93, 259.

81. Cassar, I. *J. Organomet. Chem.* **1975**, 93, 253.

82. Sonogashira, K.; Tohda, Y.; Hagihara, N. *Tetrahedron Lett.* **1975**, 16, 4467.

83. Norton, N. N. 'Biomedical sensors: Fundamentals and Applications, ed. N. M. Norton, Noyes Publications, Inc., **1982**, pp.1-44.

84. Clark, L. C. Jr.; Lyons, C. *Ann. NY Acad. Sci*. **1962**, 102, 29.

85. Wei, H.; Li, B.; Li, J.; Wang, E.; Dong, S. *Chem. Comm.* **2007**, 3735.

86. Dubertret, B.; Calame, M.; Libchaber, A. J. *Nat. Biotechnol.* **2001**, *19*, 365.

87. Xiao, Y.; Patolsky, F.; Katz, E.; Hainfeld, J.F.; Willner, I. *Science* **2003**, *299*, 1877.

88. Nam, J .M.; Stoeva, S. I.; Mirkin, C. A. *J. Am. Chem. Soc.* **2004**, *126*, 5932.

89. Astuti, Y.; Palomares, E.; Haque, S. A.; Durrant, J. R. *J. Am. Chem. Soc.* **2005**, *127*, 15120.

90. Nam, J. M.; Thaxton, C. S.; Mirkin, C. A. *Science* **2003**, *301*, 1884.

91. Stoeva, S. I.; Lee, J. S.; Thaxton, S. S.; Mirkin, C. A. *Angew. Chem. Int. Ed.* **2006**, *45*, 3303.

92. Lavigne, J. J.; Anslyn, E. V. *Angew. Chem. Int. Ed*. **2001**, *40*, 3118.

93. Goodey, A.; Lavigne, J. J.; Savoy, S. M.; Rodriguez, M. D.; Curey, T.; Tsao, A.; Simmons, G.; Wright, J.; Yoo, S. J.; Sohn, Y.; Ansyln, E. V.; Shear, J. B.; Neikirk, D. P.; McDevitt, J. T. *J. Am. Chem. Soc*. **2001**, *123*, 2559.

94. Wiskur, S. L.; Floriano, P. N., Anslyn, E. V.; McDevitt, J. T. *Angew. Chem. Int. Ed*. **2003**, *42*, 2070.

95. Lavigne, J. J.; Savoy, S. M.; Clevenger, M. B.; Ritchie, J. E.; McDoniel, B.; Yoo, S. J.; Anslyn, E. V.; McDevitt, J. T.; Shear, J. B.; Neikirk, D. P. *J. Am. Chem. Soc*. **1998**, *120*, 6429.

96. Curey, T. E.; Goodey, A.; Tsao, A.; Lavigne, J. J.; Sohn, Y.; McDevitt, J. T.; Anslyn, E. V.; Neikirk, D.; Shear, J. B. *Anal. Biochem*. **2001**, *293*, 178.

97. McCleskey, S. C.; Griffin, M. J.; Schneider, S. E.; McDevitt, J. T.; Anslyn, E. V. *J. Am. Chem. Soc*. **2003**, *125*, 1114.

98. Lee, J. W.; Lee, J. S.; Kang, M.; Su, A. I.; Chang, Y. T. *Chem. Eur. J.* **2006**, *12*, 5691.

99. Rakow, N. A.; Suslick, K. S. *Nature* **2000**, *406*, 710.

100. Greene, N. T.; Shimizu, K. D. *J. Am. Chem. Soc.* **2005**, *127*, 5695.

101. Folmer-Andersen, J. F.; Kitamura M.; Anslyn E. V. *J. Am. Chem. Soc.* **2006**, *128*, 5652.

102. Buryak, A.; Severin, K. *J. Am. Chem. Soc.* **2005**, *127*, 3700.

103. Wright, A. T.; Anslyn, E. V. *Chem. Soc. Rev.* **2006**, 35, 14.

104. Lee, J. W.; Lee, J.-S.; Chang, Y.-T. *Angew. Chem. Int. Ed.* **2006**, *45*, 6485.

105. Daniels, M. J.; Wang, Y.; Lee, M.-Y.; Venkitaraman, A. R. *Science* **2004**, *306*, 876.

106. Ross, J. S.;Fletcher, J. A. *Stem Cells* **1998**, *16*, 413.

107. Haab, B. B. *Curr. Opin. Biotech.* **2006**, *17*, 415.

108. Baldini, L.; Wilson, A. J.; Hong, J.; Hamilton, A. D. *J. Am. Chem. Soc.* **2004**, *126*, 5656.

109. Zhou, H.; Baldini, L.; Hong, J.; Wilson, A. J.; Hamilton, A. D. *J. Am. Chem. Soc.* **2006**, *128*, 2421.

110. Wright, A. T.; Griffin, M. J.; Zhong, Z.; McCleskey, S. C.; Anslyn, E. V.; McDevitt, J. T. *Angew. Chem. Int. Ed.* **2005**, *44*, 6375.

111. Sandanaraj, B. S., Demont, R., Aathimanikandan, S. V., Savariar, E. N., Thayumanavan, S. *J. Am. Chem. Soc.* **2006**, *128*, 10686.

112. Sandanaraj, B. S., Demont, R., Thayumanavan, S. *J. Am. Chem. Soc.* **2007**, *129*, 3506.

113. Sutter, J. M.; Jurs, P. C. *Anal. Chem.* **1997**, *69*, 856.

114. Shaffer, R. E.; Rose-Pehrssen, S. L.; McGill, R. A. *Anal. Chim. Acta* **1999**, *384*, 305.

115. Shaffer, R. E.; Rose-Pehrssen, S. L *Anal. Chem.* **1999**, *71*, 4263.

116. Brown, R. G., "Introduction to Random Signal Analysis and Kalman Filtering", John Wiley & Sons, Inc., New York, **1983**, pp. 165-169.

117. *SYSTAT11.0*, SystatSoftware, Richmond, CA 94804, USA, **2004**.

118. Sih, B. C.; Wolf, M. O. *Chem. Commun.* **2005**, 3375.

119. Fan, C. H.; Wang, S.; Hong, J. W.; Bazan, G. C.; Plaxco, K. W.; Heeger, A. J. *Proc. Nat. Acad. Sci.* **2003**, 100, 6297.

120. Brust, M.; Bethell, D.; Schiffrin, D. J.; Kiely, K. J. *Adv. Mater.* **1995**, 7, 795; Advincula, R. C. *Dalton Trans.* **2006**, 2778.

121. Stern, O.; Volmer, M. *Phys. Zeitschrift* **1919**, 20**,** 183.

122. Swager, T. M.; Zhou, Q. *J. Am. Chem. Soc.* **1995**, 117, 12593.

123. Lee, J. S.; Seferos, D. S.; Giljohann, D. A.; Mirkin, C. A. *J. Am. Chem. Soc.* **2008**, 130, 5430.

124. Simard, J.; Briggs, C.; Boal, A. K.; Rotello, V. M. *Chem. Commun.* **2000**, 1943.

125. Daniel, M. C.; Astruc, D. *Chem. Rev.* **2004**, 104, 293.

126. You, C. C.; Miranda, O. R.; Gider, B.; Ghosh, P. S.; Kim, I. B.; Erdogan, B.; Krovi, S. A.; Bunz, U. H. F.; Rotello, V. M. *Nature Nanotechnol.* **2007**, 2, 318.

127. Phillips, R. L.; Miranda, O. R.; You, C. C.; Rotello, V. M., Bunz, U. H. F. *Angew. Chem. Int. Ed.* **2008**, 47, 2590.

128. Bajaj, A.; Miranda, O. R.; Kim, I.-B.; Phillips, R. L.; Jerry, D. J.; Bunz, U. H. F.; Rotello, V. M. *Proc. Nat. Acad. Sci. (USA)* **2009**, 106, 10912.

129. Kim, I. B.; Phillips, R.; Bunz, U. H. F. *Macromolecules* **2007**, 40, 5290.

130. Bunz, U. H. F. *Chem. Rev*. **2000**, 100, 1605.

131. You, C. C.; De, M.; Han, G.; Rotello, V. M. *J. Am. Chem. Soc*. **2005**, 127, 12873.

132. Wang, J.; Wang, D. L.; Miller, E. K.; Moses, D.; Bazan, G.C.; Heeger, A. J. *Macromolecules* **2000**, 33, 5153.

133. Fan, L.J.; Zhang, Y.; Jones, W.E. *Macromolecules* **2005**, 38, 2844.

134. Hunter, C. J.; Sanders, J. K. M. *J. Am. Chem. Soc.* **1990**, 112, 5525.

135. Hostetler, M. J.; Templeton, A. C.; Murray, R. W. *Langmuir* **1999**, 15, 3782.

136. Albert, K. J.; Lewis, N. S.; Schauer, C. L.; Sotzing, G. A.; Stitzel, S. E.; Vaid, T. P; Walt, D. R. *Chem. Rev.* **2000**, 100, 2595.

137. Wright, A. T.; Anslyn, E. V. *Chem. Soc. Rev.* **2006**, 35, 14.

138. You, C.-C.; Verma, A.; Rotello, V. M. *Soft Matter* **2006**, 2, 190.

139. Rosi, N. L.; Mirkin C. A. *Chem. Rev.* **2005**, 105, 1547.

140. Fischer, N. O.; McIntosh, C. M.; Simard, J. M.; Rotello V. M. *Proc. Natl. Acad. Sci. USA* **2002**, 99, 5018.

141. Bayraktar, H.; Ghosh, P. S.; Rotello, V. M.; Knapp, M. J. *Chem. Commun.* **2006**, 1390.

142. Nath, S.; Ghosh, S. K.; Kundu, S.; Praharaj, S.; Panigrahi, S.; Pal, T. *J. Nanoparticle Res.* **2006**, 8, 111.

143. Bunz, U. H. F. *Adv. Polym. Sci.* **2005**, 177, 1.

144. Zheng, J.; Swager, T. M. *Adv. Polym. Sci.* **2005**, 177, 151.

145. Kim, I.-B.; Dunkhorst, A.; Gilbert, J.; Bunz, U. H. F. *Macromolecules* **2005**, 38, 4560.

146. Aguila, A.; Murray, R. W. *Langmuir* **2000**, 16, 5949.

147. Jurs, P. C.; Bakken, G. A.; McClelland, H. E. *Chem. Rev.* **2000**, 100, 2649.

148. Caplan, A. J.; Mandal, A. K.; Theodoraki, M. A. *Trends Cell Biol.* **2007**, *17*, 87.

149. Castro, M. J. M.; Anderson, S. *Biochem.* **1996**, *35*, 11435.

150. Cavalieri, F.; Chiessi, E.; Paradossi, G. *Soft Matter* **2007**, *3*, 718.

151. Censarek, P.; Beyermann, M.; Koch, K. W. *Biochem.* **2002**, *41*, 8598.

152. Censarek, P.; Beyermann, M.; Koch, K. W. *Febs Letters* **2004**, *577*, 465.

153. Chakrabarti, R.; Klibanov, A. M. *J. Am. Chem. Soc.* **2003**, *125*, 12531.

154. Chalfie, M.; KainIn, S. R. *Green Fluorescent Protein: Properties, Applications, and Protocols*. Wiley-Interscience: Hoboken, N. J. **2006**.

155. Chan, W. C. W.; Nie, S. M. *Science* **1998,** *281*, 2016.

156. Chapman, E.; Farr, G. W.; Fenton, W. A.; Johnson, S. M.; Horwich, A. L. *Proc. Nat. Acad. Sci. USA* **2008**, *105*, 19205.

157. Chauvin, F.; Fomenkov, A.; Johnson, C. R.; Roseman, S. *Proc. Nat. Acad. Sci. USA* **1996**, *93*, 7028.

158. Chen, C. P.; Hsu, C. H.; Su, N. Y.; Lin, Y. C.; Chiou, S. H.; Wu, S. H. *J. Biol. Chem.* **2001**, *276*, 45079.

159. Cheon, J.; Lee, J. H. *Acc. Chem. Res.* **2008**, *41*, 1630.

160. Chiti, F.; Dobson, C. M. *Ann. Rev. Biochem.* **2006**, *75*, 333.

161. Ciosek, P.; Wroblewski, W. *Analyst* **2007**, *132*, 963.

162. Wright, A. T.; Edwards, N. Y.; Anslyn, E. V.; McDevitt, J. T. *Angew. Chem. Int. Ed.* **2007**, 46, 8212.

163. Miranda, O. R.; You, C. C. ; Phillips, R. ; Kim, I. K. ; Ghosh, P. S.; Bunz, U. H. F.; Rotello, V. M. *J. Am. Chem. Soc.* **2007**, **129**, 9856.

164. Stephenson, C. J.; Shimizu, K. D. *Polym. Int.* **2007**, **56**, 482.

165. De, M.; You, C. C.; Srivastava, S.; Rotello, V. M. *J. Am. Chem. Soc.* **2007**, 129, 10747.

166. Tsien, R.Y. *Annu. Rev. Biochem.* **1998**, 67, 509.

167. Anderson, N. L.; Anderson, N.G. *Mol. Cell. Proteomics* **2002**, 1, 845.

168. Jurs, P. C.; Bakken, G. A.; McClelland, H. E. *Chem. Rev.* **2000**, 100, 2649.

169. De, M.; Rana, S.; Rotello, V. M. *Macromol. Biosci.* **2009**, 9, 174.

170. Abdelhafiz, A. H.; Myint, M. P.; Tayek, J. A.; Wheeldon, N. M. *Clin. Thera.* **2009**, 21, 1534.

171. Galic, G.; Tomic, M.; Galesic, K.; Kvesic, A.; Soljic, M.; Mozetic, V.; Loncar, Z.; Maricic, A.; Martinovic, Z. *Coll. Antropol.* **2009**, 33, 559.

172. Zismam, D. A.; Kawut, S. M.; Lederer, D. J.; Belperio, J. A.; Lynch, J. P.; Schwarz, M. I.; Tayek, J. A.; Reuben, D. B.; Karlamangla, A. S. *Chest.* **2009**, 135, 929.

173. Tricoli, J. V.; Schoenfeldt, M.; Conley, B. *Clin. Cancer Res.* **2004**, 10, 3943.

174. Masson, J.-F.; Battaglia, T. M.; Khairallah, P.; Beaudoin, S.; Booksh, K. S. *Anal. Chem.* **2007**, 79, 612.

175. Hogdall, E. V. S.; Christensen, L.; Kjaer, S. K.; Blaakaer, J.; Kjaerbye-Thygesen, A.; Gayther, S.; Jacobs, I. J.; Hogdall, C. K.; *Gynecol.Oncol.* **2007**, 104, 508.

176. Couderc, R. *Ann. Biol. Clin.* **2000**, 58, 581.

177. Pisitkun, T.; Johnstone, R.; Knepper, M. A.; *Mol. Cell. Proteomics* **2006**, *5*, 1760.

178. Andreasson, U.; Portelius, E.; Andersson, M. E.; Blennow, K.; Zetterberg, H. *Biomarkers in Medicine* **2007**, 1, 59.

179. Kodadek, T. *Chem. Biol.* **2001**, 8, 105.

180. Soukka, T.; Paukkunen, J.; Harma, H.; Lonnberg, S.; Lindroos, H.; Lovgren, T. *Clin. Chem.* **2001**, 47, 1269.

181. Acharya, G.; Chang, C.-L. Doorneweerd, D. D.; Vlashi, E.; Henne, W. A.; Hartmann, L. C.; Low, P. S.; Savran, C. A. *J. Am. Chem. Soc.* **2007**, 129, 15824.

182. Muller, U. R. *Mol. Biosyst.* **2006**, 2, 470.

183. Engvall, E.; Perlmann, P. *J. Immunol.* **1972**, 109, 129. b) Schuurs, A. H. W. M.; Van Weemen, B. K. *J. Immunoassay* **1980**, 1, 229.

184. Li, J. N.; Zhang, Z.; Rosenzweig, J.; Wang, Y. Y; Chan, D. W. *Clin. Chem.* **2002**, 48, 1296.

185. Baggerly, K. A.; Morris, J. S.; Coombes, K. R. Bioinformatics **2004**, 20, 777.

186. Lavigne, J. J.; Savoy, S. M.; Clevenger, M. B.; Ritchie, J. E.; McDoniel, B.; Yoo, S. J.; Anslyn, E. V.; McDevitt, J. T.; Shear, J. B.; Neikirk, D. P. *J. Am. Chem. Soc*. **1998**, 120, 6429.

187. Lee, J. W.; Lee, J.-S.; Chang, Y.-T. *Angew. Chem. Int. Ed.* **2006**, 45, 6485.

188. Lewis, N. S. *Acc. Chem. Res.* **2004**, 37, 663.

189. Krantz-Rulcker, C.; Stenberg, M.; Winquist, F.; Lundstrom, I. *Anal. Chim. Acta* **2001**, 426, 217.

190. Collins, B. E.; Wright, A. T.; Anslyn, E. V. *Top. Curr. Chem.* **2007**, *277*, 181

191. Buryak, A.; Pozdnoukhov, A.; Severin, K. *Chem. Commun.* **2007**, 2366.

192. Stephenson, C. J.; Shimizu, K. D. *Polym. Int.* 2007, 56, 482.

193. Glijohann, D. A.; Mirkin, C. A. *Nature* **2009**, 462, 461.

194. Hong, R.; Fisher, N. O.; Verma, A.; Goodman, C. M.; Emrick, T.; Rotello, V. M. *J. Am. Chem. Soc.* **2004**, 126, 739.

195. Jones, S.; Thornton, J. M. *Proc. Natl. Acad. Sci. USA*, **1996**, 93, 13.

196. Stites, E. W. *Chem. Rev.*, **1997**, 97, 1233.

197. Conte, L. L.; Chothia, C.; Janin, J. *J. Mol. Biol.*, **1999**, 285, 2177.

198. Jacobson, R. H.; Zhang, X. J.; Dubose, R. F.; Matthews, B. W. *Nature* **1994**, 369, 761.

199. Craven, G. R.; Steers, E.; Anfinsen, C. B. *J. Biol. Chem.* **1965**, 240, 2468.

200. Wallenfels, K.; Weil, R. *Enzymes*, *3rd Ed.* **1972**, 7, 617.

201. Fowler, A. V.; Zabin, I. *J. Biol. Chem.* **1978**, *253*, 5521.

202. Fowler, A. V.; Zabin, I. *J. Biol. Chem.* **1970**, *245*, 5032.

203. Nikolic, M. S.; Krack, M.; Aleksandrovic, V.; Kornowski, A.; Förster, S.; Weller, H. *Angew. Chem*. **2006**, 118, 6727.

204. Adachi, J.; Kumar, C.; Zhang, Y.; Olsen, J. V.; Mann, M. *Genome Biol.* **2006**; 7: R80.

205. Li, S.-J.; Peng, M.; Li, H.; Liu, B.-S.; Wang, C.; Wu, J.-R.; Li, Y.-X.; Zeng, R. *Nucl. Acids Res*. **2009**, 37, D907.

206. Fliser, D.; Novak, J.; Thongboonkerd, V.; Argilés, A.; Jankowski, V.; Girolami, M. A.; Jankowski, J.; Mischa, H. *J. Am. Soc. Nephrol.,* **2007**, 18, 1057.

207. Magistroni, R.; Ligabue, G.; Lupo, V.; Furci, F.; Leonelli, M.; Manganelli, L.; Masellis, M.; Gatti, V.; Cavazzini, F.; Tizzanini, W.; Albertazzi, A. *Nephrol Dial Transplant*, **2009**, 24, 1672.

208. Roden, A. C.; Lockington, K. S.; Trostrud, L. J.; Katzmann, J. A. *Am. J. Clin. Pathol*, **2008**, 130, 141.

209. Nedelkolv, D.; Nelson, R. W. *Am. J. Kidney Dis.* **2001**, 38, 481.

210. Bottini, P.; Almerinda, M.; Alves, R.; and Garlipp C. R. *Am. J. Kidney Dis.* **2002**, 39, E2.

211. Berry, V.; Gole, A.; Kundu, S.; Murphy, C.vJ.; Saraf, R.F. *J. Am. Chem. Soc*. **2005**, 127, 17600.

212. Zhao, X.; Hilliard, L. R.; Mechery, S. J.; Wang, Y.; Bagwe, R. P.; Jin, S.; Tan, W. *Proc. Natl. Acad. Sci. U.S.A*. **2004**, 101, 15027.

213. Bertozzi, C. R.; Bednarski, M. D *J. Am. Chem. Soc*. **1992**, 114, 2242.

214. Amann, R. I.; Ludwig, W.; Schleifer, K. H. *Microbiol. Rev*. **1995**, 59, 143.

215. Reisner, B. S.; Woods, G. L. Reisner, B. S.; Woods, G. L. *J. Clin. Microbiol*. **1999**, 37, 2024.

216. Edmond, M. B.; Wallace, S. E.; McClish, D. K.; Pfaller, M. A.; Jones, R. N.; Wenzel, R. P. *Clin. Infect. Dis*. **1999**, 29, 239.

217. Batt, C. A. *Science* **2007**, 316, 1579.

218. Frenzen, P. D.; Drake, A.; Angulo, F. J. *J. Food Prot*. **2005**, 68, 2623.

219. Mead, P. S.; Slutsker, L.; Dietz, V.; McCaig, L. F.; Bresee, J.S.; Shapiro, C.; Griffin, P. M.; Tauxe, R. V. *Emerg. Infect. Dis*. **1999**, 5, 607.

220. Fan, C.; Plaxco, K. W.; Heeger, A. J *J. Am. Chem. Soc*. **2002**, 124, 5642.

221. Kates M. in Handbook of Lipid Reseach: Glycolipids, Phosphoglycolipids and Sulfoglycopids, ed. M. Kates, Plenum Publishing Corporation, Springer; 1st edition, **1990**, pp. 123-234;

222. Dmitriev, B.; Toukach, F.; Ehlers, S. *TRENDS in Microbiology*, **2005**, 13, 569;

223. Koch, A. L. *Clinical Microbiology Reviews*, **2003**, 16, 673;

224. Schaffer, C.; Messner, P. *Microbiology*, **2005**, 151, 643;

225. Bos, M. P.; Tefsen, B.; Geurtsen, J.; Tommassen, J. *Proc. Natl. Acad. Sci. USA.*, **2004**, 101, 9417.

226. Kim, I. B.; Erdogan, B.; Wilson, J. N.; Bunz, U. H. F. *Chem. Eur. J*. **2004**, 10, 6247.

227. Berry, V.; Gole, A.; Kundu, S.; Murphy, C.vJ.; Saraf, R.F. *J. Am. Chem. Soc*. **2005**, 127, 17600.

228. Amann, R. I.; Ludwig, W.; Schleifer, K. H. *Microbiol. Rev*. **1995**, 59, 143.

229. Reisner, B. S.; Woods, G. L. Reisner, B. S.; Woods, G. L. *J. Clin. Microbiol*. **1999**, 37, 2024.

230. Inglesby, T. V.; O'Toole, T.; Henderson, D. A.; Bartlett, J. G.; Ascher, M. S.; Eitzen, E.; Friedlander, A. M.; Gerberding, J.; Hauer, J.; Hughes, J; McDade, J.; Osterholm, M. T.; Parker, G.; Perl, T. M.; Russell, P. K.; Tonat, K. *J. Am. Med. Assoc.* **2002**, 287, 2236.

231. Brecher, M. E.; Hay, S. N. *Clin. Microbiol. Rev.* **2005**, 18, 195.

232. Shorten, P. R.; Pleasants, A. B.; Soboleva, T. K. *Int. J. Food Microbiol.* **2006**, 108, 369.

233. Ford, E. E.; Colwell, R. R. A global decline in microbiological safety: a call for action. A report from The American Academy of Microbiology, Washington, D.C., **1996**, pp. 1-40.

234. Pedley, S.; Bartram, J.; Rees, G.; Dufour, A.; Cotruvo, J. A. “Pathogenic mycobacteria in Water” World Health Organization (WHO), ISBN: 92-4-156259-5, **2004**.

235. Deisingh, A. M; Thompson, M. *Can. J. Microbiol.* **2004**, 50, 69.

236. Cole, L. A. *Sci. Am.* **1996**, 275, 60.

237. Chandler, D. P.; Straub T. M. *J. of Microbiol. Methods,* **2003**, 53, 185.

238. Straub, T.M.; Chandler, D. P. *J. Microbiol. Methods* **2003**, 53, 185.

239. Hugo, W. B.; Russell, A. D. “Pharmaceutical Microbiology” Blackwell, Oxford, 6th edn. **1998**.

240. Adams, M. R.; Moss, M. O. “Food Microbiology” Royal Society of Chemistry, 2nd ed. **2000**.

241. Safarik, I.; Safarikova, M.; Forsythe, S. J. *J. Appl. Bacteriol.* **1995**, 78, 575.

242. Harrigan, H. F. “Laboratory Methods in Food Microbiology” 3rd ed. Academic Press, San Diego, **1998**.

243. Newton, C. R.; Graham, A. “PCR”, 2nd ed. Bios Scientific, Oxford, **1997**.

244. Eeles, R. A.; Sharp, A. C. “Polymerase Chain Reaction: The technique and its applications” Landes, R.G., Austin, TX, **1993**.

245. Strachan, N. J. C.; Nicholson, F. J.; Ogden, I. D. *Anal. Chim. Acta.* **1995**, 313, 63.

246. Maughan, N. J.; Lewis, F. A.; Smith, V. *J. Pathol.* **2001,** 195, 3-6. b) T. J. Aitman, *Br. Med. J.* **2001**, 323, 611.

247. Hall, E. A. H. “Biosensors” Open University Press, Milton Keynes, **1990**.

248. Catrall, R. W. “Chemical Sensors” Oxford University Press, Oxford, **1997**.

249. Ivnitski, D.; Abdel-Hamid, I.; Atanasov, P.; Wilkins, E. *Biosensors & Bioelectronic*s **1999**, 14, 7, 599.

250. Hilpert, K.; Hancock, R. E. W. *Nature Protocols*, **2007**, 2, 1652.

251. Ji, J.; Schanzle, A.; Tabacco, M. B. *Anal. Chem.* **2004**, 76, 1411.

252. Heal, J. S.; Blom, A. W.; Titcomb, D.; Taylor, A.; Bowker, K.; Hardy, J. R. W. *J. Hosp. Infect.* **2003**, 53, 136.

253. Perkins, S. D.; Mayfield, J.; Fraser, V.; Angenent, L. T. *Appl. Environ. Microbiol.* **2009,** 75, 5363.

254. Chen, C. L.; Yu, J-C.; Holme, S.; Jacobs, M.R.; Yomtovian, R.; McDonald, C. P. *Transfusion* **2008**, 48, 1550-1557.

255. Orihuela, C.; Fillon, J. S.; Tuomanen, E. I. *Infect Immun.* **2006**, 74, 3783.

256. Wu, Y-D.; Chen, L-H.; Zhao, Z-Y. *J. Clin. Microbiol.* **2008**, 46, 2613.

257. Lee, H.; Yoon, T. J.; Weissleder, R. *Angew. Chem. Int. Ed. Engl.* **2009**, 48, 5657.

258. Grossman, H.; Myers, W.; Vreeland, V.; Bruehl, R.; Alper, M.; Bertozzi, C.; Clarke, J. *Proc. Natl. Acad. Sci. USA* **2004**, 101, 129.

259. Bruno, J. G.; Francis, K.; Ikanovic, M.; Rao, P.; Dwarakanath, S.; Rudzinski, D. E. *J. of Bionanoscience* **2007**, 1, 1.

260. Yang, S. Y.; Wang, W. C.; Lan, C. B.; Chen, C. H.; Chieh, J. J.; Horng, H. E.; Hong, C. Y.; Yang, H. C.; Tsai, C. P.; Yang, C.Y.; Cheng, I. C.; Chung, W. C. *J. Virol. Methods* **2010**, 164, 14.

261. Niikura, K.; Nagakawa, K.; Ohtake, N.; Suzuki, T.; Matsuo, Y.; Hirofumi Sawa, Ijiro, K. *Bioconjugate Chem.*, **2009**, 20, 1848.

262. Halfpenny, K. C.; Wright, D. W. *WIREs Nanomed. Nanobiotechnol*. **2010**, 2, 277.

263. Bajaj, A.; Rana, S.; Miranda, O. R.; Yawe, J. C.; Jerry, D. J.; Bunz, U. H. F.; Rotello, V. M. *Chem. Sci.* **2010**, 1, 134.

264. Berry, V.; Gole, A.; Murphy, J.; Saraf, R. F. *J. Am. Chem. Soc.* **2005**, 127, 17600.

265. Guidelines for Drinking Water, Third Edition, Volume 1 (Recommendations), World Health Organization (WHO), ISBN: 92-4-154638-7, **2004**.

266. Gerba, C. P. “Pathogens in the environment” Gerba, C. P.; Brusseau, M. L. Pollution Science. Academic press, New York, **1996**, 279.

267. McFeters, G. A. Drinking water microbiology, Springer-Verlag, ISBN: 0-387-97162-9, **1990**.

268. Holme, S.; McAlister, M. B.; Ortolano, G. A.; Chong, C.; Cortus, M. A.; Jacobs, M. R.; Yomtovian, R.; Freundlich, L. F.; Wenz, B. *Transfusion* **2005**, 45, 984.

269. Hoffmann, O.; Keilwerth, N.; Bastholm Bille, M.; Reuter, U.; Angstwurm, K.; Schumann, R. R.; Dirnagl, U.; Weber, J. R. *J. Cereb. Blood Flow. Metab.* **2002**, 22, 988.

270. Wagner, S. J. *Vox Sanguinis* **2004**, 86, 157.

271. Wu, Y-D.; Chen, L-H.; Wu, X-J.; Shang, S-Q.; Lou, J-T.; Du, L-Z.; Zhao, Z-Y. *J. Clin. Microbio*l. **2008**, 46, 2613.

272. Nguyen, B. T.; Wiskur, S. L.; Anslyn, E. V. *Org. Lett.* **2004**, 6, 2499.

273. Alivisatos, A. P.; Gu, W.; Larabell, C. *Annu. Rev. Biomed. Eng.* **2005**, 7, 55.

274. Bruchez Jr., M.; Moronne, M.; Gin, P.; Weiss, S.; Alivisatos, A. P. *Science* **1998**, 281, 2013.

275. Patange, S. B.; Mukundan, M. K.; Ashok Kumar, K. *Food Control* **2005**, 16, 465.

276. Steiner, M. S.; Meier, R. J.; Duerkop, A.; Wolfbeis, O. S. *Anal. Chem.* **2010**, AC102029J, Articles ASAP

277. Bonifacio, L. D.; Puzzo, D. P.; Breslav, S.; Ozin, G. A. *Adv. Mater.* **2010**, 22, 1351.

278. Janzen, M. C.; Ponder, J. B.; Bailey, D. P.; Ingison, C. K.; Suslick, K.S. *Anal. Chem.* **2006**, 78, 3591.

279. Filippini, D.; Gatto, E.; Alimelli, A.; Malik, M. A.; Di Natale, C.; Paolesse, R.; Damico, A. ; Lundstron, I. *J. Porphyrins Phthalocyanines* **2009**, 13, 77.

280. Bos, M. P.; Robert, V.; Tommassen, J. *Annu. Rev. Microbiol.* **2007**, 61, 191.

281. Duong, F.; Eichler, J.; Price, A.; Leonard, M. R.; Wickner, W. *Cell* **1997**, 91, 567.

282. Sutcliffe, I. C. *Syst. Appl. Microbiol.* **1995**, 17, 467.

283. Baddiley, J. *Bioessays* **1989**, 10, 207.

284. Armstrong, J. J.; Baddiley, J.; Buchanan, J. G.; Carss, B.; Greenberg, G. R. *J. Am. Chem. Soc.* **1958**, 4344.

285. Navarre, W. W.; Schneewind, O. *Microbiol. Mol. Biol. Rev.* **1999**, 63, 174.

286. Srinivas, P. R.; Kramer, B. S.; Srivastava, S. *Lancet Oncol.* **2001**, 2, 698.

287. Pantel, K.; Brakenhoff, R. H.; Brandt, B. *Nat. Rev. Cancer* **2008**, 8, 329.

288. Jen, J.; Wu, L.; Sidransky, D. *Ann N Y Acad Sci.* **2000**, 906, 8.

289. Skvara, H.; Teban, L.; Fiebiger, M.; Binder, M.; Kittler, H. *Arch. Dermatol*. 2005, **141**, 155.

290. Ward, A .M.; Catto, J. W. F.; Hamdy, F. C. *Ann. Clin. Biochem.* **2001**, 38, 633.

291. Chou, S. F.; Hsu, W.L.; Hwang, J. M.; Chen, C. Y. *Biosens. Bioelectron.* **2004**, 19, 999.

292. Alivisatos, P. *Nat. Biotechnol.* **2004**, 22, 47.

293. Soukka, T.; Paukkunen, J.; Harma, H.; Lonnberg, S.; Lindroos, H.; Lovgren, T. *Clin. Chem.* **2001**, 47, 1269.

294. Wu, G.; Datar, R. H.; Hansen, K. M.; Thundat, T.; Cote, R. J.; Majumdar, A. *Nat. Biotechnol.* **2001**, 19, 856.

295. Chen, R. J.; Bangsaruntip, S.; Drouvalakis, K. A.; Kam, N. W. S.; Shim, M.; Li, Y.; Kim, W.; Utz, P. J.; Dai, H. *Proc. Natl. Acad. Sci. U. S. A.* **2003**, 100, 4984.

296. Chen, R. J.; Choi, H. C.; Bangsaruntip, S.; Yenilmez, E.; Tang, X.; Wang, Q.; Chang, Y. L.; Dai, H. *J. Am. Chem. Soc.* **2004**, 126, 1563.

297. Wang, W. U.; Chen, C.; Lin, K. H.; Fang, Y.; Lieber, C. M. *Proc. Natl. Acad. Sci. USA* **2005**, 102, 3208.

298. Cui, Y.; Wei, Q.; Park, H.; Lieber, C. M. *Science* **2001**, 293, 1289.

299. Campagnolo, C.; Meyers, K. J.; Ryan, T.; Atkinson, R. C.; Chen, Y. T.; Scanlan, M. J.; Ritter, G.; Old, L. J.; Batt, C. A. *J. Biochem. Biophys.* **2004**, 61, 283.

300. Wingren, C.; Borrebaeck, C. A. *Curr. Opin. Biotech.* **2008**, 18, 55.

301. Sanchez-Carbayo, M. *Clin. Chem.* **2006**, 52,1651.

302. Singer, S. J.; Nicolson, G. L. *Science* **1972**, 175, 720.

303. Alberts, B.; Johnson, A.; Lewis, J. (**2002**) in *Molecular Biology of the Cell* (4th ed.).

304. Deugnier, M. A.; Faraldo, M. M.; Teuliere, J.; Thiery, J. P.; Medina, D.; Glukhova, M.A. *Dev Biol* **2006**, 293, 414.

305. Blackburn, A. C.; McLary, S. C.; Naeem, R.; Luszcz, J.; Stockton, D. W.; Donehower, L. A.; Mohammed, M.; Mailhes, J. B.; Soferr, T.; Naber, S. P.; Otis, C. N.; Jerry, D. J. *Cancer Res* **2004**, 64, 5140.